



HAL
open science

Systematic assessment of the role of Dynein regulators in oriented cell divisions by live RNAi screen in a novel vertebrate model of spindle orientation

Maria Florencia Di Pietro

► **To cite this version:**

Maria Florencia Di Pietro. Systematic assessment of the role of Dynein regulators in oriented cell divisions by live RNAi screen in a novel vertebrate model of spindle orientation. Cellular Biology. Université Pierre et Marie Curie - Paris VI, 2016. English. NNT : 2016PA066405 . tel-01592476

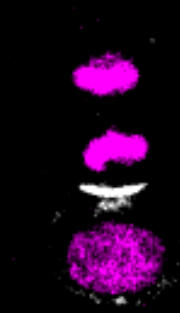
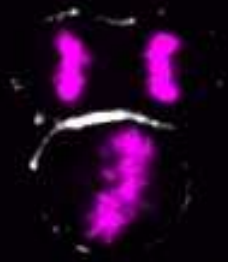
HAL Id: tel-01592476

<https://theses.hal.science/tel-01592476>

Submitted on 25 Sep 2017

HAL is a multi-disciplinary open access archive for the deposit and dissemination of scientific research documents, whether they are published or not. The documents may come from teaching and research institutions in France or abroad, or from public or private research centers.

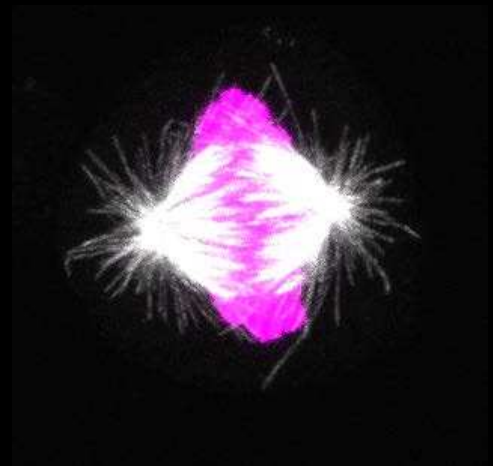
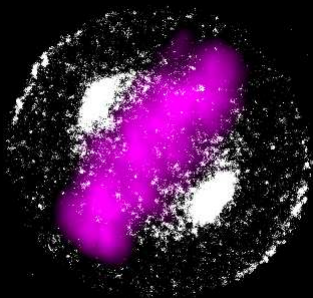
L'archive ouverte pluridisciplinaire **HAL**, est destinée au dépôt et à la diffusion de documents scientifiques de niveau recherche, publiés ou non, émanant des établissements d'enseignement et de recherche français ou étrangers, des laboratoires publics ou privés.



Systematic assessment of the role of
Dynein regulators in oriented cell divisions
by live RNAi screen in a novel vertebrate
model of spindle orientation

Maria Florencia di Pietro

PhD thesis



Université Pierre et Marie Curie

Ecole doctorale Complexité du Vivant

Institut de Biologie de l'Ecole Normale Supérieure,

Team: « Cell division and Neurogenesis »

Systematic assessment of the role of Dynein regulators in oriented cell divisions by live RNAi screen in a novel vertebrate model of spindle orientation

Par Maria Florencia di Pietro

Thèse de doctorat de Biologie Cellulaire

Dirigée par Dr Xavier Morin

Présentée et soutenue publiquement le 23 Septembre 2016

Devant un jury composé de :

Gho, Michel- Research Director- Président du Jury

Gotta, Monica- Professor- Rapportrice

Mapelli, Marina- Research Director- Rapportrice

Bellaiche, Yohanns-Research Director- Examineur

ACKNOWLEDGEMENTS

First of all I want to thank Xavier for welcoming me in his lab and for being an excellent thesis supervisor during all these years. I would like to thank him for the guidance and support during my project, for allowing me to discover the world of cell biology and imaging, and for being also great at the human level. I also want to thank him for trusting me by proposing a huge and ambitious project, for his great contribution to my development as a young researcher and for always proposing solutions and saying the right things at the right moment.

Secondly I want to thank my favorite postdocs, Mehdi and Samuel, for being invaluable colleagues, for sharing with me their experience, for sharing great conversations about science life and life in science. Each of you has enormously contributed to my PhD years in a different manner and I have greatly appreciated having you as colleagues since I joined the lab; you have been awesome.

I want to thank our technicians in the lab for helping me with cell cultures. Raphael, a former technician in the lab, for accompanying me in my first steps in the cell culture room. Rosette, our current technician, for having helped me by maintaining cell lines and assisting me in preparing materials all along these years, and for being a really nice colleague.

Next I want to thank Chooyoung and Evelyne, too more recently incorporated members of the lab, for being great colleagues in everyday life lab and for helping and being kind with me.

I have really spent great times in Xavier's lab, which I consider a treasure in my career and more generally in life. Thank all of you for creating this amazing atmosphere I could find both at the scientific and human level.

Moreover, I want to thank different people who I worked with especially during the first years. Léo, for having spent very nice times working together, and for his feedback, his interest and collaboration on my project. Simon, for our interesting collaboration working in optogenetics and for further help with other aspects of my project. More generally, I would like to thank all the

“optoclubbers”, for our meetings about optogenetics and cell division orientation, and also because we’ve had a lot of fun together. In addition, I thank a lot to Auguste Genovesio, Yingbo Li and France Rose for collaborating on my project by developing software for data analysis.

Furthermore I thank all the people of the imaging platform of the institute for assistance during these years. I also want to thank the people from 7th floor of the IBENS for being nice and helpful these years. More generally, thanks to the people that have contributed with protocols, reagents, cell lines or in other aspects of my project: Olivier Collin, Nicolas Carpi and Matthieu Piel, Salah Elias, Mickael Machicoane and Arnaud Echard, Iain Cheeseman, the Hyman lab and Maria Bagonis.

Moreover, I would like to thank Monica Gotta, Marina Mapelli, Yohanns Bellaiche and Michel Gho for accepting to participate as a jury of my thesis. Also many thanks to the members of my thesis committee, Renata Basto, Marie-Emilie Terret and Matthieu Piel, for the excellent input to my project during our two meetings.

I also want to mention great people I have known in Paris: the friends I have made at Cité U, my mates from M2, my “more Parisian” friends, people from the theater classes and every other nice person that I have met along my way. Thank you all for nice moments spent together. Thanks also to my friends from life in Buenos Aires, for supporting me and for keeping in touch all these years.

Finally I want to thank my brother, my sister and my parents who, while being 11k km far away from me, have unconditionally supported me in every aspect of life during all these years. Thanks Euge and Fede for always being there for me. Thanks Mum and Dad for adapting so well to the distance, for helping me with everything and for visiting me every year. These years would not have been the same without the support of my family.

CONTENTS

Acknowledgements	0
Figures index	7
Glossary.....	8
Abstract.....	10
Résumé	12
Chapter 1: Mitotic spindle orientation in development and disease.....	14
1-1 Generation of cellular diversity.....	14
1.1.1- Drosophila Neuroblasts	17
1.1.2- Mouse Skin progenitors.....	19
1.1.3- Vertebrate neural progenitors	20
1.2. Morphogenetic processes.....	24
1.3-Tumorigenesis.....	28
1.3.1- Deregulation of stem cells compartments.....	28
1.3.2- Epithelial disruption.....	29
1.4. Conclusion	31
Chapter 2: Mechanisms of mitotic spindle orientation.....	33
2.1. Introduction	33
2.2- The LGN complex	34
2.3. Models for studying spindle orientation.....	38
2.4. New insights into the molecular regulation of LGN complex recruitment/stability at the cortex	40
2.4.1. Molecules regulating the recruitment /stability of the LGN complex at the cortex.....	40
2.4.2. Temporal and spatial regulation of LGN complex localization	43
2.4.3. Not a monopoly: Gai/LGN independent pathways in spindle orientation.....	49
2.5- The emerging role of actin in spindle orientation.....	51
2.5.1. Requirement of an intact actin cortex	51
2.5.2. Anthrax receptor and actin polarization	52
2.5.3. Polarized subcortical actin clouds.....	53
2.5.4. ERM proteins.....	54

2.6. Modulation of spindle orientation through the specific regulation of astral microtubules.....	57
2.6.1. Astral microtubules nucleation	58
2.6.2. Astral microtubules dynamics and stability.....	59
2.6.3. Astral MT cortical capture.....	60
2.6.4. Behavior of astral microtubules at the cortex.....	61
2.6.5. Modulation of specific astral MT subpopulations	61
2.7. Extracellular stimuli influencing spindle orientation	63
2.8. Spindle orientation in context: roles of cell geometry and mechanical forces	64
2.8.1. Intrinsic cell geometry in mitosis impacts on spindle orientation	65
2.8.2. Role of surrounding forces in spindle orientation	67
2.9. Other models of Spindle positioning	71
Spindle orientation in budding yeast.....	71
Spindle orientation in Oocyte Meiosis.....	72
2.10. Conclusion.....	74
Chapter 3: Dynein and its regulators	76
3.0- Molecular motors.....	76
3.1- The Dynein family	76
3.1.1 Dynein structure.....	78
3.1.2 Motor characteristics.....	80
3.1.3- Dynein regulation	81
3.2- Dynactin.....	84
3.2.1-Dynactin structure.....	84
3.2.2- Dynactin Interaction with Dynein.....	87
3.2.3- Functions of Dynein assisted by Dynactin.....	89
3.2.4- Function of individual dynactin subunits	92
3.3-LIS1/NDE1/NDEL1	96
3.3.1-Structure and Interaction LIS1- Nde1/NdeL1-Dynein.....	96
3.3.2-Functions of Dynein assisted by LIS1/NDE1/NDEL1	97
3.4- Bicaudal D.....	99

3.5 RZZ Complex and Spindly.....	100
3.5- The Dynein family in Spindle Orientation in metazoans.....	100
3.5.1-Function of Dynein in spindle orientation in C.elegans and Drosophila	101
3.5.2- Function of Dynein in spindle orientation in vertebrate cultured cells	103
3.5.3- Function of dynein in vertebrate spindle orientation <i>in vivo</i>	108
3.6- Conclusion	109
Chapter 4: The actin Capping Proteins CAPZ- A/B (CP)	110
4.1- CAPZ A/B isoforms and structure.....	110
4.1.2-Structure of CAPZ A/B heterodimer	111
4.1.3- Structure of the CP bound to actin.....	112
4.2- CAPZ A/B actin capping activity <i>in vitro</i>	112
4.3- CAPZ A/B functions in cells and <i>in vivo</i>	113
4.3.1- Role of CAPZ A/B in actin dependent processes	113
4.3.2- CAPZ A/B in Dynactin.....	119
4.3.3- CAPZ A/B and Microtubules.....	119
4.4- Conclusion	120
Chapter 5: Questions and objectives of the project	121
5.1. Questions motivating this project	121
5.2- Objectives.....	122
A- Development of a cellular model of LGN-controlled spindle orientation	122
B- Screen for new regulators of vertebrate spindle orientation	125
C- Characterization of the mechanisms of action of interesting hits in cells	125
D- Validation of interesting hit(s) <i>in vivo</i>	126
Chapter 6: Results.....	127
6.1. Designing of a spindle orientation model specifically guided by the LGN complex in cultured cells	127
6.2. A systematic live RNAi screen identifies essential and dispensable dynein/dynactin complex members downstream of the LGN complex	133
6.2.1. Workflow.....	133
6.2.2. Candidate choice	134
6.2.3. Screen results	136

6.3. The Actin Capping protein CAPZ-B localizes to the spindle poles and cell cortex in mitosis, and regulates mitotic spindle orientation in adherent cells.....	142
6.4. CAPZ-B controls spindle orientation in an actin independent manner	145
6.5. Regulation of dynactin/dynein complexes by CAPZ-B.....	148
6.6. CAPZ-B controls the dynamics of mitotic microtubules.....	152
6.7. CAPZ-B controls planar spindle orientation in the chick neuroepithelium	155
Chapter 7: Discussion.....	159
A novel cellular model of oriented divisions: a new tool in the spindle orientation field	159
Advantages and potential uses of the model	159
Limitations of the Ed-Gai spindle orientation model	162
A live RNAi screen for spindle orientation regulators	165
Regulation of Mitotic spindle orientation by CAPZ-B.....	168
CAPZ-B localization during mitosis	168
Regulation of dynactin/dynein by CAPZ-B	169
Regulation of Microtubules by CAPZ-B.....	170
Differential role of CAPZ-B vs CAPZ-A in spindle orientation.....	174
CAPZ-B regulates spindle orientation in the chick neuroepithelium.....	174
Conclusion	176
Résumé de la thèse.....	177
Introduction.....	177
L'orientation du fuseau mitotique	177
Le complexes dynein-dynactin.....	178
Objectifs.....	179
Résultats.....	180
Développement d'un modèle d'orientation de fuseau en culture cellulaire.....	180
Un crible RNAi pour trouver des nouveaux régulateurs de l'orientation de fuseau	181
Caractérisation de la fonction de CAPZ-B dans l'orientation du fuseau mitotique	181
Conclusion	182
Appendix 1: Supplementary Figures	184
Appendix 2: Methods.....	190

Cell culture	190
Transfection.....	190
RNAi library.....	191
Plasmids and cell lines.....	191
Drug treatment.....	192
Immunofluorescence	192
In ovo electroporation	193
Image acquisition.....	194
Image analysis.....	195
Angle measurement in RNAi screen and Ed-Gai model development experiments.....	195
Description of Matlab software: Nuclei segmentation, division angle tracking and GFP cluster quantification.....	196
Quantification of cortical signals in mitotic cells	197
Analysis of MT dynamics using u-track.....	198
Appendix 3: Contribution to additional research projects.....	199
References.....	205

FIGURES INDEX

Introduction

Figure 1: Spindle orientation in binary fate decision determined by extrinsic cues.....	15
Figure 2: Spindle orientation during Neuroblast asymmetric division.....	18
Figure 3: Mitotic spindle orientation in mouse embryonic skin progenitors.....	20
Figure 4: Mitotic spindle orientation in the vertebrate neuroepithelium.....	23
Figure 5: Mitotic spindle orientation in morphogenetic processes.....	27
Figure 6: Role of spindle orientation in epithelial architecture maintenance and potential role in tumorigenesis.....	31
Figure 7: The LGN complex.....	35
Figure 8: Models of spindle orientation in 2D or 3D cultured cells.....	39
Figure 9: Temporal-spatial regulation of LGN complex localization.....	48
Figure 10: The role of actin in spindle orientation.....	56
Figure 11: Modulation of spindle orientation through regulation of astral microtubules.....	62
Figure 12: Role of cell geometry and external forces.....	70
Figure 13: Functions of Cytoplasmic dynein 1 in interphase and mitosis in metazoans.....	77
Figure 14: Crystal structure of human dynein 2.....	79
Figure 15: Structure of the Dynein complex, including catalytic and non-catalytic subunits.....	79
Figure 16: Structure of the Dynactin complex.....	84
Figure 17: Model for the interaction between the CAPZ A/B heterodimer and the Arp1 filament barbed end..	87
Figure 18: Interaction of Dynein –Dynactin when bound to MT.....	88
Figure 19: Functions and interactions for individual subunits.....	95
Figure 20: DHC function in the micropattern-guided spindle orientation model.....	104
Figure 21: Cellular phenotypes involved in spindle misorientation generated by LIS1 or Spindly depletion....	107
Figure 22: Integrin receptor and ILK recruit dynactin to the basal membrane.....	108
Figure 23: Structure of the CAPZ A/B heterodimer.....	111
Figure 24: Actin capping function of CAPZ A/B in different cellular processes.....	116
Figure 25: Effect of LGN knockdown on micropattern guided spindle orientation.....	124

Results

Figure 26: Development of a spindle orientation model controlled by the LGN complex.....	132
Figure 27: Localization of LGNGFP, NuMA and the dynactin subunit p150 in pairs of Ed-Gαi cells.....	133
Figure 28: A live siRNA screen for spindle orientation regulators: Dynein subunits and regulators.....	137
Figure 29: Effect of CAPZ-B siRNA on spindle orientation with respect to the substrate.....	143
Figure 30: Localization of CAPZ-B in mitotic cells.....	144
Figure 31: Effect of CAPZ-B depletion on the actin cytoskeleton in mitotic cells.....	146
Figure 32: CAPZ-B regulates Ed-Gαi controlled spindle orientation independently of actin modulation.....	147
Figure 33: Effects of CAPZ-B depletion on the Dynactin and Dynein complexes.....	150
Figure 34: Effect of CAPZ-B depletion on the spindle displacement towards single DHC-GFP crescents.....	151
Figure 35: Effect of CAPZ-B depletion in spindle- and astral- MT density.....	153
Figure 36: Effect of CAPZ-B depletion on astral MT dynamics.....	154
Figure 37: CAPZ-B localization in neuroepithelial progenitors.....	155
Figure 38: CAPZ-B function during planar spindle orientation of neuroepithelial progenitors.....	157

Discussion

Figure 39: Model proposed for the recruitment/ stability of Dynein/Dynactin at the cell cortex in mitosis.....	166
---	-----

Appendix 1

Figure 40: Development of the Ed-Gαi model and characterization of EdGFP cells.....	185
Figure 41: Workflow for automated anaphase angle and GFP level measurements.....	186
Figure 42: A live siRNA screen for spindle orientation (second part).....	187
Figure 43: Regulation of dynein/dynactin by CAPZ-B, p150 and Arp1A.....	189

GLOSSARY

- GSC: Germline stem cells
- LGN: Leucine-Glycine-Asparagine
- NuMA: Nuclear and Mitotic Apparatus
- Pins: Partner of Inscuteable
- Mud: Mushroom body defect
- Baz: Bazooka
- Par6: Partitioning Defective 6
- Par3: Partitioning Defective 3
- aPKC: atypical protein kinase C
- Brat: Brain tumor
- Numb?
- Insc: Inscuteable
- mInsc: mouse Inscuteable
- MCPH: Microcephaly
- Fat-Ds: Fat-Dachsous
- PCP: Planar Cell Polarity
- APC: Adenomatous polyposis coli
- VHL : von Hippel-Lindau
- MT: Microtubule
- GOA1: Guanine nucleotide-binding protein G (o) subunit alpha
- GPA16: G Protein, Alpha subunit
- GPR1/2: G protein regulator 1/2
- LIN5: Spindle apparatus protein lin-5
- TPR: Tetratricopeptide repeats
- GPR: G Protein Regulator
- GAP: GTPase activating protein
- GEF: Guanine exchange factor
- MDCK: Madin-Darby canine kidney
- Ed: Echinoid
- Dlg: Discs-large
- SOP: sensory organ precursor
- Lgl: lethal giant larvae
- NB: Neuroblast
- AurA: Aurora A
- Ran: RAs-related Nuclear protein
- HTT: Huntingtin
- Plk1: Polo-like kinase 1
- T2055: Threonine 2055
- CDK1: Cyclin dependent kinase 1
- 4.1G: band 4.1-like 2 protein/EPB41L2
- 4.1R: band 4.1 protein/EPB41
- PIP: Phosphatidylinositol phosphate
- PIP2: Phosphatidylinositol 4,5-bisphosphate
- CYK4: Rho family GTPase-activating protein CYK4 / MgcRacGAP
- MKLP1: Mitotic kinesin-like protein 1
- Fz-Dsh: Frizzled-Dishevelled
- Dsh DEP domain: Dishevelled/EGL10/Pleckstrin domain
- Antxr2a: Anthrax receptor 2a
- zdia2: diaphanous related formin 2 (in zebrafish)
- Arp3: Actin related protein 3
- ERM: Ezrin-Radixin-Moesin
- Pcnt: pericentrin
- Rab11: Ras-related protein Rab-11, recycling endosome GTPase
- EB1: End Binding family member 1
- γ -TuRCs: γ -tubulin ring complexes
- Dgrip75: Drosophila grip-motif-polypeptide 75
- MISP: mitotic interactor and substrate of Plk1
- MAP4: Microtubule associated protein 4
- EB3: End Binding family member 3
- APs: apical progenitors
- Fat/Ds/Fj: Fat/Dachsous/Four jointed
- Tre1: trapped in endoderm 1
- ECM: extracellular matrix
- NRK: Normal Rat Kidney
- EVL: enveloping cell layer
- TCJs: tricellular junctions
- Num1: NUclear Migration 1
- Bim1: Binding to Microtubules 1
- Myo2: MYOSin
- Kar 9: KARyogamy
- She1: Sensitivity to High Expression
- Dyn1: Yeast DHC
- Pac1: Perish in the Absence of Cin8p
- Bik1: Bilateral Karyogamy defect
- LIS1: Lissencephaly 1
- CLIP-170: Cytoplasmic Linker Protein 170
- Myo V: Myosin 5
- Arp2/3: Actin related proteins 2/3 complex
- SAC: Spindle Assembly Checkpoint-
- MTOC: Microtubule Organizing Center
- NEB: Nuclear Envelope Breakdown
- DHC: Dynein Heavy chain
- DIC: Dynein Intermediate chain
- DLIC: Dynein Light intermediate chains
- DLC: Dynein Light Chains
- LC8: dynein light chain LC8 family

- Roadblock: Dynein Light Chain Roadblock or LC7 family
- TCTEX: Dynein Light Chain Tctex (T-Complex-Associated-Testis-Expressed 1-Like) family
- AAA: ATPASES Associated with diverse cellular Activities
- NDE1: Nude
- NDEL1: Nude Like1
- RZZ: ROD ZW10 Zwilch
- Arp1: Actin related protein 1
- cryoEM: cryo Electron Microscopy
- CAP-Gly: Cytoskeleton-associated proteins glycine-rich domain
- MTBD: Microtubule Binding Domain
- CAPZ A/B: Capping Actin Protein of Muscle Z-Line isoforms A/B
- Arp11: Actin-Related Protein 11
- ER: Endoplasmic Reticulum
- RILP: Rab Interacting Lysosomal Protein
- SPB: Spindle pole bodies
- BICD: Bicaudal D
- BICDR: Bicaudal-D-related protein
- KT: kinetochore
- dyrb1: Dynein Light chain Roadblock type 1
- DYNLL1: Dynein Light Chain LC8-Type 1
- MEFs: Mouse Embryonic Fibroblasts
- ILK: Integrin Linked Kinase
- CP: actin capping protein
- TIRF: Total internal reflection fluorescence
- Glu MTs: MTs enriched in post-translationally deetyrosinated tubulin (Glu-tubulin)
- mDia: Diaphanous-related formin
- H2B: Histone 2B
- Patterns=micropatterns
- Ed-G α i= EdGFP-G α i
- Ed-LGN= EdGFP-LGN
- NCZ: Nocodazole
- Lat A: Latrunculin A
- AGS3: Activator of G-Protein Signaling 3
- Frmpd1: FERM and PDZ domain containing 1
- STMN2: Stathmin 2
- MACF1: Microtubule-Actin Crosslinking Factor 1
- RB1: Retinoblastoma 1
- CLASP1: Cytoplasmic Linker Associated Protein 1
- ASPM: Abnormal Spindle Microtubule Assembly
- STIL: SCL/TAL1 Interrupting Locus
- LKB1: Liver Kinase B1
- Dox: Doxycycline
- RB: Roadblock
- LT1 and 3: Isoforms of TCTEX DLC type
- E3-E4: embryonic day 3 /or 4
- indels: insertion/deletions
- gRNA: guide RNA
- TetON: Tetracycline ON transactivator
- TRE: Tetracycline response element
- NeoR: Resistance to neomycin

ABSTRACT

During cell division, the positioning and orientation of the mitotic spindle within the cell is tightly regulated in many cell types. This precise orientation may be involved in cell fate decisions, tissue morphogenesis and maintenance of epithelial structures. Therefore, this process is critical for development and tissue homeostasis, and its deregulation can lead to different pathologies. In several contexts, spindle orientation is controlled by the LGN molecular complex (composed of G α i, LGN and NuMA), whose subcortical localization determines the axis of spindle orientation. In particular, the localization of the LGN complex determines the site of recruitment of the molecular motor dynein which in turn exerts forces on astral microtubules to orient the spindle. Insights into the molecular mechanisms regulating LGN dependent spindle orientation have been obtained mainly in invertebrate models. In contrast, our understanding of vertebrate spindle orientation is somehow limited to the members of the LGN complex and its simple model of recruitment. There is missing information about the molecules regulating the formation of the complex and those working downstream of it. In particular, how molecular motors function during spindle orientation has been little explored. This prompted us to screen for new regulators of vertebrate spindle orientation. For this, I developed a novel model of spindle orientation specifically controlled by the LGN complex, using human cells cultured on micropatterns and live imaging. Using this model, I performed a live siRNA screen testing 110 candidates including molecular motors and their regulators, MAPs and a set of centrosomal proteins for their function in LGN complex-controlled spindle orientation. Remarkably, this screen revealed that dynein regulators are unequally required for spindle orientation. This reinforces the notion that regulation of this single molecular motor relies on specific subunits for the control of different cellular processes. Furthermore, within the dynactin subunits, I found that the actin capping protein CAPZ-B, whose function in the dynactin complex was previously unknown, is a strong regulator of spindle orientation. Characterization of the mechanisms of action of CAPZ-B in cultured cells revealed that CAPZ-B regulates spindle orientation independently of its classical role in modulating actin dynamics. Instead, my results suggest that CAPZ-B controls spindle

orientation by modulating the localization/activity of the dynein/dynactin complexes as well as the dynamics of spindle microtubules. Finally, we demonstrated that CAPZ-B regulates spindle orientation *in vivo* in the chick embryonic neuroepithelium where progenitors divide with a planar orientation in an LGN complex dependent manner.

I expect that my work will contribute to the understanding of dynein function during vertebrate spindle orientation and will open the path for new investigations in the field. In addition, I hope that our newly developed model of spindle orientation will be of interest for the community working on this question. Better characterizing vertebrate spindle orientation at the molecular level is essential for the understanding of this relevant question in cell and developmental biology.

RESUME

Lors de la division cellulaire, le positionnement et l'orientation du fuseau mitotique dans la cellule sont strictement régulés dans de nombreux types cellulaires. L'orientation spécifique du fuseau peut jouer un rôle dans la détermination du destin cellulaire, ainsi que dans la morphogénèse et le maintien des structures épithéliales. En conséquence, ce processus est critique pour le développement et l'homéostasie de tissus, et sa dérégulation peut conduire à diverses pathologies.

Dans certains contextes, l'orientation du fuseau est contrôlée par le complexe moléculaire LGN, dont la localisation sous-corticale détermine l'axe d'orientation du fuseau. En particulier, la localisation du complexe LGN détermine le site de recrutement du moteur moléculaire dynein, lequel exerce des forces sur les microtubules astraux pour orienter le fuseau. Les détails des mécanismes moléculaires régulant l'orientation du fuseau dépendant du complexe LGN ont été obtenus principalement chez les invertébrés. En revanche, notre compréhension de l'orientation du fuseau chez les vertébrés est plutôt limitée aux membres du complexe LGN et à leur simple mode de recrutement. Il y a des informations manquantes concernant les molécules régulant la formation du complexe et celles qui fonctionnent en aval. En particulier, comment les moteurs moléculaires fonctionnent pendant l'orientation du fuseau a été peu exploré. Ces faits nous ont motivés à initier un crible moléculaire pour trouver de nouveaux régulateurs de l'orientation de fuseau chez les vertébrés. Avec cet objectif, j'ai développé un nouveau modèle d'orientation du fuseau spécifiquement contrôlé par le complexe LGN, en utilisant des cellules humaines cultivées sur des micropatrons ainsi que la vidéo-microscopie. Avec ce modèle, j'ai réalisé un crible « *siRNA* » en évaluant 110 candidats incluant des moteurs moléculaires et leurs régulateurs, des protéines associées aux microtubules et un groupe de protéines centrosomales, pour leur fonction dans l'orientation du fuseau contrôlée par le complexe LGN. De façon remarquable, ce crible a révélé que les régulateurs de la dynein sont inégalement requis pour orienter le fuseau. Ceci renforce la notion que la régulation de ce moteur moléculaire dépend de sous-unités spécifiques pour le contrôle de processus cellulaires différents. De plus, entre les sous-unités de la dynactine, j'ai trouvé que la protéine du « capping » de l'actine, CAPZ-B, dont

aucune fonction au sein du complexe dynactine n'avait jusqu'à présent été identifiée, est un régulateur majeur de l'orientation du fuseau. La caractérisation des mécanismes d'action de CAPZ-B dans des cellules en culture a révélé que CAPZ-B régule l'orientation du fuseau indépendamment de son rôle classique comme modulateur de la dynamique de l'actine. En revanche, mes résultats suggèrent que CAPZ-B contrôle l'orientation du fuseau en régulant la localisation et l'activité des complexes dynein et dynactine ainsi que la dynamique des microtubules du fuseau. Finalement, nous avons démontré que CAPZ-B régule l'orientation du fuseau *in vivo* dans le neuroépithélium de l'embryon de poulet où les progéniteurs se divisent avec une orientation planaire d'une façon dépendante du complexe LGN. Je pense que mes travaux vont contribuer à la compréhension de la fonction de la dynein pendant l'orientation du fuseau chez les vertébrés et vont ouvrir la voie pour de nouvelles recherches dans le domaine. De plus, j'espère que notre nouveau modèle d'orientation du fuseau sera d'intérêt pour la communauté scientifique dédiée à cette question. Une meilleure caractérisation au niveau moléculaire de l'orientation du fuseau chez les vertébrés est essentielle pour la compréhension de cette question pertinente pour la biologie cellulaire et du développement.

CHAPTER 1: MITOTIC SPINDLE ORIENTATION IN DEVELOPMENT AND DISEASE

The development of multicellular organisms composed of functional tissues and organs relies on a series of morphogenetic events, and on mechanisms that generate cellular diversity in a timely manner. In the adult organism, homeostasis of mature tissues requires controlled proliferation to produce new cells in normal or repair conditions, while maintaining tissue architecture. In this chapter I will discuss some examples showing how mitotic spindle orientation contributes to these processes as well as potential links between defective spindle orientation and different diseases.

1-1 GENERATION OF CELLULAR DIVERSITY

Stem cells need to balance between proliferation and differentiation in order to maintain their pool as well as producing differentiating progeny. In this sense, one interesting stem cell feature is that they can divide asymmetrically producing a daughter cell with a distinct fate as well as a self-renewing daughter. This allows the generation of differentiating cells while conserving a precursor able to divide. The generation of different fates in one single division can be controlled both by extrinsic or intrinsic factors. In the first scenario, the positioning of the daughter cells with respect to a surrounding signaling source that dictates cell identity determines the occurrence of symmetric vs asymmetric outputs. A clear example is given by the division of the germline stem cells (GSC) in the *Drosophila* ovaries. Self-renewal of these cells depends on signals coming from the surrounding cells (cap cells) that constitute the niche. Thus, positioning of one cell away from this niche results in its differentiation while the daughter remaining in contact with the niche self-renews. In contrast, positioning of both daughter cells in parallel to the cap cells allows the generation of two GSC (Spradling et al., 2011; Xie and Spradling, 2000) (Fig.1).

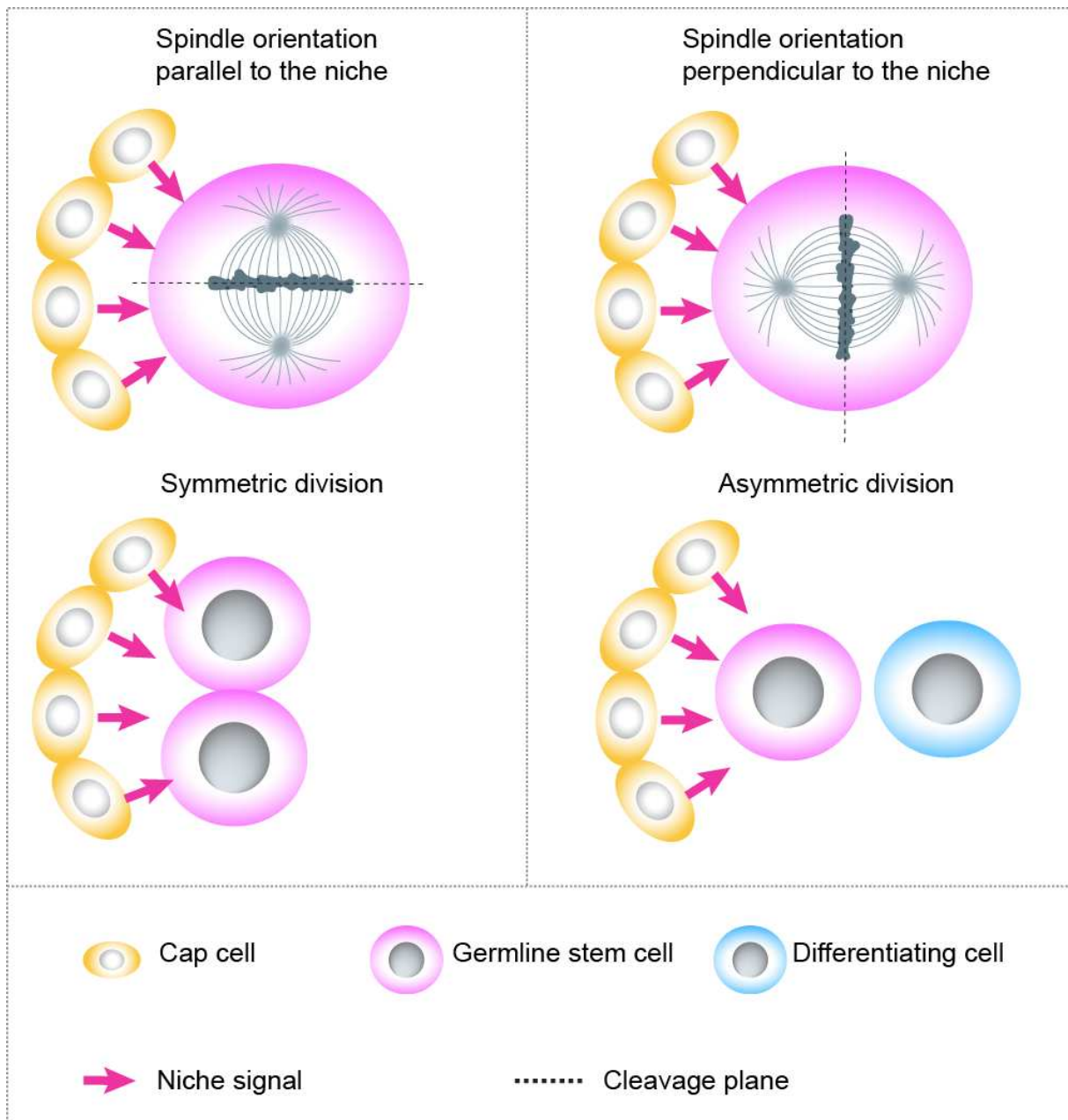


Figure 1: Spindle orientation determines the occurrence of symmetric/ asymmetric cell division by defining the position of the daughter cells with respect to a signaling niche. The example given corresponds to Germline stem cell divisions. Symmetric divisions can occur upon GSC loss, and contribute to repopulate the niche.

In the second scenario, the unequal segregation of intrinsic cell fate determinants between sibling cells accounts for the generation of two different fates. Probably the best example is constituted by the *Drosophila* neuroblasts which divide asymmetrically to self-renew and produce a ganglion mother cell. Here, the fate determinants Brat, Prospero and Numb are uniquely segregated into the ganglion mother cell, allowing for asymmetric cell division (reviewed in Homem and Knoblich, 2012; Knoblich, 2008) (Fig. 2a) (see below for additional details).

How can the differential positioning or asymmetric segregation of intrinsic fate determinants be achieved? The plane in which cell division occurs constitutes a mechanistic solution for both scenarios. In the first case, if the division plane is perpendicular to the signaling source, then both cells will remain in contact with the signal giving rise to a symmetric cell division. If the division plane is parallel, in contrast, one cell is positioned away from the niche thus generating an asymmetric division (Yamashita et al., 2003b) (Fig. 1a). In the intrinsic mode of cell fate determination, intrinsic fate determinants asymmetrically distribute in mitosis, and a cleavage plane that results in asymmetric segregation of these determinants allows the generation of distinct cell fates (Fig. 2a).

The plane of cell division is mainly controlled by the orientation of the mitotic spindle in anaphase. Thus, differential orientation of the mitotic spindle is a potential mechanism to determine the occurrence of symmetric vs asymmetric cell divisions.

It should be noted, however, that the orientation of the spindle (apico/basal, planar, etc) is not a synonym of the division outcome (asymmetric/symmetric) as I will discuss below.

In the following sections I will present some of the most studied examples linking spindle orientation with differential cell fate generation in higher eukaryotes as well as potential links between spindle misorientation and pathologies. The mechanisms of spindle orientation will be discussed in detail in chapter 2. However, to facilitate the discussion of these examples, I introduce the core mechanisms here. In short, in many tissues, spindle orientation is controlled by the specific subcortical localization of an evolutionary conserved complex composed of Gai subunits, LGN and NuMA (Gai, Pins and Mud in *Drosophila*, hereafter called “LGN complex”) which mediates the recruitment of force generators that in turn orient the spindle towards the cortical sites in which the LGN complex is enriched (reviewed in Morin and Bellaïche, 2011).

1.1.1- DROSOPHILA NEUROBLASTS

Neuroblasts are the neural stem cells in the *Drosophila* nervous system. These cells delaminate from the neuroectoderm and divide continually in an asymmetric fashion giving rise to a self-renewed neuroblast and a ganglion mother cell which will further produce two neurons. Neuroblasts are polarized along the apico basal axis with Bazooka (Par3 homolog), Par6 and aPKC localized to the apical side (Suzuki and Ohno, 2006). During prometaphase the cell fate determinants Brat, Prospero and Numb accumulate to the basal side (Betschinger et al., 2006; Choksi et al., 2006). In this context, the spindle is oriented along the apico-basal axis which allows the segregation of basal cell fate determinants to the basal cell and of the apical determinants to the apical cell, thus resulting in an asymmetric cell division (reviewed in Knoblich, 2008). In terms of mechanisms, an apically localized adaptor called Inscuteable (Insc) provides the link between the apical polarity complex and the spindle orientation machinery i.e. the $G\alpha$ /Pins/Mud complex, which is recruited to the apical membrane (Bowman et al., 2006; Yu et al., 2000) (Fig. 2a).

In the context of neuroblast division, spindle orientation is seen as one of several mechanisms favoring the occurrence of cell fate decisions. Of note, binary cell fate choices are not much affected in mud mutants in which spindle orientation is specifically perturbed without affecting the apical-basal polarity and the distribution of fate determinants. The fact that asymmetric division still takes place is attributed to a “telophase rescue” in which the fate determinants are redistributed in relation to the final spindle orientation axis in late mitosis (Bowman et al., 2006; Knoblich, 2010). However, Cabernard and Doe have found that a minority of mud mutant cells present defective distribution of cell determinants at the end of mitosis. Within this cell population, these authors have observed that when the spindle is perpendicular to the apico-basal axis, apical determinants are equally inherited and the two daughters become neuroblasts (Fig. 2b). Of note, the basal determinants are still unequally segregated in this case, suggesting that the presence of the apical determinants overrides the inheritance of basal determinants (Cabernard and Doe, 2009).

Because of the stereotypic behavior of neuroblast division as well as the powerful genetics available in flies, this model is extensively used for the study of asymmetric cell division and spindle orientation.

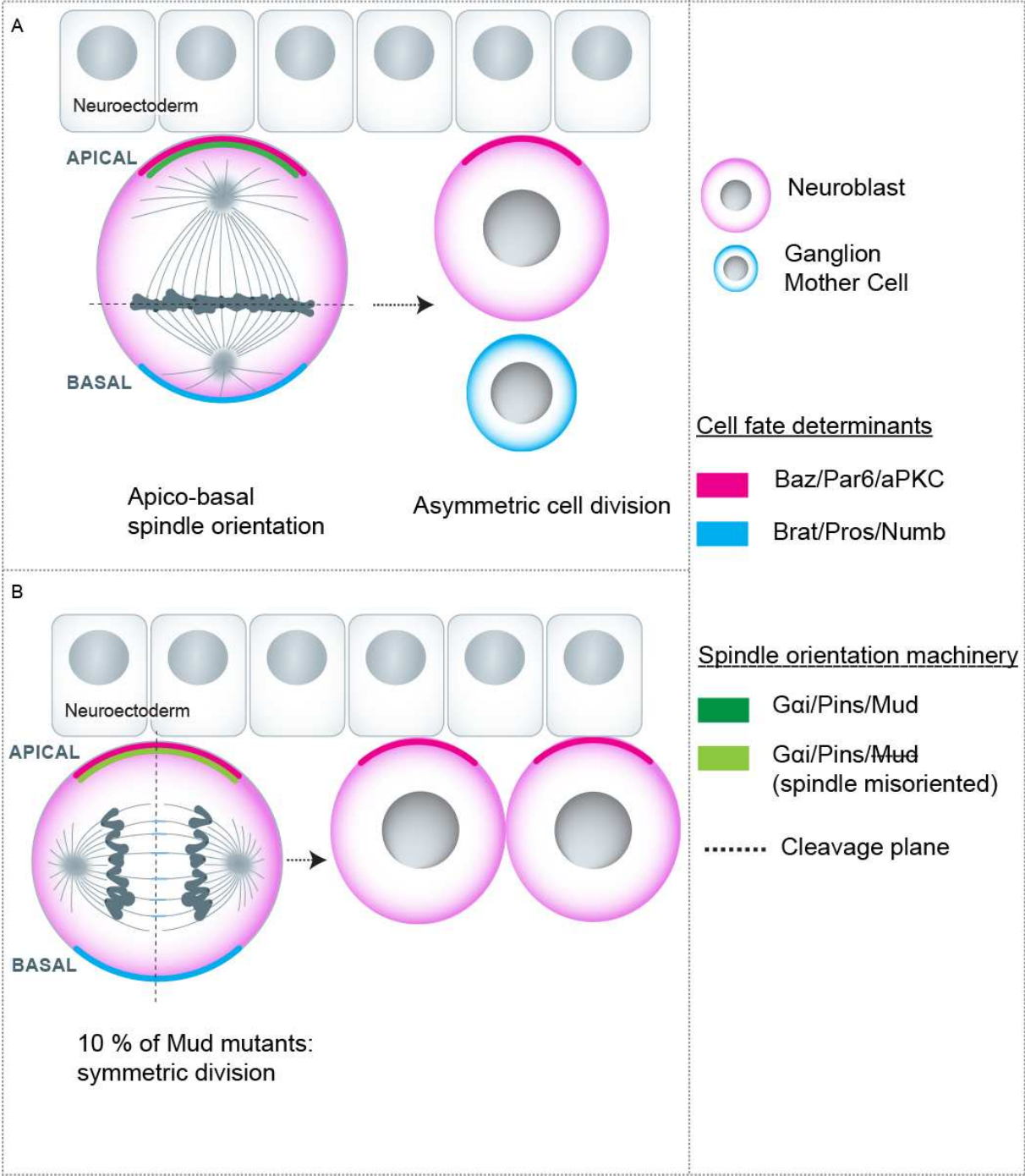


Figure 2: Spindle orientation during Neuroblast asymmetric division. a) Spindle orientation allows the asymmetric segregation of intrinsic cell fate determinants and asymmetric division.. b) A minority of Mud mutants (defective in spindle orientation) in which spindle is misoriented at late mitosis results in symmetric division.

1.1.2- MOUSE SKIN PROGENITORS

The mammalian epidermis is a stratified epithelium composed of distinct layers. In early embryonic development the epidermal tissue is constituted by a single layered epithelium that contacts the basement membrane. In this context, basal progenitors divide with a planar orientation, i.e. with the spindle oriented in the plane of the epithelium, which gives rise to symmetric divisions with both cells remaining in the plane of the epithelia. This type of division is linked with tissue expansion during these early stages of development. Later on, as the epidermis becomes multilayered, the progenitors switch to an asymmetric mode of division giving rise to cells with distinct fates and position (basal proliferative and suprabasal committed cells) which is essential for skin stratification (Lechler and Fuchs, 2005; Williams et al., 2011). Here, the switch from a symmetric to an asymmetric mode of cell division coincides with a switch in spindle orientation from planar to apico-basal orientation. Somehow similarly to the *Drosophila* neuroblast model, the spindle orientation machinery is recruited specifically to the apical domain which allows apico-basal spindle orientation (Lechler and Fuchs, 2005) (Fig. 3). Likewise, mInsc, a distant homologue of Insc makes the link between the apical polarity marker Par3 and LGN as they form a complex *in vivo* (Lechler and Fuchs, 2005).

Positioning one cell away from the basement membrane, known as a source of growth factors and extracellular matrix signaling would account for the differential cell fate (Lechler and Fuchs, 2005).

Importantly, knock-down of proteins regulating specifically spindle orientation results in divisions occurring mainly planarly, and impairs tissue differentiation and stratification (Fig.3). Hence, these data demonstrated that spindle orientation mediates asymmetric cell division and is essential for skin stratification in mice (Williams et al., 2011).

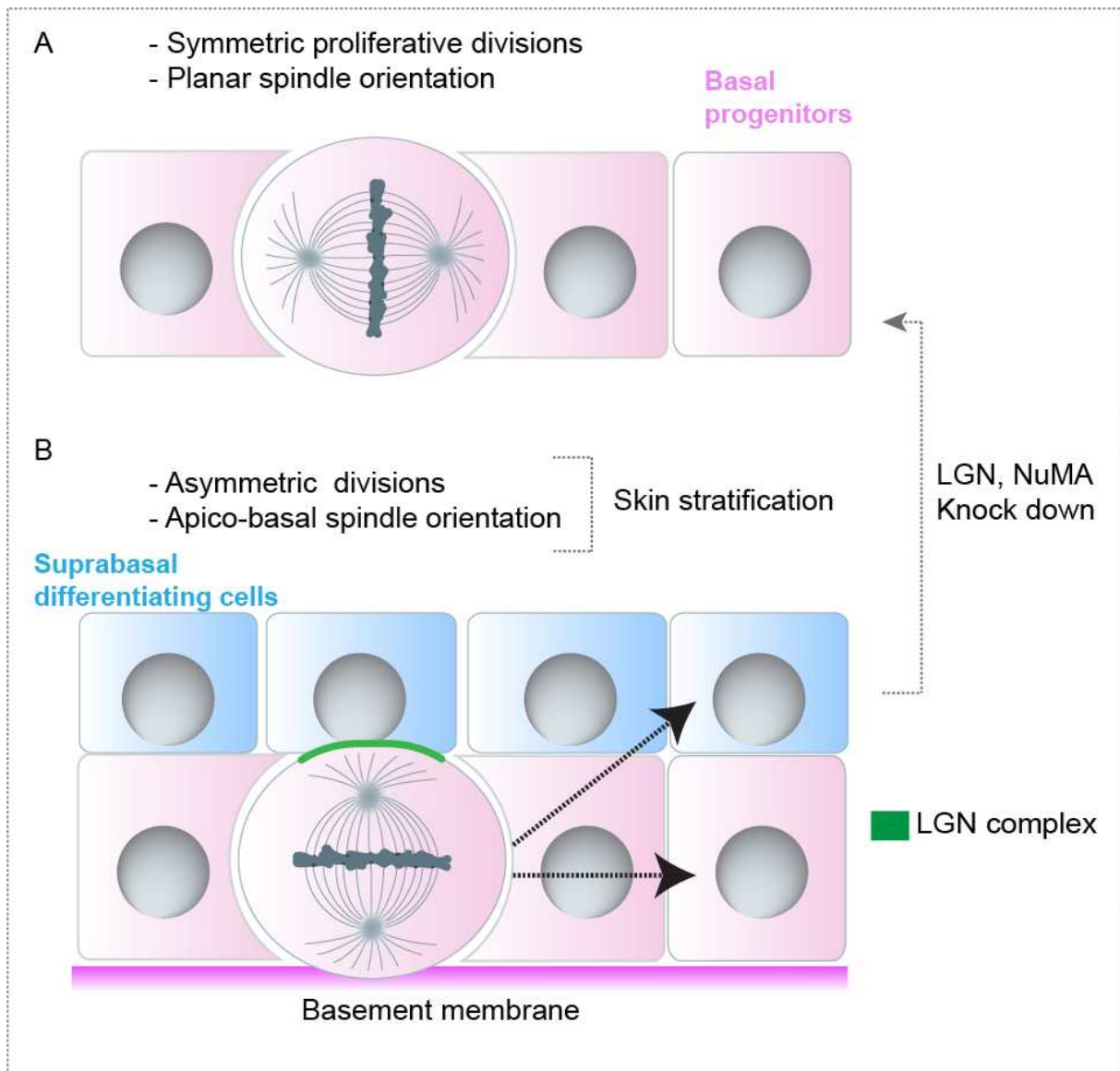


Figure 3: Mitotic spindle orientation is essential for asymmetric cell division and skin stratification during mouse embryogenesis.

1.1.3- VERTEBRATE NEURAL PROGENITORS

The vertebrate neuroepithelium is organized as a pseudostratified epithelial monolayer. Neuroepithelial progenitors are elongated cells. They have a small apical surface that faces the lumen of the neural tube, which is separated from the molecularly distinct basolateral domain by sub-apical junctions that are important for tissue cohesion and maintenance of polarity. The pseudostratified aspect of the tissue is a consequence of the so-called interkinetic nuclear movement, during which

the position of the nucleus varies along the apico-basal axis of the cell in relation to the cell cycle stage. In particular, the nucleus localizes to the apical surface when cells enter mitosis.

In a first stage, neuroepithelial cells divide symmetrically to amplify their pool. Later on in development, in particular at the onset of neurogenesis, they switch to an asymmetric mode of division which allows the production of a differentiating neuron or intermediate progenitor and the self-renewal of the progenitor (Fig.4) (Peyre and Morin, 2012). After the onset of neurogenesis, more committed and differentiated cells lose the apical attachment and start to accumulate basally in the “mantle zone”, whereas proliferative cells remain apically in the “ventricular” zone and retain the apico-basal organization.

By analogy with the asymmetric division of fly neuroblasts, it was proposed in the mid-nineties that cells dividing with a spindle oriented parallel to the apico-basal axis were undergoing asymmetric divisions, whereas cells dividing symmetrically would maintain a planar spindle orientation (Chenn and McConnell, 1995). However, careful analysis of the orientation of cell divisions showed that apical progenitors mainly divide with a planar spindle orientation even at the peak of neurogenesis (Kosodo et al., 2004; Noctor et al., 2008). This is difficult to reconcile with the idea that spindle orientation is a driver for asymmetric cell division in this context.

It was therefore proposed that small angle variations from the planar orientation (and thus from a vertical cleavage plane) would be enough for one of the daughter cells to bypass the small apical domain. The differential inheritance of the apical domain which may contain cell fate determinants would then result in different cell fates (Fig. 4) (Huttner and Brand, 1997). Indeed, while both daughters retain apical attachment, differential inheritance of the domain containing the apical polarity proteins has been shown to correlate with markers of binary cell fate decision in mouse cortical progenitors (Kosodo et al., 2004; Marthiens and French-Constant, 2009).

In support of this model, a number of loss of function studies have shown a correlation between defects in spindle orientation (resulting in an increase in the frequency of “oblique” and “vertical”

divisions”) with accelerated neurogenesis (e.g. (Feng and Walsh, 2004; Fish et al., 2006; Godin et al., 2010; Lizarraga et al., 2010). Similarly, overexpression of *Inscuteable* in the chick neural tube or mouse neocortex increases the number of vertical divisions and simultaneously accelerates neurogenesis through an increase of asymmetric (neurogenic) divisions (Das and Storey, 2012; Postiglione et al., 2011).

In line with this model, some authors have proposed that some forms of microcephaly may be a consequence of defective spindle orientation. Primary microcephaly is an autosomal recessive disorder in which patients show small brains. Smaller brains are thought to arise from a defect in the number of neurons due to early exhaustion of the progenitor pool by uncontrolled and premature occurrence of asymmetric divisions. Indeed, most genes associated with primary Microcephaly (MCPH) in humans have been involved to various extent with the regulation of spindle orientation in different experimental systems (Fish et al., 2006; Gruber et al., 2011; Kitagawa et al., 2011; Lizarraga et al., 2010), lending some credit to the hypothesis. However, MCPH1-9 genes are also involved in multiple cellular processes, making difficult to assign a role to spindle orientation in microcephaly. Of note, all MCPH genes code for centrosomal proteins and their depletion often results in defective centriole duplication or centrosome maturation (Noatynska et al., 2012; Thornton and Woods, 2009). Therefore, it is possible that multiple processes linked to centrosome function and the cell cycle contribute to generate microcephaly (Arquint and Nigg, 2014; Marthiens et al., 2013), and that the defects in spindle orientation are only a minor aspect of the phenotype.

Indeed, knocking-down LGN (which normally localizes at the lateral cortex directing planar spindle orientation) in the chick spinal cord and in the mouse cortex also resulted in randomized spindle orientation, but contrary to the models prediction, this did not significantly affect the rate of neurogenesis. Instead, this resulted in the production of ectopic progenitors in the mantle zone (Fig.4) (Konno et al., 2008; Morin et al., 2007). This suggested that oblique or vertical spindle orientations are not sufficient to induce neurogenic divisions. In the same line, both symmetric

proliferative and asymmetric neurogenic divisions were shown to be associated with variable angles of division in the chick spinal cord, with no statistical difference between the two groups (Wilcock et al., 2007). Moreover, in rat cortical slice cultures apical progenitors divide symmetrically or asymmetrically independently of the cleavage plane but depending on the developmental stage (Noctor et al., 2008).

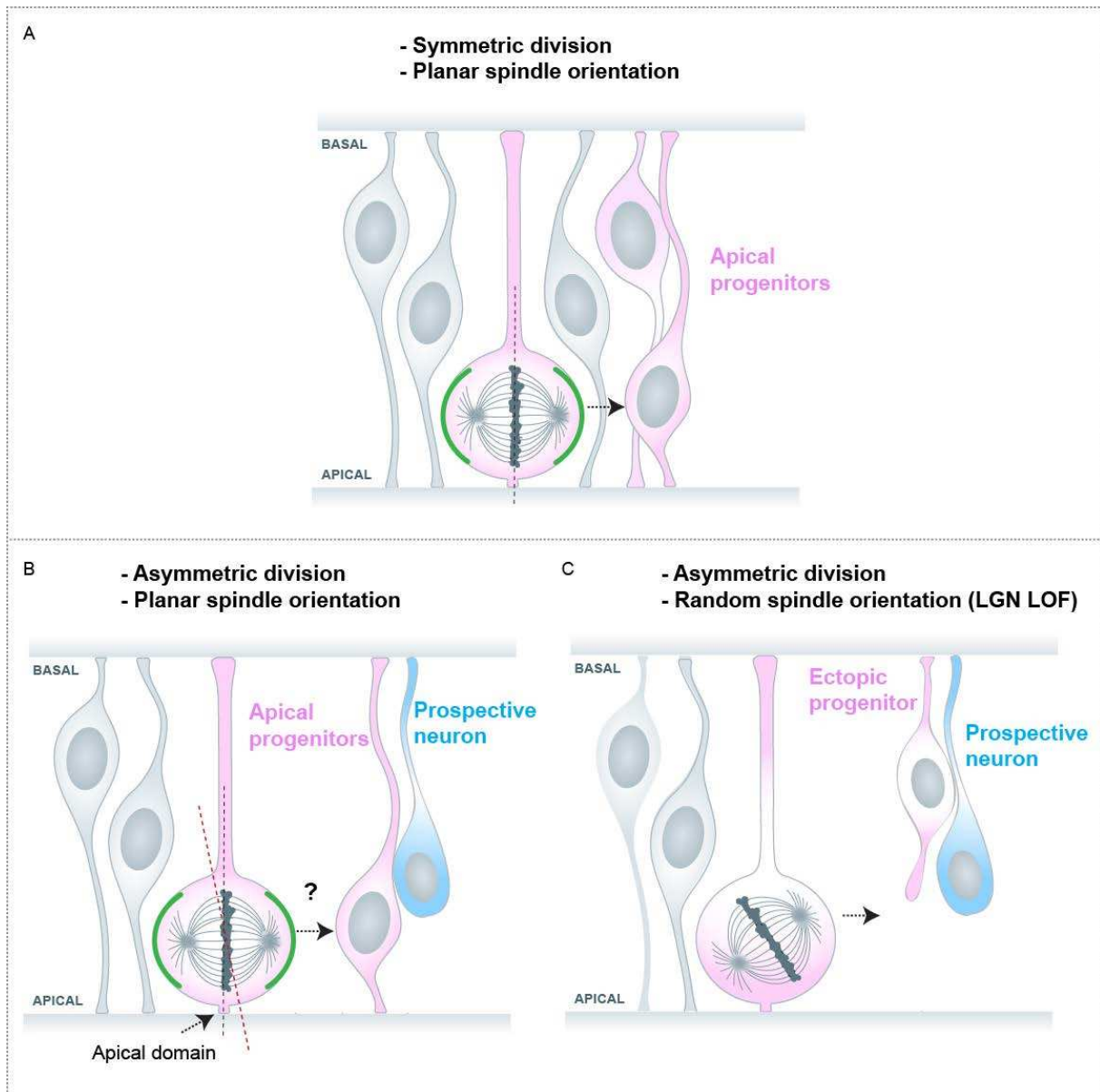


Figure 4: Mitotic spindle orientation in the vertebrate neuroepithelium. a) Apical progenitors divide symmetrically to expand their pool during the proliferative phase. b) During the neurogenic stage they switch to an asymmetric mode of division. The spindle orient mostly planarly during both phases. Subtle deviations are proposed to be sufficient to bypass the apical domain (see the red line indicating an oblique cleavage plane). However, randomization of spindle orientation by LGN loss of function does not impact the rate of neurogenesis but results in ectopic progenitors (c).

Overall, the role of spindle orientation in determining asymmetric cell division of apical progenitors and neurogenesis is controversial in vertebrates.

Alternatively, different mechanisms that allow generating asymmetric fates independently on spindle orientation have been proposed. In particular, Paridaen and colleagues have shown that the differential inheritance of cilia remnants associated with the mitotic centrosome contributes to generate distinct cell fates (Paridaen et al., 2013). Along the same line, Wang and colleagues also proposed that the intrinsic asymmetry of the mitotic spindle (due to the different maturation of spindle poles) contributes to the generation of different fates upon division of neural progenitors (Wang et al., 2009).

Finally, a more established role of spindle orientation in the neuroepithelium is to maintain the progenitors in the ventricular zone. Indeed, randomization of spindle orientation by depletion of LGN generates ectopic progenitors that overproliferate in the subventricular zone (Morin et al., 2007). This highlights the importance of understanding how spindle orientation is achieved in the neuroepithelium independently of its unclear role in neurogenesis.

1.2. MORPHOGENETIC PROCESSES

Different cellular processes are proposed to drive the shaping of organs during embryogenesis. Both oriented cell divisions and cell arrangements are predicted to contribute to this process. In principle, cell division orientation along the axis of tissue elongation would contribute to the process of elongation as in this case daughter cells are positioned along the elongation axis. Indeed, orientation of cell division along the elongation axis has been observed in several contexts (reviewed in Gillies and Cabernard, 2011). However, this does not prove a role for spindle orientation in tissue morphogenesis. Of note, higher tension in the direction of tissue elongation could affect the orientation of cell divisions and not the opposite (Campinho et al., 2013). Nevertheless, different studies have demonstrated a role for spindle orientation in different morphogenetic processes. In particular, stereotypic cell division orientations have been observed in the *Drosophila* wing and eye

discs. In the wing blade, division occurs mainly along the proximal/distal axis which coincides with the axis of preferential tissue growth (Fig. 5a). Mutation of Dachsoos or Dachs (components of the Fat-Ds PCP pathway) resulted both in cell divisions orienting randomly and a defective wing shape, which suggests a contribution of division orientation to the shaping of organs in *Drosophila* (Baena-Lopez et al., 2005; Mao et al., 2011). Remarkably, repolarization of Dachs perpendicularly to the proximal/distal axis along which it is normally polarized is sufficient to drive division orientation and tissue growth perpendicularly to the proximal distal axis (Mao et al., 2011).

Cell divisions are also oriented along the axis of kidney tubule elongation in mice. Consistently, loss of function of Fat4 generates cell division misorientation and defective tubule elongation in mouse kidney (Fischer et al., 2006).

In addition, cell division is oriented along the antero-posterior axis in the posterior region of the *Drosophila* germband, during the fast elongation phase of this tissue which occurs along the antero-posterior axis (Fig. 5b) Notably, in mutants where cell division is inhibited the elongation of the germband is compromised (da Silva and Vincent, 2007).

Moreover, during Zebrafish gastrulation, cell divisions are oriented along the animal-vegetal axis in the dorsal epiblast, which matches the axis of tissue elongation (Gong et al., 2004). Importantly, loss of function of Dsh –a molecule involved in spindle orientation in different systems- results in random spindle orientation and defective convergence and tissue extension in the Zebrafish gastrula. Of note, contribution of spindle orientation to tissue elongation is significant but only partial, suggesting that other processes such as cell intercalation are involved in tissue elongation in this context (Gong et al., 2004). However, later studies showed that when spindle orientation is perturbed by injecting blocking antibodies against the force generator dynein, this does not result in defects in body axis elongation, contradicting the idea that spindle orientation is involved in tissue elongation during Zebrafish gastrulation (Quesada-Hernandez et al., 2010).

Furthermore, cell division orientation is essential for neural tube morphogenesis in Zebrafish (Zigman et al., 2011). The immature epithelium of the Zebrafish neural keel develops into a lumenized neural tube. During the neural keel and rod stage, apical neuroepithelial cell divisions occur with an apico-basal orientation and give rise to two bilaterally distributed progenitors (Fig. 5c) (Geldmacher-Voss et al., 2003; Tawk et al., 2007). Remarkably, induction of spindle misorientation by depletion of Scribble in the neural keel generates drastic defects in morphogenesis, in particular a misaligned configuration of the apical surfaces laying the neural tube lumen in contrast to the straight wild type organization. Of note, these effects occur without problems in the apical domain organization, which suggests that the morphogenetic defects are generated by misoriented cell divisions (Zigman, Trinh et al. 2011). In the same line, oriented cell divisions are required for midline formation in the neural rod, a later stage of neurulation (Quesada-Hernandez, Caneparo et al. 2010).

In conclusion, the orientation of cell division contributes to several morphogenetic processes. However, in some tissues, there is only a correlative link between these processes. Noteworthy, perturbing certain signaling pathways may alter several cellular processes in addition to cell division orientation, probably explaining the different results obtained with respect to tissue elongation in Zebrafish (Gong et al., 2004; Quesada-Hernandez et al., 2010). Thus, careful analysis of tissue organization and different cellular processes is critical for understanding the actual contribution of spindle orientation to tissue morphogenesis.

Finally, in addition to participate in the shaping of tissues and organs, spindle orientation along the plane of epithelia is essential to maintain the two daughter cells in the epithelia both during growth and homeostasis (Macara et al., 2014; Zheng et al., 2010). Thus, defective planar spindle orientation could lead to epithelial architecture disruption as discussed below.

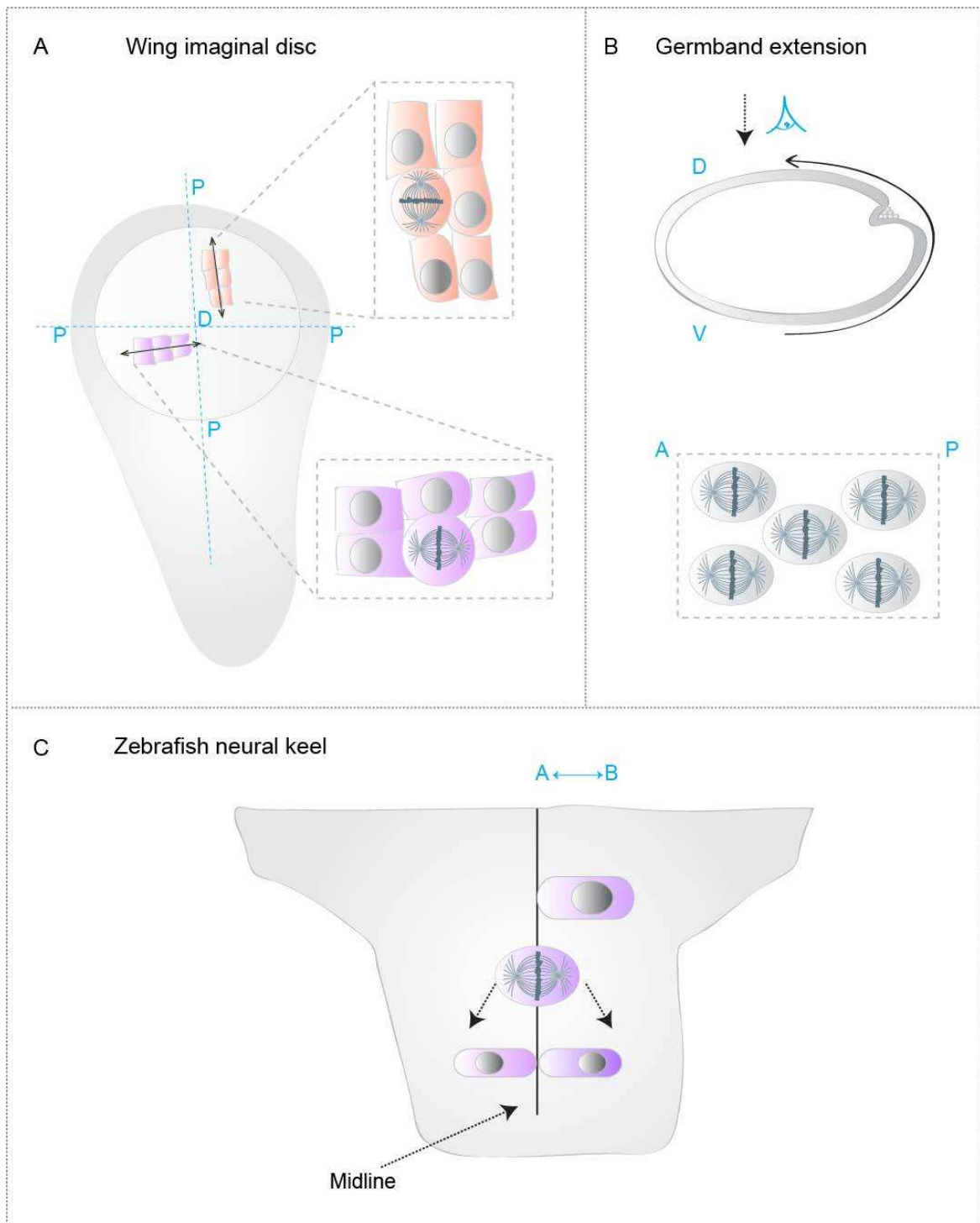


Figure 5: Mitotic spindle orientation in morphogenetic processes. a) Oriented divisions along the proximo-distal axis are important for directional tissue growth in *Drosophila* wing discs. The arrows indicate the direction of growth. b) Spindle orientation along the antero-posterior axis contributes to *Drosophila* germband extension. c) Apico-basal spindle orientation is critical for correct midline organization during neural tube formation in Zebrafish.

1.3-TUMORIGENESIS

Different observations have led to the idea that spindle orientation could be at least a contributor factor to tumorigenesis. First, misoriented spindles are seen in many tumors (Fleming et al., 2009). Second, tumor suppressors often mutated in cancer have been seen to regulate spindle orientation. This is the case of the tumor suppressors APC, E-cadherin and VHL (Pease and Tirnauer, 2011). Here I discuss two possible mechanisms by which spindle misorientation could contribute to tumor development as well as some evidence supporting these mechanisms.

1.3.1- DEREGLATION OF STEM CELLS COMPARTMENTS

Stem cells can divide both symmetrically and asymmetrically at least in some contexts. Asymmetric stem cell division is considered as critical to maintain the size of stem cell compartments by producing one stem cell and one differentiating cell. Notably, many cancers are proposed to arise from a deregulation of the stem cell compartment. Because spindle orientation is one of the mechanisms involved in determining the occurrence of asymmetric vs symmetric divisions, spindle orientation could then control the size of stem cell compartments and therefore its deregulation could contribute to tumorigenesis. The strongest evidence for this hypothesis comes from work in *Drosophila* neuroblasts (Causinus and Gonzalez, 2005). In particular, mutation of genes regulating spindle orientation and asymmetric cell division (namely Pins, Numb, Prospero and Miranda) result in hyperproliferation of larval neuroblasts transplanted in adult tissue and generation of highly proliferating invading tumors. In line with this, loss of the cell fate determinant Brat, which is considered as a self-renewal repressor, leads to a massive increase in the number of larval neuroblasts *in situ* (Betschinger et al., 2006; Lee et al., 2006).

In vertebrates, the potential link between control of asymmetric cell division and cancer has been investigated in the mouse and human gut epithelia (Quyn et al., 2010). Quyn and colleagues found that spindles are preferentially oriented perpendicularly to the apical surface specifically in the stem cell compartment. In mice gut, this orientation correlates with the asymmetric inheritance of DNA

strands which is considered as a feature of asymmetric cell division based on studies in muscle cells (Rocheteau et al., 2012). Notably, in precancerous tissue generated by heterozygous loss of the tumor suppressor APC, spindle orientation and asymmetric DNA segregation are defective. While these data do not prove a specific contribution of spindle orientation to cancer, this suggests that APC mutation could contribute to tumor formation by deregulating spindle orientation and asymmetric cell division.

1.3.2- EPITHELIAL DISRUPTION

Epithelial tumors constitute the majority of human cancers (Pease and Tirnauer, 2011). In epithelia, cells normally divide with a planar orientation allowing to maintain both cells in the plane of the tissue (Fig. 6a). In contrast, loss of planar spindle orientation can result in positioning one daughter cell on top of the other leading to disrupted epithelial tissue architecture (Fig. 6b). The cell positioned away from the extracellular matrix could follow different destinies. First, this cell could die as a consequence of losing essential signals and attachment; however apoptotic mechanisms are often perturbed in cancers. Thus, a second possibility is that the cell remains in the tissue leading to vertical tissue expansion and hyperplasia, which are premalignant features (Fig. 6c). Alternatively, if the cell detaches from the tissue, this could lead to dissemination and metastasis (Pease and Tirnauer, 2011).

Interestingly, recent work performed in the *Drosophila* wing disc epithelia, in which cell divisions occur preferentially in the plane of the epithelium, has brought support to these ideas. In this tissue, Nakajima and colleagues have shown that defective spindle orientation generated by mutation of different genes including *mud* correlates with basal cell delamination. Remarkably, while the delaminated cells normally die by apoptosis, blocking apoptosis in this context led to the formation of basal tumor-like masses with characteristics of epithelial-mesenchymal transition (Fig. 6b-c) (Nakajima et al., 2013). Whether spindle misorientation combined with apoptosis inhibition lead to epithelial disruption and tumor formation in vertebrate epithelia remains to be elucidated.

Noteworthy, the cell behavior observed by Nakajima et al in the wing disk does not apply to all fly epithelia, and Bergstralh and colleagues have shown that abnormally positioned cells generated by apico-basal orientation in different tissues (namely the follicular epithelium, the embryonic ectoderm and the neuroepithelium) reintegrate into the tissue rather than undergoing apoptosis (Fig. 6c) (Bergstralh et al., 2015). Hence different epithelial structures cope differently with defective spindle orientation, and may have different susceptibility to daughter cells mispositioning and tumor formation.

In conclusion, spindle misorientation leads to tissue overgrowth and tumor formation in specific *Drosophila* tissues and both mechanisms proposed here have somehow found support in this organism. However, clear evidence for a specific role of spindle misorientation in contributing to tumorigenesis or tumor development is lacking in mammalian organisms. In this sense, targeting pathways specifically involved in spindle orientation without perturbing tissue polarity could help to define the potential contribution of spindle orientation to mammalian tumors.

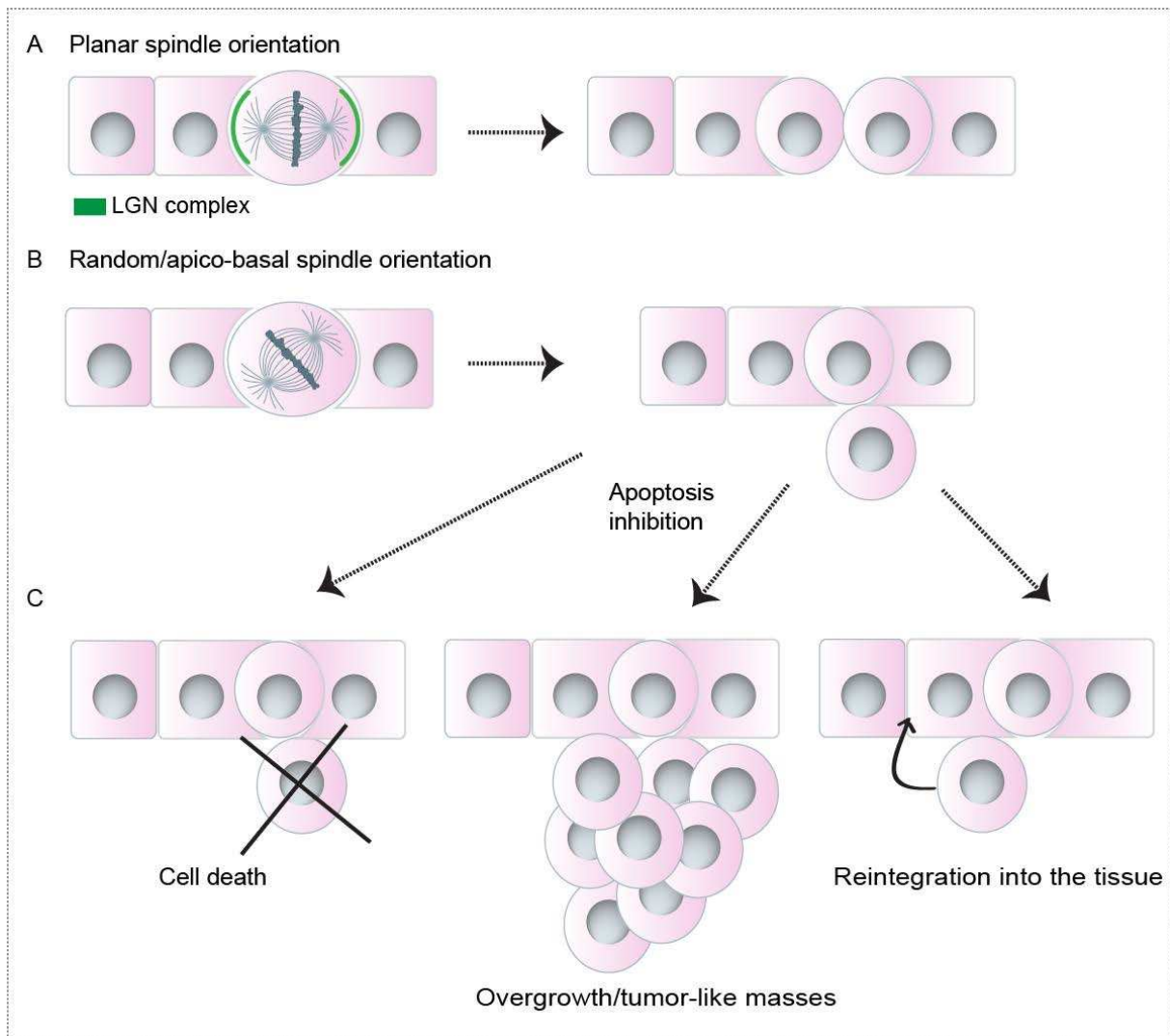


Figure 6: Role of spindle orientation in epithelial architecture maintenance and potential role in tumorigenesis. a) Planar spindle orientation maintains both daughter cells in the epithelia. b) Random or apico-basal spindle orientation leads to mispositioning of one cell out of epithelia. c) Different outcomes are possible: cell death, overproliferation and tumor-like formation or reintegration of the cell into the epithelial layer.

1.4. CONCLUSION

Mitotic spindle orientation is critical for diverse developmental processes in several organisms. In invertebrates and more specifically in *Drosophila*, spindle orientation is clearly involved in binary cell fate choices and morphogenesis and spindle misorientation can lead to tissue overgrowth. While I discussed only a few examples, it should be noted that in invertebrates we find other classical models in which spindle orientation is critical for asymmetric division. These include the asymmetric cell division of the *C.elegans* zygote and of *Drosophila* Sensory Organ Precursors, which will be further discussed in the frame of the mechanisms of spindle orientation in the next chapters. In

vertebrates, spindle orientation is linked to the morphogenesis of at least some tissues while its role in asymmetric cell division is only well defined in tissues such as the skin. The relatively better understanding of the role of oriented divisions in *Drosophila* development is partially justified by a more refined understanding of the molecular mechanisms controlling spindle orientation in this organism. That said, efforts to dissect the molecular mechanisms of vertebrate spindle orientation could be useful for a better comprehension of the function of this cellular process in normal development and disease in higher vertebrates. Notably, to understand the specific contribution of spindle orientation to development and disease, one challenge is to target spindle orientation without affecting cell polarity, centrosome function and tissue architecture. Many of the genes mutated in Microcephaly and cancer have pleiotropic roles, thus complicating the understanding of the contribution of spindle orientation defects to disease in these mutants. Thus, finding molecules that regulate specifically spindle orientation could help to address these issues.

CHAPTER 2: MECHANISMS OF MITOTIC SPINDLE ORIENTATION

This chapter is highly based on the review that we have recently published: "Regulation of mitotic spindle orientation: an integrated view" Florencia di Pietro, Arnaud Echard, Xavier Morin. EMBO Reports, Aug. 2016. The figures are adapted from the review figures as well (di Pietro et al., 2016).

2.1. INTRODUCTION

The orientation of the mitotic spindle in animal cells can be influenced by geometric cues, internal cues and external cues. More than a century ago, Hertwig proposed that cells orient their spindles along the long axis of the cell, arguing for a role of cellular geometry in controlling the plane of division (Hertwig, 1884). While this rule applies to many situations, orientation of the spindle is also often set by specific polarity cues. Early studies identified the evolutionary conserved Gai/LGN/NuMA complex as a key regulator that polarizes cortical force generators that exert pulling forces on astral MT to orient the spindle. Indeed, in most animal cell types oriented cell divisions involve the transmission of localized pulling forces located at the cell cortex to astral microtubules, resulting in the positioning the mitotic spindle. As a consequence, the cell cortex, the specific mechanisms that recruit and localize force generators, and the astral microtubule network have emerged as the three essential levels of regulation for spindle orientation.

An excellent model that contributed to the establishment of spindle orientation principles is the *C.elegans* zygote. The *C. elegans* zygote divides asymmetrically with regard to both cell size and fate, and spindle displacement towards to posterior cortex is necessary for this process. Remarkably, elegant studies performed in this embryo have demonstrated that the polarization of force generators on the posterior cortex results in the exertion of higher forces on the spindle pole closest to that cortex (Grill et al., 2001; Grill et al., 2003). In particular, Grill and colleagues used laser ablation to sever spindle poles and considered the velocity of displacement of centrosome fragments as a measure of the force previously exerted on that pole (Grill et al., 2003). With this approach, they found that the posterior pole fragments showed higher velocities than the anterior ones which is linked with the recruitment of more force generators to the posterior cortex.

In this chapter I will discuss spindle orientation mechanisms in detail. In particular, I will present the main characteristics of the LGN complex as well as recent data that shed light on how the cortical recruitment and dynamics of this complex are regulated in mitosis. Then, I will discuss a host of data illustrating how modulation of the actin cytoskeleton and astral MT control spindle orientation in different contexts. Finally, I will focus on the regulation of spindle orientation by geometric cues and external forces. The role of Dynein in spindle orientation will be separately discussed in Chapter 3. Of note, the present chapter makes emphasis in the regulation of spindle orientation mainly in *Drosophila* and vertebrate models. In the end I briefly discuss other models of spindle positioning that are relevant for the next chapter.

2.2- THE LGN COMPLEX

A number of genetic studies have revealed that an evolutionary conserved molecular complex composed of the heterotrimeric Gα protein Gαi, LGN and NuMA (respectively Gαi, Pins and Mud in *Drosophila*, and GOA1/GPA16, GPR1/2 and LIN5 in *C. elegans*, “the LGN complex for simplicity, Fig.7) is at the core of spindle orientation and positioning in different tissues both in invertebrate and vertebrate species (Du and Macara, 2004; Gotta and Ahringer, 2001; Gotta et al., 2003; Konno et al., 2008; Lechler and Fuchs, 2005; Morin et al., 2007; Peyre et al., 2011; Schaefer et al., 2001; Schaefer et al., 2000; Srinivasan et al., 2003; Yu et al., 2000) (reviewed in Morin and Bellaïche, 2011). During mitosis, this complex is localized to a particular subcortical domain and directs the recruitment of the minus end-directed microtubule motor dynein (Couwenbergs et al., 2007; Kotak et al., 2012; Nguyen-Ngoc et al., 2007) (Fig. 1a). The directed movement of cortically anchored dynein along astral microtubules generates pulling forces on spindle poles leading to the orientation and/or positioning of the spindle. Therefore, the specific localization of the LGN complex determines the site of force concentration and the axis of spindle orientation. Consistently, the apical localization of Pins/Mud or LGN/NuMA directs spindle orientation along the apico-basal axis in *Drosophila* neuroblasts (Fig. 7B) and mouse skin progenitors, respectively (Bowman et al., 2006; Izumi et al., 2006; Lechler and Fuchs, 2005; Siller et al., 2006; Williams et al., 2011; Yu et al., 2000).

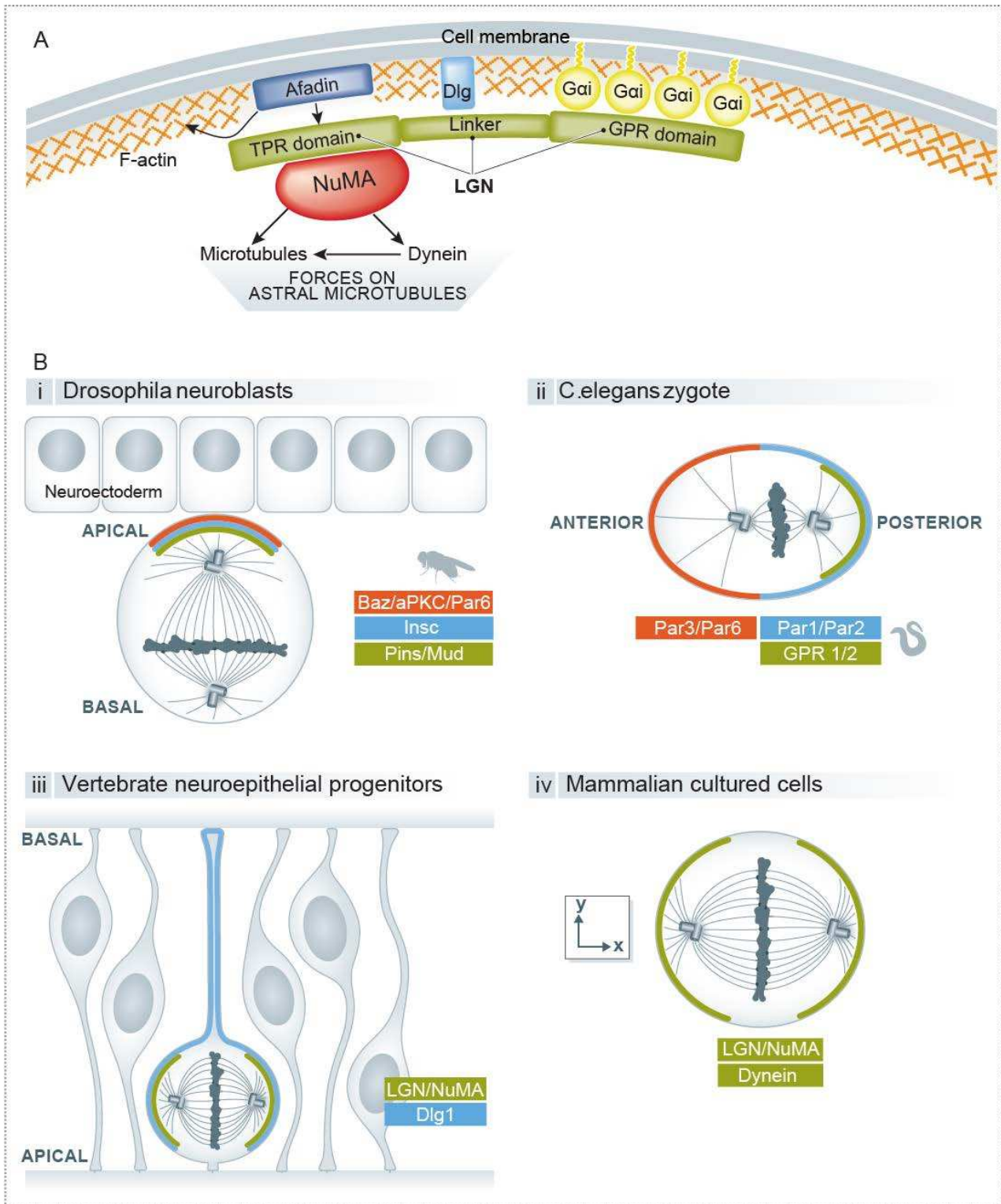


Figure 7: The LGN complex A) Schema showing the LGN domains and its interactions with Gai membrane anchored subunits, and with NuMA, as well as the interaction with cortical proteins (Dlg, Afadin) that regulate LGN cortical localization. B) LGN complex localization in different systems, showing the polarity proteins regulating this specific localization when applicable. i) *Drosophila* embryonic neuroblasts, ii) *C. elegans* zygote, iii) neural progenitors in the vertebrate neuroepithelium, iv) mammalian cell lines. Adapted from di Pietro et al. 2016.

In the *C. elegans* zygote, enrichment of GPR1/2 at the posterior cortex is necessary for spindle positioning along the antero-posterior axis (Gotta et al., 2003; Srinivasan et al., 2003) (Fig.7b).

Furthermore, the lateral localization of the LGN complex regulates planar spindle orientation of progenitors in chick and mouse neuroepithelium (Konno et al., 2008; Morin et al., 2007; Peyre et al., 2011) as well as during epithelial morphogenesis of *Drosophila* and mammalian cells (Bergstralh et al., 2013; Zheng et al., 2010) (Fig.7b).

Biochemical and structural analysis revealed the different components of the LGN complex which are briefly presented below:

G α i. G α i subunits localize to the plasma membrane through myristylation, where they serve as an anchor to the complex. By default, G α i subunits cover the whole cell inner surface, and do not contribute to the polarization of LGN and NuMA crescents.

LGN. LGN was first identified as a biochemical interactor of G α i subunits (Mochizuki et al., 1996). LGN is a modular protein composed of three main domains. Its N-terminal TPR domain contains 7 (6 or 8 depending on the authors) Tetratricopeptide repeats, which mediate interaction with multiple binding partners, including NuMA, Afadin and Inscuteable. Its central “linker” domain does not show any recognizable organization or binding motif, but is crucially required for its function through its interaction with Dlg (Fig. 7a). The C-terminal GPR (G Protein Regulator) domain contains four (3 in *Drosophila* Pins and 1 in *C. elegans* GPR1/2) Goloco domains that mediate interaction with G α i/o subunits. LGN interacts with G α i only when it is bound to GDP, and has a guanine dissociation inhibitory (GDI) activity (Willard et al., 2004).

The GTPase activating protein (GAP) RGS14/LoCo/RGS-7 (in vertebrates, *Drosophila* and *C. elegans*, respectively) and the Guanine exchange factor (GEF) Ric8a control the interaction between LGN and G α i, and therefore the stability of the complex, by modulating the GTPase activity of G α i subunits and thereby the phosphorylation state of bound guanosine (Afshar et al., 2004; Couwenbergs et al., 2004; David et al., 2005; Hampoelz et al., 2005; Hess et al., 2004; Wang et al., 2005; Woodard et al., 2010; Yu et al., 2005).

NuMA. NuMA is a coiled coil protein that can interact with LGN, dynein as well as with microtubules (Fig. 7a) (Bowman et al., 2006; Du et al., 2001; Haren and Merdes, 2002; Kotak et al., 2012; Merdes et al., 1996). NuMA is also present on the spindle, enriched near the poles, and regulates spindle formation and organisation.

In dividing cells, LGN and NuMA are usually observed as cortical crescents facing one or both spindle poles (Fig. 7b), and it is established that this specific cortical localization is instructive for spindle orientation in many systems.

Because G α i subunits localize all over the cortex, additional factors, and in particular polarity proteins, must regulate the polarized cortical distribution of LGN and NuMA. Indeed, the LGN homolog Pins (Partner of Inscuteable) was initially identified in *Drosophila* in interaction screens with Inscuteable (Schaefer et al., 2000; Yu et al., 2000), an apical protein known for its role in apico-basal spindle orientation in neuroblasts (Kraut et al., 1996). Apical localization of Insc, and consequently of Pins, requires the polarity protein Bazooka (*Drosophila* Par3) (Yu et al., 2000), as well as atypical protein kinase C (aPKC) (Izumi et al., 2004; Wodarz et al., 2000). Similarly, the posterior cortical enrichment of GPR1/2 requires the Par2 and Par3 polarity proteins during the first division of the *C. elegans* embryo (Gotta et al., 2003).

Later work has revealed a surprising diversity in the mechanisms that control LGN localization at restricted cortical domains. While Pins/LGN localizes apically in *Drosophila* neuroblasts, it is found in a ring at the lateral cortex during planar spindle orientation in different epithelial contexts (Bergstralh et al., 2013; Peyre et al., 2011; Zheng et al., 2010). Remarkably, while aPKC is required for the apical recruitment of Pins in neuroblasts (Izumi et al., 2004), it inhibits the apical localization of LGN and favours its lateral enrichment during cystogenesis in MDCK cells (Zheng et al., 2010), see section 2.3). The mechanism mediating this inhibition involves the phosphorylation of LGN by apical aPKC, which increases locally LGN affinity to a 14-3-3 protein, competing with the interaction of LGN

with G α i at the apical domain (Hao et al., 2010), and favouring the planar orientation of the spindle in these cells.

Additional mechanisms are discussed in section 2.4. In the next section I present cell culture models that have greatly contributed to the fine comprehension of LGN complex regulation.

2.3. MODELS FOR STUDYING SPINDLE ORIENTATION

The core components of spindle orientation have been discovered in invertebrate *in vivo* models of spindle orientation, which continue to be useful for dissecting new regulators and understanding the dynamics of this cellular process. In addition, an induced polarity assay has been developed in *Drosophila* S2 cells (Johnston et al., 2009). In this model, intracellular fusion to the transmembrane and extracellular domains of the Echinoid (Ed) homophilic cell–cell adhesion protein is used to localize a protein of choice to the contacts between clustered cells, in this way generating a polarized distribution in each cell. Polarized localization of Pins by using this trick results in spindle orientation in the direction of the Ed-Pins enrichment, constituting a model where the function of molecules in spindle orientation downstream of Pins can be evaluated (Fig.8i). Alternatively, by fusing proteins or protein domains to Echinoid, their ability to orient the spindle has been evaluated in different studies (Johnston et al., 2009; Johnston et al., 2013; Segalen et al., 2010; Wee et al., 2011).

In vertebrate systems, in addition to the *in vivo* models of spindle orientation (e.g. mouse skin progenitors, mouse and chick neuroepithelial cells, fish epiblast cells), *in vitro* cultured cells are frequently used to study the molecular details and dynamics of this cellular process. The most frequently used *in vitro* models are:

- MDCK cysts: a 3D model of epithelial morphogenesis. By culturing dog MDCK cells in matrigel, cysts with a central lumen and defined polarity domains are generated. In this context, spindle orientation occurs in the plane of the epithelium and depends on LGN which localizes to the lateral cell cortex (Fig.8i) (Zheng et al., 2010). Defective spindle orientation

commonly results in cysts with multiple lumina. The Caco-2 3D system is used in a similar manner (Jaffe et al., 2008).

- HeLa cells cultured on a fibronectin substrate: This human cell line has been shown to orient the mitotic spindle parallel to the substrate (Fig.8iii), which depends on astral microtubules (Toyoshima et al., 2007). While this is the most frequently used cell line, other cell types also show this orientation.

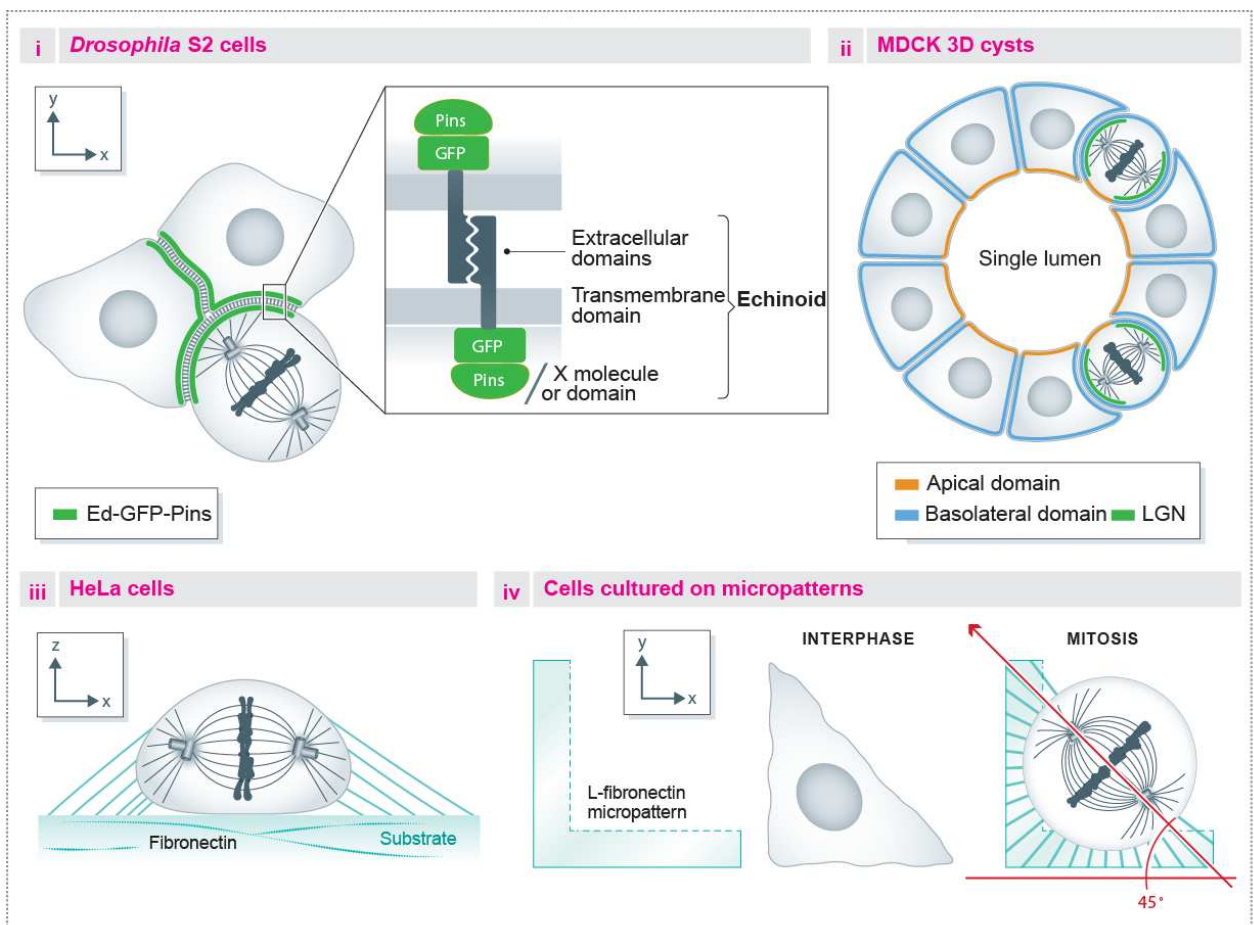


Figure 8: Models of spindle orientation in 2D or 3D cultured cells. i) Induced polarity assay in *Drosophila* S2 cells. ii) MDCK cysts, a model of epithelial morphogenesis and planar spindle orientation. iii) HeLa cells cultured on a fibronectin substrate align their spindle parallel to the growth surface. iv) Single cells cultured on fibronectin micropatterns align their spindle with respect to the geometry of the adhesion pattern.

- Cells cultured on micropatterns (HeLa cells, fibroblasts, MCF cells): In this model, single cells are cultured on micro surfaces of defined geometry, which dictates a specific shape and

adhesion pattern to the cells. The adhesion pattern can induce a specific spindle orientation in the xy-plane (Fig.8iv). This orientation is dependent on the distribution of actin retraction fibres as well as on astral microtubules (Fink et al., 2011; Machicoane et al., 2014; They et al., 2007; They et al., 2005).

It should be noted that knockdown of LGN or NuMA only results in partial loss of spindle orientation (i.e. angle distributions remain biased to the control angles) in these last two systems, suggesting that the involvement of the LGN complex is only marginal, and that it acts in combination with, or as a complement to, additional pathways. This point will be further discussed in chapter 5.

2.4. NEW INSIGHTS INTO THE MOLECULAR REGULATION OF LGN COMPLEX RECRUITMENT/STABILITY AT THE CORTEX

2.4.1. MOLECULES REGULATING THE RECRUITMENT /STABILITY OF THE LGN COMPLEX AT THE CORTEX

DISCS LARGE

In contrast to MDCK cysts, aPKC does not regulate the lateral localization of Pins/LGN in *Drosophila* follicular epithelia and chick embryonic neuroepithelium (Bergstralh et al., 2013; Peyre et al., 2011). This function relies at least in part on the polarity protein Discs-large (Dlg), known as a tumor suppressor in *Drosophila*. Dlg was previously shown to regulate spindle orientation in *Drosophila* larval sensory organ precursor (SOP) cells, where it regulates Pins localization to the anterior cell cortex (Bellaïche et al., 2001). In addition, Dlg is part of a non-essential microtubule-based pathway driving cortical localization of LGN, acting in parallel to the dominant Inscuteable recruitment pathway in neuroblasts (Siegrist and Doe, 2005) (reviewed in Morin and Bellaïche, 2011). While Dlg shows a polarized localization in SOP and NB, it presents baso-lateral localization in canonical epithelia. Recent studies have shown that depleting Dlg/Dlg1 results in defects in planar spindle orientation in *Drosophila* epithelia and in chick neuroepithelium (Bergstralh et al., 2013; Saadaoui et al., 2014). Quite remarkably, Dlg/Dlg1 acts differently in each of these tissues. In *Drosophila* follicular

epithelia, Pins becomes localized all around the cortex upon Dlg depletion, indicating that Dlg may act by restricting the Pins localization to the lateral cortex (Bergstralh et al., 2013). In contrast, in the chick neuroepithelium, LGN cortical loss upon Dlg1 depletion suggests that Dlg acts to recruit/stabilize LGN at the cortex in this context (Saadaoui et al., 2014). Similarly, DLG1 depletion in human HeLa cells reduces LGN-NuMA cortical localization in association with defects in micropattern guided-spindle orientation (see section 2.3, (Saadaoui et al., 2014). Direct interaction between Dlg/Dlg1 and Pins/LGN relies on the phosphorylation of a conserved Serine residue in the LGN linker domain (Johnston et al., 2012; Johnston et al., 2009; Sans et al., 2005; Zhu et al., 2011) (Fig.7a). In *Drosophila*, Pins phosphorylation by Aurora A (AurA) regulates the interaction between Dlg and Pins. In contrast, AurA activity would not be required for LGN-DLG1 interaction as LGN cortical recruitment in HeLa cells is not affected by AurA inhibition (Gallini et al., 2016).

Importantly, acute depletion of Dlg/Dlg1 does not generate obvious defects in tissue polarity in follicular epithelia or in the neuroepithelium, indicating that this protein plays a specific role in spindle orientation independent of its function in cell polarity (Bergstralh et al., 2013; Saadaoui et al., 2014).

AFADIN6

The scaffolding protein Canoe/AFADIN6 regulates LGN complex formation and spindle orientation. This role was initially described in *Drosophila* neuroblasts, where Canoe localizes to the apical cortex and regulates apical-basal spindle orientation (Speicher et al., 2008). The molecular details have been dissected in the S2 cell induced polarity assay (section 2.3) (Wee et al., 2011), where Canoe interacts with Pins and acts specifically in the spindle orientation pathway mediated by Pins^{TPR}/Mud (Johnston et al., 2009). In particular, Canoe is necessary for Mud recruitment to cortical Pins crescents through its interaction with the TPR domains (Speicher et al., 2008; Wee et al., 2011). Canoe interaction with Ran^{GTP} is also required for Mud recruitment and spindle orientation (Wee et al., 2011). The vertebrate homolog of Canoe, Afadin, also plays a role in spindle orientation in

adherent cells and in 3D cell cultures (section 2.3), albeit through a distinct mechanism: Afadin6 binds simultaneously cortical F-actin and the TPR region of LGN (Fig. 7a). Afadin6 interaction with LGN is in competition with the NuMA/LGN interaction, although the affinity for Afadin6 is lower. However, upon Afadin6 depletion, LGN cortical recruitment is reduced, and NuMA and dynein are not recruited (Carminati et al., 2016). As NuMA is nuclear in interphase and only released upon nuclear envelope breakdown, one possibility is that Afadin6 is necessary for the initial recruitment of LGN to the cortex and its interaction with G α i subunits in early mitosis, before LGN interacts with and recruits NuMA at the cell cortex.

More generally, the interplay between G α i, Afadin6 and Dlg1 in LGN cortical localization is not well understood. G α i appears as an obligate membrane anchor, since LGN is completely absent from the cortex when the G α i/LGN interaction is disrupted; in contrast LGN cortical levels are only reduced in the absence of Afadin6 and Dlg1 (Carminati et al., 2016; Saadaoui et al., 2014). Whether Afadin6 and Dlg1 are important for the initial recruitment of LGN by G α i, or whether they are involved in maintaining LGN at the cortex, remains unclear. In addition, Dlg1 is involved in the polarization of LGN cortical localization at least in *Drosophila* epithelia.

HUNTINGTIN

A series of recent investigations have focused on the role of Huntingtin (HTT) in spindle orientation. This protein, mutated in Huntington's disease, regulates spindle orientation in mouse neural progenitors and basal mammary cells *in vivo*, as well as in *Drosophila* neuroblasts (Elias et al., 2014; Godin et al., 2010). The mechanisms of action of HTT have been further evaluated in cultured mammalian cells, where it regulates spindle orientation with respect to the substrate (section 2.3) (Elias et al., 2014). HTT depletion leads to a decrease in the cortical levels of LGN, NuMA, and members of the dynactin/ dynein complex. Contrary to the LGN interactors Afadin6 and Dlg1, HTT localizes to spindle poles during mitosis. Because HTT plays a role in anterograde vesicular transport

in neurons, the proposed hypothesis is that HTT regulates the transport of LGN and dynein complex members via astral MTs from the spindle poles to the cortex. Accordingly, this transport depends on the plus-end directed motor kinesin 1 (Elias et al., 2014).

PHOSPHORYLATION OF MUD AND NUMA

Two recent reports identified the serine phosphorylation of Mud and NuMA as necessary for their cortical localization. In *Drosophila*, phosphorylation of a serine residue in the coiled-coil domain of Mud by the Hippo pathway kinase Warts induces a conformation change that uncovers the Pins binding domain and allows interaction with cortical Pins (Dewey et al., 2015). On the other side, phosphorylation of a distinct Serine residue in another domain of NuMA by the mitotic kinase AurA is necessary for NuMA cortical recruitment in human cells (Gallini et al., 2016). While the two mechanisms are different, it is remarkable that both Warts and AurA kinases localize to spindle poles, suggesting that they act there to promote the release of phosphorylated Mud/NuMA from the spindle pole and thereby allow its interaction with cortical Pins/LGN. Accordingly, upon pharmacological inhibition or knockdown of AurA, NuMA is lost from the cortex and its concentration increases at the spindle poles (Gallini et al., 2016; Kotak et al., 2016). Of note, phosphorylation on a NuMA threonine residue differentially affects NuMA cortical recruitment as I will discuss below. Finally, the *C.elegans* AIR-1 AurA kinase, while not essential, is also involved in spindle positioning in the one cell embryos. However, in this context, it seems to act in a different manner, as inhibiting AIR-1 resulted in exaggerated spindle oscillations, which is in principle not compatible with reduced cortical levels of LIN-5 (Kotak et al., 2016).

2.4.2. TEMPORAL AND SPATIAL REGULATION OF LGN COMPLEX LOCALIZATION

In specific cell types, the centrosome maintains its position during all the cell cycle and the spindle forms directly with its correct orientation (Rebollo et al., 2009; Yamashita et al., 2003b). However, in many cases, the spindle forms in prometaphase with a random orientation, and the final axis of division observed at anaphase is set through spindle rotation during prometaphase and metaphase

(Peyre et al., 2011). The switch from interphase to mitosis, and mitotic progression itself, are accompanied by the sequential activation of numerous signaling pathways and major changes in the organization of cellular structures. This section highlights a number of recent studies that describe the dynamics and molecular regulation of the LGN complex sub-cellular recruitment in relationship to mitotic progression (Fig.9).

TEMPORAL REGULATION OF THE LGN COMPLEX FORMATION IN EARLY MITOSIS

In the last few years, different labs have studied the temporal and spatial aspects of LGN/dynein complexes formation by mainly using mammalian cell lines. In HeLa cells, LGN protein levels increase during mitosis (Du and Macara, 2004), which contributes to restrict LGN complex formation only in mitosis, but the molecular regulation of this increase is unknown. In addition, Du and Macara have also demonstrated that during interphase, LGN exists in a closed conformation and because it interacts poorly with Gai in this state, it does not localize to the cortex. They proposed that interaction with NuMA is necessary to switch LGN to an open conformation that increases its ability to bind Gai subunits. Because NuMA localizes to the nucleus during interphase, the formation of the Gai/LGN/NuMA cortical complex would then be further restricted to mitosis in vertebrate cells (Du and Macara, 2004) (Fig. 9). However, whether NuMA is required for LGN cortical recruitment is unclear: knockdown of the NuMA homolog lin-5 in *C. elegans* embryos results in the loss of cortical GPR1/2 (LGN) (Srinivasan et al., 2003), whereas knockdown of NuMA in the chick neuroepithelium does not prevent LGN cortical localization (Peyre et al., 2011). Besides, upon AurA inhibition NuMA is lost from the cortex, but not LGN (Gallini et al., 2016). In contrast to vertebrate cells, *Drosophila* Mud is not nuclear and shows cortical localization during interphase in neuroblasts and the overlying neuroectoderm (Bowman et al., 2006; Yu et al., 2000). This may explain why Pins shows also cortical patterns in interphase in these cells. Similarly, LIN5 in *C. elegans* is not a nuclear protein.

SPATIAL REGULATION OF LGN LOCALIZATION IN EARLY MITOSIS

The subcellular localization of the LGN complex is very dynamic throughout mitosis (Fig.9). Using HeLa cells that stably express GFP-LGN cultured on fibronectin, Kiyomitsu and Cheeseman showed that LGN is initially recruited all around the cell cortex during prometaphase but its localization is later restricted to two cortical crescents facing the spindle poles during metaphase and anaphase (Kiyomitsu and Cheeseman, 2012). Using different drugs that affect spindle organization and chromosome alignment, they observed that an abnormal proximity of chromosomes with the cortex inhibited LGN and NuMA cortical localization, and concluded that chromosome derived signals normally exclude LGN-NuMA from cortical sites in proximity to the chromosomal plate. Using a Ran^{T24N} dominant-negative mutant to disrupt the Ran^{GTP} chromosomal gradient, they went on to show that this gradient is responsible for LGN cortical exclusion (Kiyomitsu and Cheeseman, 2012). Therefore, the spatio-temporal restriction of LGN complex localization during mitosis is proposed to rely on a gradient of Ran^{GTP} that inhibits the formation of the complex in the vicinity of chromosomes. Once the metaphase plate is formed, LGN and NuMA are excluded from this location and appear enriched as two cortical crescents overlying each spindle pole (Fig. 9). Therefore, in this model the localization of the complex is established once spindle orientation is set. This is in marked contrast to models in which the orientation is constrained by polarized molecular cues, such as the asymmetric division of fly neuroblasts. Interestingly, when HeLa cells are cultured on polarized micropatterns (see section 2.3), the asymmetric distribution of retraction fibers imposes such a constraint, and both LGN and dynein complexes show a restricted cortical localization before the spindle is oriented along the correct axis (Machicoane et al., 2014; Tame et al., 2014).

In mitotic HeLa cells, the cortical distribution of dynactin-dynein complexes is dynamic during metaphase. Live imaging revealed redistribution of a polarized crescent that alternates between the cortical domains that face each spindle pole (Kiyomitsu and Cheeseman, 2012). Remarkably, these oscillations are independent of the distribution of LGN and NuMA, which remain localized in two cortical crescents (Fig.9). They are followed by an asymmetric positioning of the spindle, whose poles

are alternatively attracted to the dynein enriched cortical domains. Here, the kinase Plk1, localized at the spindle poles, negatively controls the cortical localization of dynein/dynactin. The proximity of a spindle pole to the cortex excludes dynein from this cortical site. Concomitantly, dynein/dynactin accumulates to the side of the cell facing the opposing (and more distant) spindle pole and generates pulling forces which in turn will reposition the spindle (Kiyomitsu and Cheeseman, 2012). Cortical targeting of dynein/dynactin during this oscillatory phase depends on astral microtubules (Tame et al., 2014).

A SPECIFIC SPATIO-TEMPORAL REGULATION IN ANAPHASE

More recently, different labs have described changes in the cortical recruitment of NuMA between metaphase and anaphase (Kiyomitsu and Cheeseman, 2013; Kotak et al., 2013, 2014). In contrast to LGN levels, cortical levels of NuMA increase from metaphase to anaphase. These changes are related to its phosphorylation state at T2055, which is regulated by the balance between the activities of the CDK1 kinase and the PP2CA phosphatase. During metaphase, phosphorylated NuMA is observed at spindle poles, while the cortical protein would correspond to non-phosphorylated NuMA. At anaphase onset, the decrease in CDK1 activity results in an increase in non-phosphorylated NuMA, which allows further enrichment of this protein at the cortex (Fig. 9). Accordingly, altering NuMA phosphorylation states results in defects in spindle orientation with respect to the substrate (Kotak and Gonczy, 2014).

In contrast to metaphase, an absence of LGN or G α i in anaphase does not result in complete loss of NuMA from the cortex. Besides, LGN cortical levels do not increase in anaphase, indicating that additional molecules contribute to NuMA localization after the metaphase/anaphase transition. Kiyomitsu and Cheeseman showed that cortical 4.1G and 4.1R proteins interact directly with non-phosphorylated NuMA in anaphase, providing a potential mechanism for this increase (Kiyomitsu and Cheeseman, 2013). However, whereas depletion of both LGN and 4.1 proteins completely deplete cortical NuMA in anaphase, depletion of 4.1 proteins alone had no effect (Kiyomitsu and

Cheeseman, 2013). Moreover, Kotak et al. found that a GFP-tagged version of NuMA lacking the interaction domain with 4.1 proteins shows the same localization and levels during metaphase and anaphase than wild-type GFP-NuMA (Kotak et al., 2014). As an alternative model, they proposed that an interaction between NuMA and the phosphoinositides PIP/PIP2 is involved in NuMA cortical recruitment in anaphase: using different approaches to perturb PIP2 levels, they show changes in the NuMA and dynein levels in anaphase. The authors found that this PIP2 mediated-recruitment pathway is anaphase specific. The dependence of the NuMA-PIP2 interaction on NuMA phosphorylation states remains to be elucidated (Fig.9). In the same study, Kotak and colleagues found that NuMA is excluded from the equatorial cortex by the centralspindlin proteins CYK4 and MKLP1 during anaphase (Fig.9) (Kotak et al., 2014), therefore maintaining the exclusion initiated in metaphase by the Ran-GTP signal. Increased cortical levels of NuMA in anaphase are important for spindle elongation and chromosome separation in human cultured cells (Kotak et al., 2013). However, whether this increase is also important for spindle orientation itself is not clear.

Altogether, these recent experiments in symmetrically dividing human cultured cells have revealed complex regulations of the dynamics of LGN, NuMA and dynein localization during mitosis by molecules located on chromosomes, centrosomes and at the cortex. Several questions remain. Firstly, are these pathways active and necessary to achieve oriented divisions *in vivo*? In the neuroepithelium, it is unlikely that the Ran-GTP mechanism is at play in metaphase. A continuous and homogenous ring of LGN/NuMA is observed at the lateral cortex, and the levels of LGN/NuMA are not lower in the vicinity of the metaphase plate, despite the very small cell size (Peyre et al., 2011). Secondly, how do they integrate with the instructive signals, such as polarized Inscuteable, that control spindle orientation in complex tissues? New investigations in the field are expected to shed light on these aspects.

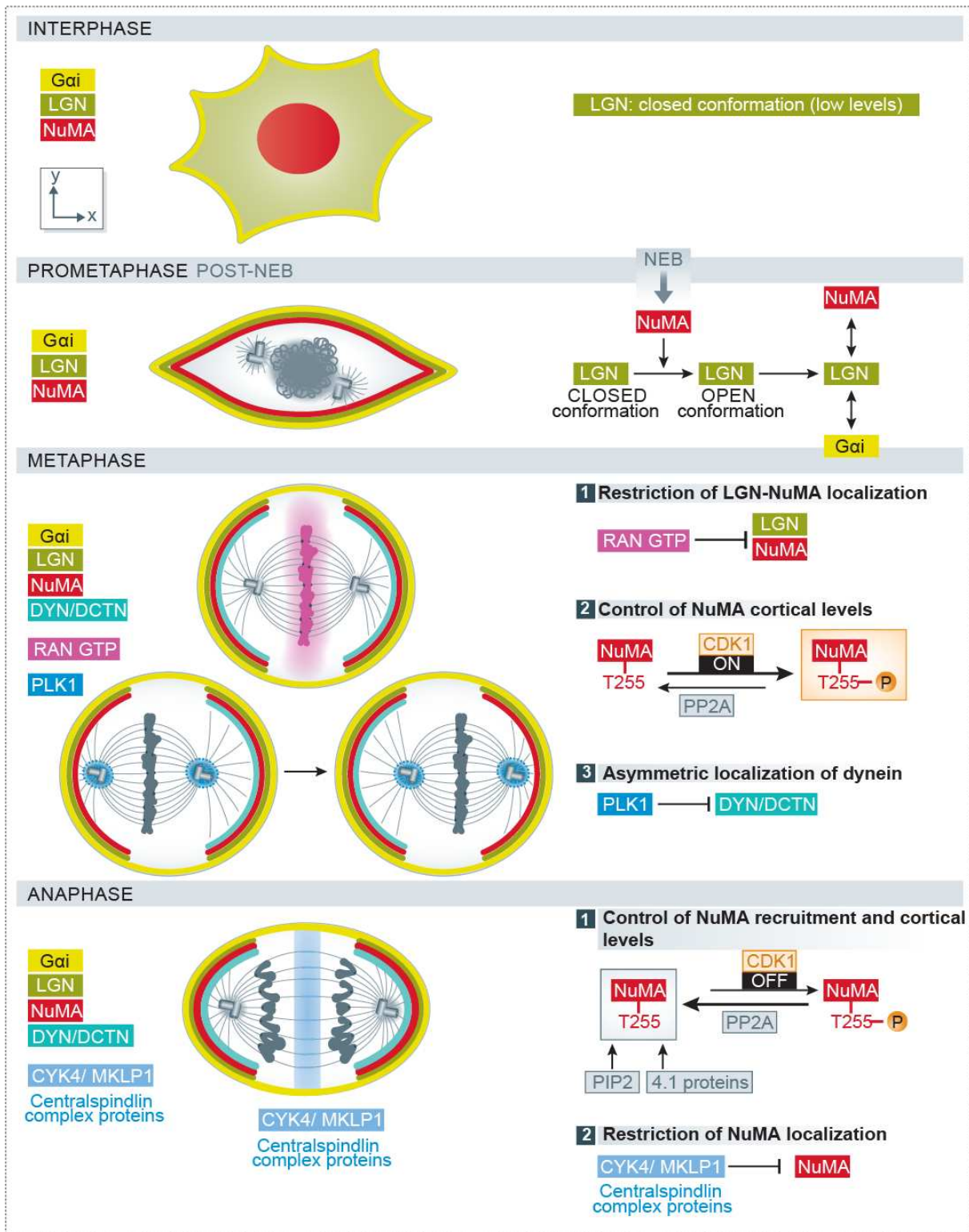


Figure 9: Temporal-spatial regulation of LGN complex localization. Left: Scheme of interphase and mitotic phases indicating the distribution of LGN, NuMA and dynein, as well as the localization of specific molecules (RAN GTP, PLK1 and Centralspindlin proteins) that are involved in controlling this distribution in cultured HeLa cells. Note that NuMA and dynein cortical levels increase in anaphase. Right: Detail of the molecular mechanisms involved in the control of LGN /NuMA localization and of dynein by RANGTP/Centralspindlin and PLK1, respectively. The control of NuMA cortical levels by CDK1 activity is also indicated.

In this subsection, I have shown how cell cycle regulated changes in the activity of kinases and the assembly of central spindle complexes in anaphase, result in a differential regulation of the cortical localization of NuMA. Remarkably, this reveals that NuMA can be recruited to the cortex independently of Gai and LGN in anaphase. In the next section, I further discuss this notion by presenting alternative spindle orientation complexes that converge on NuMA and dynein cortical recruitment, independently of LGN.

2.4.3. NOT A MONOPOLY: GAI/LGN INDEPENDENT PATHWAYS IN SPINDLE ORIENTATION

The Frizzled-Dishevelled (Fz-Dsh) PCP pathway regulates spindle orientation in different contexts, including zebrafish gastrulation and asymmetric division of the SOP pl cell (reviewed in Segalen and Bellaiche, 2009). pl cells on the fly notum divide along the antero-posterior axis, and the spindle is slightly tilted relative to the tissue surface. Although Gai, Pins and Dlg accumulate at the anterior cell cortex and are involved in the near planar orientation of the spindle, they are not necessary for its antero-posterior alignment (David et al., 2005). This orientation is regulated by the Fz receptor and its cortical effector Dsh, which are localized at the posterior cortex. Using the S2 cell induced polarity assay (Johnston et al., 2009), see section 2.3), Segalen and colleagues identified Mud as the downstream effector of Dsh (Segalen et al., 2010). Accordingly, they showed that Mud recruitment by Dsh at the posterior apical cortex of the pl cell is necessary for spindle orientation along the antero-posterior axis (Fig. 10a). Similarly, during Zebrafish gastrulation, Dishevelled and NuMA are necessary for spindle orientation along the animal-vegetal axis in epiblast cells (Segalen et al., 2010). This suggests that the Dishevelled-NuMA pathway is conserved across different species.

Mechanistically, the Dsh DEP (Dishevelled/EGL10/Pleckstrin) domain mediates the recruitment of Mud and Dynein. However, Johnston and colleagues found that the Dsh/NuMA pathway does not act alone and uncovered an accessory pathway in Dsh-mediated spindle orientation (Johnston et al., 2013). Using the induced polarity assay in S2 cells (section 2.3), they found that the DEP domain of Dsh on its own indeed recruits Mud, but surprisingly this was not sufficient to orient the spindle.

Robust spindle orientation required the C-terminal domains of Dsh in addition to the DEP domain (DEP-CT) and an interaction of the Dsh-PDZL domain with Canoe. Indeed, RNAi experiments showed that Canoe is necessary for robust spindle orientation in this assay. However, contrary to its previously described role downstream of Pins (Wee et al., 2011), in this case Canoe does not work through the recruitment of Mud. Instead, it is required for the recruitment of RhoA and the formin Diaphanous to the DEP-CT construct. Both RhoA and the actin nucleation activity of its effector Diaphanous are necessary for spindle orientation. Consistently, actin accumulates in the cortical domain where DEP-CT is localized. The mechanisms that link cortical actin nucleation to spindle rotation, however, remain to be investigated. In support of their *in vitro* data, the authors demonstrated that Diaphanous is indeed necessary for Dsh mediated spindle orientation along the antero-posterior axis in *Drosophila* SOP cells (Johnston et al., 2013) (Fig. 10a).

In addition to the Dsh/Mud pathway in which Pins is not involved, Bergstralh and colleagues have recently shown that Pins is not required for Mud lateral localization and anaphase planar spindle orientation in the *Drosophila* wing disc epithelia (Bergstralh et al., 2016). Of note, the absence of spindle orientation phenotypes was seen also in metaphase suggesting that this is not due to an anaphase-specific correcting mechanism. In contrast, Mud is required for planar spindle orientation in this epithelium (Bergstralh et al., 2016; Nakajima et al., 2013). However, how Mud is recruited to the cortex remains to be elucidated in this context. In section 2.8, I will present new evidence that shows Mud localization to specific junctions in this context.

While NuMA is a central component in several spindle orientation pathways (see also section 2.8 for an additional Pins independent/NuMA-dependent pathway), the molecular details of how it regulates spindle orientation remain to be clarified. Artificial targeting of dynein to the cell membrane independently of its interaction with endogenous NuMA induces excessive spindle rotation (Kotak et al., 2012). This suggests that dynein alone is sufficient to exert forces on astral microtubules, and that NuMA may only be a passive anchor for the motor complex. However,

artificially high levels of cortical dynein may cause excessive spindle rotations and bypass a regulation of dynein by NuMA that may occur at physiological expression levels. Alternatively, NuMA could itself contribute to force generation, either by regulating the motor activity of dynein, or through its ability to directly interact with microtubules (Haren and Merdes, 2002). It was proposed that NuMA localization to microtubule ends via its MT binding domain is necessary for spindle orientation (Seldin et al., 2016). Mouse keratinocytes depleted for the NuMA MT binding domain showed spindle orientation defects without changes in the localization of the dynein complex. However, the exact mechanisms by which MT end-localized NuMA contributes to spindle orientation remain to be elucidated.

2.5- THE EMERGING ROLE OF ACTIN IN SPINDLE ORIENTATION

In the previous sections, the words “cell cortex” and “cortical recruitment” were used in an improper (but very widely employed) manner while referring to the inner surface of the cell membrane. The cell cortex is actually defined as a cross-linked network of actin, myosin, and associated proteins located directly underneath the plasma membrane. In this section, I present emerging roles of this network in spindle orientation. The mechanics of the cell cortex are essential in the control of cell deformations that occur during cell division, and contribute to the transmission of forces. Furthermore, as already alluded to in the previous paragraph, several studies show that specific polarization of the actin cortex controls spindle orientation.

2.5.1. REQUIREMENT OF AN INTACT ACTIN CORTEX

When a cell enters mitosis, remodeling of its actin cytoskeleton leads to cell rounding and the establishment of a thinner, but stiffer actin-myosin cortex (Clark et al., 2013 and reviewed in Cadart et al., 2014). Impairment of the actin cortex by latrunculin A/B or cytochalasin D treatment generates spindle orientation defects in cultured cells and *in vivo* in the mouse embryonic skin and in *Drosophila* wing discs (Luxenburg et al., 2011; Nakajima et al., 2013; Zheng et al., 2013). In cultured cells and in the developing mouse skin, LGN cortical localization was perturbed by these treatments

(Luxenburg et al., 2011; Machicoane et al., 2014; Zheng et al., 2013). Hence, an intact cortex is required for the correct localization of the spindle orientation machinery and for the stabilization of force generators. How F-actin influences force generator localization at the cortex remains elusive. Recent data showing that Afadin6 can bind simultaneously actin and LGN provide for the first time a direct mechanistic link between cortical actin and the force generator machinery (Carminati et al., 2016). Simultaneously, a sufficiently stiff actin cortex is likely important to prevent membrane deformations and to balance the forces exerted by force generators at the cell surface that pull the spindle, as suggested by experiments in the *C. elegans* zygote (Redemann et al., 2010). In addition, changes in cellular shape generated by disruption of the actin cortex may be involved in the observed phenotypes, as I will discuss in detail in section 2.8. While the presence of an intact and stiff actin cortex can be seen as permissive for the correct localization of force generators and mitotic cell rounding, an active (or instructive) role of actin and actin related molecules in guiding spindle orientation is becoming more apparent (as discussed below).

2.5.2. ANTHRAX RECEPTOR AND ACTIN POLARIZATION

In the context of Zebrafish gastrulation, Castanon and colleagues described a novel molecular cascade controlling oriented divisions in epiblast cells (Castanon et al., 2013). Interestingly, the authors have observed the formation of an F-actin cap that co-localizes with an Anthrax receptor (Antxr2a) cap during cell division. Depletion of Antxr2a causes spindle misorientation. By following spindle rotation and cap formation in a series of gene knockdown experiments, the authors dissected the cascade of events that leads to cap formation and spindle rotation. They propose that local activation of RhoA by Wnt leads to the cortical enrichment of actin in an oriented manner. Actin recruits Antxr2a to the actin cap where it contributes to the activation of a diaphanous related formin, *zdia2*, which in turn allows spindle rotation in the direction of the cap (Fig.10b). However, it is not clear whether this pathway acts on Dynein, which is also involved in spindle orientation in

these cells (Quesada-Hernandez et al., 2010). It is also unknown whether Dsh and NuMA (Segalen et al., 2010) act in parallel to or downstream of the Antxr2a orientation pathway.

2.5.3. POLARIZED SUBCORTICAL ACTIN CLOUDS

In addition to cortical actin, Mitsushima and colleagues described the presence of a subcortical cluster of actin during mitosis in cultured cells. This actin cloud undergoes a rotational movement during metaphase, and disappears into the contractile ring upon cytokinesis. The formation of this amorphous actin-rich structure depends on Arp3 (Mitsushima et al., 2010). Further studies support a role for the actin cloud in spindle orientation. When cells are cultured on micropatterned surfaces (section 2.3), the adhesion pattern of the cell controls spindle orientation in the plane (xy axis) in an actin and microtubule dependent manner (Fink et al., 2011; They et al., 2007). The polarized distribution of retraction fibers during mitosis constitutes a memory of the adhesion pattern in interphase and influences the orientation of the spindle, as seen by laser ablation experiments (Fink et al., 2011). Interestingly, the adhesion pattern and distribution of retraction fibers influenced the polarized distribution and movements of actin clouds, and dynamic analyses suggested that clouds influence the rotation of the mitotic spindle in an astral MT dependent manner (Fink et al., 2011). More recently, the function of these actin clouds in spindle orientation was formally demonstrated by inhibiting the Arp2/3 complex (Kwon et al., 2015). Kwon and colleagues further demonstrated that the unconventional microtubule binding Myosin 10, an actin motor involved in spindle formation and integrity (Woolner et al., 2008), regulates spindle orientation with respect to polarized actin clouds in cells cultured on micropatterns. This activity depends on its MT binding domain. Interestingly, Myosin 10 localizes to retraction fibers and to dynamic actin clouds but it does not modify their dynamics or assembly. In contrast, depletion of Myosin 10 specifically increases astral microtubule dynamics and decreases the cortical dwell time of these MT at the cortex, as demonstrated by dynamic analyses of EB3 in metaphase. This suggests that actin localized Myosin 10 regulates spindle orientation by modulating astral MT dynamics, constituting a link between actin

and microtubules in the context of spindle orientation (Fig. 10c). Of note, the action of Myosin 10 differs from that of dynein, as Myosin 10 depletion does not change the frequency of microtubule lateral transitions in anaphase, in contrast to cells lacking cortical dynein caused by depletion of LGN using RNAi. In addition, depletion of Myosin 10 and LGN together results in more dramatic defects on spindle orientation than depleting each protein alone, suggesting that the actin-Myosin 10 and LGN-dynein pathways act in parallel to orient the spindle (Kwon et al., 2015). This reinforces the idea that in some cellular contexts, multiple pathways act to promote robust spindle orientation.

2.5.4. ERM PROTEINS

The ezrin-radixin-moesin (ERM) proteins are a family of actin-membrane cross-linkers which control cortical rigidity and stability (Fehon et al., 2010). Depletion of Moesin, the single member of the family in *Drosophila*, leads to massive cortical instability and blebbing in mitotic S2 cells. This results in exaggerated spindle oscillations and mispositioning (Carreno et al., 2008; Kunda et al., 2008). Defects in spindle morphology (such as short spindle and asymmetric asters) make it difficult to properly evaluate spindle orientation in this model. In contrast, in the *Drosophila* larval wing disk, Moesin RNAi does not induce massive blebbing during division, but affects cell rounding so that cells are more elongated along the apico basal axis. This correlates with a loss of planar spindle orientation (Nakajima et al., 2013). ERM proteins have been recently studied for their role in spindle orientation in vertebrate cells. In dividing human cells cultured on L-shaped micropatterns, activated ERM proteins are asymmetrically distributed, with an enrichment in the cortical domain facing the adhesive surface (Machicoane et al., 2014; They et al., 2005) (Fig.10d). Here, depletion of the three proteins as well as impairment of their activation through depletion of the SLK kinase (which was found to directly activate ERM proteins through phosphorylation) leads to spindle misorientation in the xy axis (section 2.3) (Machicoane et al., 2014). This phenotype is associated with the loss of LGN and NuMA cortical localization and with reduced spindle rotation, suggesting that activated ERM proteins are necessary for LGN/NuMA cortical recruitment or stability in this context. Importantly, in

contrast to the effects observed upon depletion of Moesin in *Drosophila* (Carreno et al., 2008; Kunda et al., 2008), depletion of ERM proteins does not generate obvious alterations in cell shape and spindle morphology in human cells, arguing for a specific role of these proteins in orienting the spindle by the control of LGN/NuMA localization (Machicoane et al., 2014). ERM proteins probably act at the level of LGN, since no effect was observed on G α i localization upon ERM inactivation or depletion. Remarkably, perturbing ERM activation in mouse apical neural progenitors *in vivo* impairs spindle orientation (Machicoane et al., 2014). However, whether ERM proteins regulate LGN complex localization also in this context remains to be studied. Intriguingly, activated ERM can also bind microtubules and thus could also influence spindle orientation directly (Solinet et al., 2013). Detailed time lapse microscopy indicated that spindles rotate in prometaphase in cells cultured on L-shaped micropatterns (Machicoane et al., 2014; They et al., 2005). The finding that LGN and NuMA are first localized asymmetrically as a large crescent facing the adhesive matrix (Machicoane et al., 2014) likely explains the stereotyped spindle orientation in this system, as anticipated by previous theoretical modeling (They et al., 2007).

This section highlighted the role of actin and actin regulators in spindle orientation in different model systems. An important challenge is to understand the crosstalk between actin- and NuMA-Dynein pathways. Remarkably, actin related pathways are seen both to modulate or to act independently of the LGN/ NuMA pathways. Indeed, ERM actin crosslinkers regulate the cortical localization of the LGN complex in cultured cells (Machicoane et al., 2014). Whether this regulation goes through modulation of the actin cortex or if alternatively there is a direct molecular link between ERMs and LGN/NuMA, remains to be determined. In contrast, actin subcortical clouds and myosin 10 act in parallel to the LGN/ dynein pathway to regulate spindle orientation in cells cultured on micropatterns (Kwon et al., 2015). Similarly, Dishevelled controls spindle orientation in *Drosophila* S2 and SOP cells by activating two parallel cascades: a NuMA-Dynein and a RhoA- Diaphanous-actin

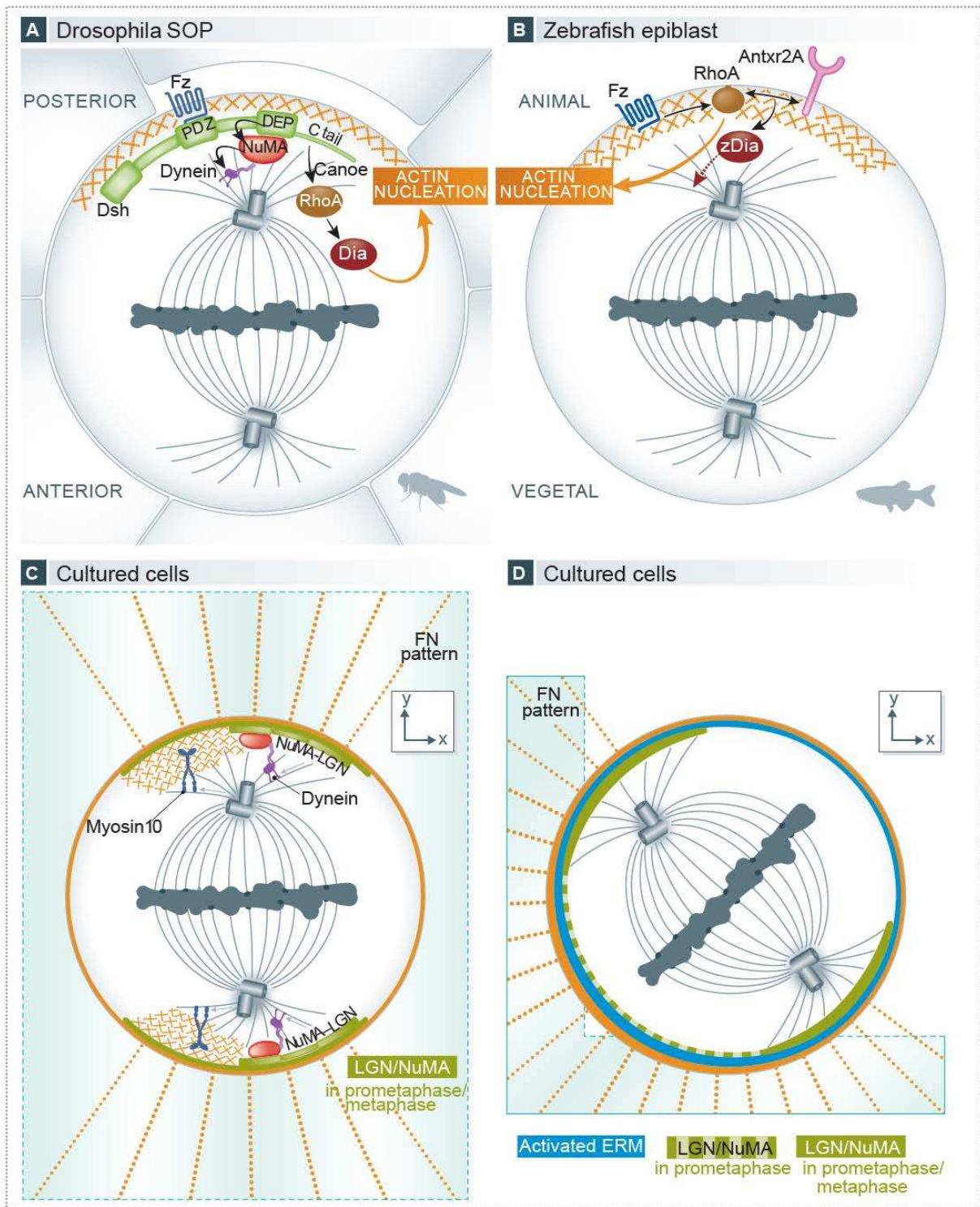


Figure 10: The role of actin in spindle orientation. Actin is shown in orange. a) In *Drosophila* SOP, Dishevelled localizes to the posterior cortex activating two parallel pathways required for spindle orientation: i) The recruitment of NuMA via the DEP domain allows dynein enrichment at this site, ii) a molecular cascade involving the tail domain of Dishevelled, and the Canoe and RhoA molecules leads to the activation of the actin nucleator Diaphanous at this cortical site. b) RhoA and the Anthrax receptor 2 A (Antxr2A) orient the spindle along the animal-vegetal axis in Zebrafish epiblast. Activation of Fzz promotes RhoA recruitment to the “animal cortex”. In turn, RhoA induces actin nucleation leading to the formation of an actin cap, and together with the Anthrax receptor activates the downstream effector zDia. c, d) Involvement of different actin related molecules in xy spindle orientation in single cells cultured on fibronectin micropatterns. In this context, the distribution of actin retraction fibers dictates the orientation of the spindle. C) Polarized actin subcortical clouds make the link between the distribution of retraction fibers and spindle orientation. Myosin 10 mediates the link between

actin and microtubules in this context. The classical LGN/ dynein complexes are proposed to act in parallel to this pathway, leading to robust spindle orientation. D) The Ezrin-Radixin-Moesin proteins are enriched in the adhesive cortex in cells cultured in L patterns. These proteins control the initial distribution of LGN and NuMA, during prometaphase, which favor spindle rotation along the depicted axis.

pathway (Johnston et al., 2013). In these cases, it would be interesting to study if parallel pathways act simultaneously or not during spindle orientation. For instance, it could be imagined that one pathway determines the initial orientation of the spindle, having a more instructive role, while the other cascade maintains the orientation once it is set.

The molecular complexes that recruit force generators are located at the plasma membrane. Despite the size of these complexes, due to the thickness of the mitotic cortex (190nm: Clark et al., 2013), it is unlikely that force generators stick out beyond the cortex in the cytoplasm, and more probable that astral microtubules reach motor complexes close to the plasma membrane by growing through the actin meshwork. This also provides an additional layer of regulation for the cortical capture of microtubules, which will be addressed in the following section, dedicated to the regulation of astral microtubules. It will be interesting to explore whether the actin regulators described above influence this meshwork.

2.6. MODULATION OF SPINDLE ORIENTATION THROUGH THE SPECIFIC REGULATION OF ASTRAL MICROTUBULES

Except for positioning of meiotic spindles, which lack astral microtubules (reviewed in Almonacid et al., 2014, see also section 2.9), spindle orientation is thought to be achieved by the interaction of astral microtubules with force generators at the cellular cortex (in the broader definition that includes the plasma membrane). Therefore, defects in spindle morphology and/or astral MTs can affect spindle orientation. Shorter spindles may indirectly affect the distance between astral microtubules and the cortex. Alternatively, abnormal astral microtubules may affect the correct transmission of forces necessary to orient the spindle. Indeed, many proteins affecting astral

microtubules perturb spindle orientation. Here I will discuss how modulation of A) astral MT nucleation/anchoring at the centrosome, B) astral MT dynamics and stability, C) astral MT cortical capture, D) astral MT behavior at the cortex and E) astral MT subpopulations impact on spindle orientation (Fig. 11).

2.6.1. ASTRAL MICROTUBULES NUCLEATION

The role of the centrosomal protein pericentrin (Pcnt) in spindle orientation has been addressed by using cultured MEFs derived from Pcnt $-/-$ knock-out mice (Chen et al., 2014). In these cells, both astral microtubule length and density (determined by measuring α -tubulin signal intensity) are decreased, and spindle orientation with respect to the substrate (section 2.3) is impaired. In addition, Pcnt was found necessary for spindle pole localization of a particular set of centrosomal proteins including Ninein, Centriolin and Cep215. While the localization of these proteins at the centrosome is required for spindle orientation, it remains to be analysed how each of them affects astral microtubules. However, the data obtained so far suggest that defective recruitment of centrosomal proteins by Pcnt depletion leads to defects in astral microtubules nucleation at the centrosome and thus induces spindle misorientation (Fig. 11c-i). Importantly, the cortical localization of NuMA and the dynactin subunit p150 glued are not affected in Pcnt $-/-$ cells, suggesting that their transport and/or turnover are not affected by the observed defects on astral microtubules. This suggests that defects in centrosomal protein localization and/or astral microtubule density are responsible for the observed defects in spindle orientation. In agreement with the *in vitro* data, the authors found spindle orientation defects in neural progenitors and in heart septums of Pcnt $-/-$ mice (Chen et al., 2014).

Related to MT nucleation activity, a novel role of Rab11 recycling endosomes (RE) in spindle orientation has been recently demonstrated in human cells (Hehnly and Doxsey, 2014). These endosomes associate with the spindle and with spindle poles in a Rab11 dependent manner. Impairment of Rab11 function generates spindle misorientation with respect to the substrate. The

authors proposed that disruption of astral microtubules is related to this phenotype, which could be explained by the fact that Rab11 RE transport microtubule nucleation components like γ tubulin and GCP4 (Fig.11c-i). These effects may not be astral MT-specific as the overall spindle microtubule density is affected upon Rab11 depletion. Assays of microtubule nucleation from spindle poles in Rab11 depleted vs control cells demonstrated that Rab11 is indeed important for spindle pole MT nucleation. In conclusion, Rab11 endosomes would be important for the delivery of MT-nucleating components to the spindle poles, which would affect MT nucleation, spindle morphology and consequently, spindle orientation. However, it should be noted that Rab11 depletion also generates misaligned chromosomes. The proximity of misaligned chromosomes to the cortex could affect the cortical localization of LGN-NuMA in a Ran^{GTP} mediated manner and thus indirectly affect spindle orientation, as described above (Kiyomitsu and Cheeseman, 2012). Alternatively, recent data show that artificially induced chromosomal misalignments result in kinetochore-derived Plk1 signaling, whose proximity to the cortex can locally inhibits LGN and NuMA recruitment (Tame et al., 2016), which may also explain the phenotype of Rab11 depletion. In any case, these results originally link membrane traffic with spindle orientation.

2.6.2. ASTRAL MICROTUBULES DYNAMICS AND STABILITY

Defects in astral microtubule stability also affect spindle orientation. Toyoshima and Nishida have first shown that depletion of the microtubule plus end protein EB1, a regulator of microtubule stability, results in spindle misorientation with respect to the substrate in cultured cells (see section 2.3), accompanied by a reduction in spindle length and of astral microtubules (Toyoshima and Nishida, 2007). More recently, Bouissou and colleagues have shown in *Drosophila* S2 cells and human HeLa cells that γ -tubulin ring complexes (γ -TuRCs) localize to astral microtubules in addition to their well-known localization at centrosomes and spindle microtubules. Depletion of the γ -TuRCs component Dgrip75 in *Drosophila* impairs spindle orientation mediated by Ed-Pins^{TPR+Linker} in the S2 induced polarity assay (see section 2.3) and apico-basal spindle orientation in neuroblasts (Bouissou

et al., 2014). Similarly, depletion of GCP4, the human Dgrip75 ortholog, generates defects in spindle orientation with respect to the substrate in cultured human cells. Associated with these defects, spindles show longer astral microtubules in S2 cells. Interestingly, changes in astral microtubules do not result from defects in microtubule nucleation activity, a canonical function assigned to γ -TuRCs. In contrast, γ -TuRCs act by regulating astral microtubule dynamics. Indeed, depletion of Dgrip75 increases astral MT dynamics and the time that MTs spend in the growing state, possibly explaining the overall increase in MT length (Fig.11c-ii). Importantly, by suppressing MT dynamics using drug- and knockdown-based approaches, the authors were able to rescue spindle orientation defects in S2 cells (Bouissou et al., 2014). This suggests that perturbed astral MT dynamics is directly responsible for the spindle orientation phenotypes observed.

While the effects on spindle orientation generated by the absence or shortening of astral MTs can easily be explained by the lack of interactions between the spindle and the force generators, the link between longer and more dynamic astral MTs and defective spindle orientation is less clear. One possibility is that longer astral microtubules establish abnormal interactions with the cortical sites facing the initial axis of spindle orientation, which in consequence could affect the rotation of the spindle to the cortical domains enriched in force generators (They et al., 2007). Alternatively, the interaction of force generators with highly dynamic microtubules may be less effective. Consistently, exaggerated spindle oscillations are seen upon Dgrip75 depletion in S2 cells, which could indicate unstable MT-cortex interactions (Bouissou et al., 2014).

2.6.3. ASTRAL MT CORTICAL CAPTURE

While microtubule nucleation and dynamics regulate the number of microtubules reaching the cortex, these microtubules need to establish proper contacts with the cortex. The interaction between the cortex and astral MTs can be modified by molecules localized at the cortex. For instance, the actin associated protein MISP localizes to the cellular cortex during mitosis and regulates spindle orientation with respect to the substrate in HeLa cells (Zhu et al., 2013). Depletion

of MISP results in reduced astral microtubule intensity, which is not caused by defects in microtubule nucleation, as *in vitro* and *in vivo* polymerization assays showed. Because MISP does not localize to the spindle but to the cortex, the authors proposed that astral MT attachment to the cortex is impaired in the absence of MISP, resulting in destabilized astral MTs (Fig.11c-iii). However it is noteworthy that MISP depletion generates fragmented centrosomes that are often located at the interior of the spindle, which could also contribute to disrupt astral MTs.

2.6.4. BEHAVIOR OF ASTRAL MICROTUBULES AT THE CORTEX

Once microtubule plus-ends contact the cortex by end-on attachment, two different scenarios have been observed. After a few seconds of cortical dwell, they either undergo catastrophe and shrink or continue to grow along the cell cortex, a process known as side-on sliding. Samora and colleagues have shown that the microtubule associated protein MAP4 regulates spindle orientation and positioning in HeLa cells by modifying the behaviour of astral MTs at the cellular cortex (Samora et al., 2011). Dynamic analyses of EB3-Tomato during metaphase revealed that upon depletion of MAP4, side-on sliding of astral microtubules at the cortex is increased and leads to spindle pole displacement (Fig.11c-iv). Interestingly, these effects are lost upon the impairment of dynein activity, suggesting that MAP4 acts by moderating dynein dependent forces that generate abnormal MT-cortex interactions.

2.6.5. MODULATION OF SPECIFIC ASTRAL MT SUBPOPULATIONS

While most of the studies describing the role of astral MT in spindle orientation have been performed in cultured cells, progress has been made recently to understand their characteristics and *in vivo* function in apical progenitors (APs) of the mouse neocortex (see section 1.1.3) (Mora-Bermudez et al., 2014). The authors defined two different astral MT subpopulations, which are differentially regulated between proliferating and neurogenic APs. In neurogenic APs, the numbers of apical and basal astral MTs (but not of central MTs), decrease with respect to proliferating APs, in correlation with an increase in the amplitude of spindle oscillation during metaphase.

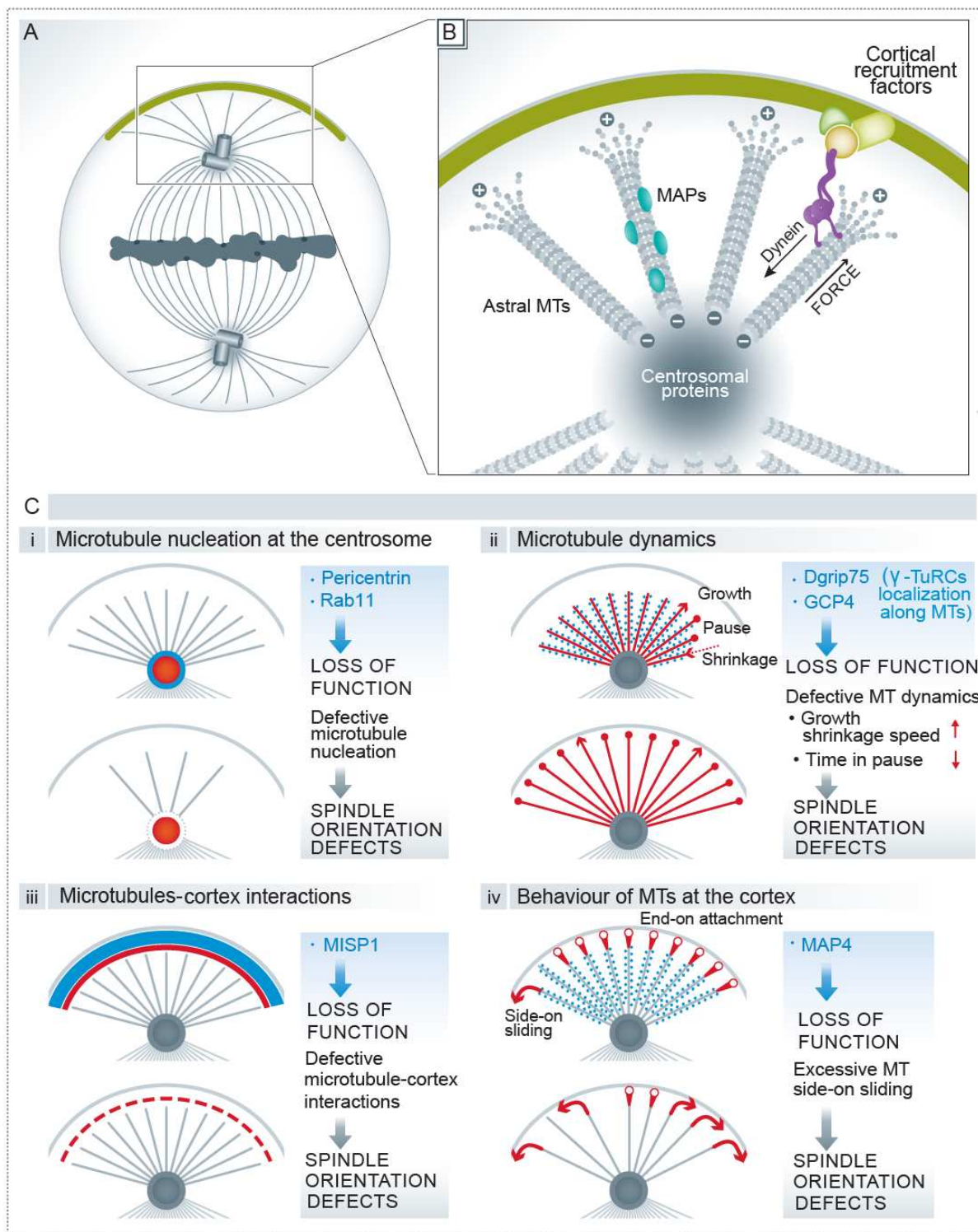


Figure 11: Modulation of spindle orientation through regulation of astral microtubules. a, b) Schema illustrating the centrosome and astral microtubules as well as generic proteins localized on these structures. Cortically recruited dynein is believed to walk on the minus end direction of astral MT, generating the force that orients the spindle. c) Regulation of different processes (I-IV) controls the density, length and behavior of astral microtubules, and thus spindle orientation. Left, the process and cellular structure concerned are indicated in red. Right: Loss of function of specific proteins (in light blue) results in defects in the indicated processes and spindle misorientation. In iii) MISP acts from the cellular cortex regulating Cortex- MT interaction.

Therefore, the density of apical/basal astral MTs may regulate the stability of spindle orientation. Indeed, specific perturbation of this astral MT subpopulation impacts the amplitude of spindle oscillations observed in proliferating APs. Interestingly, this subpopulation of astral MTs is in part controlled by LGN enrichment in the basal cortex, which is higher in proliferating than in neurogenic progenitors. This suggests that cortical anchoring of apical/basal astral MTs by the LGN complex regulates their stability. While it could be imagined that a broader cortical distribution of the LGN complex would lead to a less stable spindle orientation, the authors propose that it acts in the opposite manner: basal LGN would favor the stabilization of the spindle by anchoring apical/basal astral MTs. It can be hypothesized that forces exerted on apical/basal astral MTs are smaller than those exerted on central astral MTs. This would allow spindle orientation along the plane of the tissue, which will be further stabilized by the anchoring of astral MTs to the apical/basal domains. Whether specific subpopulations of astral MTs exist in other cellular contexts and how they regulate spindle orientation remains to be investigated.

Finally, it should be pointed out that shortening of astral MTs may differentially impact spindle orientation depending on the spindle size relative to the cell size. In addition, reduced astral MT density can result in different outcomes depending on the available cues for spindle orientation that in turn determine the level of enrichment of force generators at the cortex.

2.7. EXTRACELLULAR STIMULI INFLUENCING SPINDLE ORIENTATION

In a tissue, cells are exposed to a variety of environmental stimuli that can influence their axis of division by mobilizing and polarizing the internal machinery for spindle orientation discussed above. Recent research has shown an increasing diversity in signalling pathways involved in the upstream regulation of spindle orientation. For reasons of length, I will not extensively discuss the evidence illustrating the diversity of extracellular stimuli regulating spindle orientation in this manuscript. This topic has been further reviewed in (di Pietro et al., 2016). In short, extracellular molecules of

different nature are able to regulate spindle orientation in diverse models. These stimuli include semaphorins (Arbeille et al., 2015; Xia et al., 2015), ECM signalling (Lechler and Fuchs, 2005; Toyoshima and Nishida, 2007) as well the classical Wnt/Fz and Fat/Ds/Fj PCP pathways (Gong et al., 2004; Habib et al., 2013; Mao et al., 2011; Morin and Bellaïche, 2011; Saburi et al., 2008; Segalen and Bellaïche, 2009; Segalen et al., 2010).

2.8. SPINDLE ORIENTATION IN CONTEXT: ROLES OF CELL GEOMETRY AND MECHANICAL FORCES

Mitotic rounding is a common and remarkable feature of most dividing animal cells, whether in adherent cell culture or in intact tissues. Mitotic rounding implies reorganization of the actin cytoskeleton (reviewed in Lancaster and Baum, 2014), and cell ballooning is achieved through an increase in intracellular osmotic pressure (Stewart et al., 2011). The mitotic actin cortex is thinner, but stiffer than in interphase (Clark et al., 2013). Mitotic rounding is viewed as a way to generate sufficient intracellular space to accommodate spindle formation and is indeed important for chromosome capture and bipolar spindle maintenance (Lancaster et al., 2013 and reviewed in Cadart et al., 2014). Apart from non-adherent cells (such as one-cell zygotes), mitotic rounding in mitosis implies a profound remodeling of cells adhesion with their neighbors and/or the extracellular matrix.

Despite their rounding, mitotic cells are exposed to external forces generated by the contact with neighboring cells and with the substrate. These forces depend on the position of the cell within a tissue and on the changes in the tissue itself, especially during morphogenesis, and reflect a memory of cell shape and adhesion in interphase. In addition, rounding itself is often imperfect and cells retain a slightly elongated shape that corresponds to their shape in interphase and scales with tissue tension. In the following section, I will describe that both the memory of cell shape in interphase and a more direct sensing of cell shape in mitosis can influence spindle orientation.

2.8.1. INTRINSIC CELL GEOMETRY IN MITOSIS IMPACTS ON SPINDLE ORIENTATION

The empirical century old “long axis” or “Hertwig rule”, initially proposed by Oscar Hertwig in the late 19th century, posits that cells usually place their cleavage plane at the center of their mass and perpendicular to their longest axis (Hertwig, 1884). Hertwig had explored this property through experimental deformation of single cell echinoderm embryos. These cells are normally perfectly spherical, and their first division is symmetrical with no preferential orientation. However, by gently squeezing embryos between glass plates, Hertwig observed that the orientation of division could be controlled by the deformation and aligned with the elongated axis. In line with Hertwig’s observations, O’Connell and Wang used a similar approach to probe the relationship between cell shape and spindle orientation in cultured mammalian cells (O’Connell and Wang, 2000). Using micromanipulation with glass pipettes, they forced shape deformations in dividing Normal Rat Kidney (NRK) cells, which do not round up during mitosis and keep their interphase shape. In these cells, although the mitotic spindle can sometimes be observed orthogonal to the cell’s longest axis in early metaphase, by anaphase it is aligned parallel to the longest axis. They observed that upon experimental deformation of mitotic cells, the spindle constantly reacted to cell shape changes and adapted by moving to the new cell center and realigning with the induced longest axis. They further showed that spindle movements occurred in an astral microtubule and dynein dependent manner.

Hertwig’s rule was recently revisited in sea urchin embryos by Minc and colleagues, who used microfabricated 3-D molds to apply specific anisotropic shape deformations (Minc et al., 2011). While the rule applied to most shapes, some specific shapes did not conform to its predictions. A model in which forces applied to spindle poles scaled with the length of individual astral microtubules predicted much better the orientations observed in all tested shapes. This model is difficult to reconcile with force generators combined at or near the cell cortex, which is the dominant model in other cell types, and it implies a role of force generators in the cytoplasm (Minc et al., 2011). It should also be noted that single cell zygotes are usually very large and their spindle is comparatively small, with very long astral microtubules. In contrast, in many cell types, the size of

the spindle scales with cell size (Courtois et al., 2012; Good et al., 2013); mitotic rounding is indeed essential to allow sufficient space for the formation of the spindle, and artificial confinement results in chromosome missegregation (Lancaster et al., 2013).

Recently, Lazaro-Diequez and colleagues studied the relationship between spindle orientation and cell shape in the context of imperfect rounding, making use of the natural variability of rounding in adherent MDCK and HeLa cells in mitosis (Lazaro-Diequez et al., 2015). In control conditions, adherent cells divide very precisely in the plane of the substrate, making it difficult to address the question (section 2.3). Disruption of force generation either by knock down of the LGN pathway or pharmacological removal of astral microtubules disrupts this orientation, but a strong bias towards planar orientation remains. The authors attribute this bias to imperfect cell rounding: they compared the orientation of the spindle in cells treated with low doses of nocodazole (that primarily disrupt astral microtubules and abolish force generation) between perfectly round and more “flat” mitotic cells, and found that the bias towards planar orientation was much more pronounced in flat cells (relative to the substrate), while orientation was close to random in cells with a more spherical shape. This indicates that cell shape can directly influence orientation independently of cortical force generators. The authors observed frequent deformation of the metaphase plate in these flat cells, suggesting that the effect on orientation may be a direct consequence of steric hindrance in cells where cytoplasmic volume and cell size are just sufficient to accommodate the size of the metaphase spindle.

This notion can be transposed to *in vivo* situations, where cell packing imposes constraints on cell shape both in interphase and during mitosis, and where rounding is unlikely to be perfect. In the mouse developing skin, where interphase cells are flat (eg. with a relatively short apico-basal length), orientation of the spindle is biphasic: symmetric divisions orient in the plane of the tissue and asymmetric divisions are perpendicular to this plane in an *Insc/Gai/LGN/NuMA* dependent manner (Lechler and Fuchs, 2005; Williams et al., 2014). Remarkably, disruption of force generators via

knockdown of NuMA or p150 does not lead to random spindle orientation, but most divisions are planar, according to the main axis of cell elongation (Fig. 12a). This suggests that a cell shape sensing mechanism independent of cortical force generators contributes to a default planar orientation in this tissue (Williams et al., 2011).

2.8.2. ROLE OF SURROUNDING FORCES IN SPINDLE ORIENTATION

EXTERNAL FORCES INFLUENCE SPINDLE ORIENTATION IN SINGLE CELLS IN VITRO

In cultured adherent cells, the distribution of retraction fibers in mitosis reflects the geometry of the adhesion of the cell to its substrate in the previous interphase. As mentioned above, the distribution of retraction fibers dictates, and can indeed be used to predict the orientation of the mitotic spindle within the plane of the substrate (Fink et al., 2011; They et al., 2007; They et al., 2005). Fink and colleagues demonstrated the function of retraction fibers by performing laser ablation of these cellular structures and by analyzing spindle movements (Fig. 12b). Importantly, these authors observed changes in cell shape upon retraction fiber ablation, suggesting that retraction fibers exert forces on the cell. Indeed, this was confirmed upon measurement of the forces associated with retraction fibers by using optical tweezers. Remarkably, applying stretch forces to a cell without affecting its shape is sufficient for spindle rotation along the axis of the dominant force field (Fink et al., 2011). Collectively, these experiments demonstrate that adhesion-related forces can control spindle orientation in single cells. In these experiments, reorientation was reduced in the presence of low doses of nocodazole that disrupt astral microtubules, indicating that force generators acting on the microtubule network work downstream of retraction fibers. The entire molecular cascade that links external forces from retraction fibers to the recruitment and activation of internal force generators is not completely understood, and involves several pathways, as already detailed. On one hand, activation of the actin cloud/Myosin 10 pathway provides a direct link with microtubule dynamics (Kwon et al., 2015); on the other hand, forces exerted on the cortex influence local ERM activation (Machicoane et al., 2014; They et al., 2005), which directly or indirectly promotes the

asymmetric localization of LGN/NuMA and presumably of dynein to the cortex (Machicoane et al., 2014).

While retraction fibers have not been described in tissues, distinct structures may mediate the establishment of forces in an analogous manner through cell-matrix attachment or cell-cell interactions, as described below.

INFLUENCE OF EXTERNAL FORCES ON SPINDLE ORIENTATION *IN VIVO*

The influence of external forces on spindle orientation has also been addressed *in vivo* in developing tissues. During the spreading of the enveloping cell layer (EVL) of Zebrafish gastrula (Campinho et al., 2013), cells orient their spindle along the animal-vegetal axis which coincides with the axis of maximal tension in this tissue. Importantly, artificial induction of local tension in the perpendicular direction induces spindle rotation and reorientation towards the axis of induced tension. Using a computational model, the authors found that the cell shape parameter in interphase can reliably be used to predict the visualized orientation of divisions in the EVL. Mechanistically, they showed that the molecular motor Myosin II is involved in cell shape regulation and in mediating the connection between shape and spindle orientation (Campinho et al., 2013).

Wyatt et al used micromanipulation to apply stretch forces to a suspended monolayer of cultured MDCK cells (Wyatt et al., 2015). In response to stretch, cells elongate parallel to this homogeneous field force and divide along their longest axis. This restores cell shape isotropy in the stretched tissue; in short, divisions relieve tension. Similar results were obtained in the developing *Drosophila* wing disc, where cells divide according to local tension fields, therefore reducing the tension in the tissue (Legoff et al., 2013; Mao et al., 2013). During this morphogenetic process, the tension fields themselves are generated by local variations in proliferation rates, showing an interesting feedback loop between proliferation, tissue tension, and oriented cell divisions.

How do cells sense “tension” and translate it into spindle orientation? When a tissue is under tension, cells tend to adopt an elongated shape that generally aligns with the axis of maximal tension. However, a minority of cells does not behave like this. Remarkably, Wyatt et al found that the spindle aligns with the long axis even in the minority of cases when the long axis is not aligned with the stretch applied to the tissue, indicating that cell shape may be a better predictor than global tissue tension itself (Wyatt et al., 2015). However, a recent study by Bosveld and colleagues shows that while cell shape in interphase is a good indicator of spindle orientation when anisotropy is high, it does not predict orientation as efficiently in nearly isotropic cells. Under these conditions the topology of a cell’s contacts with its neighbors during interphase is a better parameter (Bosveld et al., 2016). In the epithelium of the fly pupal notum, the authors found that tricellular junctions (TCJs; the vertex where three neighboring cells are in contact) localize force generators in a Mud-dependent manner. Remarkably, Mud starts to accumulate at TCJs during the G2 phase. When cells round up for mitosis, the position of cortical patches of Mud reflects the geometry of the cell contacts with its neighbors and dictates where greater forces will be generated. The authors show that a model using the position of the TCJs, and therefore of the Mud patches (“Mud intensity model”), to predict force generation faithfully recapitulates experimental data in this tissue. Remarkably, predictions in this particular tissue are more accurate than with a model that uses cell shape as one of its main parameters (Minc et al., 2011). Bosveld and colleagues proposed that in addition to their function as epithelial barrier structures, TCJs serve as polarity cues promoting geometry and mechanical sensing in epithelial tissues (Bosveld et al., 2016) (Fig. 12c). Quite remarkably, this new orientation mechanism depends on Mud, Dynein and Dlg, but does not require Gai or Pins, providing another example of a Pins-independent, but Mud-dependent pathway. In contrast to *Drosophila* Mud, vertebrate NuMA is nuclear in interphase and has not been described at cellular junctions in epithelia; it is therefore unclear whether the mechanism described above reflects a generic property of TCJs. Future experiments in other model systems, either in tissues or in

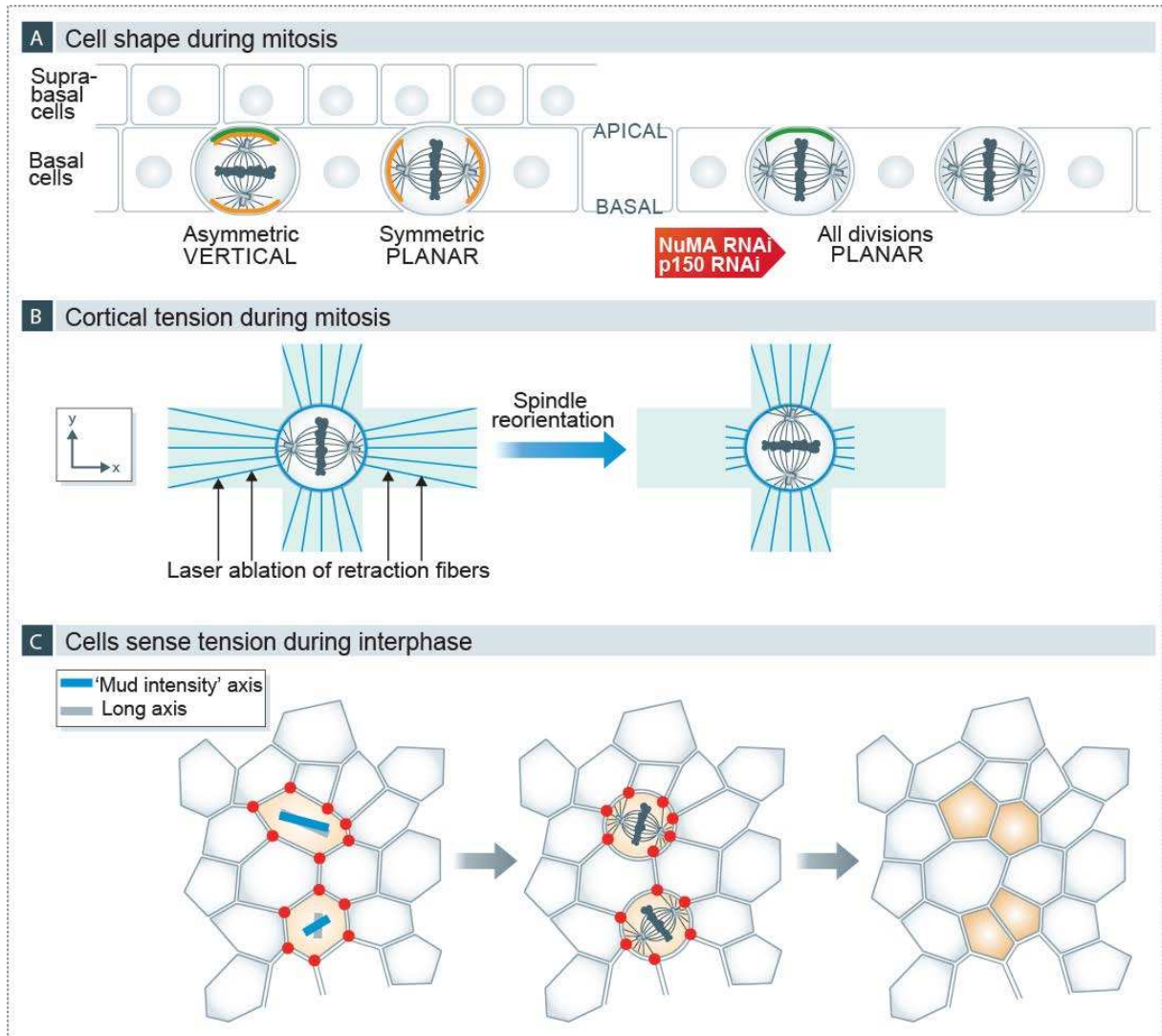


Figure 12: Role of cell geometry and external forces: a) Cells in the basal layer of the developing mouse epidermis adopt a binary orientation: symmetric divisions occur in the plane of the epithelium, and asymmetric divisions divide along the apico-basal axis in an *Insc/Gai/LGN/NuMA/Dynein* manner, with one daughter cell delaminating into the suprabasal cell layer. Upon NuMA or p150 depletion, cortical force generators are not functioning and most divisions now take place in the plane of the epithelium, suggesting that the “default” planar orientation may be dictated by the flat cell shape in this tissue. Green lines: *Insc* and *Gai3* apical accumulation; Orange lines: Force generators (Dynein). See Williams et al, 2011. b) In single cells cultured on fibronectin micropatterns (light blue), a field of maximal force is associated with polarized retraction fibers (blue lines). Cells cultured on “cross” shaped patterns orient their spindle along the long arms of the cross, where maximal forces are observed. Laser ablation of retraction fibers on the long arms induce a 90° spindle rotation and alignment to face the “new” maximal forces. See Fink et al, 2011. c) In the fly notum epithelium, NuMA accumulates at tricellular junctions in the G2 phase. Left panel: a vector corresponding to the cells long axis (grey bar) or to the geometry of tricellular junctions (or Mud accumulation, red dots) can be drawn (blue bar). In elongated cells, both vectors are aligned (top cell), whereas they do not always align in cells with an isotropic shape (bottom cell). Middle pane: the “Mud accumulation” vector predicts the orientation of cell divisions more accurately than the long axis. Right panel: position and shape of the daughter cells after division. See (Bosveld et al., 2016).

experimentally stretched cell layers (like those described by Wyatt et al.), should explore whether TCJs carry a similar geometric information independently of NuMA.

In summary, it appears that mechanisms acting in interphase and during mitosis sense extrinsic tension and intrinsic geometry and contribute to translate these cell shape parameters into an oriented spindle. Despite the increase in osmotic pressure, mitotic rounding is probably never perfect in a tissue where cells are subjected to forces of adhesion and compaction. It is therefore difficult to completely uncouple the factors that depend on external forces from those related to intrinsic shape.

2.9. OTHER MODELS OF SPINDLE POSITIONING

Spindle positioning mechanisms are also extensively studied during asymmetric division of the budding yeast and in the asymmetric division of mammalian oocyte meiosis. As I will talk about these models later in the manuscript, here I present the basics for each of these models. Of note, both models show important differences to the mechanisms observed in higher eukaryote cells in embryonic development or in cell culture presented in the precedent sections.

SPINDLE ORIENTATION IN BUDDING YEAST

Spindle positioning is well characterized in the asymmetric division of the budding yeast *S. cerevisiae* (McNally, 2013). In this model, the spindle is positioned in relation to the bud neck to allow the correct segregation of chromosomes between mother and daughter cells. Spindle orientation in this system also depends on the interaction of astral microtubules with cortically localized factors; however, cortical factors (e.g. Num1, reviewed in Moore et al., 2009) are not homologous to those found in higher eukaryotes. In addition, spindle positioning is achieved by two sequential and clearly distinct pathways (Markus and Lee, 2011a). In pre-anaphase, spindle orientation along the mother-bud axis is not linked to dynein dependent forces but instead, depends on the displacement of astral microtubules along actin cables. This process depends on the interaction between the MT tip protein Bim1 (homologous to EB1) and the myosin Myo2 via the yeast specific adaptor Kar 9 (homologous to

APC) (Markus et al., 2012; Markus and Lee, 2011a). In anaphase, spindle displacement into the bud neck is mediated by pulling forces exerted by cortically anchored dynein. The switch between both pathways is linked to the removal of the dynein inhibitor She1 from astral microtubules in the metaphase-anaphase transition (Woodruff et al., 2009). In anaphase, dynein (Dyn1) is delivered to the cortex, where it binds to the cortical factor Num1 through a mechanism of “off-loading” from astral microtubules (Markus and Lee, 2011b). Thus, pre-targeting of dynein to microtubule plus ends is necessary for spindle positioning (Markus and Lee, 2011a, b). Dynein pre-targeting depends on Pac1 and Bik1 (LIS1 and CLIP-170 homologues, respectively) (Markus and Lee, 2011a). Interestingly, in mammalian interphase cells, dynein localizes to MT plus ends in a CLIP170 and EB1 dependent manner (Lansbergen et al., 2004). However, whether the localization of dynein to MT plus ends is important for its delivery to the cortex during vertebrate mitosis remains to be investigated. Notably, both pathways acting in spindle positioning in yeasts do not rely on the polarization of cortical anchors as it is seen in higher eukaryotes. Instead, they rely on the asymmetric localization of Kar 9 and Dyn1, to the astral microtubule plus ends emanating from the daughter spindle pole (Markus et al., 2012).

SPINDLE ORIENTATION IN OOCYTE MEIOSIS

Oocytes divide asymmetrically during Meiosis I and II, giving rise to a small polar body and an oocyte inheriting most of the cytoplasmic content. The asymmetric positioning of the meiotic spindle allows the asymmetric division in these big cells. In prophase I, the oocyte shows no signs of polarization and the spindle is assembled in the center of the cell. Thus, a symmetry breaking event and the migration of the spindle towards the cortex are necessary (Almonacid et al., 2014). Of note, meiotic spindles lack centrosomes and astral MT in many species; thus, most of the mechanisms described in the precedent sections are not compatible with spindle positioning in this system. The direction of spindle migration is determined randomly by the position of the spindle pole closer to the cortex on which higher forces are applied. In mouse oocytes, the spindle is surrounded by an actin cage and

decorated with active Myosin 2 molecules at both spindle poles. In particular, Myosin 2 contributes to spindle migration by allowing attaching and pulling of the spindle (Schuh and Ellenberg, 2008).

Several studies performed in the mouse oocyte model have allowed to uncover different mechanisms contributing to spindle migration during Meiosis I. All these mechanisms involve actin based networks which are fine-modulated to allow spindle migration. In particular, a dense cytoplasmic F-actin network is essential for spindle migration. This network is composed of numerous thin filaments and crossing points and depends on the actin nucleators Formin 2 and Spire 1/ 2 (Azoury et al., 2008; Dumont et al., 2007; Pfender et al., 2011; Schuh and Ellenberg, 2008) . Upon Meiosis I resumption, a drop in the levels of Formin 2 and a concomitant destabilization of the actin network are proposed to allow for symmetry breaking and spindle migration (Azoury et al., 2011). More recently, a vesicle-driven mechanism was proposed to regulate the cytoplasmic actin meshwork. In particular, vesicles coated with Formin 2, Spire 1/ 2, Myosin V and Rab11 serve to nucleate actin filaments. The meshwork density and the vesicle number are reciprocally regulated. Interestingly, the presence of Myo V and actin nucleators allow these vesicles to generate tracks for their own movement, and the outward directed movement of these vesicles contributes to spindle migration (Holubcova et al., 2013).

Furthermore, an essential modulation of actin dynamics takes place at the oocyte cortex. Upon resumption of Meiosis I, a remarkable thickening of the actin cortex occurs in an Arp2/3 dependent manner. This cortical thickening results in a drop in cortical tension, leading to a softer actin cortex. Notably, this cortex softening is required for correct spindle migration. Concerning the function of this cortex thickening, mathematical modelling predicts that a softer cortex amplifies the initial imbalance of forces that act on both poles accelerating spindle movement (Chaigne et al., 2013).

2.10. CONCLUSION

Landmark studies performed in invertebrate models of asymmetric division have allowed identification of the evolutionary conserved LGN complex whose specific localization dictates spindle orientation and positioning from worms to higher vertebrates.

In the last years, an increasing amount of investigations have provided further details of how the cortical localization of this complex is regulated. *In vivo* and *in vitro* work in *Drosophila* and vertebrate models of symmetric and asymmetric divisions has uncovered different molecules that regulate this complex at the level of LGN recruitment. More recently, the phosphorylation of NuMA by different kinases has been shown to be critical for its cortical recruitment. These investigations also illustrated that protein orthologues act differently in different models. Finally, elegant experiments performed in human symmetrically dividing cells showed how centrosomes, chromosomes and the central spindle as well as mitotic phosphorylation events control the dynamics of LGN complex assembly in space and time during mitosis. Whether these regulations occur *in vivo* and in highly polarized cells remains to be elucidated.

In addition, recent data demonstrated that many spindle orientation models do not depend on LGN but only on NuMA, pointing NuMA as a central component of diverse spindle orientation pathways.

On the other side, modulation of the actin cortex and astral MT are obvious candidates to regulate spindle orientation. However, a fine understanding of the multiple ways in which these networks regulate spindle orientation has only started to emerge. These studies have revealed that the actin cortex is not just permissive for the correct exertion of forces but specific polarization of the actin network also guides spindle orientation at least in specific contexts. An open question is how the actin cortex interacts with the classical NuMA/dynein pathways during spindle orientation. Concerning astral MT regulation, multiple aspects from their nucleation to their behaviour at the cortex are able to regulate spindle orientation, opening the path for new investigations in the field.

While both the regulation of the actin cytoskeleton and the astral MT still need to find evidence in additional spindle orientation models, this underscores the importance of evaluating how these cellular aspects are modulated when studying the function of particular proteins in oriented divisions.

Furthermore, how the link between the cortical complexes whatever their nature and the astral MT is regulated is much less understood as I will discuss in the following chapter.

Finally, apart from molecules, the geometry of the cell can dictate spindle orientation as proposed a long time ago, and recent investigations have refined this initial observation. Likewise, external forces can modulate spindle orientation at least in specific systems. This highlights the importance of considering these factors when studying the role of specific pathways in spindle orientation.

CHAPTER 3: DYNEIN AND ITS REGULATORS

3.0- MOLECULAR MOTORS

The size and complexity of eukaryotic cells make them dependent on specialized “vehicles” to transport diverse materials -such as vesicles and mRNA- between different organelles and regions of the cell. To accomplish this function, different molecular motors which move along actin and microtubule tracks have evolved in cells. Three different types of motors exist in eukaryotes: Myosins, Kinesins and Dyneins. Myosins use actin filaments as tracks, while Kinesins and Dyneins move along microtubules. Most kinesins move preferentially in the plus end direction of microtubules, while Dynein moves preferentially in the MT minus end direction.

In addition to serve intracellular transport, molecular motors are involved in many other cellular functions requiring force generation, such as spindle formation and chromosome movements in mitosis. In this chapter, I will focus on the Dynein family of molecular motors.

3.1- THE DYNEIN FAMILY

Two main classes of dyneins can be distinguished based on their clearly distinct functions: i) Axonemal dyneins, which are critical for ciliary and flagellar beating, and ii) Cytoplasmic dyneins, which serve diverse cellular processes including intracellular transport, mitosis and cell polarization. Remarkably, while numerous forms of axonemal dynein have been identified, only two forms of cytoplasmic dynein are found in cells (Hook and Vallee, 2006). The most abundant cytoplasmic form is known as Dynein 1, and is present in all MT containing cells. Dynein 1 is critically involved in several cellular functions (Fig.13) (Kardon and Vale, 2009; Roberts et al., 2013), including:

- Transport of Golgi elements, late and recycling endosomes, lysosomes and RNA-protein complexes into the minus end direction of microtubules.
- Nuclear positioning and migration.
- Perinuclear positioning of the Golgi Apparatus.

- Nuclear Envelope breakdown.
- MT capture at the kinetochore, which results in the rapid poleward movement of chromosomes during the alignment process in prometaphase.
- Removal of checkpoints proteins (Spindle Assembly Checkpoint-SAC- proteins) from the kinetochores to poles when sister chromatid pairs become bioriented. This allows silencing the SAC and anaphase initiation.
- Focusing MT (-) ends at the spindle poles.
- Generation of force from fixed sites, e.g. force generation at the cellular cortex during spindle positioning and orientation.

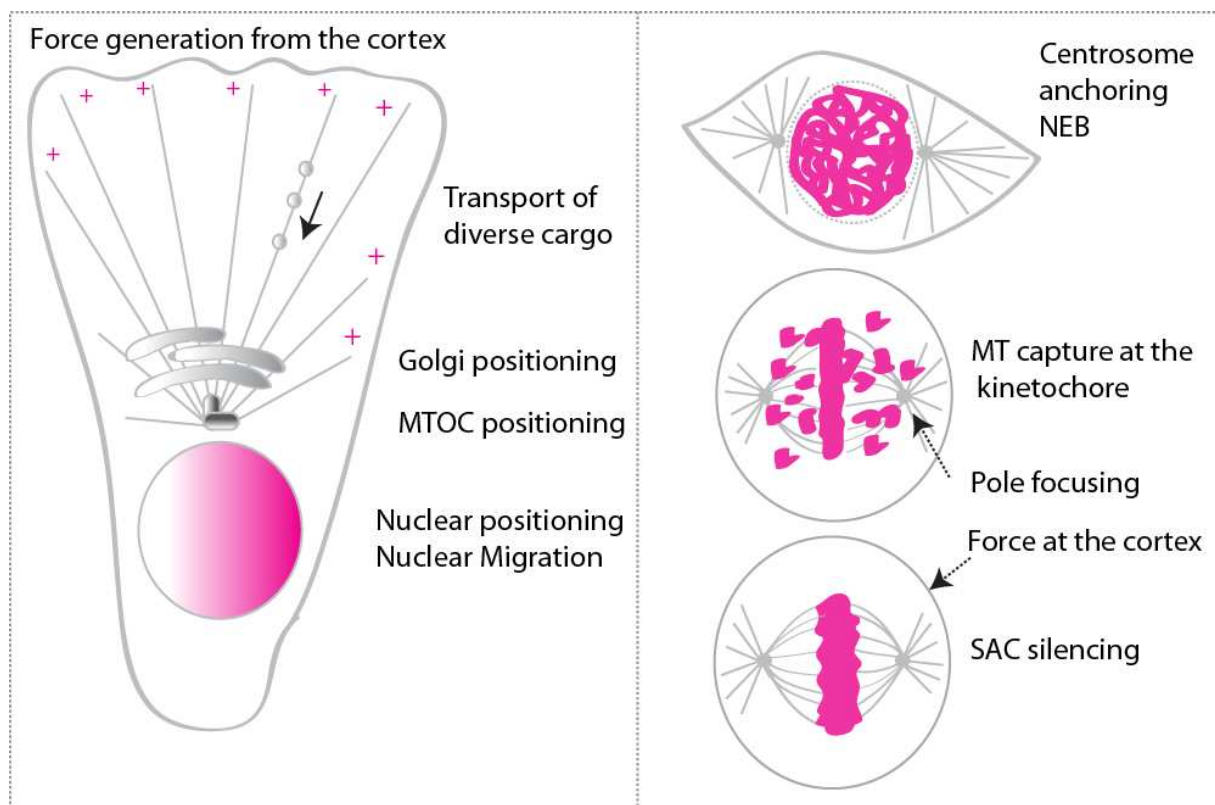


Figure 13: Functions of Cytoplasmic dynein 1 in interphase and mitosis in metazoans.

In contrast, cytoplasmic Dynein 2 is found almost exclusively in cilia and flagella, where it coexists with axonemal dyneins. Dynein 2 is involved in retrograde intraflagellar transport and transport in modified cilia (Mikami et al., 2002; Pazour et al., 1999).

3.1.1 DYNEIN STRUCTURE

Dynein is assembled as a multi-subunit complex of about 1.2 Mda. The Dynein complex is composed of two Heavy chains (DHC), two Intermediate chains (DIC), two Light intermediate chains (DLIC) and three dimers of different light chains (DLC) types: LC8, LC7 or Roadblock, and TCTEX (Chowdhury et al., 2015; Vallee et al., 2012) (Fig.15).

The Dynein Heavy Chains (DHC) are the biggest subunits (~500 kda) and contain the motor domain. The organization of both the motor and non-motor parts of DHC is remarkably well conserved (Hook and Vallee 2006). The DHC assemble as homodimers and present different structural regions (Fig.14) (Carter et al., 2011; Kon et al., 2012; Kon et al., 2011):

- A globular head containing the motor domain (380 kDa), which is composed of an asymmetric ring of six AAA ATPase domains encoded as a single polypeptide (Carter et al., 2011). ATP hydrolysis occurs in three of these domains, hydrolysis at AAA1 being critical for dynein motility (Cho et al., 2008; Kon et al., 2004). In addition, the motor domain is associated with three appendages that project from the globular domain and are important for dynein function: i) the stalk, at whose tip the MT binding domain (MTBD) is found (Carter et al., 2008; Gee et al., 1997; Hook et al., 2009), ii) the buttress, which connects AAA5 with the stalk and may regulate stalk function (Carter et al., 2011; Kon et al., 2011) and iii) the linker, a primary mechanical element of the motor domain implicated in force transduction (Burgess et al., 2003; Roberts et al., 2009). In accordance, the highest sequence conservation within the DHC is found in the motor and linker domains (Hook and Vallee, 2006), more specifically in the boundaries of the linker and the first two AAA domains. Indeed, this area corresponds to the source of dynein force production.
- An N-terminal domain or tail (160 kda) at the base of the molecule, which is involved in DHC homodimerization and serves as a scaffold for the binding of non-catalytic dynein subunits (Chowdhury et al., 2015; Tynan et al., 2000; Urnavicius et al., 2015).

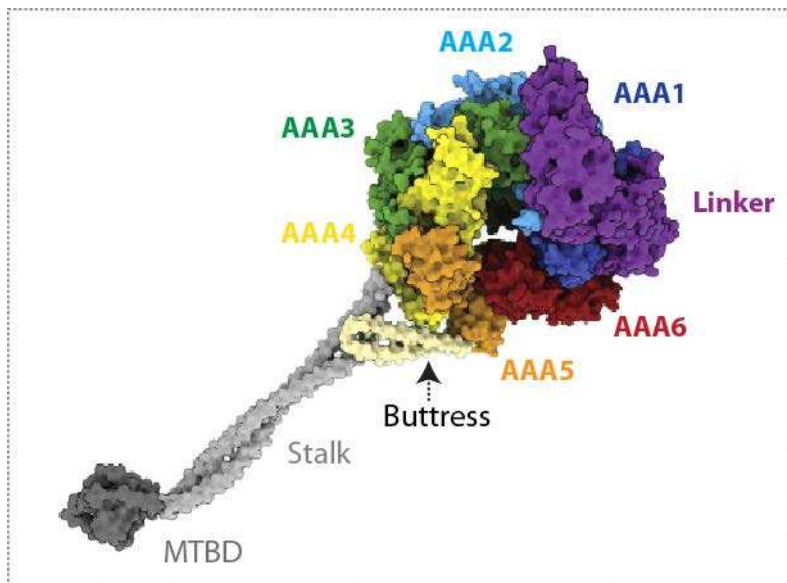


Figure 14- Crystal structure of human dynein 2. The Dynein globular motor domain and its appendages are shown. The position of the linker changes in relation to the nucleotide bound. The configuration shown corresponds to the ATP bound state in AAA1. Adapted from (Bhabha et al., 2016).

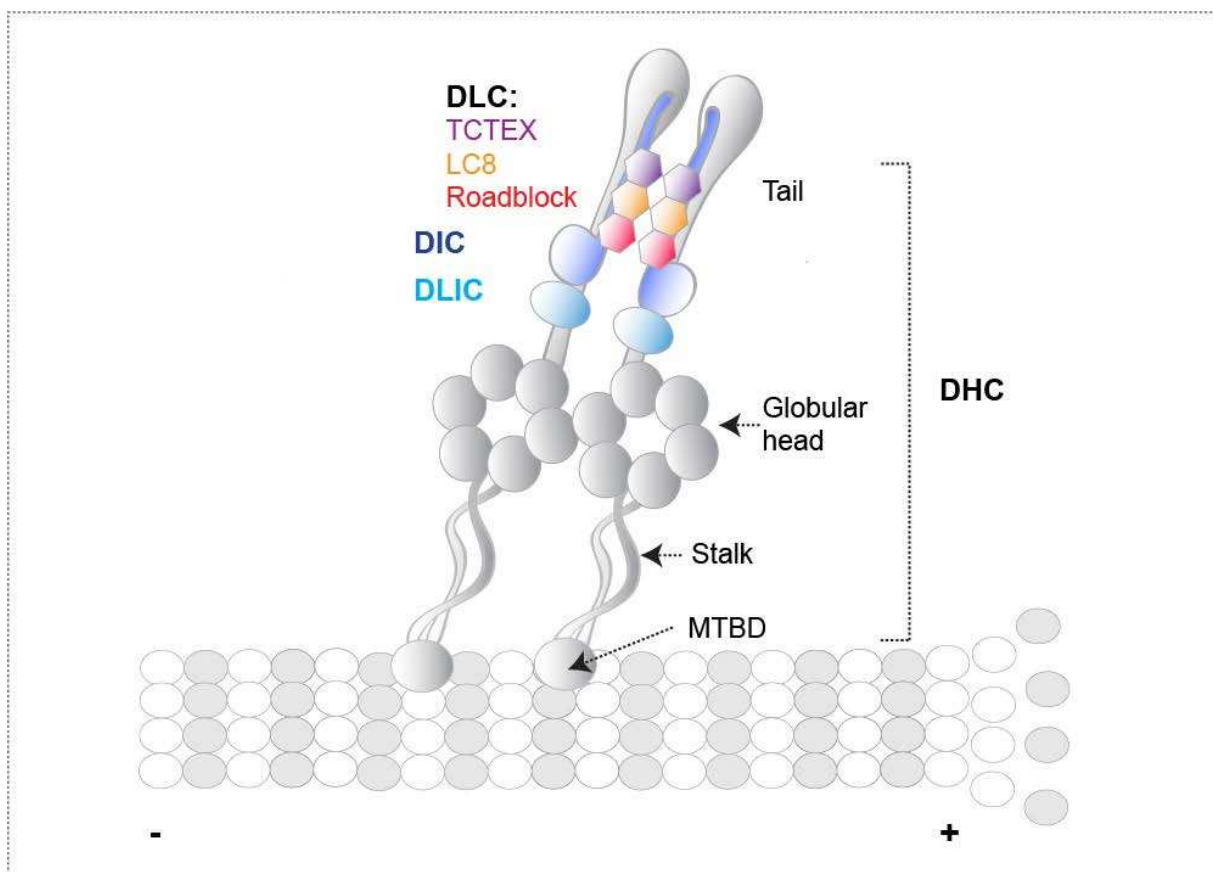


Figure 15: Structure of the Dynein complex, including catalytic and non-catalytic subunits. The main regions of the DHC are indicated.

Concerning the non-catalytic subunits, they all assemble as dimers on the DHC tail. DIC and DLIC bind directly to DHC, while DLC assemble on DIC (Chowdhury et al., 2015; Makokha et al., 2002; Tynan et al., 2000) (Fig. 15). These accessory subunits are not required for dynein activity *in vitro*, but may

serve for dynein activity *in vivo*, as I will discuss later in the manuscript. Interaction studies suggest that non-catalytic subunits link dynein to cargos and adaptors that regulate dynein function.

3.1.2 MOTOR CHARACTERISTICS

Dynein is a processive motor that can undergo μm scale displacements without detaching from MT (King and Schroer, 2000). The speed of movement is of about $0.1 \mu\text{m/s}$ for yeast dynein, and $1\text{-}3 \mu\text{m/s}$ for vertebrate dynein (Vallee et al., 2012), which highlights the need for characterizing the behavior and regulation of dyneins from different species separately. Interestingly, several features related to the stepping behaviour distinguish Dyneins from Kinesins and Myosin motors.

- The size of each dynein step is more variable than in myosin or kinesins. While being in general around 10 nm , both yeast and bovine dynein steps can range from 8 to 32 nm . This step size can vary in response to load, with shorter steps under higher load (Bhabha et al., 2016; Mallik et al., 2004; Reck-Peterson et al., 2006).
- Dynein moves preferentially into the minus end direction of MT. However, this directional bias is less strong than in kinesin and myosin. Yeast dynein steps backwards 20% of the time. In addition, dynein can step sideways (Reck-Peterson, Yildiz et al. 2006).
- Studies of yeast dynein demonstrated that each individual dynein motor domain acts as an autonomous stepper: the two heads step largely independently from each other. In contrast to kinesins, one dynein head can perform consecutive steps before the other head moves (DeWitt et al., 2012; Qiu et al., 2012; Bhabha et al. 2016). This behavior clearly differs from the hand-over-hand stepping observed in the two other molecular motors.

While these detailed characteristics have been obtained from *in vitro* studies of dynein motility, which may differ from dynein behavior in cells, these features could be significant for dynein function in cells. For instance, one could imagine that the higher variability in size stepping and directionality make the dynein molecule more flexible and adaptable to accomplish diverse cellular functions and to work with different adaptors that regulate its function, as discussed below. Furthermore, we could

hypothesize that the dynein stepping behavior is different between different cellular functions. Does the stepping behavior vary between dynein cortical force generation during spindle orientation and dynein long range movement during vesicle transport along MT tracks? During spindle orientation, the cell membrane can be considered as the dynein cargo, which represents a very different load compared to a vesicle. In addition, the fact that dynein contacts the depolymerizing MT end during spindle orientation while dynein displaces far from the MT ends during intracellular transport may have an impact on its way of movement.

Another interesting possibility is that within one single function dynein changes its behavior in relation to the obstacles found, such as the encounter of a kinesin in the way, to which dynein could adapt by stepping sideways, or the dynein distance from their target. While observation of dynein motility is far more complex *in vivo*, it would be interesting to investigate these possibilities in the future.

3.1.3- DYNEIN REGULATION

In order to introduce the complex landscape of dynein regulations, it is worth to start by comparing the dynein family with the myosin and kinesin families. In particular, multiple classes of kinesins and myosins have been identified (at least 14 for kinesin and 17 for myosin) (Hirokawa and Noda, 2008; Krendel and Mooseker, 2005). These different classes are in general associated with distinct cellular functions. In this sense, while the motor domain is highly conserved in kinesins and myosins, a wide range of tail domains allows interaction with different cargos. In marked contrast, only two classes of Dynein exist: axonemal and cytoplasmic ones. Axonemal dyneins and Cytoplasmic Dynein 2 are known to be dedicated to ciliar and flagellar functions (Mikami et al., 2002; Pazour et al., 1999). Remarkably, only one form of Cytoplasmic Dynein (Dynein 1) accounts for a diversity of cellular functions, including all cytoplasmic transport and several mitotic functions, and therefore is associated with multiple subcellular structures. How can one single type of dynein mediate this diversity of cellular activities? The key seems to lie in the regulation of dynein by its multiple

interactors. In other words, differential dynein regulation by non-catalytic subunits and by distinct dynein adaptors would help dynein to accomplish numerous functions.

As mentioned above, DHC interacts with a large assembly of non-catalytic subunits, which have been proposed to be points of attachment for some dynein cargos and dynein regulators. In particular, the Dynein Intermediate Chains (DIC) are known to interact with the dynactin subunit p150 and Nde/L (King et al., 2003; Stehman et al., 2007). Within the dynein light chains, the LL type interacts with the adaptor Bicaudal through its binding partner Egalitarian and with the dynein regulators NDE1 and NDEL1 (Navarro et al., 2004; Stehman et al., 2007).

To date, relatively few studies have addressed the specific role of the non-catalytic subunits in regulating dynein function. Knowledge about the functional role of non-catalytic subunits is sparse, and the contribution of different subunits to each single cellular function has rarely been addressed (Pfister et al., 2006). One of the few exceptions is given by the budding yeast model, where the role of different dynein subunits in spindle positioning has been investigated. Of note, dynein function in yeast is restricted to its role in spindle positioning, as intracellular transport is based on actin tracks. During spindle positioning, both the DHC and the accessory subunits localize to MT+ ends. This localization is a prerequisite for DHC cortical localization and force exertion, as DHC is then loaded from MT+ ends to the cortex (see chapter 2 for more details). Yeast homologues of the DIC (Pac11), DLIC (Dyn3), and DLC (Dyn2) present a dynein-like mutant phenotype, that is, defects in spindle positioning (Geiser et al., 1997; Lee et al., 2005; Moore et al., 2009). Insights into their mechanisms of action showed that DIC/Pac11 is necessary for DHC localization to the MT+ ends, while DLIC/Dyn3 is required for DHC to localize to the cortex (Lee, Kaiser et al. 2005). Finally, mutants for any of the dynein subunits showed defective dynactin targeting to MT+ ends, which might contribute to the phenotypes observed as I will discuss below (Moore et al., 2008).

Furthermore, the role of different dynein subunits in several mitotic functions has been recently examined in human cultured cells. In the table below (table 1), I summarize the requirement for

different dynein subunits in specific mitotic functions as determined by RNAi single knock-down experiments (Raaijmakers et al., 2013).

Function	Dynein subunits required
Pole Focusing	DHC, DIC2, DLC: Roadblock1
Chromosome alignment	DHC, DIC2,DLIC 1/ 2, DLC: Roadblock1
Mitotic progression	DHC, DIC2,DLIC 1/ 2, DLC: Roadblock1
Inward force generation in the spindle	DHC, DIC2,DLIC 1/ 2, DLC: Roadblock1
Centrosome anchoring at Prophase	DHC, DIC2,DLIC 1/ 2, DLC: Roadblock1
DHC Nuclear Envelope localization	DIC2
DHC Kinetochores Localization	DIC2,DLIC 1/ 2, DLC: Roadblock1 and TCTEX1

Table 1: Dissection of the dynein subunits required for different mitotic functions. Based on (Raaijmakers, Tanenbaum et al. 2013)

Thus, this study contributed to the dissection of the different dynein subunits required for numerous dynein mitotic functions. However, several questions remain unanswered. How do these different subunits contribute to each specific cellular function? In this sense, DIC is known to interact with p150, RZZ and NDE/L; accordingly, these regulators are required for at least some of these functions (see below). This suggests that DIC may contribute to dynein regulation by mediating these interactions. However, to my knowledge, no specific interactions have been assigned to DLIC, raising the question of how these chains contribute to dynein function. Finally, it becomes apparent that DIC, DLIC and Roadblock are required for almost all the mitotic functions evaluated. Are they all required for other dynein mitotic functions as well?

As deduced from this section, the dynein complex interacts with different complexes and adaptors which indeed regulate dynein function. In the next section, I focus on the different dynein regulators and on how they regulate dynein function in specific cellular contexts.

3.2- DYNACTIN

Dynactin (name derived from “Dynein activator”) has been proposed as being necessary for nearly all cellular functions of cytoplasmic dynein. In particular, dynactin has been shown to regulate dynein targeting to specific locations, as well as to link dynein to cargos and to modulate dynein processivity as I will detail below. In this section I aim to give a complete view of the dynactin structure, its interaction with dynein and its specific functions, which I consider relevant in the frame of my results.

3.2.1-DYNACTIN STRUCTURE

Dynactin is a multisubunit complex of 1 MDa, composed of eleven types of subunits. Its structural and compositional complexities suggest that dynactin function might be tightly regulated by its different components and interactions. Different structural domains can be recognized in the dynactin complex (Schroer, 2004; Urnavicius et al., 2015). In particular, dynactin is composed of an actin-like 40 nm filament of Arp1 subunits, which is capped at both ends by different sub-complexes, in analogy with actin filaments. In addition, a shoulder/arm region projects from the filament near its barbed end (Fig. 16).

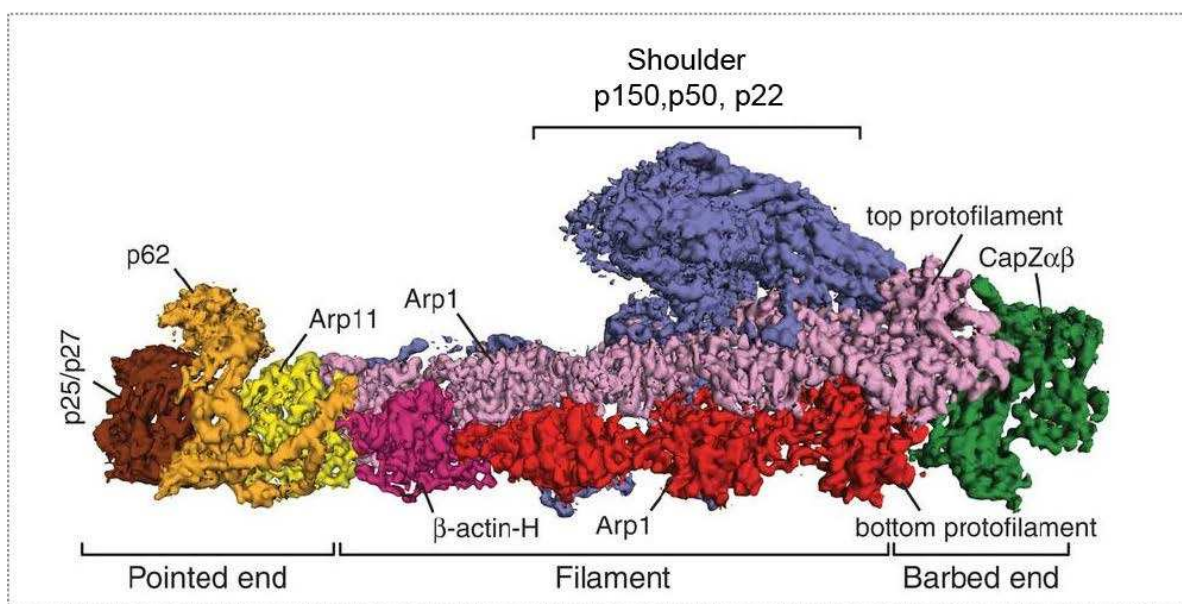


Figure 16: Structure of the Dynactin complex as determined by cryoEM. Adapted from (Urnavicius et al., 2015).

SHOULDER/ARM

The shoulder/arm region is composed of a dimer of p150 subunits, a dimer of p22 and four p50 subunits (Figs. 16, 19). The p150 dynactin subunit presents distinct domains that mediate interactions with different cellular components. At its N-terminal portion, a CAP-Gly domain interacts with MT (MTBD), while its C-terminal domain interacts with the Arp1 filament. The CAP-Gly domain is necessary for dynactin localization to MT+ ends in mammalian cells. In the middle region, a domain of interaction with the Dynein Intermediate Chains is found (Schroer, 2004).

Recent cryo electron microscopy analyses have allowed to obtain a detailed structure of native mammalian dynactin molecules (Chowdhury et al., 2015; Urnavicius et al., 2015), fig. 16). Most p150 is contained in the projection arm; hence, the shoulder is mainly composed of p50 and p22 subunits. The shoulder is formed by two identical arms and it is symmetric until it contacts the Arp1 filament where its symmetry is broken. P150 enters the shoulder between the two arms. Interestingly, extended regions from the shoulder expand the length of the dynactin filament, contacting every Arp1 subunit. These regions may correspond to the N-terminal domain of p50, and are proposed as a mechanism to specify the size of the dynactin filament (Urnavicius et al., 2015)

ARP1 FILAMENT

The high resolution structure has allowed obtaining details on the composition and structure of the dynactin filament and its associated complexes. The Arp1 polymer presents a two stranded helical organization, with four subunits in one strand and five in the other strand. The two strands wraps around each other. The filament contains one single actin protomer that lies at the pointed end of the four strand polymer. As mentioned before, the dynactin filament is similar to an actin filament, which goes in accordance with the high sequence homology between β -actin and Arp1 (Urnavicius et al., 2015).

At its barbed (+) end, a heterodimer of the actin capping proteins CAPZ-A and B caps the structure (Schroer, 2004). Indeed, in the high resolution dynactin structure, helices corresponding to the α and

β tentacles (the C-terminal regions) of CAPZ-A and CAPZ-B are seen bound to the first Arp1 in each filament strand at the barbed end (Urnavicius et al., 2015). The CAPZ A/B heterodimer interacts with the dynactin complex in the same way as proposed for the actin filament (Narita et al., 2006; Urnavicius et al., 2015). However, the interaction modes present some differences. In particular, Arp1 contains a loop where four negative residues are found. These residues are close to four positive residues in CAPZ-A (Fig. 17). In contrast, the actin loop contains one single negative residue. Interestingly, these observations predict that CAPZ-A/B binds to Arp1 with higher affinity than to actin (Urnavicius et al., 2015). This goes in accordance with the fact that a pool of CAPZ A/B remains bound to dynactin but not to actin upon CAPZ RNAi treatment (Cheong et al., 2014). Of note, the tight binding of CAPZ A/B to dynactin suggests a role for the heterodimer in stabilizing the dynactin complex (Urnavicius et al., 2015).

At the opposite (-) end of the dynactin filament, a complex of Arp11, p62, p25 and p27 subunits forms the pointed end complex (Schroer, 2004). In particular, Arp11 contacts protomers of both filament strands (which are Arp1 and actin), and is proposed to prevent further subunit addition by sterically blocking this end (Urnavicius et al., 2015). While in the pointed end additional subunits are found, the only one seen as capping the filament is Arp11, suggesting that p25, p27 and p62 have a different role. P25 and p27 contact Arp11 while p62 wraps around the contact site of Arp11, p25 and p27 (Fig.16). Of note, some fungal species express Arp11 but lack p25, p62 and p27 (Hammesfahr and Kollmar, 2012).

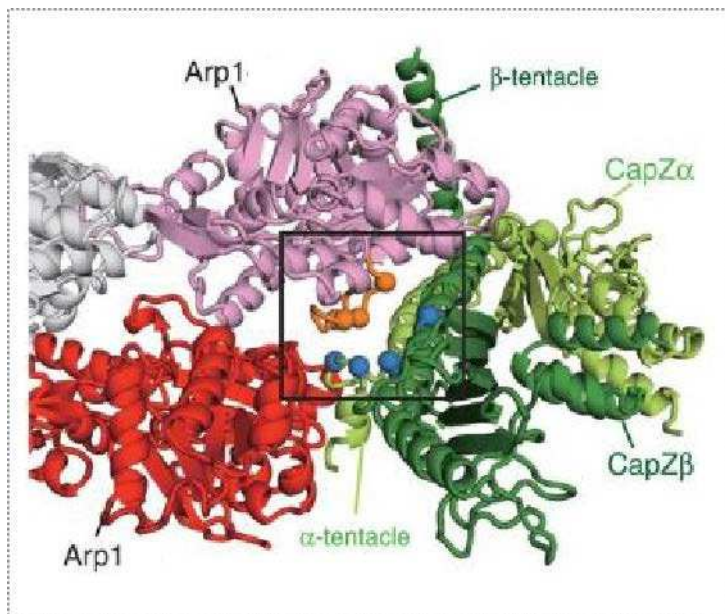


Figure 17: Model for the interaction between the CAPZ A/B heterodimer and the Arp1 filament barbed end. The residues proposed to be involved in the tight interaction are shown in the square. Picture extracted from (Urnavicius et al., 2015).

3.2.2- DYNACTIN INTERACTION WITH DYNEIN

Twenty years ago, different studies demonstrated an interaction between p150 and DIC, which has prevailed in the field as the interaction connecting dynein and dynactin for many years (Karki and Holzbaur, 1995; King et al., 2003; Vaughan and Vallee, 1995). However, recent cryo electron microscopy data allowed demonstrating a second site of interaction between the dynein and dynactin complexes. In particular, in purified complexes of dynein tail, dynactin and the dynein adaptor Bicaudal 2, Urnavicius and colleagues observed that the dynein tail interacts with the dynactin filament from the β -actin subunit to the barbed end (Fig. 18). Interestingly, the sites of contact between the DHC and the Arp1 filament are proposed as equivalent to the myosin binding sites on actin. Of note, the authors suggested that the flexible dynein motor domains lie close to the barbed ends based on the projection of a Dynein-Dynactin-Bicaudal complex (Urnavicius et al., 2015). In contrast, the pointed end complex lies at the opposite side of the motor domain, which is compatible with the proposed function for this complex as a cargo adaptor (see section 3.2.4). Noteworthy, the newly described interaction is stabilized by Bicaudal 2, which is necessary for dynein-dynactin complex stability at least *in vitro*. Finally, concerning the function of this novel

interaction, the authors proposed that it allows reorientation of the DHC and activation of the motors though the *in vivo* functional significance of this interaction remains to be elucidated.

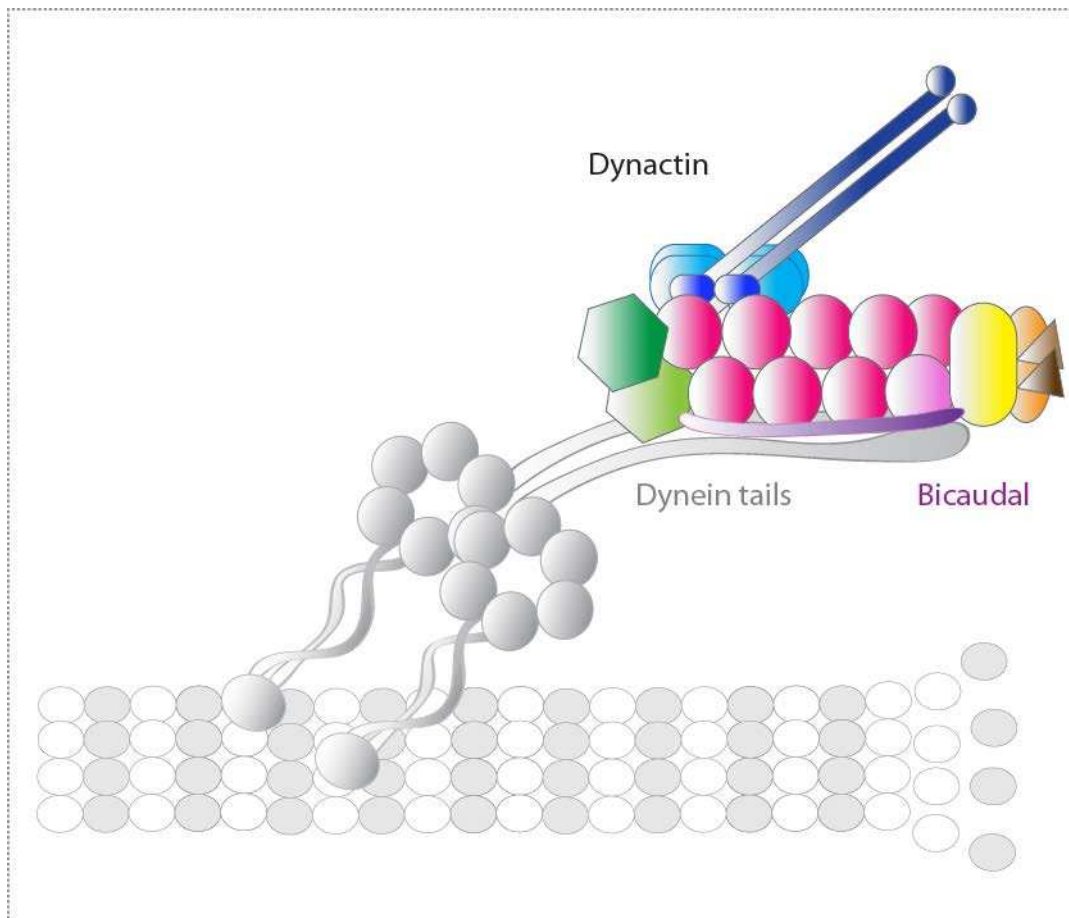


Figure 18: Interaction of Dynein –Dynactin when bound to MT. Schema based on (Chowdhury et al., 2015) model.

Likewise, Chowdhury and colleagues obtained a detailed structure of the dynein-dynactin-Bicaudal complex bound to MT, observing a similar interaction between the dynein tail and the Arp1 filament. Accordingly, the dynein accessory subunits are exposed which would allow cargo binding (Fig. 18). Intriguingly, the shoulder/arm of dynactin which contains a MTBD on p150 is located in the opposite site to MT in the structure described (Chowdhury et al., 2015). This last observation is of particular interest in the frame of contradictory results availing or not the requirement of the p150 MTBD for dynein activity modulation (see 3.2.3).

Importantly, the occurrence of this novel interaction does not prevent the interaction between p150 and the DIC assembled on the dynein tail (Chowdhury et al., 2015; Urnavicius et al., 2015). In this sense, the high flexibility of the p150 projection arm would allow the interaction between p150 and the DIC to occur in a configuration like the one described.

3.2.3- FUNCTIONS OF DYNEIN ASSISTED BY DYNACTIN

Dynactin is often considered as essential for all dynein functions. However, in the context of this manuscript, it is worth to detail the specific functions and contexts in which dynein function requires dynactin, as well as the approaches employed to propose those functions. In the following table I summarize the context/cellular function studied as well as the level of dynein regulation and dynactin subunit/domains implicated. Of note, dynactin function in metazoan spindle orientation will be specifically discussed in section 3.5.

Level of dynein regulation	Context/model	Dynactin subunit/domain	Experimental approach	Refs
Targeting of Dynein to MT+ ends	Nuclear positioning during hyphae growth/ <i>Aspergillus Nidulans</i>	p150/CAP-Gly domain Arp1	Mutation of dynactin subunits	(Xiang et al., 1994; Zhang et al., 2003; Xiang et al., 2000)
Transfer of Dynein from MT+ ends to cell cortex (offloading model)	Cell division/spindle positioning/ <i>S.cerevisiae</i>	p150/CAP-Gly domain p50 p22 Arp1	Deletion/Mutation of Dynactin subunits	(Moore et al., 2008)
Cargo transport: Targeting dynein				
Localization of dynein to MT+ ends for cargo transport	Cargo transport/certain Metazoans Contradictory data: cargo transport in HeLa, S2 and Xenopus cells is not affected in CAP-Gly mutants	p150/CAP-Gly domain	Mutation of CAP-Gly domain	(Kardon and Vale, 2009)
Linking Dynein to cargos for transport initiation	ER to Golgi dynein mediated transport	p150 →regulatory GTPases	OE p150-C: inhibits delivery of proteins from ER to Golgi	(Watson et al., 2005)

		P150-C → SEC 23		
Linking Dynein to cargos for transport initiation	Transport of late endosomes	P150-C → RILP (Rab7 GTPase effector)	Recruitment of p150 to Late endosomes by OE RILP (in dynactin dissociation conditions)	(Johansson et al., 2007)
Linking Dynein to cargos for long range transport	<i>In vitro</i> liposomes transport/transport of late endosomes?	Arp1A → βIII spectrin (present in Golgi and other vesicles)	<i>In vitro</i> reconstitution of liposomes transport using purified components/βIII spectrin shRNA	(Holleran et al., 2001; Johansson et al., 2007; Muresan et al., 2001)
Targeting Dynein to Golgi	ER to Golgi transport/ Cultured vertebrate cells	?	p50 Overexpression (dissociation of Arp1 filament from p150)	(Roghi and Allan, 1999)
Not determined; Dynein targeting to virus not affected	Human cells/Virus transport by Dynein	P150-N term	-P50 Overexpression -Mutant Δp150 N term	(Bremner et al., 2009)
<i>In vitro</i> dynein movement				
Dynein processivity (positive regulation)	<i>In vitro</i> dynein movement.	p150-N: -CAP-Gly -Basic domain (→MT) <u>Conclusion:</u> Dynactin considered as a tether between Dynein and MT, preventing Dynein from diffusing away from MT.	1)-Bead adsorbed with dynein: movement on MT. - Addition p150/ Ab αp150 N-term: effect suppressed 2) TIRF to follow movement of mammalian Dynein- p150 complexes /truncated constructs	1)(Culver-Hanlon et al., 2006; King and Schroer, 2000) 2)(Ayloo et al., 2014)
Dynein processivity (positive regulation)	<i>In vitro</i> movement of mammalian Dynein vs Dynein-Dynactin+adaptor	-Dynein alone is not processive - Dynactin dependent increase of dynein processivity depends on the presence of adaptors which increase dynein affinity for dynactin (BICD2, Spindly)	TIRF to follow movement of purified complexes on MT-(Single molecule motility)	(McKenny et al. 2014)

Dynein processivity (positive regulation)	- <i>In vitro</i> transport of purified recombinant proteins from <i>S.cerevisiae</i>)	- Dependent of p150 N-term coiled coil and Arp1. - Independent of p150 MTBD: <u>Conclusion:</u> Dynactin regulates Dynein processivity in a different manner	- <i>In vitro</i> single molecule motility assays. - Complexes dynein-dynactin - Truncated forms	(Kardon et al., 2009)
Mitotic functions				
Kinetochores dynein targeting	Human cells/ mitosis	p150, Arp1A, p50, p22, p62, p25	RNAi	(Raaijmakers et al., 2013)
Mitotic progression	Human cells/ mitosis	p50, p22, Arp1A, p62	RNAi	
Nuclear Envelope Dynein targeting	Human cells/ prophase	p150, p50, p62	RNAi	
Centrosome anchoring to Nuclear Envelope	Human cells/prophase	p150, p22, Arp1A, p62, p25, p27	RNAi	

Table 2: Dynein functions assisted by dynactin as determined by *in vitro* or *in cellulo* studies. Arrows indicate demonstrated interactions. Grey arrows indicate weaker interactions than black arrows, which is relevant for a model of dynactin-dynein interaction during transport initiation vs long range transport (see below).

Of note, most of the studies addressed the role of p150 in regulating dynein function. One interesting exception is given by the function of dynactin in linking dynein to cargos. It has been proposed that p150 interaction with receptors like the regulatory GTPase SEC23 is needed for transport initiation while the interaction of Arp1 with β III spectrin would be important during long range transport from ER to Golgi. Consistently, p150 – SEC23 interaction is weaker than Arp1- β III interaction in support of this model. In the same line, sequential recruitment of dynactin by p150-RILP interaction followed by Arp1- β III spectrin interaction has been proposed to mediate transport of late endosomes (Holleran et al., 2001; Johansson et al., 2007; Muresan et al., 2001; Watson et al., 2005). The function of different dynactin subunits will be further discussed in the next section.

From this table I conclude that both *in cellulo* and *in vitro* studies support a role for dynactin in targeting dynein to cargos and different cellular structures during intracellular transport and mitosis. Of note, the modulation of dynein processivity by dynactin has been only demonstrated *in vitro*. As

perturbing dynactin function primarily seems to affect dynein localization, demonstrating that dynactin also modulates dynein activation in cells could prove more difficult.

3.2.4- FUNCTION OF INDIVIDUAL DYNACTIN SUBUNITS

The constant and complex composition of native Dynactin suggests that each of its subunits are important for dynactin structure and function itself and/or for directly modulating dynein activity. It should be noted, however, that many studies consider only p150 as the working subunit, while other studies are based in the overexpression of p50 which destroys the complex and alter dynein related functions in an unknown manner.

Knowledge about the specific role of the different dynactin subunits other than p150 is limited. As mentioned above, Arp1 would mediate the dynein-dynactin interaction with β III spectrin rich vesicles during transport. In this sense, it is tempting to speculate that Arp1 could mediate dynactin-dynein interaction with other types of spectrins present in different cell membranes. In addition, the recently discovered interaction between the dynein tail and the Arp1 filament probably plays a role in regulating dynein function. Interestingly, yeast dynactin lacking Arp1 is unable to stimulate dynein processivity *in vitro* (Table 2, Kardon et al., 2009). On the other side, the pointed end complex composed of Arp11, p62, p25 and p27 has been proposed to be important for cargo targeting. In particular, depletion of p25 or p27 perturbed the motility and distribution of early and recycling endosomes in COS-7 cells. Accordingly, dynactin levels in isolated membranes were diminished in those depletion conditions (Yeh et al., 2012).

However, multiple questions remain unanswered. How do the multiple dynactin subunits contribute to each specific dynein function and in what manner? Are there subunits essential for specific functions and dispensable for others? Does dynactin contain subunits totally dispensable for its function? How do the different subunits act together to regulate dynactin stability, localization, interaction with dynein and modulation of dynein targeting and activation? Efforts to characterize all these aspects upon individual subunit depletion in a single context could help provide answers to

these questions. In this sense, a fine dissection of the role of individual dynactin subunits in modulating dynein function has been performed in the context of spindle positioning in yeast (Moore et al., 2008, see section 2.9). *S. cerevisiae* homologues have been described for all the dynactin subunits except for the pointed-end components p62, p27 and p25. The yeast protein Arp10 can be considered as a member of the Arp11 family, and it also interacts with the pointed end of the Arp1 filament. However, while the homologues of p150, p50, p22 and Arp1 are required for dynein function in spindle positioning, the Arp11 homologue seems dispensable (Kahana et al., 1998; Moore et al., 2008; Muhua et al., 1994). More specifically, Moore and colleagues observed all these dynactin subunits to localize with dynein to spindle pole bodies (SPB), MT+ ends and cortical foci, dynein being necessary for this localization. In turn, dynactin is necessary for the transfer of dynein from MT+ ends to the cortex, since dynactin mutants showed accumulation of dynein to the MT+ ends (Moore et al., 2008). In addition, these authors studied the interdependence between the different subunits for their localization at MT+ ends and SPB which I summarize in the next table:

Mutant					
Localization ↓	p150	p50	P24	Arp1	Arp10
P150	NA	+++	+++	+++	+++
P50	-	NA	-	MT + ends: + SPB: -	+++
P24	-	-	NA	-	+++
Arp1	-	+	+	NA	MT+ ends:+++ SPB: ++
Arp 10	-	+	+	-	NA

Table 3: Interdependence of dynactin subunits for their localization to MT+ ends and SPB.

From this table, it becomes apparent that p150 and Arp1 are essential for localizing the rest of the dynactin complex to MT+ ends and spindle pole bodies. Finally, biochemical analyses of dynactin complex composition in different mutants led to the conclusion that all three components of the shoulder/arm (p150, p50 and p22) are required for optimal stability of the shoulder. In addition, the shoulder complex is important for the association of Arp1A with p150 (Moore et al., 2008).

In summary, p150 and Arp1 are critical for targeting of the entire complex to MT+ ends, while p50 and p22 seem to regulate the stability of the complex in yeast. Concerning their role in dynein regulation, depletion of any of these dynactin subunits compromised dynein targeting from MT+ ends to the cell cortex, explaining their phenotypes in spindle positioning in this context (Moore et al., 2008; Sheeman et al., 2003). Whether dynactin regulates dynein function at other levels such as its activation remains elusive in this context.

Furthermore, recent work by Raaijmakers and colleagues (Raaijmakers et al., 2013) demonstrated the role of specific subunits of Dynactin (p150, p50, p22, Arp1, p25, p62) in several mitotic functions of Dynein in human cells. As shown in table 2 (bottom part), some subunits of this subset are necessary for specific mitotic functions but not for others, revealing specific roles for each subunit instead of a general requirement of the same set of subunits for all dynactin/dynein mitotic functions.

What are the roles of different Dynactin subunits in regulating Dynactin/ Dynein function in mitosis? While depletion of shoulder/arm subunits mutually affects the levels of each other, depletion of Arp1 does not affect the levels of shoulder/arm subunits, suggesting that Arp1 filament is indeed important for dynactin mitotic function itself rather than for complex subunits stability. This is interesting in the frame of the recent data demonstrating Dynein interaction with the Arp1 filament. Alternatively, interactions of Arp1 with other cellular components as proposed for the intracellular transport of vesicles (see table above) could be necessary for regulation of dynein function. Finally, disruption of dynactin structure by depletion of Arp1 may affect the localization/function of individual dynactin components.

The mechanism of action of additional subunits of dynactin such as p62, p25 and p27 remains also unclear in mitosis. Individual depletion of these subunits results in partial reduction of Arp1 protein levels, which could indirectly affect dynactin function. Similarly, p62 depletion perturbed dynactin integrity in COS-7 cells (Yeh et al., 2012). Finally, none of the pointed and barbed ends capping factors (Arp11, CAPZ A/B) are essential for the mitotic functions studied. This is somehow

contradictory to the structural data proposing these subunits as stabilizers of the complex and raises the question of the role of these components in this complex. In Fig.19, I summarize the different interactions and functions proposed so far for each specific dynactin subunit by *in vitro* and *in cellulo* studies.

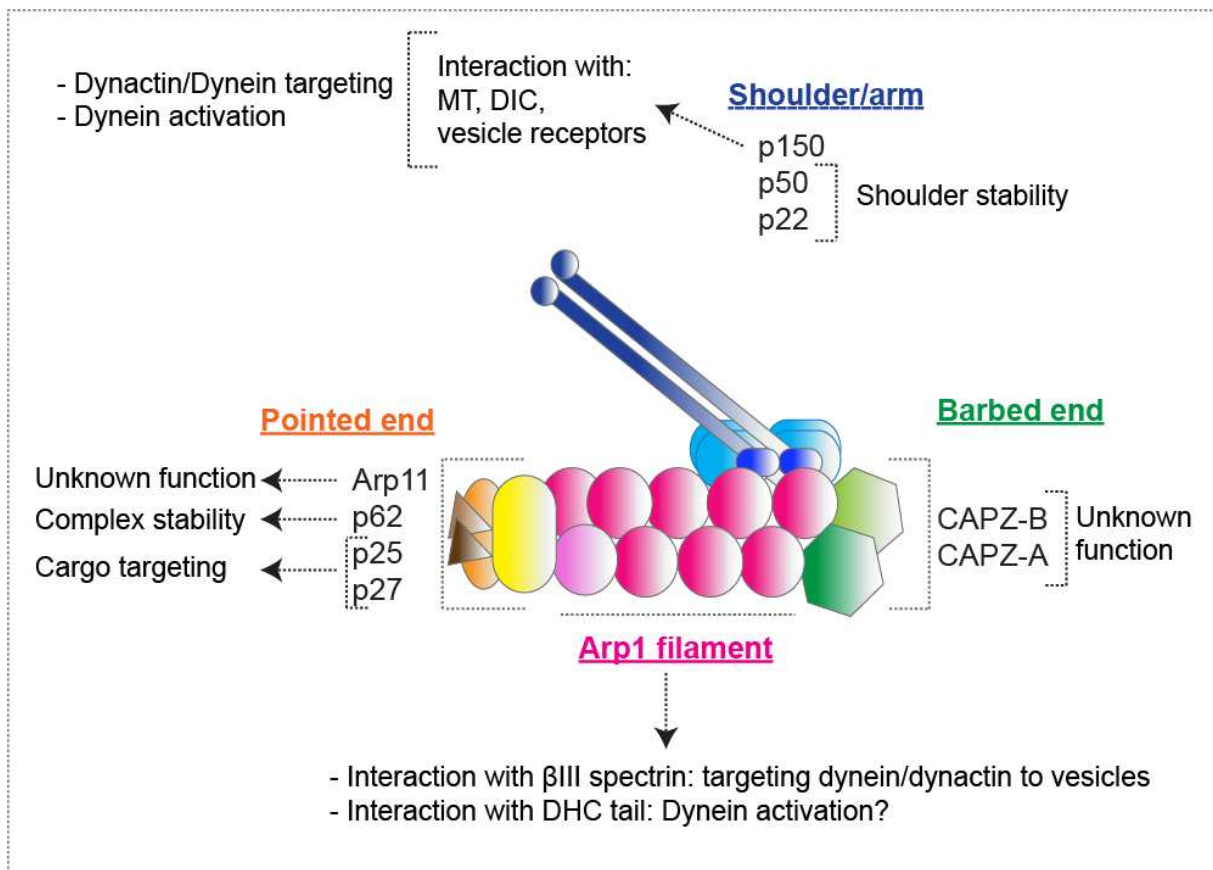


Figure 19: Schema of the dynactin complex specifying proposed functions and interactions for individual subunits.

In addition, Raaijmakers and colleagues observed that dynactin was not necessary for force generation in the spindle as they observed no phenotypes in pole focusing or inward force generation upon dynactin subunit depletion. Therefore, dynactin would not be required for modulating dynein activation at least in these processes (Raaijmakers et al., 2013). Whether dynactin serves to activate dynein in other cellular functions remains to be elucidated. In addition, much evidence point dynactin as a targeting factor at least in the contexts evaluated so far.

In conclusion, different levels of dynein regulation by dynactin (targeting vs. activation) have been observed in different *in vitro/in cellulo* contexts, in interphase and mitosis. In addition, the dissection of the contribution of specific dynactin subunits to dynein functions has only started to emerge, and shows that specific subunits are required for specific cellular functions but not for others. This highlights the importance of understanding how dynactin and its subunits regulate dynein during each specific cellular function.

3.3-LIS1/NDE1/NDEL1

LIS1 (for Lissencephaly 1), NDE1 (Nude1) and NDEL1 (Nude Like1) are known as general regulators of dynein function. Organisms with loss of function of any of these three proteins present similar phenotypes (see table 4). Studies in fungi and metazoans species have shown that these proteins regulate dynein function during nuclear and spindle positioning, kinetochore function and organelle and mRNA transport (see table below). NDE and NDEL are highly homologous proteins. Fungi contain only one gene expressing NDE while metazoans contain both homologues (Feng et al., 2000; Niethammer et al., 2000).

3.3.1-STRUCTURE AND INTERACTION LIS1- NDE1/NDEL1-DYNEIN

LIS1, NDE1/NDEL1 and dynein colocalize at Kinetochores, centrosomes, cell cortical regions and at the Nuclear Envelope. NDE/NDEL interacts both with Dynein through DIC and DLC LC8 and with LIS1. The ability of LIS1, NDE1/NDEL1 and dynein to form a triple complex and their sites of interaction, suggests that NDE1/NDEL1 recruits LIS1 to the dynein complex and help it to localize close to the motor domains, which has found support in recent *in vitro* experiments (McKenney et al., 2010). Accordingly, LIS1 is proposed to directly interact with the AAA1 subdomain of the Dynein Motor subunits (Sasaki et al., 2000; Tai et al., 2002). In addition, an interaction between the N-terminal region of NDE1/NDEL1 and the dynein motor domain of DHC has also been proposed but not yet proven (Sasaki et al., 2000).

In terms of structure, LIS1 is a dimer of subunits containing LIS-homology, coiled-coil and WD40 repeat domains, the latest including the sites for NDE/NDEL and dynein binding (Vallee et al., 2012). NDE and NDEL also assemble as homodimers and contain domains for interaction with Dynein at the N and C termini and with LIS1 (Sasaki et al., 2000). In contrast to dynactin, neither LIS1 nor NDE/NDEL contains microtubule binding domains.

3.3.2-FUNCTIONS OF DYNEIN ASSISTED BY LIS1/NDE1/NDEL1

In the following table I summarize numerous dynein functions requiring LIS1 and NDE/NDEL both in interphase and mitotic cells.

Level of Dynein regulation	Context/model	Protein	Experimental approach	Refs
Localization of Dynein to MT+ ends and cell cortex	Nuclear positioning/ <i>S.cerevisiae</i>	LIS1/Nde homologues LIS-CLIP170 interaction possibly involved	Δ LIS, Δ NudEL homologues	(Lee et al., 2003; Li et al., 2005)
Release of dynein from MT+ ends, Dynein motility towards (-) ends	Nuclear distribution/A <i>Nidulans</i>	Nde, NdeL homologues	LOF NDE, NDEL homologues	(Kardon and Vale, 2009)
Targeting dynein to membranes				
Dynein recruitment to membranes	Organelle transport /Neurons-HeLa	NDEL/ NDEL1 LIS1	NdeL blocking antibody. RNAi	(Lam et al., 2010; Zhang et al., 2009)
- Localization of Dynein to cell cortex, idea mainly based on observation of LIS1 at the cellular cortex (Cockell et al., 2004; Faulkner et al., 2000; Swan et al., 1999). However, there are no known receptors for LIS1-Nde/L1 - Possibly other levels of regulation	MTOC positioning - Nuclear positioning- Neuronal migration- interkinetic nuclear movements/ Metazoans	LIS1-NDE LIS1-NDEL	OE, mutants, RNAi	(Feng et al., 2000; Shu et al., 2004; Tanaka et al., 2004; Tsai et al., 2005)

Dynein activation				
Dynein motor activity	<i>In vitro</i> : recombinant LIS1 and NDE1, purified vertebrate dynein	<ul style="list-style-type: none"> - LIS1 alone: Increase MT-Dynein interaction. Persistent force dynein state. - NDE1 alone: Decrease MT dynein interaction. Decrease dynein force production - LIS1 + NDE1: Increase duration of MT-Dynein interaction under load 	<i>In vitro</i> : MT-dynein interaction assay Dynein adsorbed to beads-single molecule tracking: Evaluation of force (optical trapping)	(McKenney et al., 2010)
Modulation of Dynein ATPase activity	<i>In vitro</i> : recombinant LIS1 and NDE1, purified vertebrate dynein	LIS1: stimulation LIS1 and Ndel: inhibition of MT-stimulated ATPase activity.	<i>In vitro</i> enzymatic assay	(McKenney et al., 2010; Mesngon et al., 2006)
Mitotic functions				
KT dynein targeting	Mitosis/ Human cells	LIS1, NDE1/NDEL1	RNAi	(Raaijmakers et al., 2013)
Mitotic progression	Mitosis/Human cells	LIS1, NDE1/NDEL1	RNAi	
Localization of Dynein to Nuclear Envelope	Mitosis prophase/ Human cells	LIS1	RNAi	
Centrosome anchoring to Nuclear Envelope	Mitosis Prophase/Human cells	LIS1	RNAi	
Spindle Pole focusing	Mitosis/Human cells	LIS1, NDE1/NDEL1	RNAi	
Chromosome alignment	Mitosis/Human cells	LIS1, NDE1/NDEL1	RNAi	
Inward force generation in the spindle	Mitosis/Human cells	LIS1, NDE1/NDEL1	RNAi	

Table 4: Functions of Dynein assisted by LIS1 and/ or Nde/NdeL as determined by *in vitro*, *in cellulo* or *in vivo* studies.

In summary, both LIS1 and Nde/L1 are proposed to function as targeting factors and regulators of Dynein activation. With regard to this second function, the interaction of LIS1/NDE1/L1 with the dynein motor domain positions these factors as good candidates to be general regulators of dynein activation (Sasaki et al., 2000). Indeed, recent *in vitro* observations demonstrated the regulation of dynein force by both factors (McKenney et al., 2010). Moreover, depletion of LIS1 or NDE/L generates defects in spindle pole focusing and inward force generation, that is, processes requiring dynein force production in the spindle. Targeting of dynein to the spindle, while not quantified, does

not seem much affected in these depletion conditions. This also favors the idea that these factors regulate dynein activation (Raaijmakers et al., 2013).

3.4- BICAUDAL D

Bicaudal D (BICD) is a metazoan specific dynein adaptor that links dynein to its cargoes. Mammals have two BICD homologs, BICD1 and BICD2 as well as two related proteins named BICDR-1 and BICDR-2 (Hoogenraad and Akhmanova, 2016). Bicaudal is involved in vesicle transport from ER to Golgi and within the Golgi Apparatus in mammalian cells; in this context, interaction of Bicaudal with cargoes may occur through its membrane receptor Rab6 (Kardon and Vale, 2009; Matanis et al., 2002). In addition, Bicaudal participates in MT organization in cultured mammalian cells (Fumoto et al., 2006), nuclear positioning in *Drosophila* (Swan et al., 1999), and localization of dynein at the nuclear envelope in mitotic prophase in human cells (Raaijmakers et al., 2013).

Moreover, Bicaudal is involved in Dynein mediated localization of mRNA in the oocyte and during embryo development in *Drosophila*. In this context, overexpression of BICD or its binding partner Egalitarian increases the transition of mRNA transport from MT (+) to (-) ends, which led to the idea that BICD could activate dynein motor activity (Bullock et al. 2006). Similarly, overexpression of BICD 2 or BICDR1 in HeLa cells increases the velocity of Rab6-GFP vesicles movement in a dynein dependent manner. The effect of BICDR1 was more important than the one of BICD2, while no difference in dynein recruitment between the different overexpression conditions were seen. This suggested that BICD2 and BICDR1 modulate dynein motility during transport of Rab6 vesicles (Schlager et al., 2014). This idea is supported by the recently observed interaction between the Dynein tail and Dynactin filament which is in turn proposed to help dynein activation, and requires the presence of BICD in the complex (Urnavicius et al., 2015). However, it should be noted that dynein force production in the spindle do require neither BICD2 nor dynactin (Raaijmakers et al., 2013) which suggests that the contribution of BICD2 in activating dynein might be context dependent.

3.5 RZZ COMPLEX AND SPINDLY

The RZZ complex (composed of ROD, ZW10 and Zwilch) and Spindly are dynein adaptors mainly known for their functions at the kinetochore (KT) where they work by docking dynein and other adaptors. In particular, the RZZ complex recruits dynein and SAC (Spindle assembly Checkpoint) proteins to the KT in *C. elegans* and human cells (Gassmann et al., 2008; Raaijmakers et al., 2013). Depending on the model, Spindly also recruits dynein and SAC proteins to the KT (both in *C.elegans*, and only dynein in human cells) and participates in the removal of dynein (in *C.elegans*) and SAC proteins (in S2 cells) from the KT when sister chromatids become bioriented (Chan et al., 2009; Kardon and Vale, 2009). In accordance, depletion or mutation of Spindly results in chromosome misalignment in *C. elegans* and human cells, chromosome missegregation in *C.elegans* and mitotic progression defects in human cells (Chan et al., 2009; Gassmann et al., 2008; Raaijmakers et al., 2013).

In addition, ZW10 localizes at the ER in interphase and participates in Golgi and endosomes dynein dependent - transport independently of the rest of the RZZ complex (Hirose et al., 2004).

3.5- THE DYNEIN FAMILY IN SPINDLE ORIENTATION IN METAZOANS

Mitotic spindle orientation relies on cortical force generators that exert forces on astral MT. Pioneer studies in yeast demonstrated the role of Dynein in spindle positioning (Li et al., 1993)-see section 2.9, 3.1.3 and 3.2.4) making dynein a good candidate for those cortical force generators. In yeast, dynein function is restricted to the process of spindle positioning, facilitating the analysis of dynein family mutants in this cellular process. However, important mechanistic differences in spindle positioning (see section 2.9) as well as in the composition and regulation of the dynein family (Moore et al., 2008; Moore et al., 2009) between yeast and higher eukaryotes make it difficult to transpose the available knowledge on yeast to metazoans models.

In the last twenty years, a number of studies have contributed to prove the role of dynein in spindle positioning and orientation in higher eukaryotes. Mc Grail and colleagues studied the role of the

dynein heavy chain (DHC) in spindle orientation in germline cell divisions in *Drosophila* (McGrail and Hays, 1997). In this context, spindles are usually oriented and anchored to the fusome, a spectrin rich multivesicular structure found in these cells. In the dynein mutant, spindles did not contact the fusome and were randomly oriented. In addition, dynein was seen enriched in the fusome area specifically in mitosis, and each spindle pole was associated with this enrichment in the control situation. These data suggested the involvement of dynein in mediating spindle anchoring to the fusome (McGrail and Hays, 1997). However, the dynein mutation also induced defects in the fusome, making the interpretation of these data more difficult.

First evidence for the cortical localization of dynein in higher eukaryotes comes from work performed in MDCK epithelial cells. In these cells, the spindle is oriented in parallel to the plane of the monolayer when cultured in 2D. In this context, Busson and colleagues observed lateral cortical patches of the Dynein Intermediate Chain subunit and the Arp1 dynactin component, both in prometaphase and metaphase cells. Interestingly, the authors observed astral MT contacting the cortex at the dynein/dynactin spots. In addition, in fully polarized MDCK cells cultured in 3D, the dynactin staining was restricted to the lateral domain below tight junctions and aligned with the spindle axis (Busson et al., 1998). These data, together with the fact that dynein cortical staining is seen from prometaphase, i.e. before the spindle finds its final orientation, suggested a potential role for cortically localized dynein in epithelial spindle orientation (Busson et al., 1998). Dynein localization at the cortex has since been demonstrated in several models (e.g. Kiyomitsu and Cheeseman, 2012; Kotak et al., 2012; Williams et al., 2011).

3.5.1-FUNCTION OF DYNEIN IN SPINDLE ORIENTATION IN *C.ELEGANS* AND *DROSOPHILA*

Initial studies in *C.elegans* embryos, showed endogenous DHC to localize to the mitotic spindle in one cell embryos and to the cell boundaries in 2 cell-embryos, suggesting DHC enrichment at the cortex (Gonczy et al., 1999). In the same study, RNAi partial depletion of DHC impaired the centration and rotation of the centrosome pairs and the pronuclei associated before mitosis, resulting in spindle

orientation perpendicular to the anterior-posterior axis in one cell embryos (Gonczy et al., 1999). Likewise, depletion of p150 or p50 dynactin subunits resulted in similar phenotypes (Gonczy et al., 1999; Skop and White, 1998). In addition, depletion of p150 or p50 induced spindle misorientation in the P1 blastomere in two cell- *C.elegans* embryos. Moreover, the spindle was seen aligned to the p150 sites of enrichment in the cell-cell contacts in wild type P1 blastomeres (Skop and White, 1998).

Further and formal demonstration of the involvement of cortical dynein in exerting forces on the spindle comes from different studies performed in the context of spindle positioning in the *C.elegans* zygote (Couwenbergs et al., 2007; Nguyen-Ngoc et al., 2007). Nguyen-Noc and colleagues used temperature sensitive mutants of DHC1 to circumvent the lack of spindle assembly in DHC1 mutants. Upon temperature shift, the authors observed defects in the length of spindles, the oscillations of the posterior spindle pole and the peak pole velocities in laser severing experiments (see section 2.1). All these defects are hallmarks of defective pulling forces exerted on the spindle, suggesting that dynein is required for generating these forces (Nguyen-Ngoc et al., 2007). In addition, partial depletion of LIS1 resulted in similar defects than DHC1 mutation. Moreover, co-immunoprecipitation analyses demonstrated that LIS1 interacts with LIN5 and GPR1/2, which allowed to establish the link between the dynein complex and the cortical anchors. Accordingly, Gai, GPR 1/2 and LIN-5 were required for dynein cortical localization in the *C.elegans* zygote. Of note, in contrast to the asymmetric localization of GPR 1/2 and LIN-5, DHC is uniformly localized along the cortex in these embryos, suggesting that an asymmetry in the activation of dynein would be at the base of the asymmetry of cortical force generation observed in these embryos (Nguyen-Ngoc et al., 2007).

In parallel, Couwenbergs and colleagues studied the role of *dyrb1* (the unique dynein light chain of the roadblock family in nematodes) in force generation in the *C.elegans* zygote. DsRNA mediated depletion of *dyrb1* resulted in delayed rotation of the pronucleus-centrosome, shorter spindles and diminished spindle oscillations at the posterior pole (Couwenbergs et al., 2007). However, depletion of *dyrb1* does not impair spindle formation suggesting that dynein function is only partially

compromised upon removal of *dyrb1*. Importantly, depletion of *dyrb1* reduced the peak velocities of both the anterior and posterior poles in laser ablation assay. In addition, both genetic and biochemical interaction between *dyrb1*, *LIN-5* and *GPR1/2* demonstrated that these proteins act in the same pathway to regulate force generation in the *C.elegans* zygote. Intriguingly, depletion of *LIN5* or *GPR 1/2* did not affect the cortical localization of *dyrb1-gfp* (Couwenbergs et al., 2007), in contrast to what was observed for DHC localization (Nguyen-Ngoc et al., 2007).

On the other side, in *Drosophila* neuroblasts, Siller and Doe demonstrated that *LIS-1* and the dynactin subunit *Glued* (the *Drosophila* p150 homologue) regulate spindle alignment with respect to the cortical polarity axis in metaphase cells. Moreover, by live imaging analyses, the authors showed that astral MT dependent-spindle oscillations observed in wild type neuroblasts were suppressed in *LIS-1* mutants. This suggested that *LIS-1* controls the forces exerted on astral MT (Siller and Doe, 2008). However, in contrast to other models, neither *LIS1* nor *Glued* have been detected at the cell cortex or at astral MT in neuroblasts (Siller et al., 2005). Finally, *LIS1* and *Glued* mutants showed wild type spindle orientation in telophase suggesting that independent pathways exert forces on the spindle rescuing its orientation during late mitosis.

3.5.2- FUNCTION OF DYNEIN IN SPINDLE ORIENTATION IN VERTEBRATE CULTURED CELLS

In the last years, a number of studies have addressed the role of dynein or its regulators in vertebrate spindle positioning and orientation, by mainly using cultured cells. As a first approach, Kotak and colleagues have shown that artificial dynein targeting all around the cellular cortex induces excessive spindle rotation suggesting that force generation exerted by dynein can control spindle movements in HeLa cells. In addition, these authors showed that DHC siRNA results in mild but significant defects in spindle orientation with respect to the growth surface (Kotak et al., 2012). Later on, different groups showed that depletion of DHC or the dynactin subunit p150 induces defects in xy spindle orientation with respect to the adhesion pattern in cells cultured on micropatterns (Kiyomitsu and Cheeseman, 2012; Tame et al., 2014). Of note, micropattern guided-spindle orientation is partially

controlled by the motor Myosin 10 which links subcortical actin clouds to astral MT (Fig.20) (see section 2.5) (Kwon et al., 2015). How does dynein contribute to spindle orientation in this context? Does it help establishing the initial orientation or is it mainly necessary to maintain spindle orientation once it is established? In this sense, dynein has been seen to polarize into two cortical crescents already in early prometaphase in cells cultured on bar micropatterns, and later spindle rotation aligns the spindle axis with these crescents (Fig. 20). This suggests that dynein participates in establishing spindle orientation in this context (Tame et al., 2014), and that its localization is not merely established by the position of the chromosome plate downstream of the RAN^{GTP} inhibition of

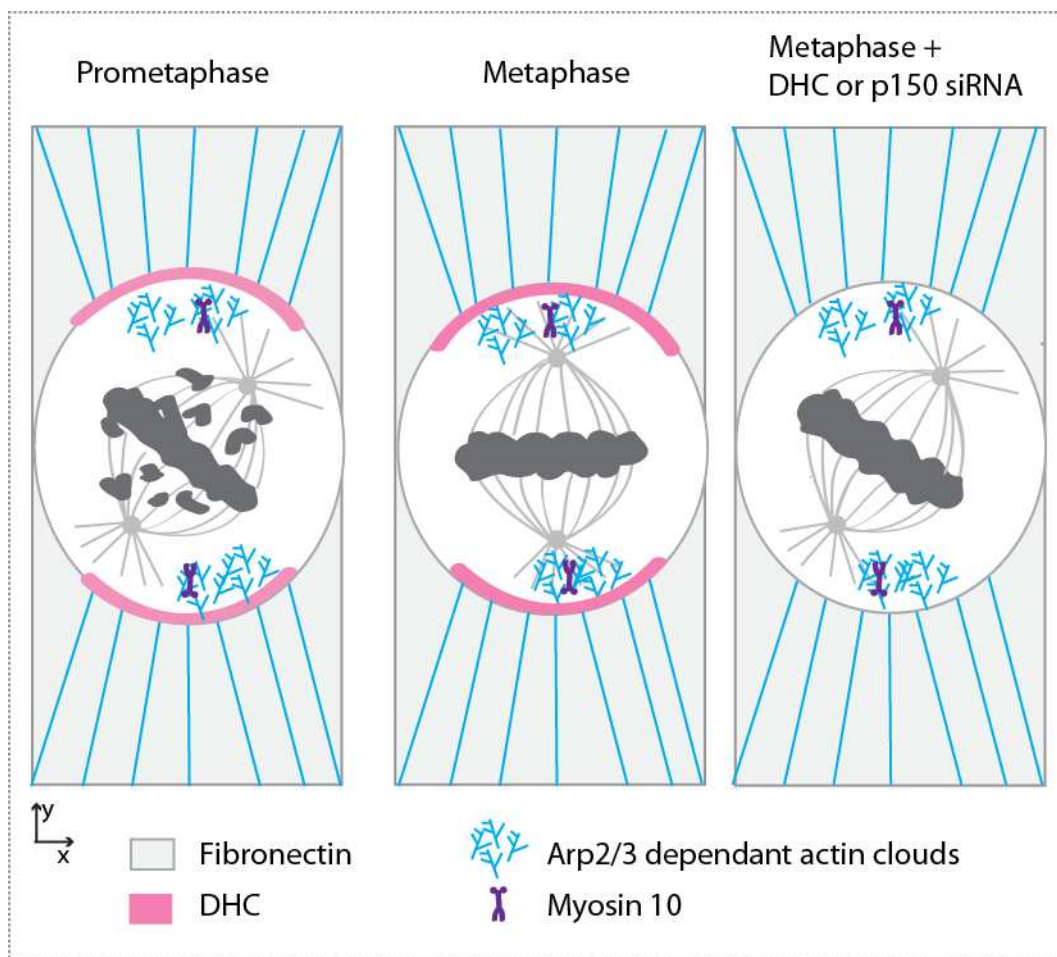


Figure 20: Summary of the experiments investigating the DHC function using HeLa cells and the micropattern-guided spindle orientation model.

LGN-NuMA as discussed in chapter 2. In addition, in HeLa cells expressing DHC-GFP, the spindle continuously moves towards single DHC-GFP crescents in a very dynamic manner (Kiyomitsu and Cheeseman, 2012) further supporting the role of dynein as a cortical force generator capable of positioning the spindle.

Moreover, the role of a few dynein regulators has been investigated in independent studies based on the widely used model of spindle orientation with respect to the substrate. From these studies we will learn how different aspects of the spindle orientation machinery can be affected by depletion of different dynein regulators leading to spindle misorientation in a context where the force generation machinery is only mildly enriched in the cellular cortex.

In particular, Dunsch and colleagues studied the role of the Dynein Light Chain DYNLL1 in spindle orientation. Depletion of the DYNLL1 misorients the spindle with respect to the substrate in metaphase HeLa cells (Dunsch et al., 2012). In contrast to DHC, DYNLL1 does not localize to the cell cortex but only to the mitotic spindle, where it is necessary for spindle orientation. In the same line, DYNLL1 forms specific complexes with dynein subunits and other spindle adaptors, but not with dynactin or NuMA. Concerning its mechanism of action, the loss of DHC-GFP asymmetry observed upon depletion of DYNLL1 led the authors to propose that DYNLL1 acts as by displacing dynein complexes from the cortex (Dunsch et al., 2012). However, how symmetrizing dynein can result in spindle misorientation in the xz plane remains unclear. Considering DYNLL1 as an inhibitor of DHC cortical localization, one possibility is that upon DYNLL1 depletion, the DHC cortical domain broadens in the z axis. In turn, a broader DHC domain along the z axis could result in spindle rotation and misorientation in that axis.

Furthermore, LIS1 is critically involved in spindle orientation. LIS1 was first seen to regulate spindle orientation in mouse neural progenitors *in vivo* (Yingling et al., 2008). Further studies performed in mitotic MEFs allowed to clarify the precise role of LIS1 in mitosis (Moon et al., 2014). LIS1 localizes to

spindle MT and to the spindle poles and it regulates spindle orientation with respect to the substrate (Moon et al., 2014). In particular, decrease in LIS1 levels reduced the length and density of astral MT (Fig. 21) (Moon et al., 2014; Yingling et al., 2008). The authors proposed that interactions between the cortex and astral MT are impaired. Indeed, dynamic analysis of EB3 comets during metaphase showed that less astral MT reached the cortical area in LIS1 mutant cells. This, together with the decrease in dynactin cortical levels observed in depletion conditions would lead to spindle misorientation. However, decreased LIS levels also generate abnormal spindle poles due to an increased number of centrosomes which cluster together in the two spindle poles (Moon et al., 2014), which could affect astral MT nucleation and anchoring. As discussed in section 3.3.2, LIS1 is necessary for numerous mitotic functions of dynein (Raaijmakers et al., 2013), which is probably at the base of the phenotypes observed in LIS1 mutants. LIS1 has been shown to function as a dynein motor activator (McKenney et al., 2010), but whether LIS1 regulates dynein motor activation specifically at the cortex remains to be elucidated.

Furthermore, the dynein adaptor Spindly, which is mainly known as a regulator of kinetochore function, has been shown to regulate spindle orientation in different models (Fig. 21) (Chan et al., 2009; Tame et al., 2016). Spindly localizes to kinetochores but also to the spindle poles before chromosome alignment (Chan et al., 2009). Depletion of spindly in human cells generated spindle misorientation with respect to the substrate (Chan et al., 2009) and with respect to the adhesive substrate in cells cultured on bar micropatterns (Tame et al., 2016). While Spindly is required for dynein/dynactin localization to KT (Chan et al., 2009), it does not appear to control the cortical recruitment of p150 and DHC (Chan et al., 2009; Tame et al., 2016). Instead, spindle misorientation defects upon Spindly depletion are indirectly generated by the chromosome misalignment phenotype related to Spindly KT function. In line with this, different conditions generating chromosome misalignment resulted in spindle misorientation in single cells cultured on micropatterns. Remarkably, in chromosome misalignment conditions, LGN localization is inhibited in cortical sites near unaligned chromosomes. Live analyses showed that upon being delocalized near

chromosomes, LGN accumulates in other cortical regions, which is followed by spindle rotation in the direction of LGN patches. This behavior would then explain the spindle misorientation phenotypes observed. In addition, LGN cortical delocalization has been seen to be mediated by kinetochore localized Plk1, which is high when chromosomes are misaligned (Tame et al., 2016). In conclusion, Spindly depletion results in spindle misorientation through an indirect effect on LGN cortical localization generated by a chromosome misalignment phenotype (Fig. 21)

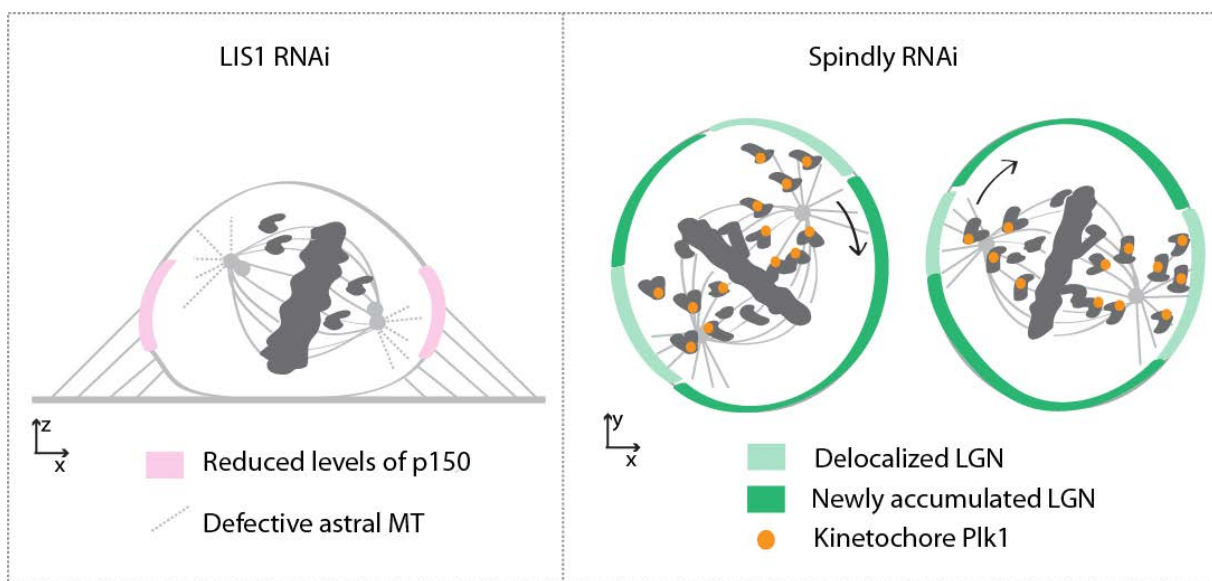


Figure 21: Cellular phenotypes involved in spindle misorientation generated by LIS1 or Spindly depletion.

Finally, Morris and colleagues have recently proposed an alternative complex for the recruitment of cortical dynein and the control of spindle orientation with respect to the substrate. This complex involves the integrin receptor and the integrin partner ILK (Integrin linked kinase) which localize to the border of the basal membrane in mitosis (Morris et al., 2015). ILK interacts with the dynactin subunits p150 and p50, and it is necessary for p50 recruitment to the basal membrane (Fig. 22). Of note, p50 depletion (which affects the stability of the dynactin complex (Raaijmakers et al., 2013)) resulted in significant but mild phenotypes on spindle orientation in the xz plane, suggesting that other pathways might be controlling spindle orientation in this context.

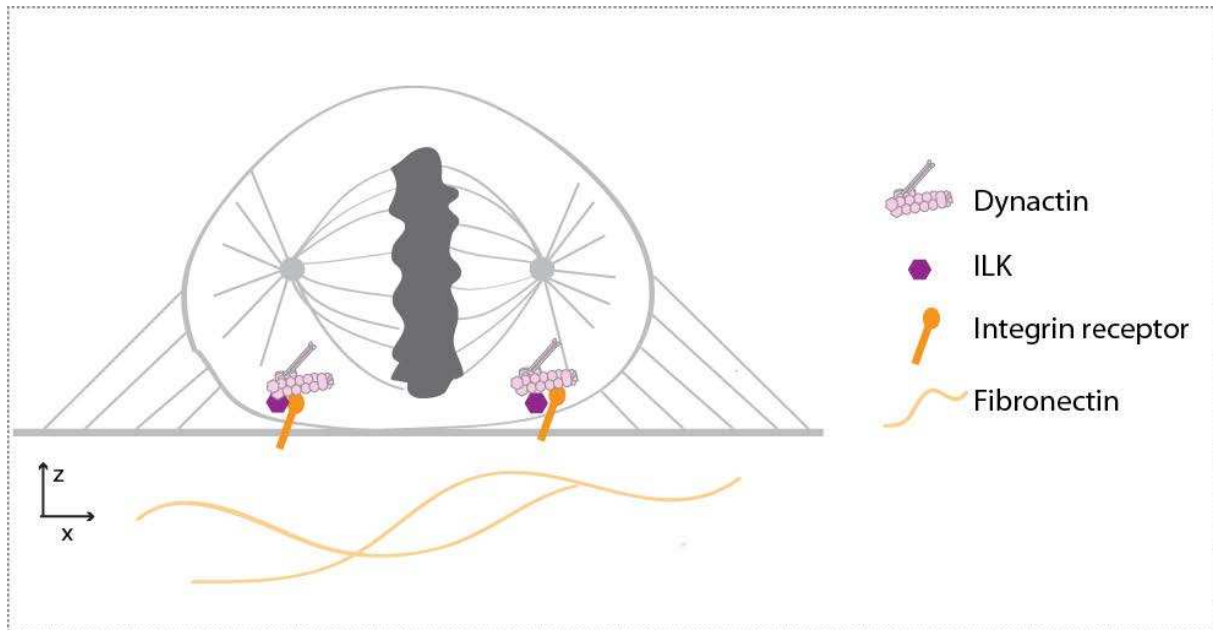


Figure 22: Integrin receptor and ILK recruit dynactin to the basal membrane, which is necessary for spindle orientation with respect to the growth surface

3.5.3- FUNCTION OF DYNEIN IN VERTEBRATE SPINDLE ORIENTATION *IN VIVO*

As mentioned in the previous section, a role for LIS1 in spindle orientation has been demonstrated in mouse neural progenitors *in vivo* (Yingling et al., 2008). Similarly, mitotic spindle orientation is defective in cortical progenitors of Nde1 knock out mice (Feng and Walsh, 2004). However, the mechanisms by which Nde1 depletion generates spindle misorientation remain unclear. Notably, multiple mitotic defects are observed in Nde1 knock out mice, including chromosome misalignment and progenitor mitoses occurring away from the ventricular surface, defects that could contribute to spindle misorientation. Concomitantly, expression of dominant negative forms of Nde1 in 293T cells induced mitotic arrest, aberrant spindles and chromosome misalignment, though the extent of the effects is unclear. These observations, together with the fact that Nde1 localizes to the spindle poles, suggest that Nde1 acts primarily by regulating spindle assembly, and thus spindle functioning (Feng and Walsh, 2004). Again, a specific role for Nde1 in regulating cortical dynein dependent forces remains to be determined.

Finally, during mouse skin stratification, p150 localizes to the apical cortex in mitotic cells dividing with an apico-basal orientation, in a similar pattern to LGN (Williams et al., 2011). Concomitantly, *in*

vivo knock-down of p150 in mouse skin impairs spindle orientation of basal progenitors during stratification. Of note, depletion of LGN, NuMA or p150 in this context affected primarily spindle orientation along the apico-basal axis, as a bias towards planar angles in angle distributions is observed in depletion conditions (Williams et al., 2011). This suggests that additional mechanisms control planar divisions in this context as discussed in chapter 2.

3.6- CONCLUSION

The dynein complex and its regulators are essential for several cellular functions. Both Dynactin, LIS/NDE/L and the other adaptors are recognized as critical for targeting dynein to specific cellular locations in interphase and/or mitosis. Whether this targeting function applies to the mitotic cellular cortex and thus to spindle orientation is not fully understood. Moreover, activation of dynein by Dynactin or LIS1 has been only proven *in vitro*, raising the question of whether this type of regulation is necessary for dynein function in cells, and if the case, if this applies to cortical dynein activation during spindle orientation. In addition, specific dynein related molecules have been seen to control spindle morphology and chromosome alignment, which indirectly impacted spindle orientation at least in the contexts evaluated.

Furthermore, while a detailed and vast knowledge on the structure and subunit composition of the dynein family and regulators is available, much less is known about the specific role of different subunits in each specific cellular function. In this sense, studies comparing the contribution of different subunits and regulators to specific cellular functions are sparse, and the understanding of the mechanisms of action of individual subunit is still limited.

CHAPTER 4: THE ACTIN CAPPING PROTEINS CAPZ- A/B (CP)

The actin capping protein (CP) was discovered and defined for its ability of capping the barbed ends of actin filaments. CP was called β -actinin when first characterized and purified from muscle in the 1960s and 1970s (Cooper and Sept, 2008; Maruyama, 2002). CP purified from skeletal muscle was called “CapZ” because of its presence at the Z-disc of the sarcomere (Casella et al., 1987). In addition, non-muscle CP was purified from *Acanthamoeba* in 1980 and shown to cap barbed ends (Isenberg et al., 1980). Remarkably, CP is found in essentially all eukaryotic organisms and every metazoan cell type (Cooper and Sept, 2008).

4.1- CAPZ A/B ISOFORMS AND STRUCTURE

CP is an A/B heterodimer with each subunit having a mass of 30 kDa. Homologs of both subunits exist in vertebrates, invertebrates, plants, fungi and protozoa. In vertebrates, the sequence similarity between the A and B subunits is very low. In contrast, when comparing the individual subunits in different organisms, sequence similarity is much higher. Interestingly, the sequence of the B subunit is more strongly conserved than that of A subunit. The regions of conservation and variability are localized in a complementary manner on the two subunits. This gives rise to an inherent asymmetry in the heterodimer where the half of the molecule containing the body of the B subunit and the actin binding C-terminal region of the A subunit is more conserved than the half containing the A subunit body and the B C-terminal region (Fig. 23) (Cooper and Sept, 2008).

Organisms other than vertebrates have single genes encoding each CP subunit. In contrast, vertebrates present two somatically expressed isoforms of each subunit and one male germ-cell specific isoform (Hart et al., 1997; Hurst et al., 1998; Schafer et al., 1994b; von Bulow et al., 1997). For the A subunit, the somatic isoforms, A1 and A2, are encoded by different genes (Cooper et al., 1991), while the B subunit isoforms are produced from a single gene by alternative splicing (Schafer et al., 1994b). The sequences of both the A1 and A2 and B1-B2 isoforms are conserved across vertebrates suggesting that they have distinct functions (Hart et al., 1997). Both the A1 and A2

isoforms were detected in brain, heart, liver, ovaries, testes, skeletal muscle, uterus, spleen, kidney and lung tissues. However, the ratio A1: A2 varies between tissues. In testes and uterus, A1 is more abundant than A2 while in brain and in skeletal muscle A2 is more abundant than A1. In heart and liver, the levels of A1 and A2 are similar (Hart et al., 1997). The B1 isoform is located specifically at the Z-disc of the sarcomere of striated muscle; while B2 is the predominant form in non-muscle tissues (Schafer et al., 1994b).

4.1.2-STRUCTURE OF CAPZ A/B HETERODIMER

Most of the structural information about the capping proteins A/B concerns the heterodimer and its interaction with the actin filaments, as this is the function more widely associated with these proteins. The A and B subunits have very similar secondary structures, in spite of the low sequence similarity (Cooper and Sept, 2008).

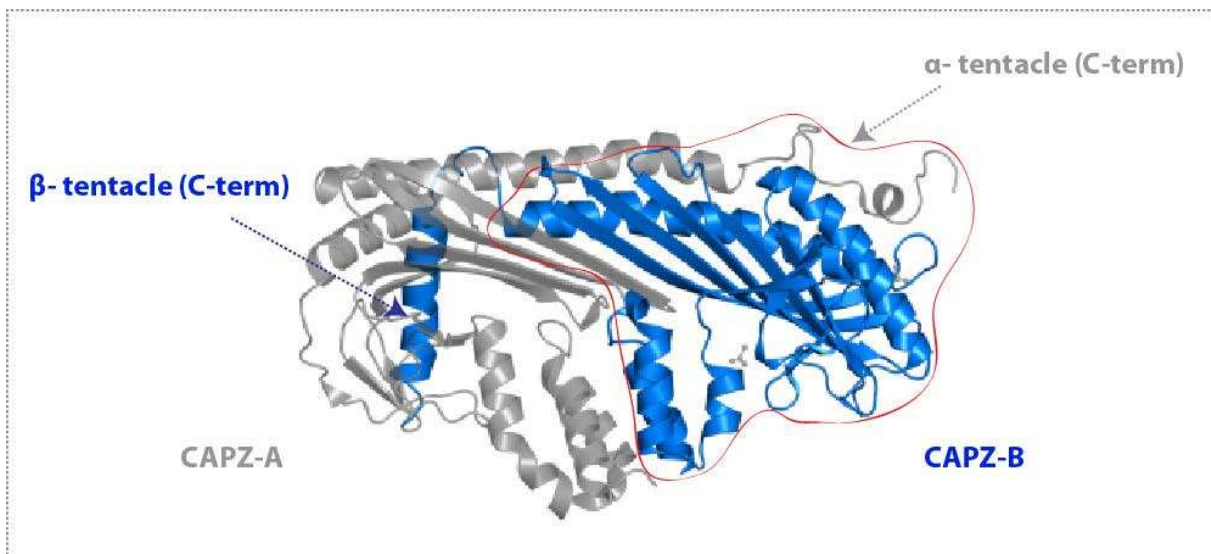


Figure 23: Structure of the CAPZ A/B heterodimer. The region delimited by the red line (including parts of CAPZ-A and B subunits) is more conserved than the rest of the heterodimer. Image adapted from: <http://www.ebi.ac.uk/pdbe>.

The x-ray crystal structure of chicken CP A1/B1 showed that the molecule has the shape of a mushroom (Yamashita et al., 2003a). The N-termini of the subunits are located at the base of the mushroom stalk, and the subunits are intertwined, with a large β -sheet at the core of the mushroom

cap structure. On the top surface of the mushroom, both subunits have C-terminal amphipathic α -helices (or tentacles) which are important for high affinity actin capping (Fig. 23) (Wear et al., 2003).

4.1-3- STRUCTURE OF THE CP BOUND TO ACTIN

Early cryo-electron microscopy analyses have allowed obtaining of a low resolution (23 Å) structure of CP bound to the barbed end of actin filaments (Narita et al., 2006). The A and B subunits are unambiguously identified in this structure. The position of the subunits with respect to the actin protomers suggests that the body of the B subunit, together with the C-terminal of the A subunit establish the primary contacts with the last actin protomers of the filament. This finding is supported by the sequence conservation observed in each subunit region. In addition, the C terminus of the B subunit can bind to a hydrophobic cleft on the actin subunit (Cooper and Sept, 2008; Kim et al., 2010). These observations led to the proposition of a model in which CP binds to the actin filament in two steps: first, by the C-terminus of the A subunit and surrounding residues, and second, by the flexible C-terminus of the B subunit (Narita et al., 2006). This raises the possibility that once CP is bound to the barbed end of the actin filament, it remains only associated by the B subunit tentacle, allowing the CP body to move in place.

4.2- CAPZ A/B ACTIN CAPPING ACTIVITY *IN VITRO*

The presence of CP at the barbed end inhibits the addition and loss of actin subunits at that end. CP binds to the barbed end of the actin filament with high affinity, generally less than 1 nM (Cooper and Sept, 2008; Wear et al., 2003). One molecule of CP appears to be sufficient to bind and attach a filament barbed end to a glass surface, based on direct observation of single actin filaments by light microscopy, and recent TIRF microscopy studies (Bearer, 1991; Pavlov et al., 2007). TIRF microscopy confirms that adding CP to growing actin filaments stops their growth (Kim et al., 2007b).

Bacteria such as *Shigella* or *Listeria* are capable of inducing actin assembly on their surface and use it to move themselves in living cells. CP was one of the proteins found as essential for the *in vitro* reconstitution of bacteria motility based on actin assembly from pure proteins (Loisel et al., 1999).

One idea about the essential role of CP in this system is that CP caps barbed ends that are older and thus located away from the surface of the object to be moved, in this case the bacteria. By preventing actin subunits from adding in these undesired locations, the addition of actin subunits in the optimal locations can be promoted (Carlier and Pantaloni, 1997).

4.3- CAPZ A/B FUNCTIONS IN CELLS AND *IN VIVO*

4.3.1- ROLE OF CAPZ A/B IN ACTIN DEPENDENT PROCESSES

The actin capping activity of CP is critically involved in different cellular and developmental processes. Of note, the concentration of CP in cells is in the micromolar range, comparable to the number of actin filament barbed ends, and the binding affinity is in the sub-nanomolar range (Wear et al., 2003). I will first discuss cellular studies demonstrating the importance of CAPZ actin capping activity for different cellular processes (Fig.24) and then move to describe the role of CAPZ A/B in morphogenesis and other complex processes at the tissue level.

CONTROL OF ACTIN BASED PROTRUSIONS AND CELL MIGRATION

To introduce the role of the actin capping activity of CAPZ A/B proteins in controlling actin based protrusions, I will first briefly introduce simple models of Lamellipodia vs Filopodia formation in cells. Lamellipodia formation is mainly driven by dendritic actin nucleation mediated by Arp 2/3 (Borisy and Svitkina, 2000). In this context, capping is needed in order to limit the elongation of actin filaments, increasing in this way the number of short actin filaments and a branched actin network (Borisy and Svitkina, 2000; Mejillano et al., 2004). In contrast, if branching and capping are prevented, this leads to continuous elongation of parallel actin filaments and filopodia formation (Svitkina et al., 2003). Therefore, the elongation status of the actin filament barbed ends, and thus the capping and anticapping activities, determine the formation of lamellipodia vs filopodia protrusions.

The high affinity of CP for actin filaments *in vitro* made CP an interesting candidate to regulate lamellipodia formation. In line with this, Mejillano and colleagues studied the function of CP in lamellipodia formation in B16F1 mouse melanoma cells, as well as in fibroblast cell lines. These cells are highly motile and present both types of protrusions. In this context, depletion of CP by shRNA against CAPZ-B led to a decrease in lamellipodia protrusions and an explosion of filopodia. In addition, the authors observed a reduction in the lamellipodial actin network and in Arp2/3 at the leading edge. An increased actin filament assembly away from the leading edge also suggested uncontrolled actin polymerization in the absence of CP. In accordance, endogenous CP was seen localized to the leading edge of Lamellipodia (Fig. 24) (Mejillano et al., 2004).

Demonstrating a role for an actin capping protein in determining lamellipodia vs filopodia formation suggested that the predominance of one type of protrusion over the other in specific cell types could be related with the levels of CP and uncapping proteins found in each cell type.

In addition of being detected at lamellipodia, CP localizes to the cell body, to the lamella (that is, the region behind the lamellipodia) and shows a punctated localization to filopodia in multiple cell types (Fig. 24) (Sinnar et al., 2014). In relation to this filopodial localization, CP depletion reduces filopodia length and affects filopodia morphology as well as filopodia dynamics as seen by time lapse analyses (Sinnar et al., 2014). However, whether these effects reveal a specific role of CP in filopodia dynamics or instead are an indirect consequence of excessive filopodia formation upon CP depletion remains to be determined. Of note, the authors observed that CP depletion increases F- actin concentration (Sinnar et al., 2014) as previously observed in other cell types (Hug et al., 1995), indicating increased actin polymerization in the absence of CP. The burst in actin polymerization occurring upon CP depletion possibly reduces the cellular levels of G-actin which could in turn affect filopodia length and dynamics.

In correlation with defects in the formation of actin based protrusions, shRNA depletion of CP impairs cell migration of cultured mouse melanoma cells and mouse cortical neurons from the ventricular

zone to the cortical plate *in vivo* (Sinnar et al., 2014). These cell migration defects could be related with defective lamellipodia and/or filopodia dynamics, given that both types of protrusions have critical roles in cell migration (Small et al., 2002).

Interestingly, in addition to these global inactivation approaches, acute local inactivation of CAPZ-B has been performed by chromophore assisted laser inactivation of GFP-CAPZ-B in fibroblasts depleted of endogenous CP. This treatment generated a local increase in the concentration of free barbed ends, the polymerization of actin and the formation of actin based protrusive structures (Vitriol et al., 2007). These results support the notion that CAPZ A/B indeed caps barbed ends preventing actin polymerization in cells.

CAPZ AND REGULATION OF AUTOPHAGY

The autophagosomes are double membrane structures that are formed by expansion and bending of flat membrane cisternae, a process that occurs on the ER surface. Recently, Mi and colleagues found that actin branched polymerization drives membrane bending during autophagosome formation in mammalian cells (Mi et al., 2015). Accordingly, CAPZ-B knockdown impaired autophagosome formation and autophagy in this context. More specifically, CAPZ-B knockdown perturbed actin polymerization and the shaping of membranes during autophagosome formation (Mi et al., 2015). This suggests that CAPZ A/B is involved in different cellular processes requiring specific actin dynamics other than cell migration.

CAPZ-B AND SPINDLE MIGRATION IN OOCYTES

Spindle positioning and asymmetric division during oocyte meiosis requires a dynamic actin cytoplasmic meshwork as well as proper cortical actin dynamics (Fig.13). Thus, diverse actin nucleators including Formin 2, Spire and Arp2/3 are critically involved in this process (Almonacid et al., 2014, see section 2.9). Hence, the actin cappers are obvious candidates to regulate spindle positioning in oocytes. In this sense, Jo and colleagues have recently shown that simultaneous

depletion of CAPZ A1 and B2 subunits generates defects in spindle migration and asymmetric division in the mouse oocyte (Jo et al., 2015). These defects correlate with a marked reduction of the oocyte cytoplasmic actin meshwork upon depletion of CAPZ proteins, which normally localize to the oocyte cytoplasm (Fig. 24). These results suggest that CAPZ A/B controls spindle migration and asymmetric division in oocytes by regulating the cytoplasmic actin meshwork (Jo et al., 2015). Of note, CAPZ depletion in oocytes decreases the density of the F-actin meshwork while in cultured mammalian cells this depletion increases the concentration of F-actin.

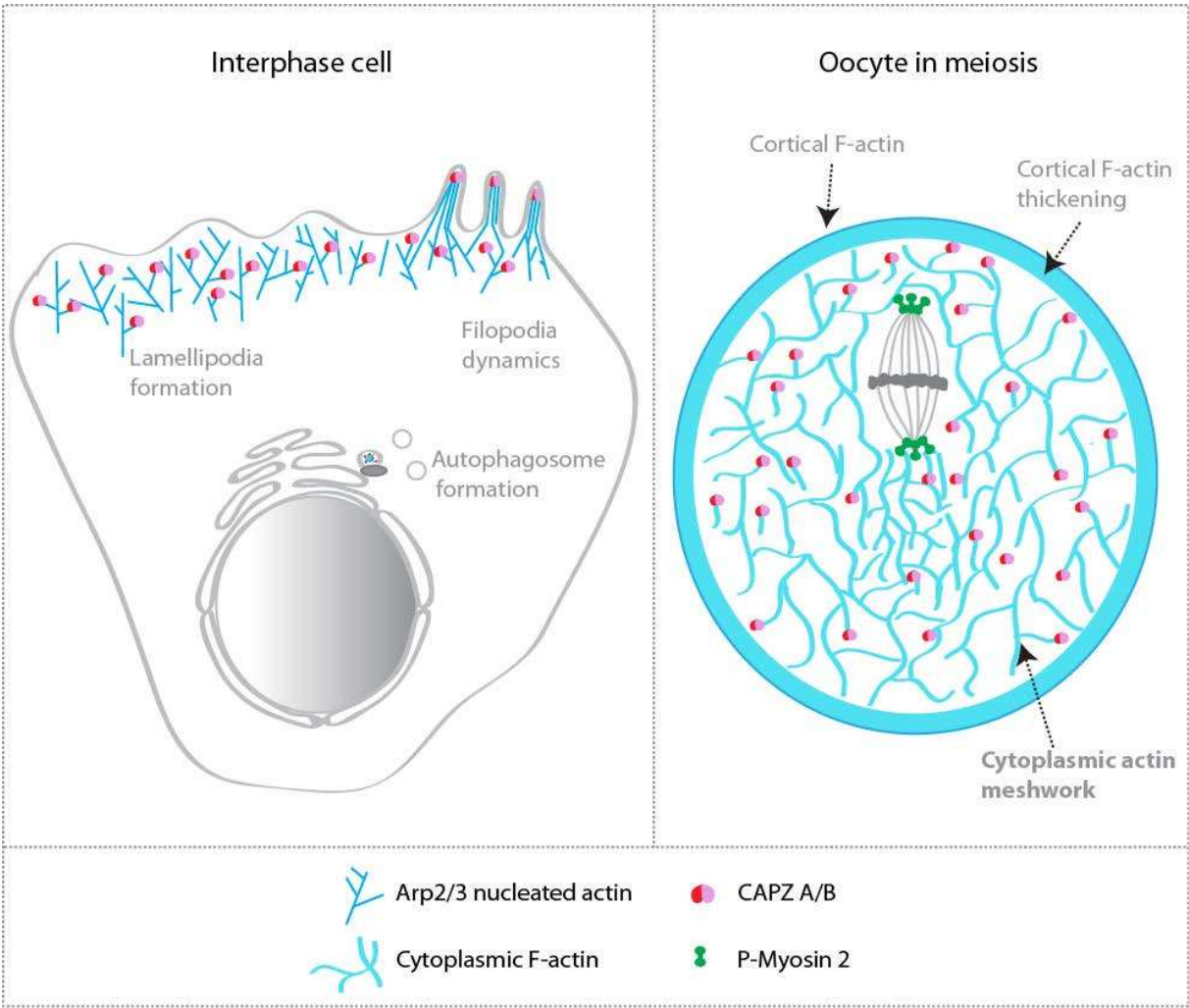


Figure 24: Actin capping function of CAPZ A/B in different cellular processes.

CAPZ A/B IN DEVELOPMENT

In *Drosophila*, CP is essential for the viability of the organism, and loss-of function mutants die as embryos (Hopmann et al., 1996). Alternative approaches to circumvent the embryonic lethality have allowed to characterize the function of CAPZ A/B in several tissues. Indeed, mutation of CP affects the development of different structures in flies. In particular, bristle morphology is affected in CP mutants. The bristles structure is defined by the formation of actin bundles during development. In line with this, CP depletion results in increased levels of F-actin and cytoskeleton disorganization during development, and defective bristle morphology in the adult (Frank et al., 2006; Hopmann et al., 1996; Hopmann and Miller, 2003).

Moreover, CP plays an important role during *Drosophila* wing development (Janody and Treisman, 2006). In particular, CAPZ-A and CAPZ-B mutant cells are extruded from the epithelium to the basal surface and die; a phenotype specific to the wing blade primordium. This effect was correlated with defective localization of the Adherens junctions components Armadillo and DE Cadherin to the basolateral membrane. Consistently, CAPZ-A partially localizes with components of epithelial junctions, including Armadillo, Dlg and Crumbs. Of note, the observed phenotypes were specific to the blade region and were not found in the notum (Janody and Treisman, 2006). This specificity was linked to the identity of the cells, as misexpressing Vestigial (a wing blade fate determinant) in the notum allows CP mutations to generate these defects in this area. In contrast, an increase in F-actin concentration was seen in all regions of the wing disc in CP mutant cells. Interestingly, CAPZ proteins have been previously seen to localize to cell-cell junctions in different chicken epithelial tissues- including adult intestinal epithelia and embryo kidney and retinal epithelia (Schafer et al., 1992)

In addition, eye mutant patches for either one of the *Drosophila* orthologues of A or B CP subunits present photoreceptor degeneration features (blackened tissue, lack of ommatidial facets, etc.) that might be related to the F-actin accumulation generated by these mutations in the eye imaginal discs (Delalle et al., 2005).

Finally, flies with partial depletion of CAPZ-B present defective oogenesis. During *Drosophila* oogenesis, follicular cells show specific patterns of migration, which are dependent on actin cytoskeleton dynamics. In addition, nurse cells transport their cytoplasm to the oocyte in an actin dependent manner. In this context, CAPZ-B depletion conditions showed impaired migration of both border and centripetal follicular cells in correlation with abnormal organization of actin rich protrusions. Moreover, CAPZ-B depletion resulted in defective actin organization and ring canal formation in nurse cells (Ogienko et al., 2013). These phenotypes could be involved in the defective oogenesis found in CAPZ-B mutants.

Recently, Mukherjee and colleagues studied the role of CAPZ-B during Zebrafish embryonic development (Mukherjee et al., 2016). CAPZ-B homozygote mutants present defects in multiple tissues. In particular, craniofacial development is affected as seen by the presence of cleft palate and a short lower jaw observed. These phenotypes correlated with defective migration of cranial neural crest cells to the palate structure, a phenotype that could be explained by the function of CAPZ-B as an actin capping protein. Indeed, in these mutants both the actin distribution and concentration of actin as well as cell morphology are perturbed in epidermis; and defective melanocyte migration in somites was observed. In addition to these defects, zebrafish homozygote mutants present defects in muscle development (see next subsection), microcephaly and smaller body size and die at 4.5 days post fertilization (Mukherjee et al., 2016).

Finally, CAPZ-B knock out mice die at embryonic day 8 (Jeremy Reiter, personal communication).

CAPZ A/B IN MUSCLE

CP localizes at the Z-disc of the muscle sarcomere (Casella et al., 1987). The barbed ends of the actin-based thin filaments are also located at the Z-disc, and one molecule of CP appears to cap each barbed end. Capping of the barbed ends in this context may help anchoring the thin filament to the Z-disc, or it may prevent the growth of the filament into the adjacent sarcomere (Cooper and Sept, 2008). Indeed, CP and its capping activity appear to be important for assembly of the sarcomere. In

cultured myotubes, injection of an anti-CP antibody that inhibited the actin-binding ability of CP or expression of a CAPZ-B mutant that does not bind actin disrupted the early steps in myofibrillogenesis. In particular, CP is required for actin filament organization in the sarcomere (Schafer et al., 1995). Moreover, expression of a capping-deficient CAPZ-B1 subunit during mouse heart development caused disruption of myofibril architecture (Hart and Cooper, 1999).

4.3.2- CAPZ A/B IN DYNACTIN

As mentioned before, CP is a biochemical component of vertebrate dynactin (Schafer et al., 1994a; Schafer et al., 1994b; Schroer, 2004), and structural studies showed it as a member of the dynactin complex possibly required for Dynactin stability (Urnavicius et al., 2015). However, the function of CAPZ A/B in Dynactin remains elusive.

In yeast, null mutations of the CAPZ homologues Cap1/2 produce no major defects on dynactin/dynein function, in particular in spindle positioning. However, biochemical approaches have not revealed CP to be a component of dynactin in yeast (Moore et al., 2008).

Remarkably, depletion of CAPZ subunits in human cells did not generate any significant phenotypes in several mitotic processes (Raaijmakers et al., 2013). These processes include the anchoring of centrosomes to the nuclear envelope at prophase, mitotic progression and dynein targeting to the nuclear envelope and kinetochores, which in contrast depend on the dynactin subunits Arp1 and/or p150. This raises the question of what is the function of CAPZ A/B in vertebrate dynactin.

4.3.3- CAPZ A/B AND MICROTUBULES

While most studies on the CP function are focused on the role of this protein as a modulator of the actin cytoskeleton, recent evidence suggested that CP also regulates the microtubule network. In this sense, Davis and colleagues found that CAPZ-B2 co-immunoprecipitates with β III-tubulin in brain lysates. In addition, CAPZ-B2 decreases MT polymerization in *in vitro* assays (Davis et al., 2009). Notably, the authors mapped a region in CAPZ-B2 (aa 106-140) as required for interaction with β III-

tubulin and modulation of MT polymerization. The authors proposed that the β III-tubulin-CAPZ-B2 interaction is involved in the regulation of growth cone morphology and neurite outgrowth in cultured hippocampal neurons. In particular, an abnormal extension of MT into the peripheral zone of growth cones observed upon CAPZ-B2 depletion is proposed to be linked to the lack of interaction of β III-tubulin with CAPZ-B2 (Davis et al., 2009). Of note, CAPZ-A2 showed no defects on MT polymerization *in vitro*, showing this feature to be specifically associated with the B2 CP subunit. Whether CAPZ-B2 regulates MT polymerization in cells and if the β -tubulin-CAPZ-B2 interaction occurs in other tissues remain to be determined.

In addition to these observations, depletion of CAPZ-B2 has been seen to reduce the number of cells containing stable (Glu) MTs in proliferating NIH3T3 cells (Bartolini et al., 2012). However, in this case, the authors proposed that the action of CP on MT stability occurs indirectly by displacing the formin mDia from actin filaments to MT, where mDia works as a MT stabilizer. Indeed, overexpression of CP (i.e. both the A and B subunits together) increases the amount of stable MTs in serum starved cells in an mDia dependent manner, in parallel to the displacement of mDia from actin filaments to the MT network (Bartolini et al., 2012).

4.4- CONCLUSION

The acting capping proteins are ubiquitously expressed in most eukaryote cell types and both A and B isoforms are highly conserved in higher eukaryotes. The actin capping activity of this heterodimer is at the core of actin dynamics regulation in many cell types. Therefore, capping proteins regulate multiple cellular processes requiring proper actin dynamics and thus are involved in morphogenesis in different tissues. On the other side, a connection between CP proteins and microtubule dynamics in specific contexts has recently been proposed. Intriguingly, capping proteins are part of the vertebrate dynactin complex but no specific functions have been linked with their presence in this complex.

CHAPTER 5: QUESTIONS AND OBJECTIVES OF THE PROJECT

5.1. QUESTIONS MOTIVATING THIS PROJECT

Several conclusions can be drawn from the previous chapters. Firstly, the specific role of spindle orientation during development and disease is only partially understood in higher vertebrates. Better characterizing the molecular mechanisms controlling spindle orientation may help to address the contribution of this process to specific developmental and pathological events. Regarding the characterization of the molecular mechanisms of oriented divisions in vertebrates, this field has mostly emerged in the last ten years, and a lot of studies addressed the role of molecules previously identified in invertebrate models, in which the most advanced spindle orientation studies had been performed during the previous decade. This has proved valuable, since despite the existence of important conservations, these studies have established that the mechanisms of action of several molecules clearly differ between invertebrate and vertebrate models (consider for instance the cases of Dlg/Dlg1, Canoe/Afadin, Moesin/ERM or RAN^{GTP}). However, molecules found in invertebrate systems should not be the only source for testing the effect of specific molecules on spindle orientation. Therefore, efforts to uncover novel regulators of spindle orientation in vertebrate models could be highly valuable in this field.

Xavier Morin's team has been studying spindle orientation in the chick embryonic neuroepithelium for several years, trying to understand both the molecular regulation of this process and its developmental relevance in this physiological context. As a reminder, planar spindle orientation of neuroepithelial progenitors depends on the specific lateral localization of the LGN complex.

Many questions remain unanswered concerning LGN dependent-spindle orientation. In particular, our understanding of vertebrate spindle orientation has been somehow limited to the core members of the LGN complex and its simple model of recruitment for several years. Recent research extensively discussed in chapter 2 has mainly focused on molecules that regulate the recruitment/stability of LGN at the cortex (e.g. Dlg1, HTT, ERM, Afadin, RAN^{GTP}). There is little

information about molecules regulating the formation of the complex downstream of LGN –such as molecules regulating the interaction between NuMA and LGN- and those working downstream of the LGN complex itself. In particular, despite the known involvement of molecular motors, how they are recruited and how they function during spindle orientation remains poorly understood. Similarly, studies addressing the role of microtubule associated proteins and centrosomal proteins are sparse.

All these reasons have prompted us to screen for novel vertebrate spindle orientation regulators which constitutes the main goal of my thesis project.

5.2- OBJECTIVES

A- DEVELOPMENT OF A CELLULAR MODEL OF LGN-CONTROLLED SPINDLE ORIENTATION

Our interest in the end was to uncover novel regulators of spindle orientation that could be relevant during LGN dependent planar spindle orientation in the neuroepithelium. Screening for tens of genes in the chick neuroepithelium was not feasible for several reasons. Firstly, embryo manipulation requirements make impractical to evaluate tens of candidates. Secondly, the tools to deplete proteins in the chick neuroepithelium are not standardized; there are no validated shRNA libraries available and previous experience in the lab showed that the optimization of protein depletion tools requires intense efforts that are not compatible with the idea of a big screen. Therefore, we decided to privilege the use of cultured cells for our screen. However, we thought that classical models of spindle orientation in cultured cells (eg X-Z orientation relative to the substrate or micropattern induced orientation in the X-Y plane) would not be ideal for our screen for the reasons exposed below.

SPINDLE ORIENTATION WITH RESPECT TO THE SUBSTRATE

The requirement of the LGN-NuMA-Dynein-astral MT pathway for spindle orientation parallel to the substrate has been addressed in different studies. Kotak and colleagues have found that siRNA mediated depletion of $\text{G}\alpha\text{i}$, LGN, NuMA or DHC1 all resulted in spindle orientation phenotypes in

metaphase (Kotak et al., 2012). Of note, these molecules are core components of spindle orientation in other contexts, and inactivating them generates random spindle orientation (Konno et al., 2008; Peyre et al., 2011). However, spindle orientation with respect to the growth surface is far from being random in HeLa cells in those depletion conditions. Remarkably, in all depletion conditions mentioned, more than 70 % of the angles remain below 20° (Kotak et al., 2012), suggesting that other parallel pathways are extensively controlling spindle orientation parallel to the substrate. This could reflect that the LGN complex is involved in stabilizing but not in defining this specific orientation.

Similarly, recent studies by Morris and colleagues showed a subtle effect of depleting p50 (a dynactin subunit required for dynactin stability) on the distribution of division angles with respect to the growth surface (Morris et al., 2015). Of note, Matsumura and colleagues did not observe spindle orientation defects upon LGN knock-down in HeLa cells (Matsumura et al., 2012).

Concerning the involvement of astral MT in this type of orientation, Toyoshima and Nishida showed that specific perturbation of astral MT by applying low doses of nocodazol indeed resulted in spindle misorientation (Toyoshima and Nishida, 2007).

Interestingly, Lazaro-Diequez et al. proposed a reason for the bias of orientation angles parallel to the substrate that they indeed observed upon inhibition of LGN, dynein or astral MT function. As described in chapter 2, the authors attributed this bias to the flat morphology that some cells retain in mitosis (Lazaro-Diequez et al., 2015). This confirmed the idea that other factors independently of the LGN-NuMA-Dynein-astral MT pathway are at play to control this specific orientation.

In addition, it should be noted that spindle orientation phenotypes observed in the different treatments described above correspond to measurements in metaphase, and not to the final anaphase orientation.

MICROPATTERN-GUIDED SPINDLE ORIENTATION IN SINGLE CELLS

The requirement of astral MT for micropattern guided spindle orientation has been clearly demonstrated in several studies (Fink et al., 2011; They et al., 2005). However, the existent data is less clear with regard to LGN and dynein. Kiyomitsu and Cheeseman reported that depleting LGN or p150 results in a decrease in the percentage of cells with a “correct spindle orientation” when dividing on L-shaped micropatterns. While the expected orientation on these patterns is 45°, they did not define the extent of variation around this value that they consider as “normal” and which orientation is considered “incorrect”, so it is difficult to deduce the true extent of the phenotype in this study. Interestingly, they proposed that LGN and p150 are involved in the maintenance of the orientation in accordance to what is observed in their example movie (Kiyomitsu and Cheeseman, 2012). In my hands, I observed only minor defects of LGN depletion on spindle orientation in the same culture system (Fig. 25).

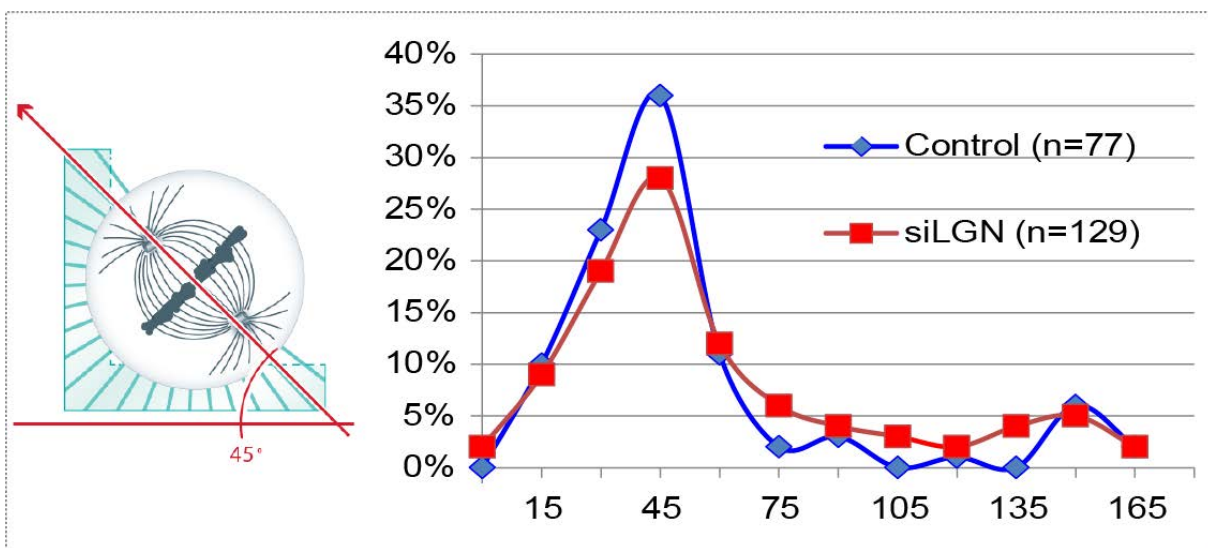


Figure 25: Effect of LGN knockdown on micropattern guided spindle orientation. Cells were seeded on L-micropatterns and the angle of division was measured in anaphase as indicated in the left schema.

Likewise, Kwon and colleagues have found significant differences in spindle orientation between control and LGN-depleted cells seeded on L-patterns, but they observed that angles were not random and remained strongly biased to the normal orientation. In contrast, when they simultaneously depleted Myosin 10 (see chapter 2), spindle orientation was random suggesting that the LGN-dynein pathway acts in parallel to the Myosin 10 pathway (Kwon et al., 2015).

Thus, these data suggest that LGN-Dynein complexes are partially involved in controlling micropattern guided spindle orientation. However, Tame and colleagues found that depletion of DHC or LGN resulted in random spindle orientation in cells cultured on rectangular patterns (Tame et al., 2014). Overall, the contribution of LGN-Dynein complexes in this type of orientation remains unclear.

In conclusion, the LGN-dynein-astral MT pathways are indeed involved in both cell culture models of spindle orientation presented above, but their contribution to the establishment or maintenance of spindle orientation are probably partial in these contexts. Therefore, my first objective was to develop a new cell culture model of spindle orientation specifically controlled by the LGN complex.

B- SCREEN FOR NEW REGULATORS OF VERTEBRATE SPINDLE ORIENTATION

My second objective was to perform a mid-scale screen for novel spindle orientation regulators, using our newly developed model. Before the screen, several validation and optimization steps were needed. Firstly, it was necessary to validate the model as a tool to find regulators of spindle orientation by siRNA screen. Secondly, optimization of the model to use it in the frame of a mid-scale screen was required. This involved the development of software to automate the analysis of spindle orientation angles, which we did in collaboration with different research groups with expertise in bioinformatics.

C- CHARACTERIZATION OF THE MECHANISMS OF ACTION OF INTERESTING HITS IN CELLS

After finding interesting candidate(s), my next objective was to characterize their function by using immunofluorescence and live imaging of different cell lines. The general idea was to evaluate how depletion of novel hits affected different cellular features known for influencing spindle orientation, namely the recruitment of cortical complexes, the actin cortex and the spindle characteristics as detailed in chapter 2.

D- VALIDATION OF INTERESTING HIT(S) *IN VIVO*

My final objective was to test the function of at least one interesting hit in the context of the LGN-based planar orientation of neural progenitors in the chick neuroepithelium, in order to validate the function of a hit from the screen in an *in vivo* physiologically relevant context. Noteworthy, a lot of the mechanistic details obtained in cell culture systems that are discussed in chapter 2 have not been assessed in more physiological contexts. We consider that when possible, this is an essential step to understand the relevance of the identified molecules or mechanisms.

The chick neuroepithelium is a routinely used model in the lab and thus several techniques including electroporation, dissection, staining, mounting, and imaging in live and fixed conditions are optimized in the team. However, knock-down approaches are less optimized for this organism. The team has successfully used shRNA approaches for depleting some proteins, including LGN, NuMA and Dlg1 (Morin et al., 2007; Peyre et al., 2011; Saadaoui et al., 2014) but this approach has also proved less efficient for other molecules studied in the group, including my own attempts with CAPZ-B. Therefore, *in vivo* validation has also required the optimization of techniques to deplete the protein of interest, as I will describe in the next chapter.

CHAPTER 6: RESULTS

The Results and Discussion chapters are extended versions of the article “The actin capping protein Z β (CAPZ-B) controls mitotic spindle orientation through the dynactin pathway”. di Pietro, F., Valon, L., Li Y., Goïame, R., Coppey, M, Genovesio, A., Morin, X. This article is still in preparation and will be submitted later this month. I chose to extend the content of the article in order to present and discuss my results more extensively in this manuscript.

6.1. DESIGNING OF A SPINDLE ORIENTATION MODEL SPECIFICALLY GUIDED BY THE LGN COMPLEX IN CULTURED CELLS

In order to design a screening system for regulators of spindle orientation that function downstream of the LGN pathway, we sought to construct an *in cellulo* system of oriented cell divisions that would be amenable to large scale genetic screening for an unambiguous spindle orientation phenotype. We decided to use HeLa cells for our model as their robust growth and standardized transfection, as well as the availability of standardized human siRNA libraries make them ideal for performing an RNAi screen. We aimed to generate a model of spindle orientation with several constraints: 1) spindle orientation would be dictated by the specific localization of LGN complex components; 2) defects in the pathway would result in strong orientation phenotypes observable in the x-y plane, allowing imaging at low magnification; 3) the system would be highly reproducible and amenable to large scale imaging, and 4) the system would be compatible with multi-well plate culture and RNAi treatment.

To conform to the first constraint, we thought of inducing a polarized distribution of the G α i subunit, which is the most upstream component of the LGN pathway. G α i is normally anchored to the cell membrane by myristylation, and this anchoring is required for the membrane recruitment of LGN and all downstream pathway components (section 2.2). Hence inducing a restricted cortical localization of G α i is expected to drive spindle orientation perpendicular to the site of G α i enrichment, through the application of pulling forces to one spindle pole. To control spindle orientation within the x-y plane (our second constraint), we thought of recruiting G α i at the interface between two adjacent cells by hooking G α i to the intracellular portion of a transmembrane, homophilic adhesion molecule (see schema in Fig. 26a). The extracellular and transmembrane

domains of the *Drosophila* Echinoid (Ed) homophilic adhesion molecule, fused to an intracellular GFP reporter sequence (EdGFP), have previously been used in a spindle orientation assay designed in *Drosophila* S2 cells that took advantage of their ability to be enriched at cell-cell contacts (see section 2.3) (Johnston et al., 2009). We cloned the EdGFP coding sequence in a mammalian expression system and introduced it in HeLa cells, where I observed that EdGFP is also enriched in cell-cell contacts (Fig. 40 in appendix 1). Importantly, this enrichment remains when cells round up to enter mitosis. Similar results were obtained for the fusion protein EdGFP-Gai (data not shown). I next developed cell lines stably expressing the chromatin marker H2B-Cherry (to follow cell divisions) and containing one of the Ed fusion constructs whose expression are Doxycycline inducible (see methods and Fig. 40a in appendix 1).

To increase reproducibility and standardize image acquisition and analysis, we thought to set-up the cell pair Ed-assay on micropatterns. Micropatterns have been extensively used to control cell size, shape, and polarity in a highly reproducible fashion. In addition, the geometry of the pattern can dictate spindle orientation in single cells (section 2.3) (They et al., 2007; They et al., 2005), and the organization of cell-cell contacts in pairs of cells (Tseng et al., 2012). As extensively discussed in section 2.8, both the shape and the adhesion pattern of the cell can influence cell division orientation. Thus, by using micropatterns to standardize these features on our cell-pair assay, we aimed at reducing the variability of spindle orientation due to geometry of adhesion factors. In addition, this provides a standardized way of isolating pairs of cells in contrast to culturing cells on a homogeneous fibronectin substrate.

We thus designed a “paired-cell assay” in which we would measure spindle orientation in the first cell that divides in a pair of cells. With a few exceptions, micropatterns have been mainly used for culturing single cells. I thus tested several shapes and sizes of micropatterns to accommodate our pairs of cells, including double circular patterns, H patterns and circular patterns of different diameters. The ideal pattern geometry should allow standardizing the shape of both cells and at the

same time allowing them to reproducibly establish and keep a contact between them all along the cell cycle. To evaluate the behavior of cells on different patterns, I performed experiments in which I fixed EdGFP cells 30 hr after seeding, an optimal time to observe many patterns occupied by a pair of cells originated from a round of cell division. For some pattern geometries, I also performed long-term movies to follow cell pair behavior in real time. In figure 40 c and d (appendix 1), examples of cell pair configuration on H or 30 μm circular patterns are shown. On circular patterns, the two cells tend to migrate in a revolving fashion on the pattern during interphase, but they each permanently occupy roughly one-half of the circular adhesion pattern which gives the cells a similar shape. In contrast, cell pairs cultured on H patterns were seen each on one bar of the H only 2/3rds of the time, and were spread over the two bars the rest of the time, resulting in highly variable cell shapes on these patterns. We therefore decided to use circular patterns with a diameter of 30 μm (Fig. 40). Importantly, cells maintain a large contact between them during all the cell cycle when seeded on those circular patterns.

To evaluate spindle orientation in EdGFP and EdGFP-G α i cell lines, I measured the angle of division in anaphase (as depicted in Fig. 26b, right) in time-lapse sequences obtained by filming cells during 48 hr. We and others have observed that the spindle actively rotates in prometaphase/metaphase to reach its final orientation and thus the anaphase angle is a more reliable measurement of the final spindle orientation (Bergstralh et al., 2016; Peyre et al., 2011). For automating angle measurement on manually extracted individual movies, we designed a Matlab software in collaboration with Léo Valon (IBENS and Biophysics Curie, group of Maxime Dahan). This software allows measuring the anaphase angle of division with respect to the center of mass of the nucleus of the neighboring cell (as depicted in Fig. 26b, right) (see Methods and Fig. 41 in appendix 1 for further details). Using a representative set of division events obtained on round patterns, we compared the angle distribution measured by this software to either manual measurements performed in the same manner (angle relative to the neighbor's nucleus center) or angle measurements with respect to the center of the EdGFP enrichment at the contact (data not shown). All three methods gave the same average

distribution, validating both the use of the neighbor's nucleus as a proxy for the position of the Ed enrichment, and the automated method. In addition, we designed a Matlab tool to estimate the GFP level in the cell-cell contacts, in collaboration with Yingbo Li in the group (see Methods and Fig. 41 for further details). This tool can be used to filter out cell pairs with levels of transgene expression that are insufficient to drive spindle orientation.

When pairs of wild type or EdGFP expressing cells are cultured on round micropatterns, the first cell of the pair that divides orients its mitotic spindle parallel to the contact with its neighbor in a highly reproducible manner, presumably influenced by the elongated shape of the half pattern it occupies (Fig. 26b, top row, and Fig. 26c), as would be predicted from studies on single cells on elongated patterns (They et al., 2005). In contrast, in cell lines expressing EdGFP-G α i, the spindle was efficiently and reproducibly reoriented perpendicularly to the cell-cell contact (Fig. 26b, bottom row, and Fig. 26c). A similar reorientation phenotype was observed in EdGFP-LGN expressing cells (Fig. 26c); however, we chose to use EdGFP-G α i cells as the reorientation was more precise than in EdGFP-LGN cells and because G α i is more upstream than LGN in the cascade. Remarkably, knock-down of LGN in EdGFP-G α i cells disrupted the EdGFP-G α i dependent orientation. Moreover, treatment of EdGFP-G α i cells with low doses of Nocodazole that primarily disrupts astral microtubules resulted in a similar loss of G α i induced orientation (Fig. 26d). Notably, both treatments resulted in an hour-glass shape distribution of angles, suggesting that a portion of cells were reverted to the wild-type orientation upon perturbing LGN or astral MT, whereas a subpopulation remains under the influence of Ed-G α i, probably due to variability in the efficiency of the LGN RNAi transfection, and in the nocodazole reduction in astral MTs.

Remarkably, neither LGN knock-down nor nocodazole treatment had any effect on spindle orientation in wild type or EdGFP cells cultured on circular patterns (Fig. 40e). This was a surprising result for us as most spindle orientation systems are believed to rely on astral MT. Our hypothesis is that the high cell shape constraint imposed to cells on these patterns is able to make them orient

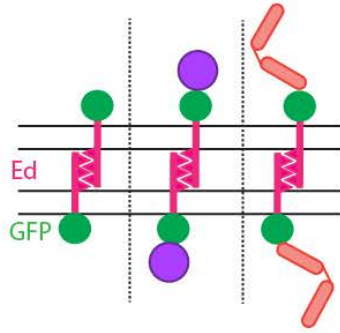
their spindles along the long interphase shape, and that this mechanism does not depend on the LGN- astral MT pathway. Likewise, cell shape has been observed to influence spindle orientation parallel to the substrate independently of astral MT (Lazaro-Diequez et al., 2015) as discussed in section 2.8. I will come back to this point in the discussion chapter.

On the other side, treatment with Latrunculin A, which disrupts actin polymerization and has been shown to affect spindle orientation on single cells cultured on some pattern shapes (Thery et al., 2005) (section 2.3), also had no effect on anaphase spindle orientation in any of our cell lines (Fig. 26d and Fig. 40e).

Finally, I studied the localization of different members of the LGN pathway in Ed-G α i cells. In dividing Ed-G α i cells, I found that LGN, NuMA, and the dynactin complex member p150 co-localized with G α i at the cell-cell contact (Fig. 27).

Overall, these results indicate that the paired-cell assay in EdGFP-G α i cells creates a specific LGN-complex and astral microtubule dependent model of oriented divisions that is independent from actin. This model conforms to our four initial constraints (spindle orientation is LGN complex-controlled, orientation defects are strong in the x-y plane, the system is reproducible and can be scaled-up for screening and the system is compatible with RNAi treatment), and we decided to use it in a live RNAi screen.

A

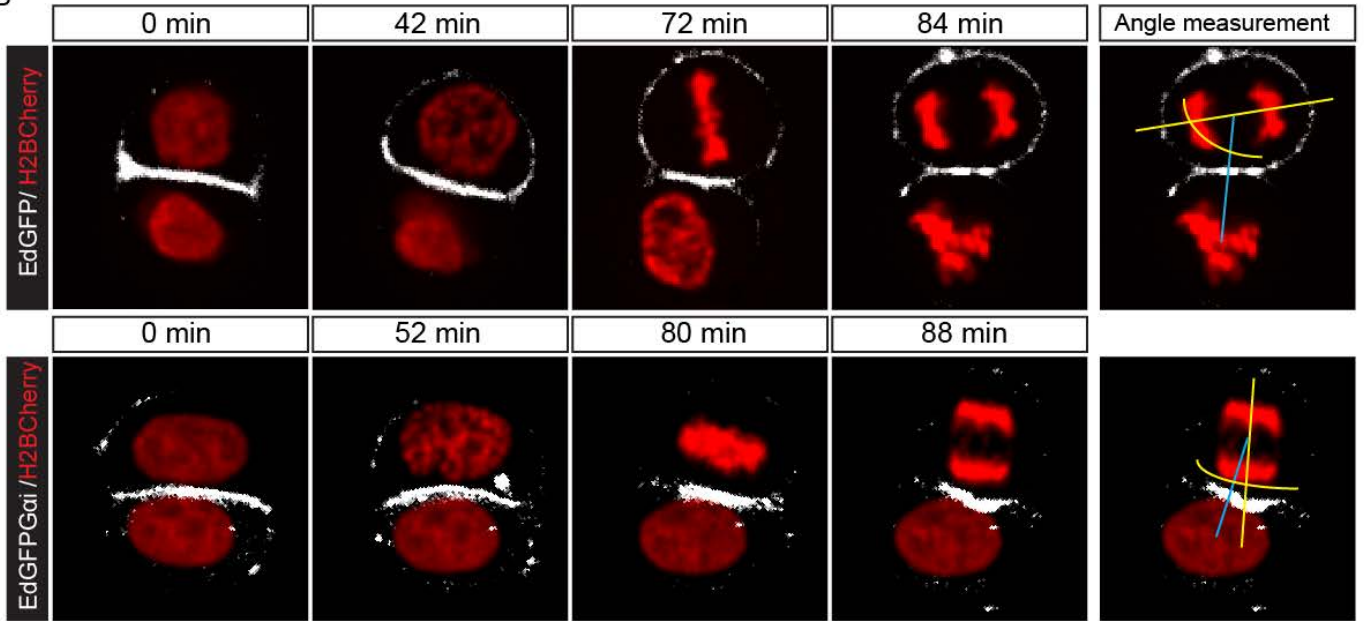


Ed/EdGai/EdLGN
HeLa cell lines

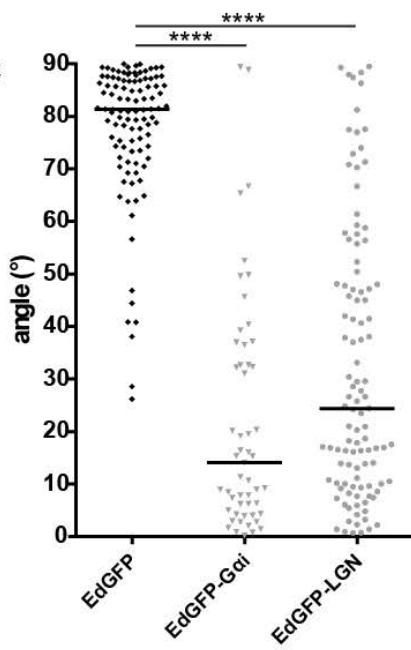
Seeding on round
micropatterns

Time-lapse
48 hr

B



C



D

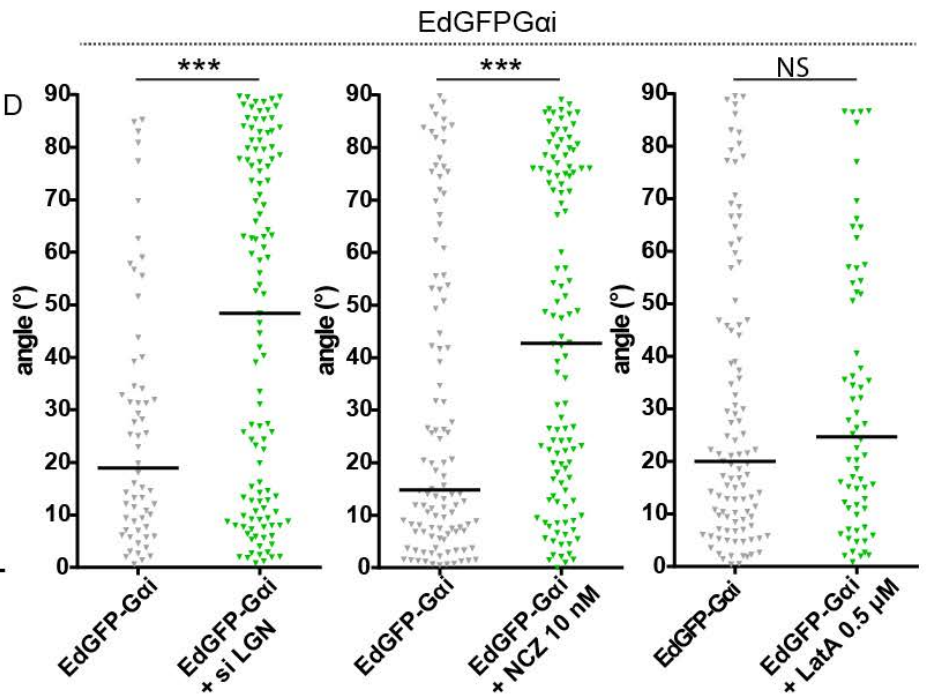


Figure 26: Development of a spindle orientation model controlled by the LGN complex. a) Left: Schema of the Ed fusion proteins in the contact between two cells, and the work flow for the experiment shown in b) b) Time lapse images of HeLa cells expressing EdGFP or EdGFPGai +H2BCherry, and seeded on 30 μm round micropatterns. c) Spindle orientation angle distributions measured in anaphase for cells expressing EdGFP, EdGFPGai and EdGFPLGN. The angles correspond to the angle between an axis connecting the two chromosome sets and an axis connecting the center of the neighboring cell and the center of the axis connecting the chromosome sets as depicted in b). Measurement of the angle of division with respect to the nucleus of the neighboring cell is consider as approximate to the angle of division with respect to the Ed enrichment. See methods for details. d) Angle distribution for EdGFPGai cells treated with siRNA against LGN, 10 nM Nocodazole to perturb astral MT or Latrunculin 0.5 μM to deplete the actin cytoskeleton.

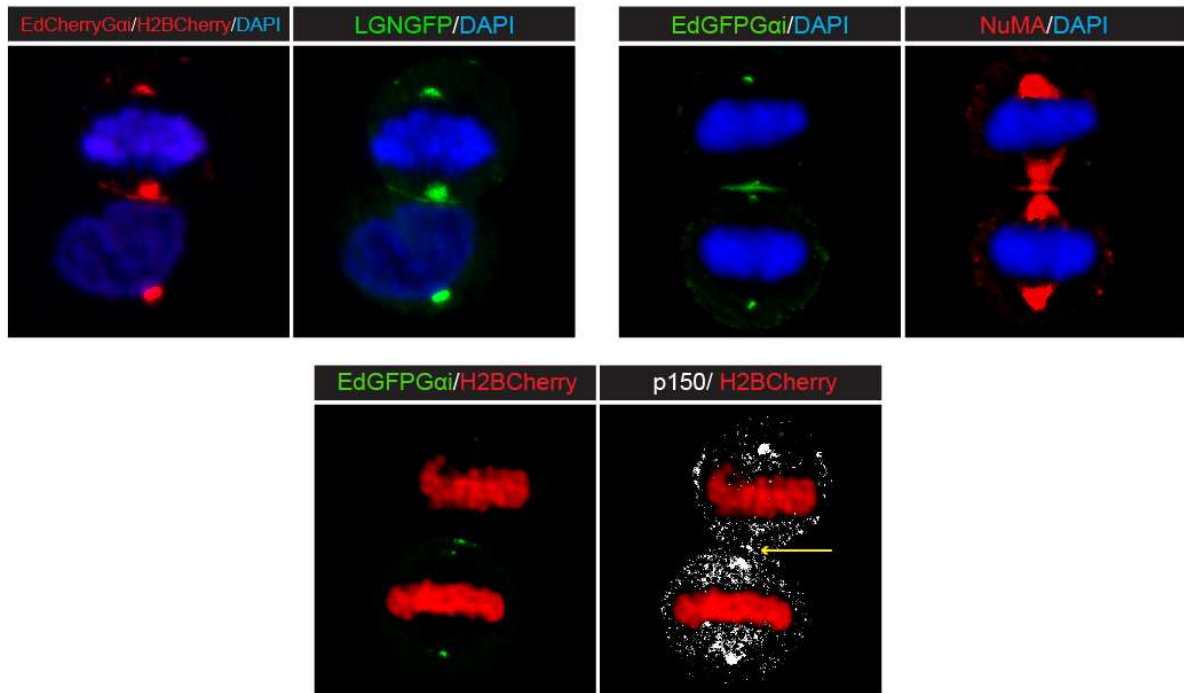


Figure 27: Localization of LGNGFP, NuMA and the dynactin subunit p150 in pairs of Ed-Gai cells seeded on round micropatterns. Cells were treated with proTame during 6 hr to enrich in metaphase cells and fixed and stained before imaging.

6.2. A SYSTEMATIC LIVE RNAI SCREEN IDENTIFIES ESSENTIAL AND DISPENSABLE DYNEIN/DYNACTIN COMPLEX MEMBERS DOWNSTREAM OF THE LGN COMPLEX

6.2.1. WORKFLOW

For our live RNAi screen, I performed similar experiments to those performed during the model development and validation steps, but at a larger scale. The workflow is provided in Figure 28a. Of note, imaging with a 10x objective was enough to measure spindle orientation angles and GFP levels. In addition, we used a microscope associated with a large field camera (13.3x13.3 μm , 2048x2048 pixels) that allowed to image more than 250 micropatterns per 10x field. Fast acquisition allowed to

image 140 positions in GFP and Cherry channels in less than seven minutes, which is the interval needed to obtain at least one image of cells in anaphase. Using these imaging conditions and commercial micropatterns in 96-well plates, I could test 24 conditions in duplicate plus control conditions in each single experiment.

For image analysis, I used the software mentioned in the previous section. Notably, the first step of image analysis that consisted in extracting all individual movies containing a cell division within a pair of cells was performed manually (see methods). In parallel, we developed software to fully automate image analysis from movie extraction to angle measurement in collaboration with Yingbo Li and Auguste Genovesio. Unfortunately, while development of this software was successful, it turned out to be more complicated than anticipated and took longer than expected to develop, and we reached a satisfactory level of functionality only after finishing our screen analysis. Nevertheless, we published this method so that it could be used in future analyses (Li et al., 2016) (see appendix 3).

6.2.2. CANDIDATE CHOICE

We chose to apply a candidate-based approach to perform a mid-scale screen for spindle orientation regulators. The LGN complex is thought to recruit dynein motors to the cell cortex in a polarized manner, therefore localizing pulling forces exerted on astral microtubules and determining final spindle orientation. Therefore, molecules regulating any level of this pathway from LGN recruitment to astral MT were good candidates to regulate LGN controlled spindle orientation.

MOLECULES POTENTIALLY REGULATING LGN COMPLEX ASSEMBLY: In this category we included molecules known for interacting biochemically with LGN or AGS3 (AGS3 is another vertebrate homolog of LGN but it is not required for spindle orientation *in vivo* - Saadaoui et al. under review) or for interacting/modulating NuMA. These molecules are: Frmpd1 (Yuzawa et al., 2011), LGL (Yasumi et al., 2005), STMN2, MACF1 (Luc de Vries, personal communication), RB1 (Uchida et al., 2014), Tankyrase (Chang et al., 2005), Rab 5 (Capalbo et al., 2011), Ubc9 (Seo et al., 2014), AurKA (Gallini et al., 2016; Johnston et al., 2009), Afadin (Carminati et al., 2016; Wee et al., 2011) and RAN (Kiyomitsu

and Cheeseman, 2012). It should be noted, however, that I observed LGN recruitment to the Ed-Gai enrichment not only in mitosis but also in interphase cells. This is probably due to the excessive levels of Gai at the cortex. Hence, it was possible that molecules regulating LGN recruitment/stability do not result in phenotypes in our model. I will come back to this point later in the discussion.

MOLECULAR MOTORS: It is now well established that the LGN complex recruits dynein to the cell cortex which is necessary for correct spindle orientation in diverse contexts (see section 3.5). However, much less is known about the regulation of dynein function by its own subunits and by its multiple adaptors during mitotic spindle orientation. The effect of some regulators has been evaluated in separate studies but it is not clear how they do regulate dynein activity at the cortex and to what extent they are specifically required for regulating the LGN-dynein- spindle orientation pathway (see section 3.5). We therefore decided to test all the dynein subunits and regulators in our spindle orientation assay.

In addition, we decided to evaluate all the kinesins in our system. Except for KIF13B, which contributes to spindle orientation in *Drosophila* (Johnston et al., 2009; Lu and Prehoda, 2013; Siegrist and Doe, 2005), the function of kinesins in metazoan spindle orientation has not been much explored. Most kinesins move in the plus end direction of MT, and it could be imagined that plus end transport of spindle orientation molecules on astral MT is necessary for their cortical localization. In addition, a set of kinesins regulate microtubule dynamics (reviewed in Walczak et al., 2013), which could in turn influence spindle orientation.

MOLECULES POTENTIALLY REGULATING MICROTUBULES FUNCTION IN MITOSIS: As extensively discussed in chapter 2, different molecules that regulate microtubule nucleation, microtubule dynamics or microtubule behavior at the cell cortex contribute to spindle orientation mainly in the context of mammalian cell divisions in parallel to the substrate. Therefore, we included a set of centrosomal proteins as well as microtubule associated proteins and + TIPs in our screen. Some of them were previously evaluated in other spindle orientation models (EB1, MAP4, CLASP1, ASPM,

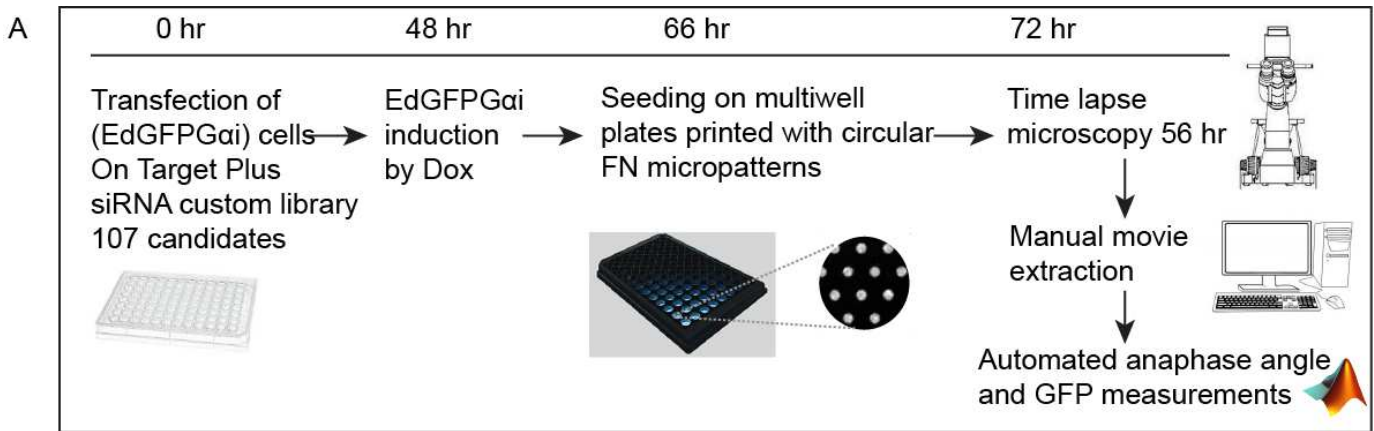
STIL, (Fish et al., 2006; Higgins et al., 2010; Kitagawa et al., 2011; Samora et al., 2011; Toyoshima and Nishida, 2007) while the function of others had not been explored to our knowledge.

Finally, we incorporated molecules that regulate spindle orientation in other systems, such as LKB1 (Wei et al., 2012), Scribble (Nakajima et al., 2013; Zigman et al., 2011), HTT (Elias et al., 2014; Godin et al., 2010), Cadherin (Tuncay and Ebnet, 2016), Diaphanous (Castanon et al., 2013; Johnston et al., 2013) and Rab 11 (Hehnlly and Doxsey, 2014).

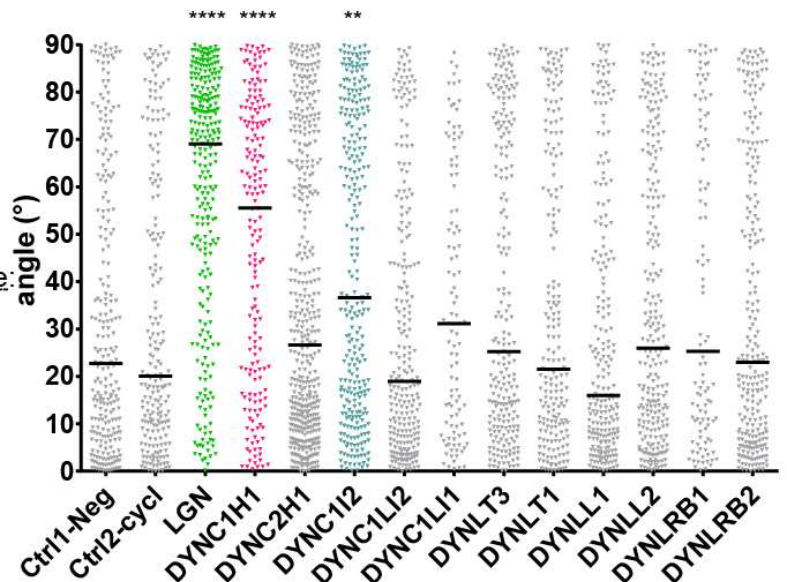
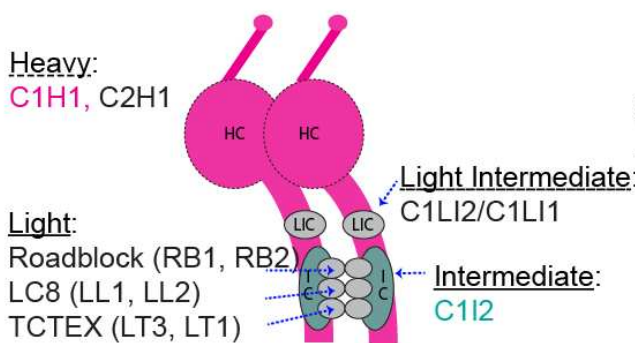
6.2.3. SCREEN RESULTS

All experiments described in this section use EdGFP-Gai cells, and the orientation imposed by EdGFP-Gai is considered as the control condition. siRNA knock-down of LGN, which results in a loss of this EdGFP-Gai control orientation, is used as a positive control of spindle misorientation. The results are presented in Figures 28 and 42. Interestingly, our screen revealed unexpected specificities concerning the regulation of the dynein molecular motor during spindle orientation, as I found that different dynein subunits and adaptors contribute differentially to spindle orientation. In particular, my results unveiled a group of dynein subunits and adaptors (DHC, p150, p50, p22, Arp1A, p62, CAPZ-B and LIS1) which are essential for Ed-Gai spindle orientation as revealed by the dramatic spindle orientation phenotype observed upon depletion of these molecules. In contrast, depletion of numerous dynein subunits and regulators (all Dynein light- and light intermediate- chains, Arp1B, Arp11, p25, p27, CAPZ-A, BICD2, Spindly, ZW10) did not generate any significant phenotype on spindle orientation angles. In addition, depletion of a subset of regulators (Nde1, NdeL1, DIC2) generated subtle but significant phenotypes on spindle orientation and thus these molecules can be considered as regulators needed to fine-tune spindle orientation controlled by the LGN complex. Therefore, this screen allowed us to finely dissect the differential role of dynein regulators in Ed-Gai controlled spindle orientation thus providing important clues for understanding the regulation of dynein in the frame of the LGN-astral MT specific spindle orientation pathway. In addition, these

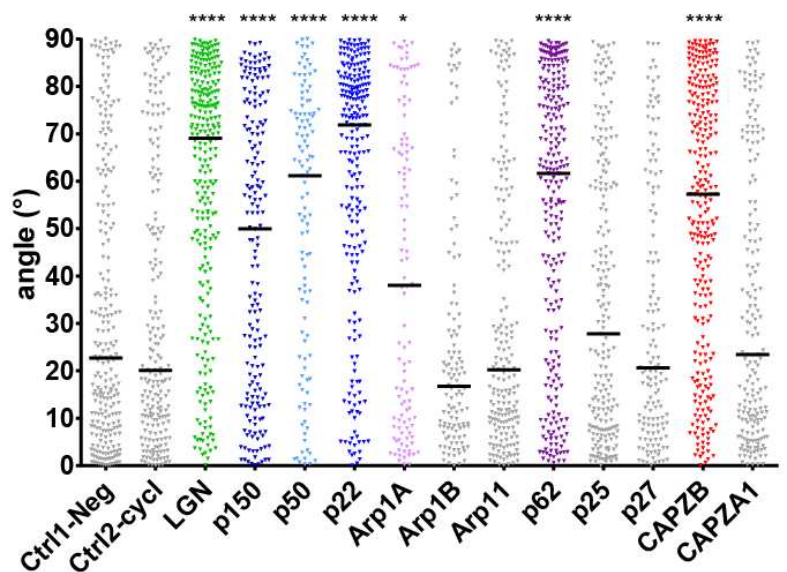
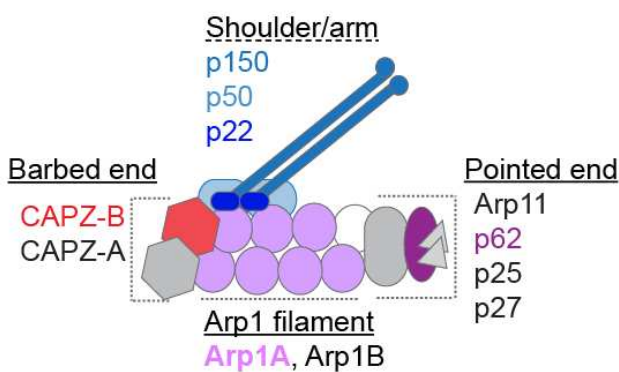
results support the notion that dynein is differentially regulated during specific cellular functions and that the formation of specific complexes varies between cellular activities.



B Dynein subunits



C Dynactin subunits



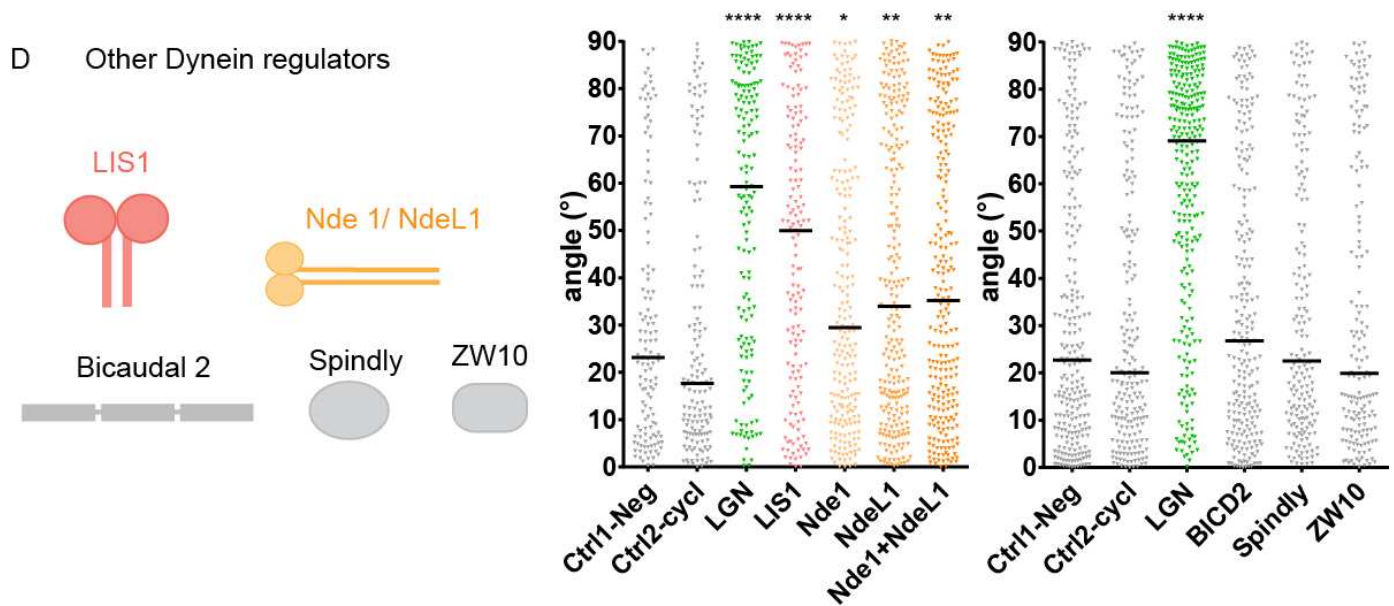


Figure 28 (starts in previous page): A live siRNA screen for spindle orientation regulators using the Ed-Gai spindle orientation model- Dissection of the role of dynein subunits and regulators. a) Workflow used for the screen experiments. b, c, d) Left: Schema of the dynein subunits and adaptors. Right: division angle distributions for cells treated with siRNA against each dynein subunit or adaptor. Treatments generating a significant phenotype are shown in the same color both in the angle distribution graph and the complex schemas. Treatments producing non-significant phenotypes are shown in grey. Two negative controls are shown. siRNA LGN is used as a positive control. b) Dynein complex c) Dynactin complex d) Other adaptors. For each condition, data shown corresponds to the measurements of two independent replicates, except for DYNC1H1 (4 independent replicates).

In the paragraphs below, I analyze in detail the results obtained for individual subunits and adaptors:

DYNEIN COMPLEX (Fig.28b): The motor subunit Dynein Heavy chain 1 (DYNC1H1, DHC1) yielded a significant and massive spindle orientation phenotype in agreement with data obtained in *C.elegans* and HeLa cells (Nguyen-Ngoc et al., 2007; Tame et al., 2014). Of note, knock-down of DHC1 was extremely detrimental, and many cells were blocked in metaphase, illustrating the pleiotropic role of DHC1 in mitosis (Raaijmakers et al., 2013). DHC2, the second “cytoplasmic dynein” heavy chain, reportedly has functions restricted to cilia formation and maintenance (Mikami et al., 2002), and is therefore not expected to control spindle orientation, nor to compensate for the loss of DHC1. Accordingly, I did not observe a significant phenotype when depleting this protein. Dynein intermediate chain 2 (DYNC1I2, DIC2) is the only intermediate chain expressed in HeLa cells (Raaijmakers et al., 2013), and its knock-down also resulted in defective orientation, although less

dramatic than the loss of DHC1 (Fig. 28b). In contrast, none of the light chains (DLC) or light intermediate chains (DLIC) appeared to be indispensable for dynein function in spindle orientation. It is unclear whether this means that dynein can function without light or light intermediate chains in this specific cellular function, or whether this simply reveals redundancy, as there are at least two genes for all these chains. To assess the second possibility, I performed double RNAi treatments to knock down either both DLIC or both DLC of each type simultaneously. Preliminary results did not show any significant phenotype of these double RNAi treatments (data not shown). I will return to this point in the next chapter (Discussion).

Of note, I did not observe any significant spindle orientation phenotype when depleting DYNLL1, in contrast to previous work by Dunsch et al. These authors proposed that increased DHC cortical levels generated by DYNLL1 depletion would be at the origin of spindle misorientation in the z axis (Dunsch et al., 2012)(see chapter 3). However, in the Ed-G α i assay, such an increase in dynein cortical levels would be unlikely to misorient the spindle in the xy axis, as dynein is expected to be strongly polarized to the Ed-G α i site of enrichment.

DYNACTIN COMPLEX (Fig. 28c): The structure of the dynactin complex has recently been described in great detail (see chapter 3) (Chowdhury et al., 2015; Urnavicius et al., 2015); knock-down of all three subunits of the shoulder and arm of dynactin (p150, p50 and p22) resulted in orientation defects as severe as LGN knock-down, indicating an essential role of these subunits in the orientation pathway. Removal of Arp1A, the most abundant component of the Arp filament, also resulted in defective orientation, whereas Arp1B knock-down had no effect. It is proposed that both Arp1A and Arp1B are present in dynactin with a ratio of 15:1 (Clark et al., 1994). One question is whether the presence of Arp1B is required in dynactin complexes for specific cellular functions or if this subunit can be replaced by Arp1A. My observation that Arp1B is dispensable for spindle orientation suggests that Arp1B knock-down can be compensated by the reportedly more abundant Arp1A at least in this specific cellular function. The reverse may not be possible due to limited availability of Arp1B in the

cell or to a preferential incorporation of Arp1A rather than of Arp1B in the dynactin complex. Concerning the complex that is assembled at the pointed end of the dynactin filament, p62 appears as an essential component for spindle orientation, while Arp11, p25 and p27 seem to be dispensable for this cellular function. Finally, within the barbed end CAPZ A/B heterodimer, while depletion of CAPZ-A did not result in any significant phenotype, depletion of CAPZ-B generated a dramatic shift in spindle orientation angles. This was surprising because CAPZ-B was described as dispensable for numerous dynactin-dynein mitotic functions (Raaijmakers et al., 2013). I pursued investigations of CAPZ-B function as described in the next sections.

OTHER DYNEIN REGULATORS (Fig. 28d): I found that LIS-1 is essential for LGN guided spindle orientation, which is consistent with previous data showing spindle orientation defects in LIS-1 depletion conditions (Moon et al., 2014; Yingling et al., 2008). Similarly to depletion of DHC, LIS-1 RNAi treatment was profoundly harmful for cells, which again agrees with the previously shown requirement of LIS-1 for several mitotic functions (Raaijmakers et al., 2013). In contrast, RNAi treatment targeting Nde1, NdeL1 or both proteins together resulted in significant spindle orientation phenotypes but much subtle than those observed for LIS-1. This agrees with previous data showing spindle misorientation in Nde1 knock out mice (Feng and Walsh, 2004). Nde1 and NdeL1 are highly homologous proteins; however, while they share several functions, they show specificity for other processes (Bradshaw et al., 2013). Notably, while Nde1 mutant embryos show defects in spindle orientation in neural progenitors (Feng and Walsh, 2004), so far defects in spindle orientation had not been associated with NdeL1 mutants (Moon et al., 2014). Hence, our screen brings the first evidence for an actual requirement of NdeL1 in oriented divisions.

Finally, BICD2, Spindly or ZW10 seem dispensable for Ed-Gai-controlled spindle orientation. Of note, Spindly was recently shown to regulate spindle orientation with respect to the growth surface (Chan et al., 2009) and with respect to the adhesion pattern in cells cultured on bar micropatterns (Tame et al., 2016) (section 3.5). However, Tame and colleagues have shown that defects on spindle

orientation observed upon Spindly depletion are an indirect consequence of chromosome misalignment generated in this condition, which in turn results in LGN delocalization from cortical sites close to misaligned chromosomes (Tame et al., 2016). The strongly polarized, Ed-G α i-recruited LGN is unlikely to be sensitive to this inhibition.

In conclusion, our screen brought novel data concerning the function of several dynein subunits and regulators in LGN complex controlled oriented divisions. Moreover, the previously shown role of certain subunits (namely DHC1, p150, p50, LIS1 and Nde1) is confirmed in our newly developed spindle orientation model, in which the phenotypes observed by depletion of most of these proteins are much more dramatic than what is generally shown in other spindle orientation models. This positions our model as a valuable tool to test the function of proteins in LGN dependent spindle orientation. In contrast, I obtained different results with respect to previous work concerning specific proteins (such as DYNLL1 and Spindly). This might reflect differences between our model and other widely used spindle orientation systems, which will be further addressed later in this manuscript.

Finally, analysis of the rest of the candidates did not reveal any of them as being essential in our spindle orientation model (Fig. 42). I observed subtle phenotypes for MAP4 and EB3 as expected from previous work showing these candidates as spindle orientation regulators in other systems. Surprisingly, I did not find any phenotype within the centrosomal proteins, suggesting that they might not regulate astral MT nucleation or alternatively, the regulation that they exert is not essential in a system where cortical cues are strongly polarized from early mitosis. Similar concepts could explain the absence of phenotypes observed for other specific proteins. I will further discuss these results in the next chapter.

6.3. THE ACTIN CAPPING PROTEIN CAPZ-B LOCALIZES TO THE SPINDLE POLES AND CELL CORTEX IN MITOSIS, AND REGULATES MITOTIC SPINDLE ORIENTATION IN ADHERENT CELLS

CAPZ-B is best known for its role as an actin capping protein clearly established by *in vitro* and *in vivo* evidence. This classical and essential function of CAPZ-B is reflected in several cellular and developmental processes that indeed require proper actin dynamics and CAPZ A/B (see chapter 4). On the other side, CAPZ-B is identified as a biochemical component of the dynactin complex. Recent structural studies have demonstrated a tight association of the CAPZ A/B heterodimer to the barbed end of the dynactin filament and proposed this association to be important for dynactin stability. However, to date, no functional studies have attributed a role to the presence of CAPZ-B in this complex. Of note, Raaijmakers et al. performed a systematic analysis of all dynein and dynactin complex core members and regulators for their function in mitosis. The phenotypic screen focused on numerous aspect of cell division, including dynein localization to the nuclear envelope and kinetochores, centrosome anchoring at the nuclear envelope, mitotic index, spindle focusing and dynein inward force generation at the spindle (Raaijmakers et al., 2013). Remarkably, CAPZ-B came out as one of the few members of the dynactin complex that did not display any noticeable phenotype in any of these categories. However, the screen did not investigate spindle orientation phenotypes. Since CAPZ-B emerged as one of the strongest hits in our spindle orientation screen, we decided to better characterize its involvement in this pathway. For this, I used HeLa cells cultured on homogeneous fibronectin coated slides.

I first investigated the effect of CAPZ-B depletion on spindle orientation with respect to the substrate. In order to avoid potential fixation artifacts on cell shape and spindle orientation, I acquired stacks of live EB3-GFP expressing cells in metaphase. CAPZ-B depletion induced a subtle but significant shift in angle distribution (Fig. 29) very much like the defects observed in LGN or NuMA knock-down.

This defect is minor in comparison to the misorientation observed in the Ed-Gai assay (Fig. 28c), highlighting the difference between models (see discussion chapter). Nevertheless, this confirms CAPZ-B function in another spindle orientation model in which other LGN-dynein complex members were seen to contribute to spindle orientation in a similar extent than CAPZ-B.

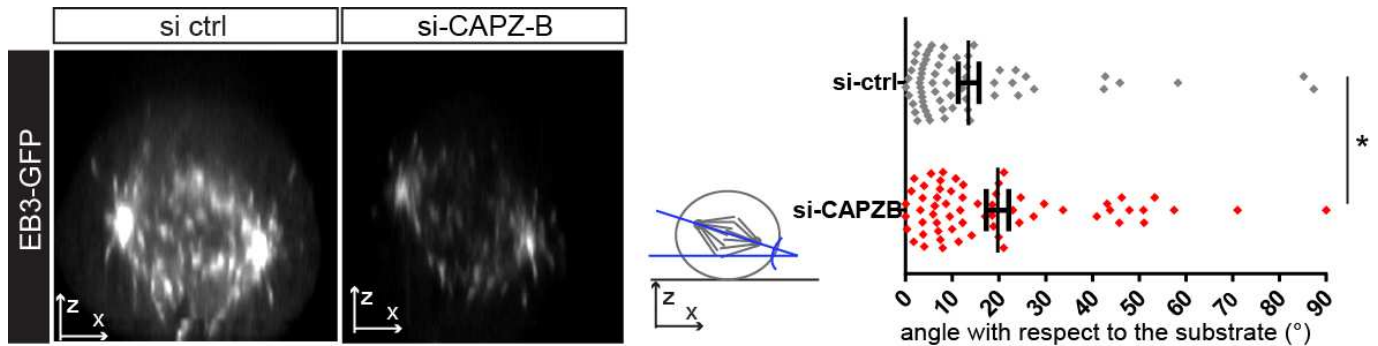


Figure 29: Effect of CAPZ-B siRNA on spindle orientation with respect to the substrate. Left: z views of live EB3-GFP cells transfected with Ctrl or CAPZ-B siRNAs. Right: Spindle orientation angles for each condition measured as depicted in the schema. Data correspond to two independent experiments.

I then investigated the localization of CAPZ-B in mitotic HeLa cells. For this, I transfected a CAPZ-B-GFP expression vector and followed the distribution of the fusion protein in live cells. In metaphase cells, CAPZ-B was enriched at the spindle poles over a diffuse cytoplasmic distribution; in addition, a slight enrichment could be observed at the cellular cortex, which was enhanced over the spindle poles (Fig.30 a-b). This cortical signal increased during anaphase (Fig.30.c-d). This localization and dynamics recapitulate the behavior previously described for molecules of the dynein and dynactin complex (e.g. DHC-GFP and Arp1A-GFP (Kiyomitsu and Cheeseman, 2012; Kotak et al., 2013) suggesting that during mitosis, CAPZ-B is part of the dynactin-dynein complex at the cortex, where it may regulate its function.

In accordance, though the cortical staining was less clear, endogenous CAPZ-B strongly localizes to the spindle poles and to the cytoplasm, and this signal is clearly decreased upon CAPZ-B siRNA treatment, as seen by immunostainings (Fig. 30e).

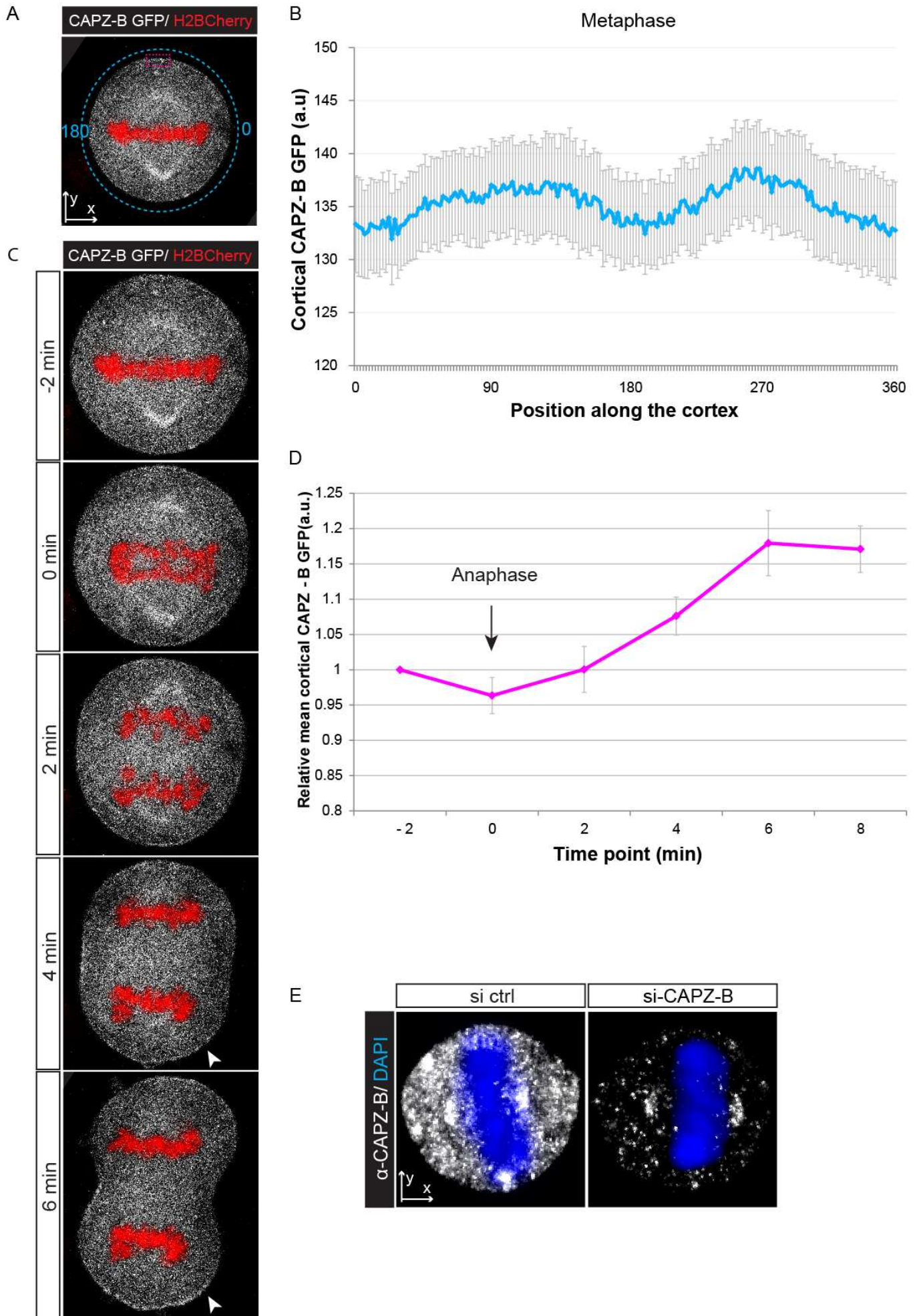


Figure 30 (previous page): Localization of CAPZ-B in mitotic cells. a, b, c, d) Localization of CAPZ-B-GFP in live cells expressing H2B-Cherry. a) shows CAPZ-B GFP in metaphase, b) shows the quantification of the CAPZ-B-GFP signal all around the cortex measured as depicted in a) . The graph shows the average curve for n= 10 cells. The curve for each cell was obtained by averaging several metaphase frames. c) Time lapse of CAPZ-B-GFP signal showing the last frame of metaphase and several frames for anaphase. d) Quantification of CAPZ-B GFP cortical signal over time. The quantification was done by measuring the fluorescence in a rectangle drawn on each cortical side (see a) in the last frame of metaphase and over the course of anaphase. Values were normalized to the values measured in the last metaphase frame. The curve is the average for n=13 cortical sides. Error bars correspond to SEM in b) and d). e) Endogenous CAPZ-B signal in ctrl or CAPZ-B siRNA treated cells.

6.4. CAPZ-B CONTROLS SPINDLE ORIENTATION IN AN ACTIN INDEPENDENT MANNER

CAPZ-B is known for its function as an actin capping protein. CAPZ-B forms a heterodimer with CAPZ-A, which binds with high affinity to the barbed ends of actin filaments. This blocks the fast growing activity of filaments by preventing the addition of new actin monomers and terminates actin elongation. The actin capping activity of CAPZ-B has been implicated in various cellular processes including cell migration, autophagy and organization of actin filaments in Z-bands in striated muscle fibers (see chapter 4).

A recent study performed in mouse oocytes identified a role of CAPZ-B in asymmetric spindle migration and polar body extrusion (Jo et al., 2015). The meiotic spindle in mammalian oocytes is devoid of astral microtubules, and its mechanisms of positioning are markedly different from classical spindle orientation in later developmental stages (section 2.9). In particular, a host of data has characterized the role of the actin cytoskeleton in this model (reviewed in Almonacid et al., 2014 and section 2.9). Indeed, the role of CAPZ-B in meiotic spindle positioning involves the actin cytoskeleton (Jo et al., 2015). However, since the actin cortex also plays a role in mitotic spindle positioning in many tissue and cell types (section 2.5), I wondered whether the spindle orientation phenotypes that I observed upon CAPZ-B depletion depend on its role in actin or in dynactin regulation.

I therefore investigated the effect of CAPZ-B depletion on the actin cortex. Remarkably, CAPZ-B depletion induced a significant increase in the density of cortical and cytoplasmic actin in mitotic cells, as revealed by phalloidin staining (Fig. 31). My experiments in the Ed-Gai system had shown

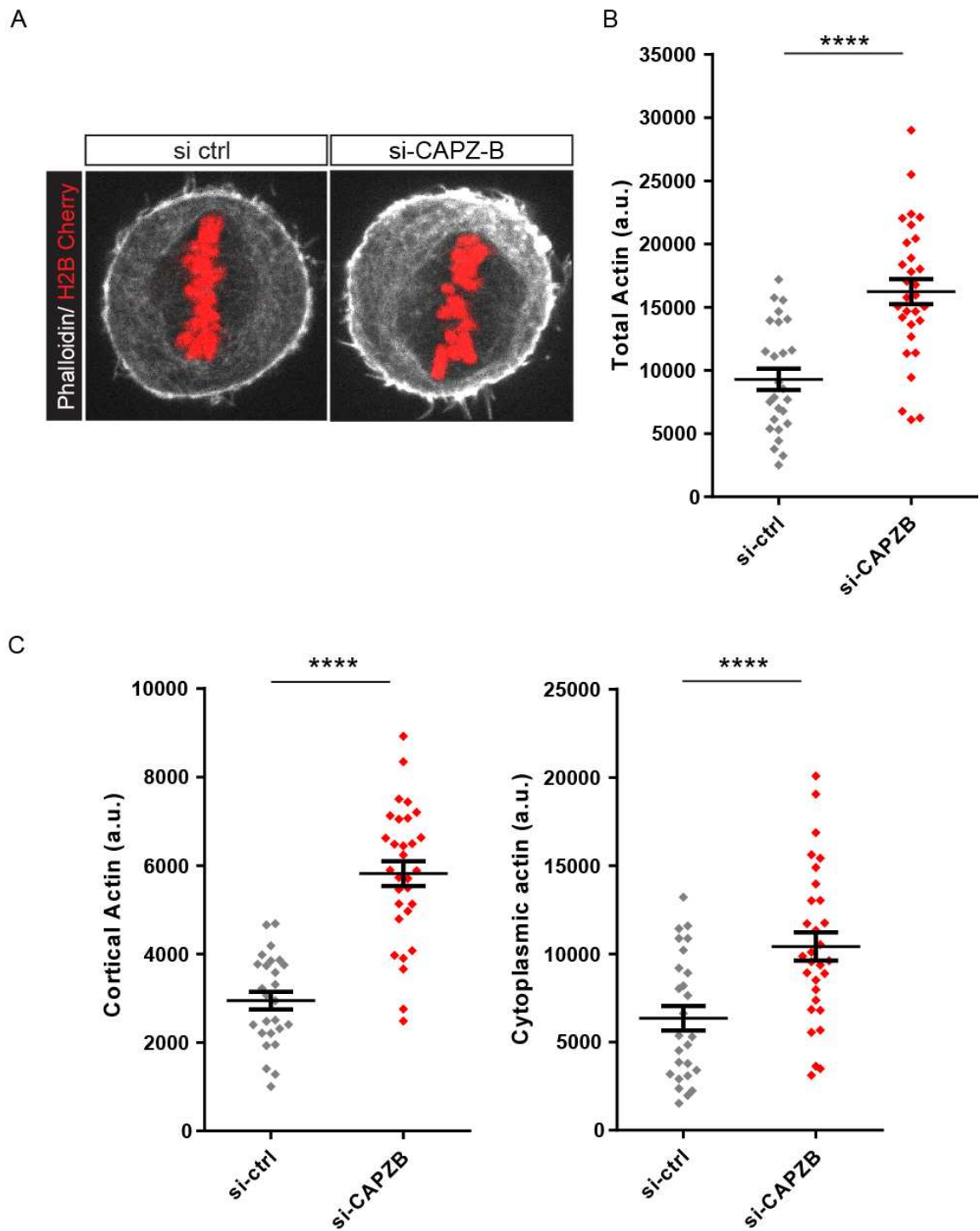


Figure 31: Effect of CAPZ-B depletion on the actin cytoskeleton in mitotic cells. a) Phalloidin staining (F-actin) in Ctrl or CAPZ-B siRNA treated cells. b) Quantification of the total phalloidin signal for one representative experience for Ctrl and CAPZ-B siRNA treated cells. c) Quantification of cortical and cytoplasmic total fluorescence. Cortical fluorescence was deduced from subtracting the cytoplasmic fluorescence to the total fluorescence.

that **reducing** the actin cortex through Latrunculin treatment did not affect G α i driven orientation (Fig. 26d), but this was not sufficient to exclude that a CAPZ-B RNAi-dependent **increase** in actin density at the cortex may affect orientation in this model.

I established that treatment of CAPZ-B RNAi cells with low doses (0.4 μ M) of Latrunculin-A reverted actin to the levels found in control cells (Fig. 32b). However, when applied in the EdGFP-G α i orientation assay, Latrunculin A treatment did not rescue the CAPZ-B RNAi spindle orientation phenotype (Fig. 32c). Altogether, these data indicate that CAPZ-B controls spindle orientation independently of its role on the actin cytoskeleton.

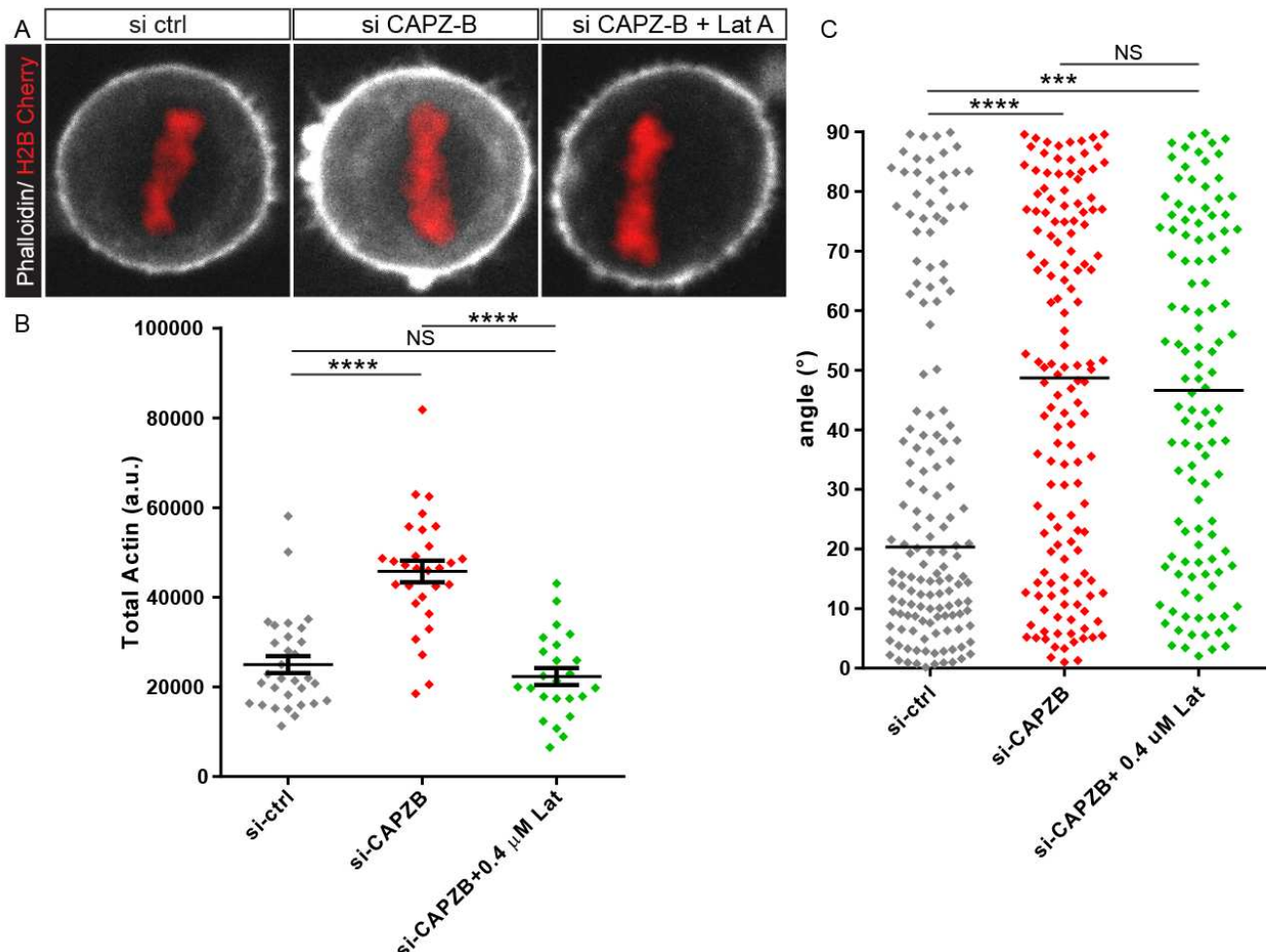


Figure 32: CAPZ-B regulates Ed-G α i controlled spindle orientation independently of actin modulation. a, b) Treatment of CAPZ-B depleted cells with Latrunculin A 0.4 μ M reduces F-actin levels to the control levels. c) Anaphase spindle orientation angles in the Ed-G α i spindle orientation assay in Ctrl-siRNA, CAPZ-B siRNA and CAPZ-B siRNA+ Latrunculin 0.4 μ M. Turning F-actin levels back to the control level does not rescue the spindle orientation phenotype generated by CAPZ-B depletion.

6.5. REGULATION OF DYNACTIN/DYNEIN COMPLEXES BY CAPZ-B

In addition to its role as an actin capping protein, numerous investigations have demonstrated that CAPZ-B is part of the dynactin complex (chapter 4); however, in human cells, no defect in dynein/dynactin functions have been seen upon depletion of this protein (Raaijmakers et al., 2013), raising the question of its functional role in the dynactin complex. The fact that CAPZ-B depletion generates a strong phenotype in our LGN-dependent OCD model, as well as the mitotic distribution of CAPZ-B, suggested that it could be regulating the function of the dynactin/dynein complexes in the context of spindle orientation. I therefore investigated the distribution of several members of the dynein and dynactin complexes during mitosis in CAPZ-B depleted cells.

I first focused on the dynactin complex. P150 and Arp1a are two major components of the projecting arm and filament structural domains of dynactin, respectively. Previous data in cycling HeLa cells have suggested that CAPZ-B depletion does not significantly affect the levels of Arp1 and p150 (Raaijmakers et al., 2013). Focusing on mitotic cells, I used an antibody against p150, and a stable cell line expressing an Arp1a-GFP fusion protein to evaluate the effect of CAPZ-B siRNA on these proteins (Kiyomitsu and Cheeseman, 2012). Both proteins showed a strongly decreased distribution at the mitotic cell cortex upon CAPZ-B depletion (Fig. 33a-b). Of note, quantification of the total levels of these proteins in pictures showed that CAPZ-B depletion also results in a decrease in the total levels of these dynactin members in mitotic cells (Fig. 43a). This suggests that CAPZ-B is important for dynactin stability, and is in agreement with predictions derived from structural analyses (Chowdhury et al., 2015; Urnavicius et al., 2015).

I then analyzed the distribution of dynein heavy chain 1 in a DHC-GFP cell line (Hutchins et al., 2010) and of the endogenous dynein intermediate chain. In contrast to dynactin complex members, both DHC1-GFP and DIC were normally distributed at the cortex upon depletion of CAPZ-B (Fig. 33c and 34a). In contrast, I observed that knock-down of either p150 or Arp1a, which both cause spindle

orientation phenotypes similar to CAPZ-B depletion in the Ed-Gai model, strongly reduced the level of DIC cortical recruitment (Fig. 43 b-c).

Hence, contrary to Arp1a and p150, CAPZ-B is not essential for dynein recruitment or stabilization at the cell cortex. However, the strong spindle orientation defects observed upon CAPZ-B depletion in the Ed-Gai assay suggest that CAPZ-B is necessary for the motor activity of dynein, most likely due to stabilization of the dynactin complex (Fig. 43d).

As presented in chapter 2, Kiyomitsu and Cheeseman (Kiyomitsu and Cheeseman, 2012) have recently described a stereotypical oscillatory movement of the mitotic spindle during metaphase, whereby the spindle is displaced along its axis so that both poles get alternatively closer to the cortex. These observations were made in a stable cell line expressing DHC1-GFP, and they described how a monopolar cortical DHC1-GFP enrichment oscillates and precedes the movement of the spindle, such that one pole is attracted to the DHC1-GFP enrichment. Subsequently the enrichment is lost through a Plk1-dependent inhibitory signal emanating from the spindle pole and reappears at the opposite side of the cortex which is most distant from spindle poles (see chapter 2). Using the same DHC1-GFP cell line, I observed the same oscillatory behavior of DHC1-GFP and of the spindle throughout metaphase in control cells; however, upon CAPZ-B depletion, when a single DHC1-GFP crescent was observed, spindle movements towards this crescent were lost (Fig. 34a-b). This agrees with the hypothesis that dynein motors are not activated at the cell cortex in the absence of CAPZ-B.

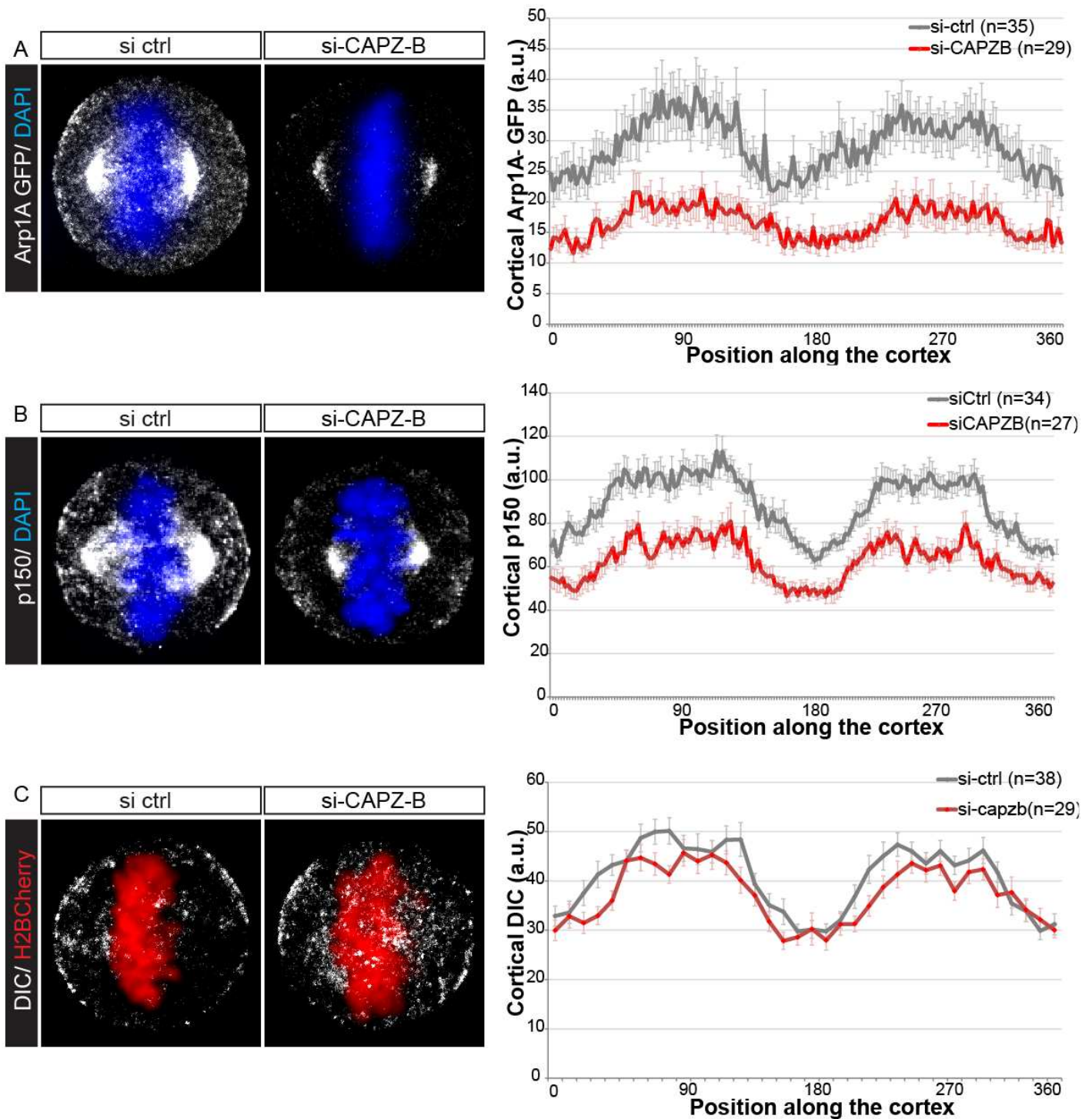


Figure 33: Effects of CAPZ-B depletion on the Dynactin and Dynein complexes. a, b, c) Cortical levels of dynactin/dynein in Ctrl or CAPZ-B siRNA treated cells. Left: Representative pictures of a) HeLa Arp1-GFP –a subunit of the Arp1 filament- or HeLa cells stained for b) p150 –a subunit of dynactin- or c) Dynein intermediate chain (DIC). Right: Quantification of cortical levels for each condition for one representative experience. The graphs show the average for n cells \pm SEM. All values are corrected by background.

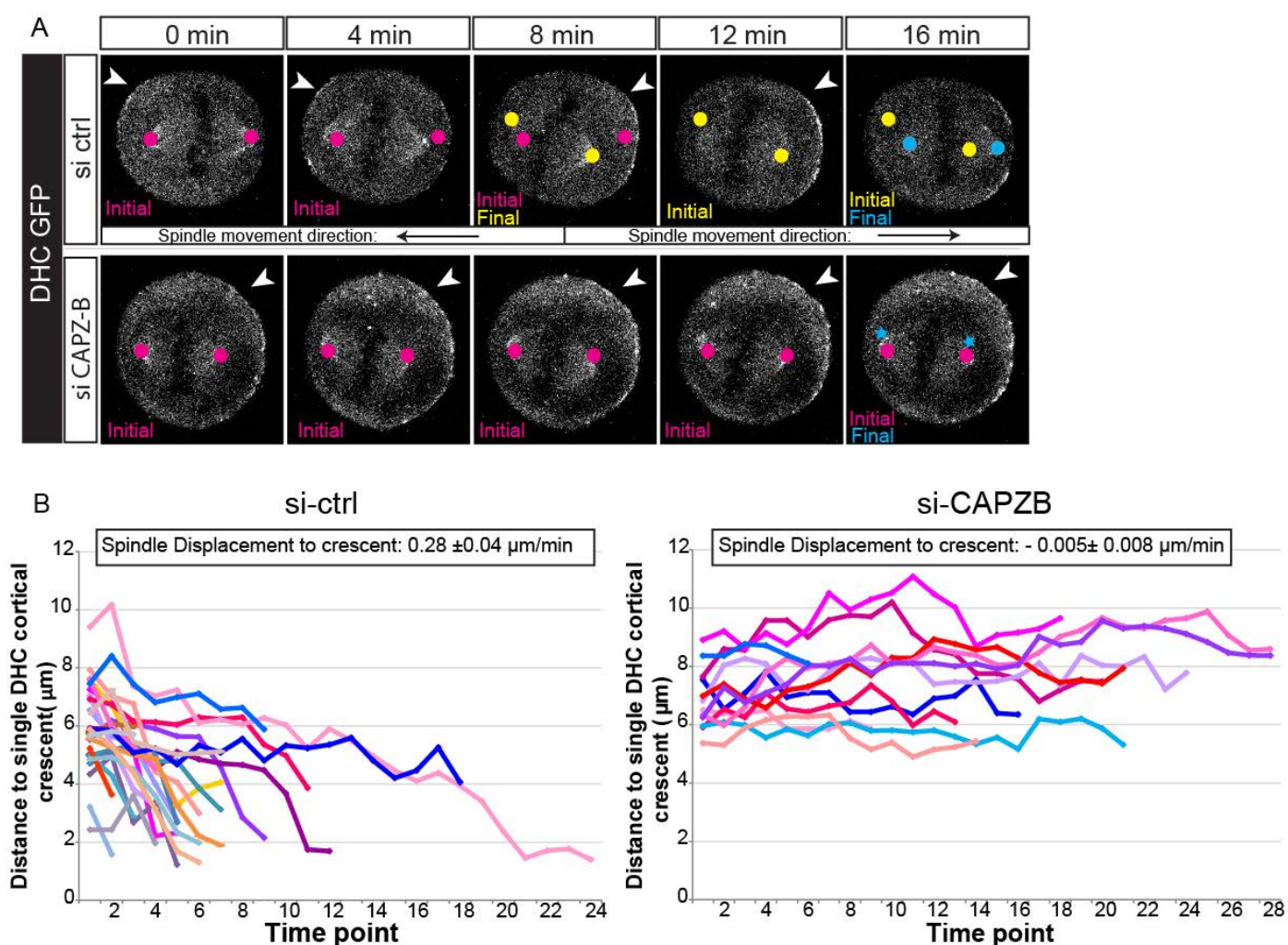


Figure 34: Effect of CAPZ-B depletion on the spindle displacement towards single DHC-GFP crescents. a) Representative time-lapse images for Ctrl or CAPZ-B siRNA treated cells. In the control condition, a first spindle displacement towards the DHC crescent on the left is shown between frames 1 and 3. Observe the difference between the initial spindle poles positions (in pink) and the final position (in yellow). A second spindle displacement towards the new DHC crescent on the right is appreciated between frames 3 and 5. In the last frame, the yellow circles depict the initial position and the light blue ones the final position. In CAPZ-B siRNA treated cells. The final position of spindle poles is marked by the light blue stars. No significant spindle movement towards the DHC crescent on the right is seen. b) Graphs illustrating the distance of the spindle pole closer to a single DHC crescent over time. In the control condition, this distance decreases over time illustrating spindle movement towards the DHC crescent. Each curve represents one distinguishable spindle displacement; thus in some cases different curves were obtained from the same cell. In CAPZ-B depleted cells, the distance does not decrease progressively over time. Each curve corresponds to a single cell. The spindle displacement values shown on top of each graph were obtained by calculating Δ distance between 2 frames (2 min) and then averaged and divided by 2 min (acquisition interval). In the control case, the Δ distance is highly variable, being minimal between some frames and on the order of μm in some others as appreciable in the curves.

6.6. CAPZ-B CONTROLS THE DYNAMICS OF MITOTIC MICROTUBULES

Spindle orientation results from the application of forces localized and generated at the cell cortex to astral microtubules. Hence, the number of astral microtubules and their stability near the cell cortex also contribute to spindle positioning (see section 2.6). CAPZ-B localizes to the mitotic spindle poles and there it could regulate spindle morphology or astral MT. In addition, it has been shown that CAPZ-B regulates microtubule polymerization *in vitro* and microtubule stability in interphase fibroblasts (see section 4.3.3).

Therefore, I next investigated whether CAPZ-B depletion would result in defects in mitotic spindle characteristics. Antibody staining for α -tubulin in HeLa cells showed that while spindle morphology appears unaffected, CAPZ-B depletion generates a significant reduction in spindle density. The reduction was visible in both the central spindle and astral microtubules (Fig. 35b-c). To further characterize this phenotype, I analyzed microtubule dynamics using the EB3-GFP reporter of microtubule +end tips. Live images of the mitotic spindle were acquired at short time interval (500 ms) with a spinning disk confocal system from cells in metaphase (see Methods), and data were analyzed using the u-track software package (Applegate et al., 2011; Matov et al., 2010)(Fig 36a). This software allows to measure several parameters of MT dynamics based on thousands of tracks automatically analyzed per cell. Compared to control cells, CAPZ-B depleted cells showed significant changes in microtubule dynamics (Fig. 36). Notably, these include an increase in growth and shrinkage speed and a decrease in growth lifetime. To evaluate if these defects were mediated by the decrease in dynactin complex levels, I performed similar experiments in p150 and Arp1A depleted cells. Remarkably, while both conditions displayed changes in growth lifetime similar to CAPZ-B depletion, growth speed showed no difference with control cells, and shrinkage speed showed an opposite tendency upon p150 depletion compared to CAPZ-B depletion. Therefore, these data suggest that CAPZ-B regulates the speed of spindle microtubules growth and shrinkage independently of its effect on p150 and Arp1A levels. In contrast, all three proteins regulate microtubules growth lifetime in a similar manner.

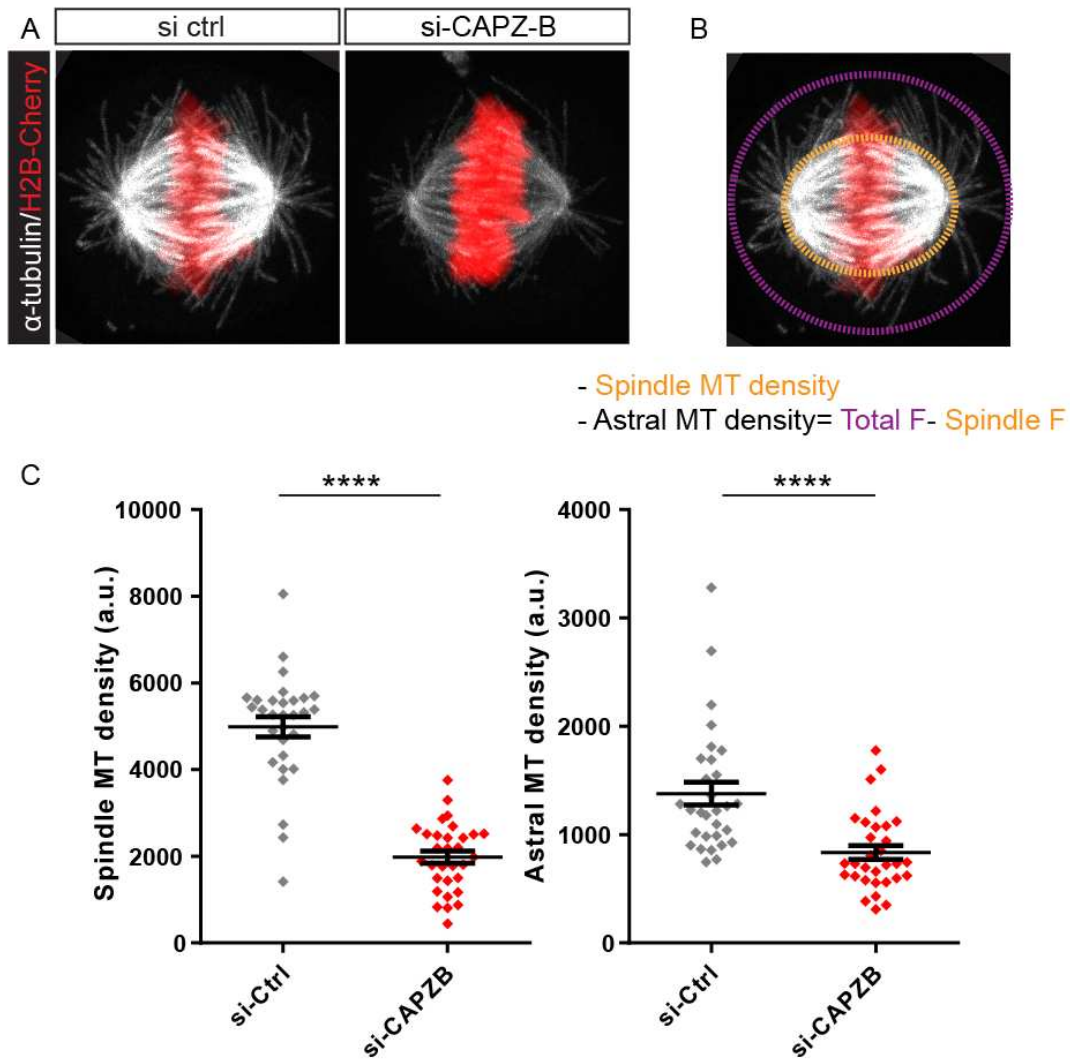


Figure 35: Effect of CAPZ-B depletion in spindle- and astral- MT density. a) Representative α -tubulin stainings for ctrl and CAPZ-B siRNA treated cells. c) Quantification of the α -tubulin fluorescence signal in the spindle and astral MT measured as depicted on the left. Astral MT fluorescence is obtained by subtracting the spindle fluorescence to the total fluorescence as indicated in b). All values are corrected by background. The graphs correspond to one representative experience.

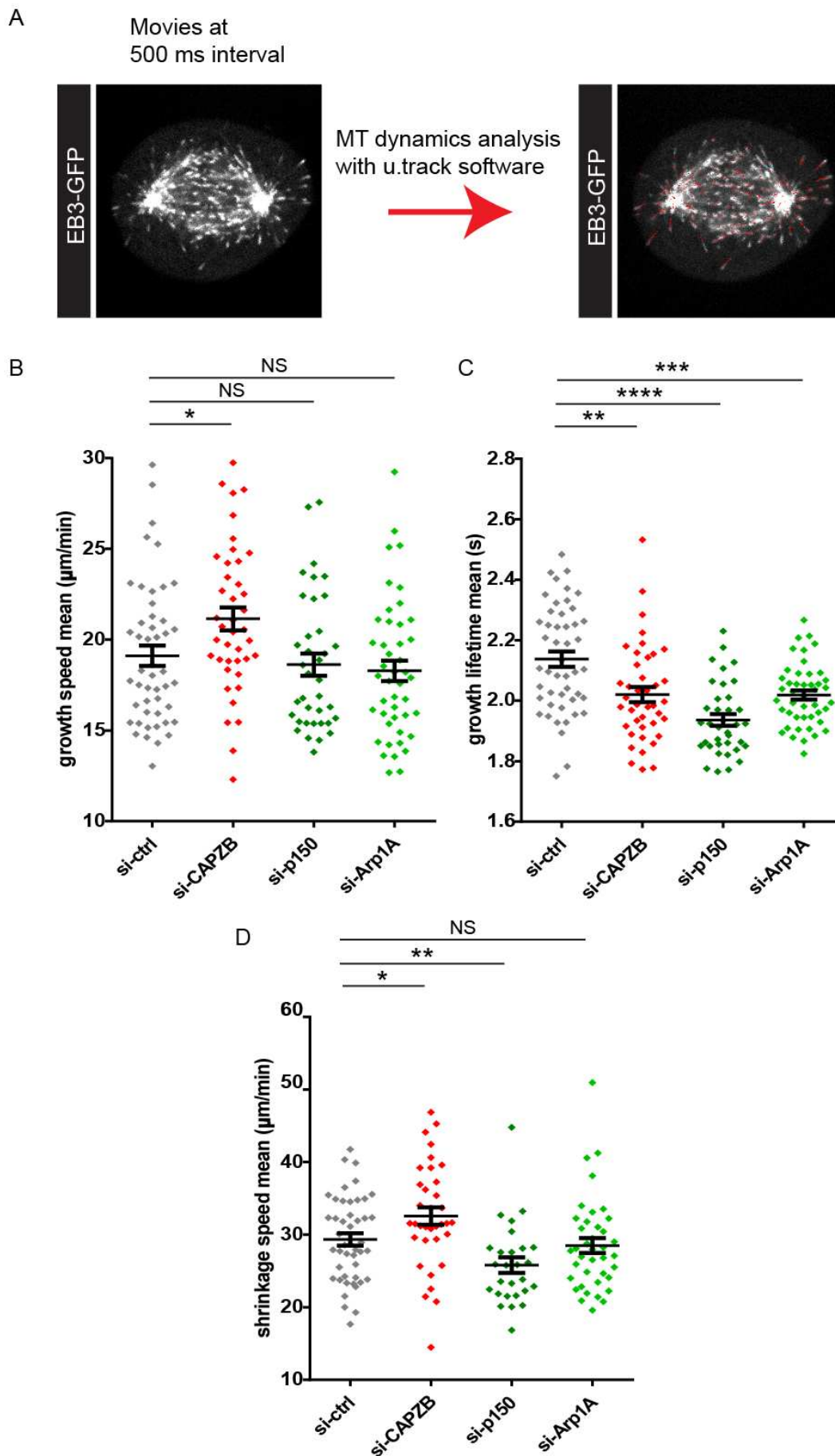


Figure 36: Effect of CAPZ-B depletion on astral MT dynamics. a) Workflow used for evaluating MT dynamics in metaphase cells, showing one example image of an EB3-GFP cell obtained in the movies, and the corresponding image obtained in the MT tracking output. Tracks are seen in red. b, c, d) Comparison of growth

speed (b), growth lifetime (c) and shrinkage speed (d) in cells treated with Ctrl, CAPZ-B, p150 or Arp1-A siRNA. Each point is the average from thousands of tracks measured in one single cell. Data correspond to two independent experiments.

6.7. CAPZ-B CONTROLS PLANAR SPINDLE ORIENTATION IN THE CHICK NEUROEPITHELIUM

We next investigated whether CAPZ-B plays a significant role in regulating oriented divisions in a developing tissue *in vivo*. Our previous experiments have shown that planar spindle orientation in the chick spinal cord neuroepithelium depends on the lateral localization of the LGN complex (Morin et al., 2007; Peyre et al., 2011; Saadaoui et al., 2014). Besides, loss-of-function experiments in neuroepithelial progenitors in the mouse cortex have shown a role for the dynein regulators Lis1 and Nde1 in spindle orientation (Feng and Walsh, 2004; Moon et al., 2014; Pawlisz et al., 2008; Yingling et al., 2008), which was confirmed in our RNAi screen for LGN complex downstream regulators (Figure 28d).

I first investigated the expression and subcellular distribution of CAPZ-B in the neuroepithelium at embryonic days 3 and 4 (E3-E4) of development. On en-face whole mounts of the neuroepithelium, the anti-CAPZ-B antibody shows a diffuse staining throughout mitotic cells, with a clear enrichment

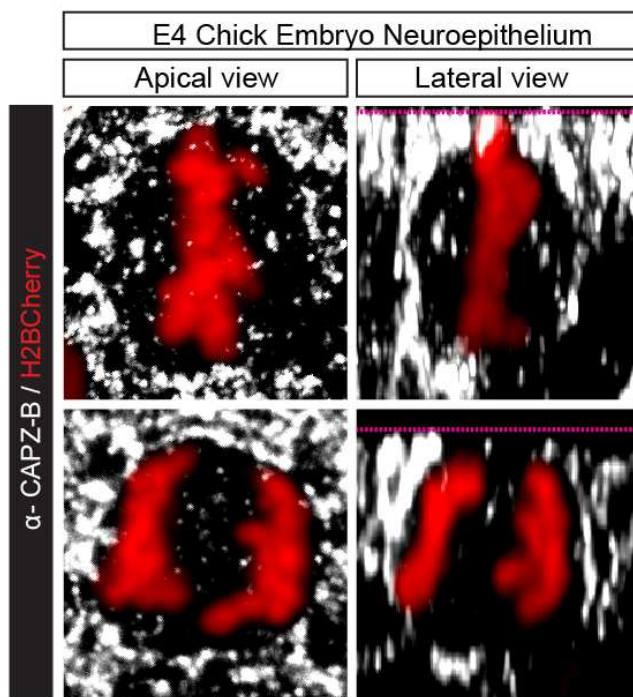


Figure 37: CAPZ-B localization in neuroepithelial progenitors in the chick embryonic neuroepithelium. Localization of endogenous CAPZ-B in neural progenitors in metaphase and anaphase. Apical and lateral (z) views are shown. Embryos were electroporated with H2BCherry.

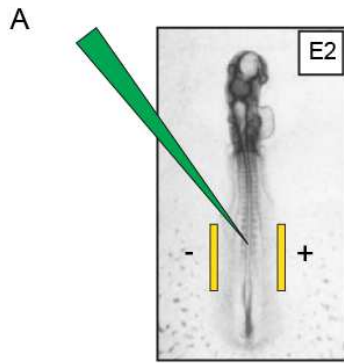
on the spindle and at the cell cortex both in metaphase and anaphase (Fig. 37). A CAPZ-B-GFP construct (mouse CAPZ-B) shows a similar distribution on the cytoplasm and spindle poles 24h after *in ovo* electroporation at E2, but the cortical staining was not detectable under these conditions (data not shown).

To address the role of CAPZ-B in spindle orientation in these cells, we used the CRISPR/Cas9 gene editing method to introduce small genomic insertion/deletions (indels) in the CAPZ-B coding sequence (Cong et al., 2013). Following a method recently described in the mouse embryonic cortex (Kalebic et al., 2016), we directly introduced the purified Cas9 nuclease complexed with *in vitro* synthesized gRNA sequences targeting the CAPZ-B coding sequence, together with a reporter plasmid coding for a human Histone2B-GFP fusion protein, through electroporation in the neuroepithelium (see methods; Fig. 38a). Electroporation *in ovo* was performed at 2 days of development (E2; HH stage 14) and embryos were harvested 48h after electroporation at E4. The effect of the CRISPR/Cas9 strategy on CAPZ-B expression was analyzed on transverse sections, using the anti-CAPZ-B antibody. In cells electroporated with a gRNA targeting coding exon 3 of CAPZ-B, a clear reduction in the staining was observed (Fig. 38b), whereas no reduction was observed in embryos electroporated with a control gRNA targeting a sequence in intron 3 of CAPZ-B (data not shown).

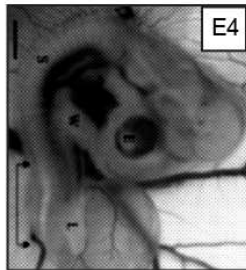
We then went on to measure spindle orientation in electroporated cells, using our previously developed method for 3D spindle measurement on flat-mounted neuroepithelia (see methods; Saadaoui et al., 2014; Fig. 38c). While mitotic control cells (electroporated either with Cas9 complexed to a control gRNA, or with the H2B-GFP expression plasmid alone) harbored a metaphase spindle that was mostly aligned with the apical surface (average angle = $\sim 12^\circ$), we observed strong defects in spindle orientation in cells electroporated with the guide RNA targeting CAPZ-B exon 3 (average angle = $\sim 27^\circ$) (Fig. 38c,e). Of note, genome targeting with the Crispr/Cas9 method by direct electroporation in cells is unlikely to yield a loss-of-function mutation in all cells that receive the Cas9/gRNA complex, nor in all cells that receive the electroporation reporter plasmid. Indeed, we

only observed a partial overlap between electroporated cells and loss of the CAPZ-B antibody signal. Hence the spindle orientation defect that we measured in cells expressing the H2B-GFP reporter is probably an underestimation of the phenotype, as only a subset of these cells might have actually lost CAPZ-B expression. Importantly, we did not observe any major perturbation of tissue polarity as determined by immunostaining of polarity markers in Crispr CAPZ-B electroporated tissue (Fig. 38d). Overall, these data show that CAPZ-B is an essential regulator of planar spindle orientation in neuroepithelial cells. Since these cells also depend on LGN for the orientation of their axis of division, we conclude that CAPZ-B also acts downstream of the LGN pathway to control planar spindle orientation in the neuroepithelium *in vivo*.

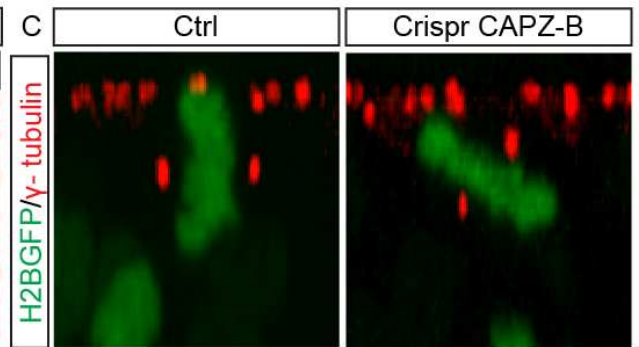
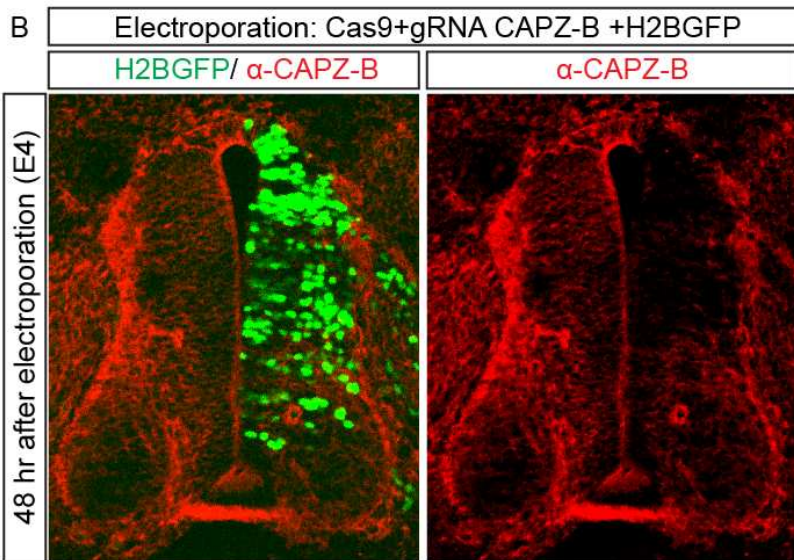
Figure 38 (next page): CAPZ-B function during planar spindle orientation of neuroepithelial progenitors in the chick embryonic neuroepithelium. a) Workflow for studying the function of CAPZ-B in spindle orientation in the neuroepithelium. b) Representative stainings of CAPZ-B in sections from embryos electroporated with Cas9+gRNA targeting the exon 3 of CAPZ-B. H2B-GFP is the electroporation marker. c) Example z- view pictures showing the metaphase spindle orientation in Ctrl or Crispr-CAPZ-B embryos. Below is a schema illustrating the measurement of metaphase spindle orientation angles with respect to the apical surface (marked by centrosome γ -tubulin stainings). d) Sections obtained from Crispr-CAPZ-B electroporated embryos were stained for the polarity markers N-cadherin and aPKC. No gross defects in these markers were seen. e) Distribution of angles for ctrl and Crispr-CAPZ-B conditions as measured in c. Data was obtained in two independent experiments from a total of 7 embryos for each condition.



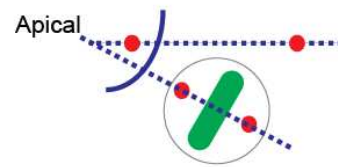
0 hr: E2 embryos: In ovo Electroporation:
Cas9 protein+ gRNA (CAPZB exon 3)

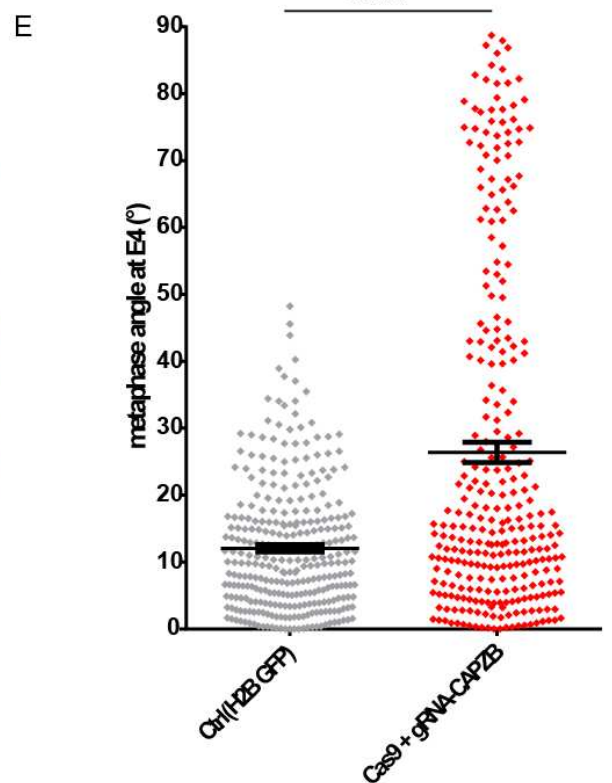
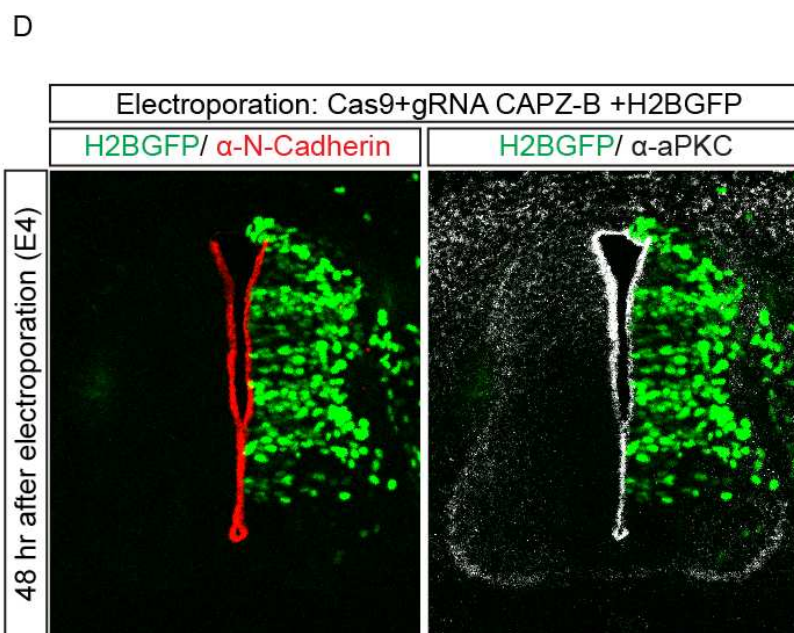


48hr: E4 embryos → Flat Mount → Angle measurement
 → Sections → - IF CAPZ-B
 → - IF Polarity markers



Angle measurement





CHAPTER 7: DISCUSSION

In this project, I first developed a novel vertebrate model of oriented divisions which is controlled by the specific localization of the LGN complex. By using this model, I performed a live RNAi screen for regulators of spindle orientation, which allowed us to dissect the differential role of all dynein subunits and regulators in LGN complex-mediated spindle orientation. Finally, I characterized the function of a novel hit, CAPZ-B, both in cultured cells and in the chick embryonic neuroepithelium. In the next sections, I will discuss the advantages and limitations of our spindle orientation model, with a focus on the screening results. Then I will discuss the results concerning the dynein family in more detail as well as the function of CAPZ-B, emphasizing on the perspectives of this work.

A NOVEL CELLULAR MODEL OF ORIENTED DIVISIONS: A NEW TOOL IN THE SPINDLE ORIENTATION FIELD

ADVANTAGES AND POTENTIAL USES OF THE MODEL

Our new *in cellulo* model of spindle orientation is based on the specific subcortical localization of the LGN complex. The specific localization of the LGN complex directs spindle orientation in several tissues. The induced polarity assay has been developed in S2 cells (Johnston et al., 2009) where it continues to be used to dissect *Drosophila* spindle orientation mechanisms. Remarkable differences in the mechanisms of several regulators between species underscore the need to interrogate spindle orientation pathways both in invertebrate and vertebrate models. Here I showed that it is possible to adapt this system to human cultured cells, extending the potential use of this strategy. In addition, I have also introduced the Echinoid constructs in MDCK cells, where they localized to the cell-cell contacts (data not shown). While I did not test spindle orientation in these cells, it is very likely that the Echinoid system is adaptable to additional vertebrate cell lines.

One remarkable feature of our model is the dramatic spindle orientation phenotypes obtained when depleting several molecules, including both known and novel proteins regulating spindle orientation. Obtaining such dramatic phenotypes (which markedly contrast with phenotypes observed in the

widely used cell culture spindle orientation models) can be attributed to two main reasons. Firstly, our model is only based on the LGN-NuMA-dynein pathway and thus depleting major actors of this pathway leads to total loss of spindle orientation. In contrast, spindle orientation in parallel to the substrate or with respect to the geometry of the adhesion pattern are probably controlled by multiple pathways, which results in mild phenotypes when targeting individual cascades. Secondly, an alternative spindle orientation induced by geometry constrains imposed to cells cultured on micropatterns is in competition with the Ed-G α i controlled orientation in our system. This probably contributes to visualize defects in the LGN-astral MT pathway. Therefore, setting the system on micropatterns not only limits variability and allows standard isolation of cell pairs but also provides a competitive spindle orientation that may help to visualize phenotypes.

Notably, spindle orientation parallel to the other cell depends neither on LGN (Fig.40), p150 and LIS1 (data not shown) nor on astral MT (Fig. 40). This was unexpected as dynein and astral MT are thought to be essential for spindle orientation downstream of any signaling or geometry cue in most contexts studied so far. We initially thought that this orientation was only dependent on actin-based mechanisms; however, I did not observe defects in anaphase spindle orientation upon Latrunculin treatment. By performing live imaging at a shorter time interval, I observed exaggerated spindle rotation in metaphase which correlated with changes in cell shape (data not shown); however, spindle orientation was rescued in anaphase. We thus thought that the geometry of the cell was controlling cell division orientation independently of actin and microtubule based pathways. Indeed, I measured cell dimensions during mitosis both in control or Latrunculin-treated cells and I observed that cells are less perfectly rounded, showing a slightly elongated shape (in parallel to the neighboring cell) during mitosis and probably this biases spindle orientation along that axis (data not shown). Previous work in models in which cell shape is the predominant cue guiding spindle orientation have proposed that cell shape is translated into longer astral MTs along a particular axis. Because forces applied on astral MT are predicted to scale with their length, the spindle would align along the longest cell axis (Minc et al., 2011). In our system, in contrast, spindle orientation seems to

be independent of astral MT, raising the question of how the spindle senses cell geometry to establish and maintains its orientation along the longest cell axis when astral MT are perturbed. Interestingly, Lazaro-Diequez et al. have recently reported that cell shape can induce spindle orientation bias independently of astral MT (Lazaro-Diequez et al., 2015). In the future, it would be interesting to study if cell shape can guide spindle orientation independently of astral MT in other systems and to investigate how the spindle can interpret cell geometry in these cases.

Our Ed-Gai spindle orientation model allows to read the angle of spindle orientation in the X-Y plane, and thus imaging cells at low magnification is sufficient to determine phenotypes, making the system adaptable to large scale RNAi- or chemical inhibition- based screens. While I performed a mid-scale screen, it would be possible to perform larger screens provided that a fully automated analysis protocol is applied (see appendix 3). Thus, screening using this model might be of interest for the scientific community. More generally, the Echinoid induced polarity assay can be used to test other spindle orientation pathways as well as the recruitment of proteins to an Ed-ProteinX cortical enrichment in HeLa cells. However, it should be noted that all the analyses presented here were done by using stable cell lines, as combining transient transfection with seeding of micropatterns did not prove efficient to obtain enough analyzable cells.

Both the development of the model and the RNAi screen were performed by using long-term time-lapse imaging. This gives the possibility of measuring the anaphase spindle orientation angle (and thus the definitive spindle orientation angle) for all cells automatically imaged, providing an extensive amount of quantitative data for each condition in one single experiment, without using synchronization drugs. In addition, live imaging at shorter time interval and higher magnification can offer a dynamic view of the spindle orientation process in different conditions. To measure spindle orientation in anaphase, live imaging is the best solution so far as anaphase is a considerably short phase and thus the proportion of anaphase cells found in cells fixed on micropatterns is quite low.

Alternatively, another possibility is to synchronize cells and analyze metaphase/anaphases in fixed conditions. However, synchronization methods are not 100 % effective (e.g. release from a thymidine block or release from a RO-3306 induced blocking at G2/M:Vassilev et al., 2006) and thus the number of events of interest found in a fixed slide is much lower than the number of cells quantified in our long-term movies. However, one synchronization method that we tested is the use of proTAME (Zeng et al., 2010) to block cells in metaphase before fixation. In comparison to other methods, this treatment generates a higher increase in the number of events of interest, and allowed me to study the localization of LGN complex members in an easy manner. However, blocking cells in metaphase may change the dynamics of spindle orientation or affect other mitotic pathways; thus, we chose not to use this approach for RNAi screen. In contrast, this strategy could be used to analyze the potentiality of a candidate X-molecule fused to Echinoid to orient the spindle.

The Ed-Gai spindle orientation model has allowed us to dissect the differential contribution of all dynein subunits and regulators to the LGN-astral MT spindle orientation pathway. Our model is certainly useful to uncover essential regulators of this pathway. In addition, I could observe mild phenotypes when depleting some dynein regulators suggesting that the system is capable of distinguishing between mild and strong regulators of spindle orientation. Remarkably, we were able to validate the function of CAPZ-B, a novel spindle orientation regulator found in our *in cellulo* assay, in the context of planar spindle orientation of neural progenitors *in vivo*. Future work investigating the function of essential regulators (e.g. p22, p62, Arp1A) vs dispensable molecules (e.g. p25, p27, Arp11) in *in vivo* contexts should be useful to establish the Ed-Gai model as a tool to dissect spindle orientation pathways having a physiological significance.

LIMITATIONS OF THE ED-GAI SPINDLE ORIENTATION MODEL

While the Ed-Gai model allowed to dissect the role of dynein regulators in spindle orientation and uncovered novel regulators of this process, I obtained unexpected results for a subset of molecules evaluated in the screen. In particular, I found no significant phenotypes for molecules that had been

shown to regulate LGN complex assembly and spindle orientation in parallel to the substrate in HeLa cells. This was the case for Afadin, Aurora Kinase A and HTT. Afadin and HTT have been shown to regulate LGN cortical localization in HeLa cells (Carminati et al., 2016; Elias et al., 2014). Of note, Ed-G α i cells recruits LGN to the cell-cell contacts not only in mitosis but also in interphase, probably due to the higher levels of Ed-G α i at the cortex. This could in turn affect the dynamics of LGN recruitment/stability at the cortex making it less susceptible to the absence of molecules that act to regulate its localization at the cortex. Therefore, our model is probably best suited to dissect spindle orientation mechanisms downstream of LGN and not at the level of LGN. However, Aurora A modulates spindle orientation in HeLa cells by regulating NuMA recruitment (Gallini et al., 2016), and I did not observe a significant phenotype upon its depletion.

In addition, depletion of CLASP1, Rab11, EB1 and STIL, which regulate spindle orientation with respect to the substrate or to the adhesion micropattern by modulating astral MTs (Hehnlly and Doxsey, 2014; Kitagawa et al., 2011; Samora et al., 2011; Toyoshima and Nishida, 2007) did not result in significant phenotypes in our screen.

Our system is based on a strongly polarized LGN complex localization which differs from the two crescent-distribution of the LGN complex established during metaphase in HeLa cells cultured on fibronectin. The levels of cortical recruitment of LGN complex members may differ between these models as our system is based on the overexpression of Ed-G α i. Therefore, the high levels of LGN complex cortical recruitment and its strong polarization may make the Ed-G α i system less vulnerable to the absence of mild regulators of LGN complex recruitment. Similarly, the strong availability of cortical cues may mask defects on astral MT. One could imagine that even when astral MT are perturbed, cortical motors might be able to attach and exert force on these microtubules, provided that at least some astral MTs reach the cortex. In contrast, the cortical attachment of microtubules might be less strong in non-polarized HeLa cells resulting in spindle misorientation with respect to the growth surface upon depletion of molecules regulating astral MTs. Nevertheless, I did find that

certain regulators of astral MT behavior and dynamics (namely MAP4 and EB3) regulate Ed-Gai controlled spindle orientation.

In conclusion, I consider that our model as it is, is suitable to find strong spindle orientation regulators working downstream of LGN, but it is less adapted to find subtle spindle orientation regulators¹. Nevertheless, optimization of the model might help to circumvent these limitations. In this sense, the expression of Ed-Gai is Doxycycline inducible and thus I tested different Dox concentrations to find the minimal dose which results in correct spindle orientation in control cells. However, it seemed that lower concentrations do not result in lower levels of Ed-Gai in each cell, but instead in less cells expressing Ed-Gai and thus correctly orienting the spindle (data not shown). In addition, another possibility was to perform the screen in a sensitized background, i.e. to simultaneously deplete a regulator of LGN complex assembly. However, our attempts to sensitize the system by depleting Dlg1 (which regulates LGN cortical localization (Saadaoui et al., 2014), did not prove useful for this objective.

On the other side, the Ed-Gai cell-pair system could be set in a different culture context than on round micropatterns. In round micropatterns, the pattern-induced orientation is competing with the Ed-Gai orientation, and while this is useful to reveal clear-cut phenotypes, the existence of this alternative orientation may result in the requirement of high levels of Ed-Gai to win over the default parallel orientation. Thus, setting the pair cell system in a less constrained environment constitutes an alternative level where to play to optimize the system.

¹ Spindle orientation defects could vary in relation to the level of protein depletion. For practical reasons, validation of protein depletion is generally not performed for large scale screen, and therefore the level of depletion is unknown. Validation of the siRNA library targeting all the dynein regulators has been performed in HeLa cells before (Raaijmakers, J.A., Tanenbaum, M.E., and Medema, R.H. (2013). Systematic dissection of dynein regulators in mitosis. *J Cell Biol* 201, 201-215.) and the knock-down efficiency ranged between 80% and 99%. Thus, it is unlikely that the efficiency of depletion could solely explain the differences in the screen phenotypes.

A LIVE RNAI SCREEN FOR SPINDLE ORIENTATION REGULATORS

Our screen revealed the differential role of dynein associated molecules in LGN controlled spindle orientation. My results brought novel evidence of the function of different dynein/dynactin subunits opening the pathway for investigating the functions of these molecules in other spindle orientation contexts. Of note, contrary to depletion of DHC or LIS1, depletion of p22, p62, Arp1A and CAPZ-B, spindle orientation regulators whose function had not been demonstrated before, does not generate massive mitotic defects followed by cell death. Therefore, it could be interesting to test the function of these molecules *in vivo*.

What is the function of the dynein regulators during spindle orientation? p150 has been typically considered as the dynactin subunit necessary for modulating dynein activity. In mitotic HeLa cells, p150 is necessary for proper dynein localization at the cell cortex (Kiyomitsu and Cheeseman, 2012), and the present manuscript). How does p150 regulate cortical dynein localization? One possibility is that p150 located at MT +ends mediates the transport of dynein from MT +ends to the cortex, as observed in budding yeast. Currently, however, there is no proof for a similar offloading mechanism in metazoans cells. Data on the requirement of astral MT to transport dynein to the cortex is sparse. Tame and colleagues have observed that astral MT are necessary to reconstitute DHC to the cortex during the oscillatory behavior of cortical DHC and the spindle (Tame et al., 2014), but the offload model needs to find further evidence. Alternatively, p150 might modulate dynein stability at the cortex. NuMA is known to interact with Dynein/Dynactin complex recruiting it to the cortex (Kotak et al., 2012; Merdes et al., 1996). Does p150 (or another dynactin subunit) interact with an unknown cortical receptor and help stabilizing dynein at the cortex? It could be interesting to determine if p150 interacts with regulatory GTPases present at the cortex as it does with receptors in vesicles (see chapter 3). Of note, NuMA depletion resulted in loss of both DHC and p150 from the cortex (Kiyomitsu and Cheeseman, 2012, 2013) suggesting that p150 also depends on NuMA-DHC for its cortical localization. Thus, one could imagine that DHC interaction with NuMA and p150 interaction with another receptor (or with NuMA itself) are both required for stabilizing DHC and p150 at the

cortex (Fig. 39). Depletion of Arp1A resulted in a strong spindle orientation phenotype in our model, and I observed that this treatment also led to reduced DHC cortical levels. Likewise, Arp1A might interact with plasma membrane receptors as it does with β III spectrin in vesicles (see chapter 3). Interestingly, DHC depletion only leads to a partial reduction of Arp1 cortical levels (Kiyomitsu and Cheeseman, 2012) suggesting that Arp1 can be recruited to the cortex independently of DHC. Of note, recent structural studies demonstrated that DHC interacts with the Arp1 dynactin filament (chapter 3). In summary, Arp1A and p150 are crucial for targeting dynein to the cortex. Whether interaction of dynein with p150 and Arp1A are also necessary for dynein activation at the cortex remains to be elucidated (see discussion of CAPZ-B function below). Importantly, depletion of Dynein intermediate chain (which is reported to interact with p150) also resulted in a significant phenotype on spindle orientation.

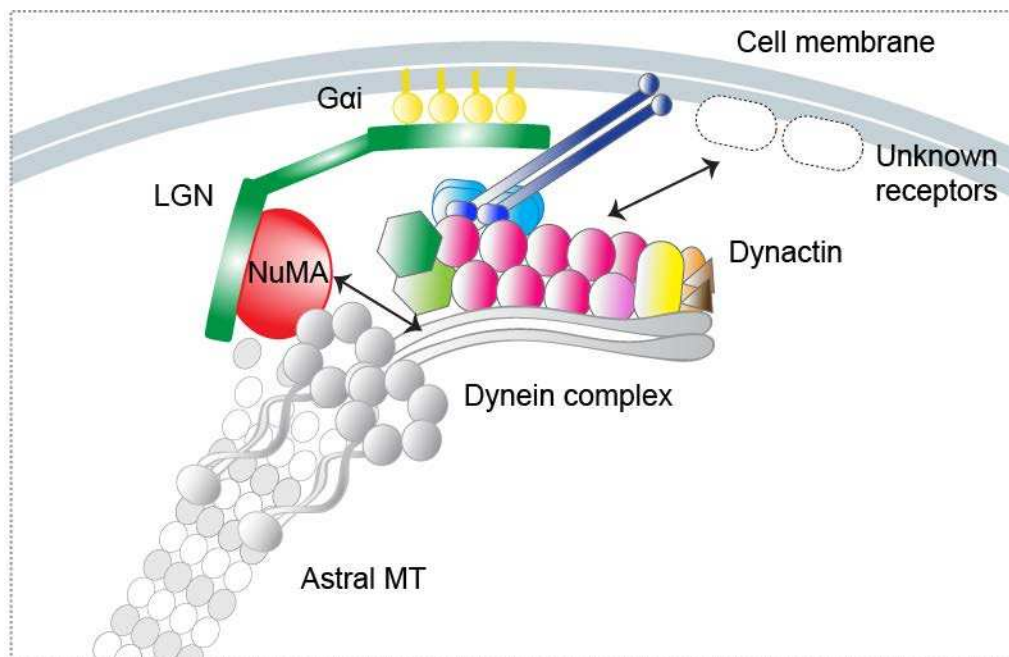


Figure 39: Model proposed for the recruitment/ stability of Dynein/Dynactin at the cell cortex in mitosis. Arrows indicate proposed interactions

Concerning the role of p22 and p50, depletion of these dynactin shoulder subunits resulted in concomitant strong reduction of p150 and partial decrease of Arp1 (Raaijmakers et al., 2013), and thus these subunits are required for the stability of the dynactin complex.

With regard to pointed end complex of dynactin, while p62 is essential for Ed-Gai spindle orientation, Arp11, p25 and p27 seem to be dispensable for this process. Depletion of p62 results in reduced levels of Arp1 (Raaijmakers et al., 2013), and thus p62 probably regulates the stability of the dynactin filament. This idea somehow contradicts the hypothesis of Urnavicius and colleagues who based on structural data proposed that Arp11, but not p62, acts as capping factor at the pointed end (Urnavicius et al., 2015).

On the other side, depletion of numerous dynein subunits did not perturb spindle orientation in our system. These include the dynein light intermediate chains and the three types of dynein light chains. One possibility is that these subunits are not essential for spindle orientation. If they play a minor role, however, our model might not be useful to reveal that (see discussion above). A second possibility is that the different isoforms that exist for each type of subunit play redundant roles in spindle orientation. In this sense, double siRNA treatment targeting both existing isoforms for each type of subunit did not generate any spindle orientation phenotype (data not shown). However, effective depletion of both subunits was not verified and as double siRNA knockdown is not as optimized as single depletion, at the moment I am not able to confirm these results. Concerning the Roadblock type of dynein light chain, the human protein atlas indicates that the RNA levels of Roadblock-2 are minimal and thus it is expected that this subunit should not compensate for the loss of Roadblock-1. In addition, Roadblock-2 does not compensate for the loss of Roadblock-1 in multiple mitotic processes (Raaijmakers et al., 2013). In conclusion, Roadblock family- Dynein light chains are probably not required in our spindle orientation assay, contrary to what was observed in *C.elegans* (Couwenbergs et al., 2007).

Finally, I did not find any significant spindle orientation phenotype within other protein families evaluated in the screen, including all kinesins, and some MAPs and centrosomal proteins. It is currently not possible to affirm that these proteins are not participating in spindle orientation, because as discussed above, our model does not seem to be optimized for unveiling subtle

regulators. However, this indicates that none of the kinesins and centrosomal proteins evaluated plays such an essential role as dynein and its regulators in LGN guided spindle orientation.

REGULATION OF MITOTIC SPINDLE ORIENTATION BY CAPZ-B

My screen results revealed that the dynactin subunit and actin capping protein CAPZ-B is essential for Ed-Gai mediated spindle orientation. This protein is typically known for its function in actin dynamics modulation in multiple cellular and developmental contexts. Here, I found that CAPZ-B regulates the localization, stability and function of the dynactin/dynein complexes during mitosis. In addition, I found that CAPZ-B localizes everywhere in the cell but it is apparently stronger at the cortex and the spindle during mitosis. This is very similar to the mitotic localization of other dynactin and dynein complex members. Moreover, I showed that CAPZ-B regulates the dynamics of spindle microtubules and thus the density of both astral and spindle microtubules. Importantly, changes in the actin cytoskeleton by CAPZ-B depletion are not responsible for the spindle orientation phenotype observed. Overall, my results support a role of CAPZ-B in regulating spindle orientation by modulating dynactin cortical localization and dynein activation. In the following subsections I discuss the different aspects of CAPZ-B function focusing on the questions that remain to be investigated.

CAPZ-B LOCALIZATION DURING MITOSIS

Further characterization of CAPZ-B cellular dynamics will be important for understanding CAPZ-B function. Remaining questions include the switch of the localization of this protein between interphase and mitosis. In interphase, cortical staining is observed (data not shown). Is it the same cortical pool that is visualized in mitosis? Is there a new pool recruited to the cortex together with dynactin members in early mitosis? When is this protein recruited to the spindle poles? In addition, the dependence of metaphase cortical localization of CAPZ-B on the LGN-NuMA-dynein pathway vs. actin pathways remains elusive. In this sense, to improve the analysis of the dynamics of CAPZ-B in cells it would be worth to develop a cell line expressing endogenous CAPZ-B tagged with a GFP by performing Crispr-Cas9 mediated knock-in.

REGULATION OF DYNAMACTIN/DYNEIN BY CAPZ-B

Another critical aspect to investigate is the exact consequence of the loss of CAPZ-B in the dynactin complex. Urnavicius et al. suggested that the CAPZ A/B heterodimer is critical for dynactin stability (Urnavicius et al., 2015). I could imagine two scenarios upon the loss of CAPZ-B from dynactin. In the first scenario, Arp1 subunits at the barbed end are lost. Of note, the shoulder/arm is assembled on the barbed end side of the filament, and thus losing the first Arp1 protomers would lead to disassembly of the shoulder/arm from the rest of the complex. Alternatively, CAPZ-B could work as an inhibitor of Arp1 monomer addition at the dynactin filament. In analogy with the increased actin polymerization seen upon CAPZ-B depletion (my results and previous work, see chapter 4), it could be imagined that additional Arp1 subunits are added to the dynactin filament in the absence of CAPZ-B. This could lead to the formation of aberrant dynactin complexes leading to destabilization and delocalization from the cortex.

To gain insights into the stability of dynactin in the absence of CAPZ-B, immunoprecipitation experiments to evaluate the presence of Arp1 and p150 in the same complex could be performed. Further biochemical analyses should provide the ratio of each subunit present in this complex when CAPZ-B is lacking. Alternatively, the Proximity ligation assay, which allows the observation of protein complexes *in situ*, could help to address these questions. In particular, I could evaluate the proximity of Arp1 and p150 to see if they are part of the same complex or not upon CAPZ-B depletion.

Interestingly, depletion of CAPZ-B leads to an increase in cortical actin levels, thus meaning that CAPZ-B is also functioning as an actin capping protein at the cortex during mitosis. Therefore, CAPZ-B molecules might be found capping either actin filaments or dynactin in a similar location. Is the assembly of the dynactin complex favored by the recycling of CAPZ-B from actin filaments at the cortex? Of note, extensive remodeling of the cell cortex occurs when cells enter mitosis. This could result in selective stabilization of dynactin at the cortex by cortical CAPZ-B. Alternatively, the

dynactin complex may be assembled at any location in the cell and then recruited as an intact complex to the cortex and the spindle at the beginning of mitosis.

Of note, while I found that CAPZ-B depletion leads to reduced cellular levels of Arp1A and p150 using immunocytochemistry, Raaijmakers et al. did not observe this effect in Western blot experiments (Raaijmakers et al., 2013). Therefore, additional experiments are required to validate my observations.

Another remarkable aspect of CAPZ-B regulation of spindle orientation is the effect of CAPZ-B depletion on the dynein motor itself. In contrast to depletion of Arp1A, p150 or other dynactin subunits, CAPZ-B siRNA does not result in the loss of dynein from the cortex. However, the spindle is no longer oriented by the Ed-Gai system, indicating that cortical dynein does not correctly exert forces on astral MTs. We hypothesize that cortical dynein is inactive when CAPZ-B is depleted. While this is difficult to prove, my results so far support this idea, as the dynamic behavior of the spindle in response to strongly polarized dynein is lost upon CAPZ-B depletion (as seen in experiments in DHC-GFP cells). Incorrect dynein activation can be attributed to reduced levels of dynactin generated by the lack of CAPZ-B. Therefore, partial loss of dynactin from the cortex would allow correct dynein localization but impaired dynein activation, in contrast to total loss of p150 or Arp1A which results in dynein loss from the cortex. This suggests that cortical dynactin is not only required for dynein cortical targeting but also for dynein motor activity.

REGULATION OF MICROTUBULES BY CAPZ-B

Furthermore, I found that depletion of CAPZ-B generates a reduction in the density of both spindle and astral MT, without gross perturbation of spindle morphology. This phenotype can be explained by the effect of CAPZ-B depletion on microtubules dynamics. CAPZ-B siRNA results in increased growth and shrinkage velocities and decrease growth lifetime of microtubules. Hence, loss of CAPZ-B results in more dynamic (and thus less stable) microtubules in mitosis. Interestingly, this phenotype seems to be mitosis-specific, as I did not observe this effect in interphase cells (data not shown).

Comparison of the same microtubule dynamics parameters upon p150 or Arp1A suggests that the effect of CAPZ-B depletion on the growth lifetime may be a consequence of reduced p150 and Arp1A levels, whose complete depletion results in an even stronger decrease in microtubule growth lifetime. In contrast, the effect of CAPZ-B loss on the speeds of growth and shrinkage seems to be independent of the reduction in those dynactin subunits.

How do these changes in microtubules dynamics contribute to spindle misorientation? As extensively discussed in chapter 2, defective microtubule dynamics could affect microtubules interaction with the cortex. Interestingly, Kwon and colleagues observed that depletion of myosin 10, which changes microtubules dynamics in a manner similar to CAPZ-B depletion, results in reduced microtubule cortical dwell times (Kwon et al., 2015). Measuring this parameter in CAPZ-B depletion conditions could provide insights into the significance of the microtubules dynamics phenotype generated by loss of CAPZ-B. In addition, restoring microtubule dynamics and testing if this partially rescues the spindle orientation phenotype would be required to definitely answer if impaired microtubule dynamics contribute to defective spindle orientation in the Ed-Gai system upon CAPZ-B depletion. In this sense, Taxol is known as a microtubule stabilizer, and thus I tested several concentrations for their effect on spindle density and morphology. High concentrations (> 30 nM) of taxol resulted in spindles with aberrant morphology, that is, with astral MT being predominant over the central spindle. Matov et al. reported that a 10 nM taxol concentration results in decrease microtubules dynamics in interphase cells (Matov et al., 2010). Thus I tested this concentration on mitotic cells; however, this treatment did not substantially change the growth speed and decreases the growth lifetime, which was not compatible with a potential microtubule stabilizing effect (data not shown). Therefore, Taxol treatment does not seem optimal to accomplish my objective, and this question remains so far unanswered. Nevertheless, while changes in astral MTs dynamics may contribute to the spindle orientation defect, they are unlikely to be the major contributor. Firstly, these changes are subtle and astral MTs reaching the cortex are still observed. Secondly, as discussed before, subtle changes in astral MT dynamics might not be sufficient to induce spindle misorientation in the Ed-Gai

model, as I did not observe significant phenotypes when depleting regulators of microtubules dynamics like EB1 or CLASP1. However, I cannot rule out that perturbed microtubules dynamics partially contribute to defective spindle orientation generated by CAPZ-B.

Regulation of microtubules dynamics by CAPZ-B is an interesting observation as this is somehow a novel facet of CAPZ-B function. As discussed in chapter 4, the role of CAPZ-B in modulating microtubules has only started to emerge, and my work brings more evidence to this aspect of CAPZ-B function. Previous evidence was based on i) *in vitro* MT polymerization assays or ii) MT stainings in interphase cells (Bartolini et al., 2012; Davis et al., 2009) and thus my work provides a characterization of the dynamics of mitotic microtubules in the absence of CAPZ-B. How does CAPZ-B modulate microtubule dynamics? CAPZ-B2 interacts with β III-tubulin in brain lysates and binds β -tubulin *in vitro* (Davis et al., 2009); notably, a region of interaction with both tubulin forms has been mapped in CAPZ-B. I have observed that CAPZ-B localizes to the mitotic spindle. Is this localization only due to its presence on the dynactin complex (p150 has a MT binding domain) or is CAPZ-B able to directly interact with microtubules during mitosis? To approximate this question, one could investigate CAPZ-B localization in the absence of p150, in addition to investigating if direct interaction of CAPZ-B2 with β -tubulin occurs in mitotic cells. Finding a direct interaction between CAPZ-B and microtubules should provide evidence for a direct modulation of microtubules dynamics by CAPZ-B. An alternative possibility is that changes in the actin cytoskeleton generated by CAPZ-B loss of function result in altered microtubule dynamics. Bartolini et al. have proposed that CAPZ-A/B overexpression increases stable microtubules by displacing the formin mDia (which stabilizes MT) from actin to MT in interphase fibroblastic cells (Bartolini et al., 2012). Hence, one could imagine that in the absence of CAPZ-B, this formin is mainly localized to actin filaments and thus MTs are less stable. However, it is unknown if this formin regulates the stability of MTs also in mitotic cells. Notably, Kwon and colleagues demonstrated that treatment with Latrunculin increases microtubule dynamics in mitosis (Kwon et al., 2015), with a similar tendency than what is observed upon CAPZ-B depletion. However, while Latrunculin inhibits actin polymerization, depletion of CAPZ-B increases

actin levels. Therefore, the CAPZ-B effect on microtubules cannot be directly attributed to changes in F-actin. However, I cannot exclude that an opposite modulation of the actin cytoskeleton by CAPZ-B might be also translated into increased MT dynamics. To investigate this possibility, I could measure MT dynamics in CAPZ-B depleted cells treated with Latrunculin at the concentration that restore F-actin to the control levels.

Moreover, as mentioned above, I found that not only CAPZ-B modulates MT dynamics but also p150 and Arp1A do so, though in a different manner. More generally, dynactin has been shown to regulate spindle formation and morphology as well as spindle pole focusing in specific systems (Echeverri et al., 1996; Gaetz and Kapoor, 2004; Kim et al., 2007a; Siller et al., 2005). However, depletion of dynactin subunits does not grossly affect spindle formation, morphology and pole focusing in human cells (Raaijmakers et al., 2013, and my own observations). Therefore, I will focus this part of the discussion on the specific modulation of microtubules dynamics by dynactin subunits. Recently, Lazarus and colleagues have shown that p150, which binds directly to MT and localizes to the MT +ends, is an anti-catastrophe factor in neurons (Lazarus et al., 2013). MT catastrophe is the conversion of a growing MT to a shrinking one. In particular, the authors showed that depletion of p150 in neurons increases the frequency of MT catastrophe. This is consistent with my observations, as an increased catastrophe frequency would result in reduced growth lifetimes as I observed upon depletion of p150. Similarly, MT growth rates were not affected by p150 RNAi in their study, in accordance with my data. In addition, *in vitro* experiments performed by Lazarus et al. suggested that p150 can control MT dynamics by itself, i.e. independently of its interaction with dynein. Of note, these authors observed that in interphase COS-7 and HeLa cells, p150 RNAi treatment did not affect MT dynamics (Lazarus et al., 2013). Hence, it is possible that the modulation of MT dynamics by p150 is specific to mitosis.

In conclusion, different dynactin subunits (namely p150, Arp1A and CAPZ-B) regulate microtubule dynamics in mitosis in specific manners, illustrating an aspect of dynactin mitotic function not much explored before.

DIFFERENTIAL ROLE OF CAPZ-B VS CAPZ-A IN SPINDLE ORIENTATION

CAPZ-A and B proteins are considered as obligate partners and the regulation of actin dynamics by these proteins is attributed to the heterodimer and not to individual subunits. Of note, depletion of CAPZ-A or CAPZ-B results in reduced levels of the other subunit at least in specific cell lines, indicating that these proteins are only stable when forming a heterodimer. Thus, it is expected that depletion of any of these subunits results in similar phenotypes. Intriguingly, I did not find significant spindle orientation phenotypes upon depletion of CAPZ-A1. One possibility is that the CAPZ-A2 isoform (which was absent from our siRNA library, but is expressed in HeLa cells though at lower levels than A1 isoform - proteatlas.org) compensates for the loss of CAPZ-A1. Alternatively, it could be imagined that when bound to dynactin, these proteins do not work as an obligate heterodimer and instead have specific roles in the complex. For instance, removal of CAPZ-B but not of CAPZ-A could compromise dynactin stability. However, this idea goes against the model of CAPZ A/B binding to Arp1 filament, which predicts that four specific residues present in CAPZ-A are involved in the tight association of the CAPZ A/B heterodimer to the dynactin filament (Urnavicius et al. 2015). Overall, the data so far do not allow to explain the differential effect of depleting CAPZ-B2 or CAPZ-A1 on spindle orientation. Nonetheless, depletion of CAPZ-A results in a mild decrease in p150 cortical levels (data not shown), suggesting that CAPZ-A may also regulate aspects of dynactin function but probably to a minor extent, not sufficiently to affect spindle orientation.

CAPZ-B REGULATES SPINDLE ORIENTATION IN THE CHICK NEUROEPITHELIUM

Finally, we have demonstrated that CAPZ-B regulates mitotic spindle orientation *in vivo* in the chick neuroepithelium. In this context, neural apical progenitors divide with a planar orientation which is essential for correct localization of progenitors to the apical surface (Morin et al., 2007). In particular

the lateral localization of the LGN complex is necessary for planar orientation in this context (Peyre et al., 2011), and LGN knock-down results in random spindle orientation. Importantly, endogenous CAPZ-B localizes to the spindle and to the cell cortex in metaphase and anaphase apical progenitors. Of note, in interphase cells CAPZ-B is enriched subapically coinciding with F-actin enrichment (data not shown). Therefore, CAPZ-B localization in polarized cells may correlate with its actin capping and dynactin functions.

Remarkably, Crispr-Cas9 mediated depletion of CAPZ-B results in strong defects in spindle orientation in metaphase. In contrast, the effect on anaphase angles is much less pronounced (data not shown). Of note, knock-down of LGN or the LGN interactor Dlg1 also results in milder phenotypes in anaphase than in metaphase (Peyre et al., 2011; Saadaoui et al., 2014). Live data in the context of Dlg-1 knock-down suggested a partial correction of orientation just before anaphase (Saadaoui et al., 2014). This indicates that an anaphase specific pathway might rescue spindle orientation in this context. Nevertheless, we demonstrated that CAPZ-B is a strong regulator of planar spindle orientation in the chick neuroepithelium. Both the localization of this protein and the strong spindle misorientation generated by its depletion suggest that CAPZ-B modulates spindle orientation through regulation of the dynactin/dynein complexes. To investigate this idea, one possibility is to analyze if CAPZ-B depletion results in reduced levels of dynactin subunits, by immunostaining for p150 or Arp1A. Noteworthy, my data so far do not allow to rule out that actin modulation by CAPZ-B is implicated in its spindle orientation activity in this tissue. In contrast to the Ed-Gai model, I have observed that Latrunculin treatment impairs spindle orientation in the chick neuroepithelium, though to a lesser extent than depletion of CAPZ-B (data not shown). Therefore, studying the effect of CAPZ-B on the actin cytoskeleton could be interesting to evaluate this possibility.

CONCLUSION

This project has covered several steps from the pure testing and optimization of a spindle orientation system in cultured cells to the validation of a novel spindle orientation regulator in a physiologically relevant context. The newly developed model of spindle orientation opens the way for further screening or alternative investigations of vertebrate spindle orientation mechanisms by adopting similar strategies, and I hope that it will be of general interest for the community working in this scientific field. Moreover, the regulation of dynein during oriented divisions, while crucial to the correct exertion of forces on astral MTs and thus for spindle orientation, had been poorly characterized before. Therefore, the fine dissection of the role of all dynein regulators in spindle orientation performed in this project sheds new light to understand how this molecular motor works during this essential cellular process.

L'ORIENTATION DU FUSEAU MITOTIQUE

Lors de la division cellulaire, le positionnement et l'orientation du fuseau mitotique dans la cellule sont strictement régulés dans de nombreux types cellulaires. L'orientation spécifique du fuseau est importante pour déterminer le destin cellulaire, ainsi que pour la morphogénèse et le maintien des structures épithéliales. En conséquence, ce processus est critique pour le développement et l'homéostasie de tissus, et sa dérégulation peut conduire à diverses pathologies (Gillies and Cabernard, 2011; Morin and Bellaïche, 2011; Peyre and Morin, 2012).

Dans plusieurs contextes, chez les invertébrés et les vertébrés, l'orientation du fuseau est contrôlée par le complexe moléculaire LGN (formé par G α i, LGN et NuMA), dont la localisation corticale détermine l'axe d'orientation du fuseau. En particulier, la localisation du complexe LGN détermine le site de recrutement du moteur moléculaire dynein qui exerce des forces sur les microtubules astraux pour orienter le fuseau (Morin and Bellaïche, 2011).

Le recrutement cortical des complexes LGN et dynein, ainsi que la modulation du cortex d'actine et des microtubules astraux constituent trois niveaux de régulation de l'orientation du fuseau (di Pietro et al., 2016). Dans les dernières années, de nombreux travaux se sont focalisés sur la dynamique de localisation du complexe LGN et l'identification des mécanismes qui la régulent. Remarquablement, le mode d'action de certaines molécules homologues varie entre différentes espèces. Enfin, il a été montré qu'outre la voie LGN, d'autres cascades sont également au cœur de l'orientation de fuseau dans certains contextes spécifiques (di Pietro et al., 2016).

En outre, plusieurs études ont récemment montré un rôle du cytosquelette d'actine dans l'orientation du fuseau mitotique. Le réseau d'actine joue un rôle autant permissif qu'instructif dans ce processus. Cependant, comment les voies dépendantes de l'actine interagissent avec les voies

dépendantes de LGN reste à clarifier. En parallèle, de nombreuses molécules impliquées dans différents aspects de la modulation des microtubules asexés régulent également par ce biais l'orientation des divisions cellulaires (di Pietro et al., 2016).

Finalement, en plus de ces voies moléculaires, la forme des cellules ainsi que les forces auxquelles elles sont exposées peuvent influencer et déterminer l'orientation de leur fuseau, et donc connaître et maîtriser ces facteurs devient important lorsque l'on interroge la fonction d'une molécule ou d'une voie particulière (di Pietro et al., 2016; Minc and Piel, 2012),

LE COMPLEXES DYNEIN-DYNACTIN

La dynein est un moteur moléculaire qui se déplace préférentiellement en direction des extrémités (-) de microtubules. La dynein cytoplasmique de type 1 est connue pour être au sein de plusieurs processus cellulaires, dont le transport de vésicules et des ARN messagers, le positionnement du noyau et des centrosomes, ainsi que de nombreuses activités pendant la mitose (Roberts et al., 2013). Le fait qu'un seul type de molécule peut être impliqué dans autant d'activités cellulaires semble être lié à sa régulation par plusieurs sous-unités du complexe, ainsi que par d'autres molécules qui interagissent avec la dynein (Kardon and Vale, 2009). La dynein est un complexe macromoléculaire composé de plusieurs sous-unités, incluant les sous-unités catalytiques (DHC) et des sous-unités non catalytiques (DIC, DLIC et DLC) pouvant potentiellement réguler la fonction de ce moteur. La localisation et l'activité de ce complexe moteur sont régulées par divers régulateurs. Un des régulateurs les mieux caractérisés est la dynactine. La dynactine en elle-même est un complexe formé par plusieurs types de sous-unités (Kardon and Vale, 2009; Schroer, 2004).

La complexité et la diversité de ces complexes suggèrent que les différentes sous-unités pourraient être différenciellement affectées à des fonctions cellulaires spécifiques. Cependant, à exception de quelques travaux, la fonction individuelle de différentes sous-unités de la dynein et de la dynactine pendant chaque processus cellulaire reste peu explorée.

OBJECTIFS

Malgré de nombreux travaux sur l'orientation du fuseau mitotique, la compréhension des mécanismes moléculaires qui la contrôlent reste limitée, en particulier chez les vertébrés. Il y a des informations manquantes concernant les molécules régulant la formation du complexe LGN et celles qui fonctionnent en aval. En particulier, comment les moteurs moléculaires fonctionnent pendant l'orientation du fuseau a été peu exploré. Les différences entre les modes d'action des mêmes molécules chez les différentes espèces soulignent l'importance d'étudier la régulation de l'orientation du fuseau dans chaque organisme. Mon objectif principal est donc de faire un crible pour trouver des nouveaux régulateurs dans des cellules de type vertébré. Notre intérêt était de trouver des régulateurs fonctionnant en aval de la voie LGN, qui est la cascade contrôlant l'orientation de divisions dans de nombreux contextes incluant notre modèle de préférence, le neuroépithélium d'embryon de poulet.

Pour faire ce crible, nous avons décidé d'utiliser des cellules en culture. Les modèles existants d'orientation du fuseau dans des cellules en culture n'étaient pas cependant satisfaisants pour notre objectif. Notamment, la voie LGN est seulement partiellement impliquée dans l'orientation de cellules par rapport au fond d'une boîte de culture (Kotak et al., 2012) ou par rapport à la géométrie d'adhésion des cellules (Kwon et al., 2015), qui sont deux références d'orientation couramment utilisées *in vitro*. En conséquence, mon premier objectif a été de développer un modèle cellulaire d'orientation du fuseau dépendant exclusivement de la voie LGN. Le second objectif était de réaliser un crible RNAi pour trouver de nouveaux régulateurs de l'orientation de divisions. Finalement, après identification d'un ou plusieurs régulateurs intéressants, l'objectif était de valider et caractériser leur fonction dans les cellules ainsi que *in vivo* chez l'embryon de poulet.

DEVELOPPEMENT D'UN MODELE D'ORIENTATION DE FUSEAU EN CULTURE CELLULAIRE

Afin de développer un modèle spécifiquement contrôlée par le complexe LGN, nous avons choisi d'utiliser un système basé sur des paires de cellules et de localiser G α i (un des membres du complexe LGN) dans la zone de contact entre les deux cellules, de façon à générer une localisation spécifique du complexe LGN pour orienter la division cellulaire.

Dans ce but, nous avons utilisé une protéine d'adhésion cellulaire nommée Echinoid, utilisée auparavant dans un système similaire d'orientation de fuseau dans des cellules de Drosophile (Johnston et al., 2009). Pour commencer j'ai montré qu'Echinoid fusionné à la GFP (ou à la GFP plus G α i) se localise aux contacts cellulaires dans les cellules HeLa.

Le deuxième outil de notre modèle est l'utilisation de micropatrons adhésifs pour cultiver les paires de cellules. La culture des cellules sur des micropatrons permet de standardiser la forme et l'adhésion cellulaire. Comme ces facteurs peuvent influencer l'orientation du fuseau, les standardiser permettra de réduire la variabilité entre cellules liée à ces facteurs (Fink et al., 2011; They et al., 2005). Nous avons décidé d'utiliser des micropatrons ronds où la forme de chaque cellule correspond à la moitié du patron indépendamment de la position des cellules.

Ensuite j'ai testé l'orientation de fuseau en anaphase au sein de paires des cellules cultivées sur des micropatrons et exprimant EdGFP (comme contrôle) ou EdGFP-G α i, en utilisant la vidéo-microscopie à long terme. Les cellules wild-type ou exprimant EdGFP orientent leur fuseau en parallèle à la cellule voisine, vraisemblablement en lien avec la géométrie des cellules sur ces patrons. En revanche, les cellules exprimant EdGFP-G α i orientent leur fuseau de façon perpendiculaire à la cellule voisine.

Remarquablement, le traitement des cellules Ed-G α i avec un siRNA contre LGN ou avec nocodazole pour perturber spécifiquement les microtubules astraux conduit à une perte de l'orientation de

fuseau perpendiculaire à l'enrichissement Ed-Gai. En conclusion, j'ai développé un système d'orientation de fuseau spécifiquement contrôlé par le complexe LGN.

UN CRIBLE RNAI POUR TROUVER DES NOUVEAUX REGULATEURS DE L'ORIENTATION DE FUSEAU

J'ai utilisé les cellules Ed-Gai pour réaliser un crible en évaluant 107 candidats pour leur rôle dans l'orientation du fuseau dépendant du complexe LGN. Nous avons choisi d'inclure toutes les sous-unités et régulateurs de la dynein, toutes les kinésines, et un groupe des protéines associées aux microtubules ou au centrosome entre autres. Remarquablement, ce crible a révélé que les régulateurs de la dynein sont inégalement requis pour orienter le fuseau. Tandis que plusieurs régulateurs sont essentiels pour cette orientation (DHC1, DIC2, LIS1, p150, p50, p22, Arp1, p62, CAPZ-B), nombre d'entre eux semblent être dispensables. Ces résultats renforcent la notion que la régulation de ce moteur moléculaire dépend des sous-unités spécifiques pour le contrôle de processus cellulaires différents. De plus, entre les sous-unités de la dynactine, j'ai trouvé que la protéine du « capping » de l'actine, CAPZ-B, dont la fonction au sein du complexe dynactine était auparavant inconnue, est un régulateur majeur de l'orientation du fuseau.

CARACTERISATION DE LA FONCTION DE CAPZ-B DANS L'ORIENTATION DU FUSEAU MITOTIQUE

Dans un premier temps, j'ai étudié la localisation de CAPZ-B dans des cellules en culture pendant la mitose, observant que CAPZ-B est localisé dans le cytoplasme cellulaire et montre un enrichissement notable au fuseau mitotique ainsi qu'au cortex cellulaire.

CAPZ-B est classiquement connue pour son rôle de protéine de « capping » d'actine, et cette fonction est reflétée dans la modulation de nombreux processus cellulaires et développementaux nécessitant une dynamique précise du cytosquelette d'actine (Cooper and Sept, 2008). D'autre part, l'actine régule l'orientation du fuseau mitotique dans plusieurs contextes cellulaires. J'ai donc évalué la possibilité de que CAPZ-B régule l'orientation des divisions en modulant le cytosquelette d'actine.

J'ai observé que la déplétion de CAPZ-B génère une augmentation des niveaux corticaux et cytoplasmiques d'actine. Cependant, le rétablissement des niveaux d'actine au niveau des cellules contrôle ne change pas le phénotype d'orientation du fuseau généré par la déplétion de CAPZ-B. Ceci nous permet de conclure que CAPZ-B régule l'orientation du fuseau indépendamment de son rôle classique de modulateur de la dynamique de l'actine.

En revanche, mes résultats suggèrent que CAPZ-B contrôle l'orientation de fuseau en régulant la localisation d'autres sous-unités du complexe dynactine, dont la localisation corticale est sévèrement affectée en l'absence de CAPZ-B. La localisation corticale de la dynein elle-même est normale en l'absence de CAPZ-B, ce qui suggère que son activité motrice est affectée en réponse à la déplétion de CAPZ-B.

De plus, j'ai trouvé que CAPZ-B exerce une modulation des microtubules pendant la mitose. En particulier, la densité de microtubules du fuseau mitotique est réduite en l'absence de CAPZ-B. Des expériences de « tracking » de microtubules dans des conditions « live » ont permis d'observer que la déplétion de CAPZ-B altère la dynamique des microtubules, pouvant ainsi expliquer le phénotype observé au niveau de la densité du fuseau.

Finalement, en utilisant la technique du Crispr-Cas9 pour réduire les niveaux de CAPZ-B dans le neuroépithélium nous avons démontré que CAPZ-B régule l'orientation du fuseau *in vivo* dans le neuroépithélium de l'embryon de poulet où les progéniteurs se divisent avec une orientation planaire d'une façon dépendante du complexe LGN.

CONCLUSION

Dans ce projet, j'ai développé un nouveau modèle d'orientation du fuseau mitotique qui présente de nombreux avantages. L'un de ces avantages est que ce modèle est uniquement contrôlé par la voie LGN, ce qui permet d'évaluer facilement le rôle des différentes molécules spécifiquement dans cette voie. En particulier, des phénotypes très marqués ont été observés face à la déplétion de molécules

essentielles pour le fonctionnement de la voie LGN-dynein-microtubules astraux. Ce modèle pourrait donc être d'intérêt pour la communauté scientifique s'intéressant à l'orientation de fuseau. D'autre part notre crible RNAi a permis de montrer un rôle différentiel des différentes sous-unités et régulateurs de la dynein dans l'orientation du fuseau mitotique. Notamment, j'ai trouvé que CAPZ-B, un membre du complexe dynactine, est un régulateur essentiel de l'orientation de fuseau dans les cellules en culture ainsi qu'*in vivo* dans le neuroépithélium d'embryon de poulet. CAPZ-B est typiquement connue par son rôle au sein du cytosquelette d'actine, mais son rôle dans l'orientation du fuseau est indépendant de cette fonction. Par contre, CAPZ-B régule la localisation de la dynactine et l'activité de la dynein ainsi que la dynamique des microtubules du fuseau mitotique, phénotypes qui expliqueraient sa fonction comme régulateur de l'orientation du fuseau.

APPENDIX 1: SUPPLEMENTARY FIGURES

Figure 40: Development of the Ed-G α i model and characterization of EdGFP cells a) Schema of the constructs used for developing HeLa cells with constitutive expression of H2BCherry and Doxycycline inducible expression of the Echinoid fusion proteins. “Tol 2” are the recognition sequences for the Tol2 transposase. Transposition of these sequences is achieved by co-transfecting low levels of the transposase vector (see methods). Tet ON is active upon Doxycycline treatment. Tet ON then can activate the transcription from the TRE promoter. b) Representative picture of HeLa interphase cells showing the enrichment of EdGFP in the cell-cell contacts. c) and d) Examples of cell pair configurations on H and 30 μ m round patterns in cells expressing EdGFP and H2B-cherry. Variable cell positions result in variable cell shape on H patterns, but similar cell shapes on round patterns. e) Effects of LGN depletion, astral MT perturbation (Nocodazole 10 nM) and actin cytoskeleton perturbation (Lat 0.5 μ M) in spindle orientation in cells expressing EdGFP and seeded on round micropatterns. In contrast to EdGFPG α i spindle orientation, spindle orientation parallel to the neighboring cell does not depend neither on LGN neither on astral MT. Results shown correspond to one representative experience.

Figure 41: Automated anaphase angle and GFP level measurements on manually extracted movies of 15 frames containing a cell division within a pair of cells a) Example time-lapse sequence showing entrance to and completion of mitosis. The angle in telophase sometimes differs from that in anaphase as a consequence of daughter cell reaccommodation on the surface pattern. Thus we measure the angle in anaphase. b) to f) image treatment for nuclei segmentation: b) Initial mCherry image c) Correlation of the initial image (b) with a Gaussian of 10 pixels spatial size. d) Filter of (c) with a 10 pixel Gaussian filter e) Binary image of (d) f) Removal of areas consisting of less than 30 pixels. Segmentation is performed in (f) figure. g) The transition from 2 to 3 nucleus in a 2-2-3 sequence is the time of anaphase (td) h) Sequence containing the 2 to 3 transition i) Measurement of division angle in td. J and k) Determination of the GFP level at the cell - cell contacts. j) GFP image showing the traced line used for measuring GFP. k) Fitting of Gaussian curves (black) to the GFP profile (in red).

Figure 42: A live siRNA screen for spindle orientation regulators using the Ed-G α i spindle orientation model. Evaluation of: a) Molecules potentially affecting the activity of LGN/ NuMA, or involved in spindle orientation in other systems. b) All kinesins (different graphs indicate separate experiments). c) a subset of centrosomal proteins, d) Microtubule associated proteins (MAPs) and MT+ end proteins. Depletion of Ubc9 and RAN are not shown as these RNAi were extremely detrimental for cells and did not provide enough cells for analysis.

Figure 43: a) Effect of CAPZ-B depletion on the total levels (determined from fluorescence images) of p150 and Arp1A-GFP. b) and c) Effect of b) p150 and c) Arp1A dynactin subunits depletion on the cortical levels of Dynein Intermediate Chain. Left: Representative images. Right: Quantification of cortical levels for each condition for one representative experience. The graphs show the average for n cells \pm SEM. All values are corrected by background. In contrast to CAPZ-B depletion, p150 or Arp1A depletion result in diminished levels of cortical DIC. D) Comparison of the effects of CAPZ-B and p150 on the dynactin and dynein complex. CAPZ-B decreases the levels of p150 but Dynein localization appears normal. Spindle misorientation might be due to ineffective dynein activation. In contrast, depleting p150 directly impacts on the cortical localization of Dynein.

Figure 40

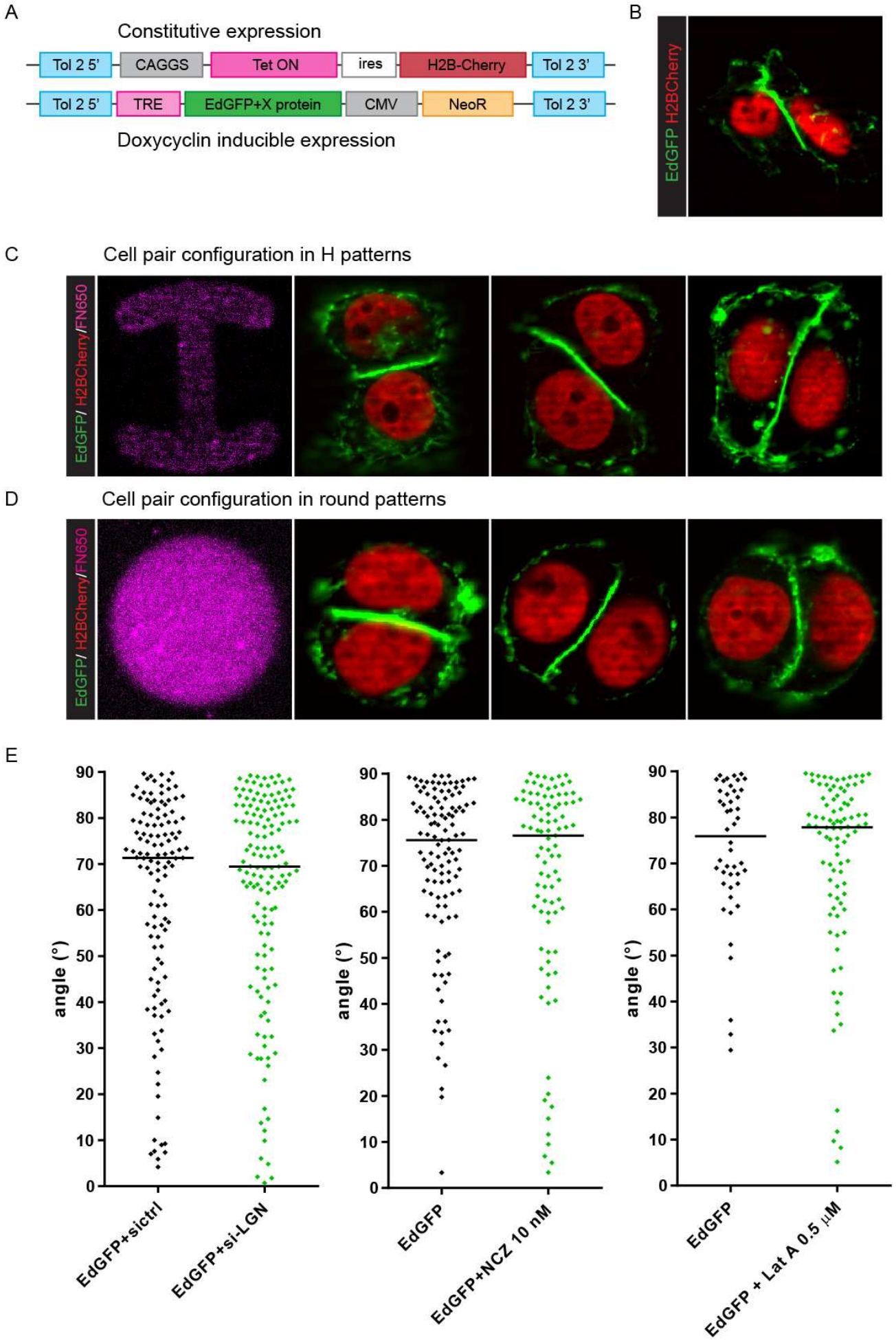


Figure 41

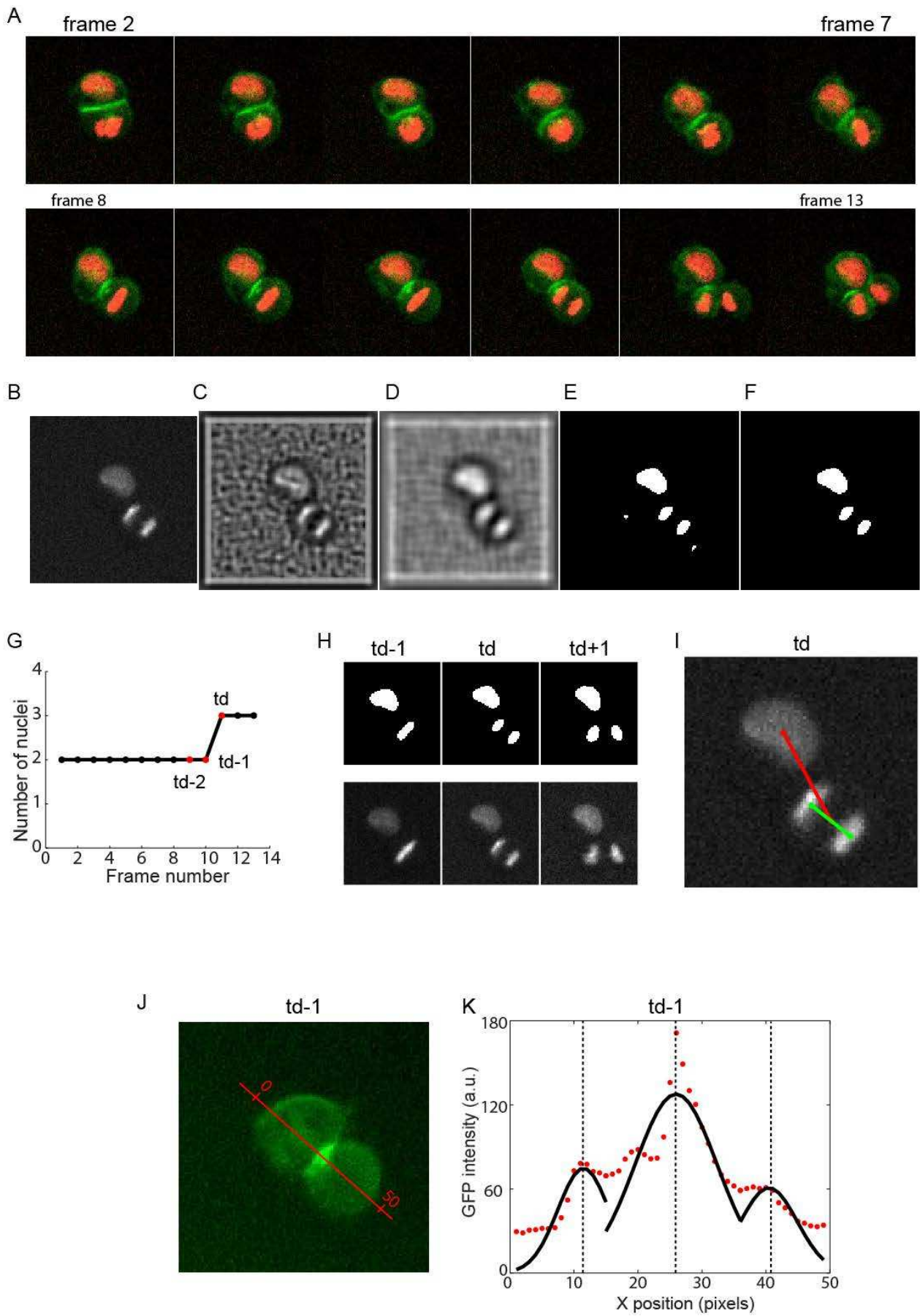
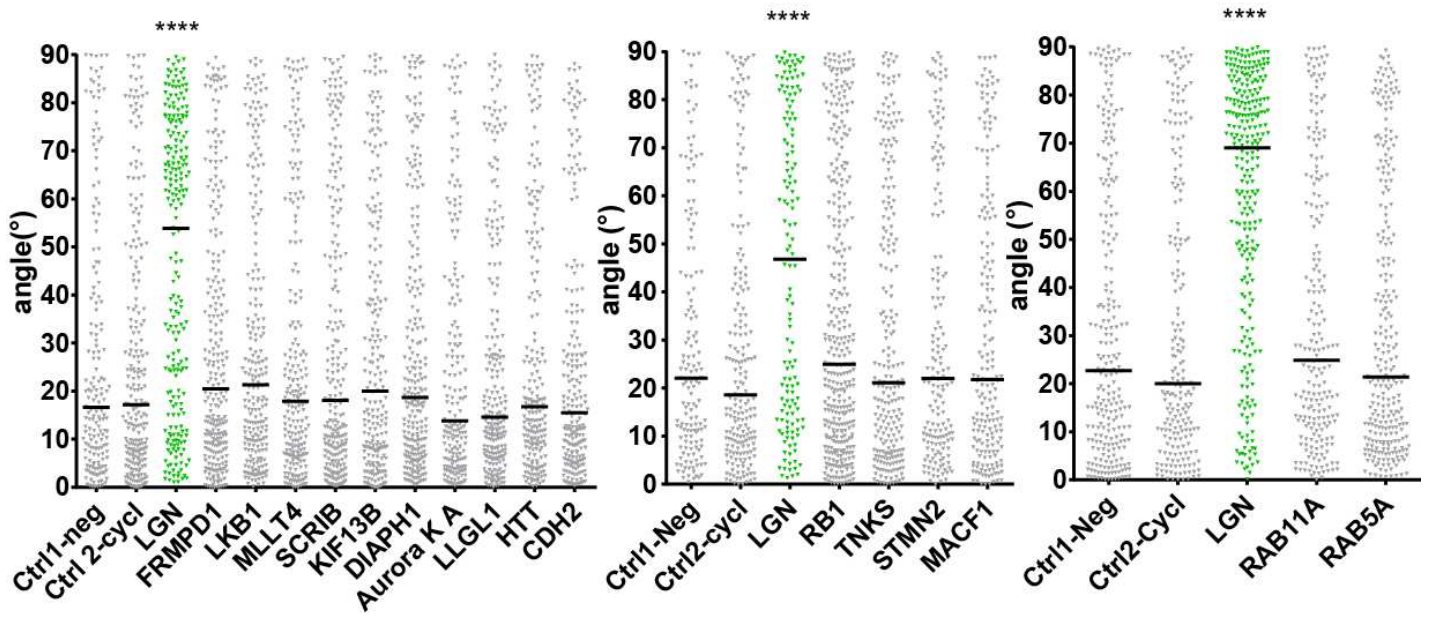
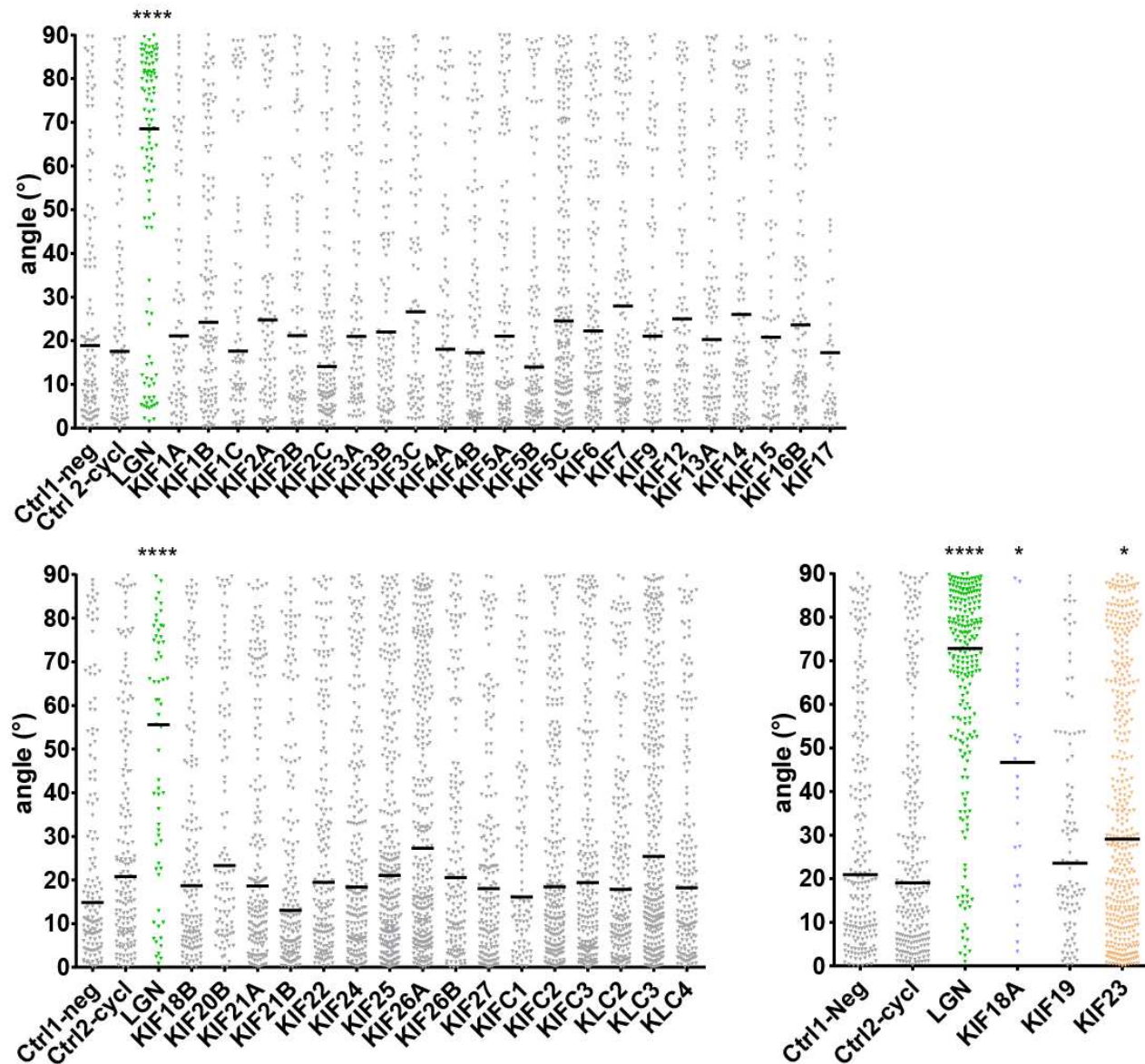


Figure 42

A Molecules potentially regulating LGN/NuMA + Molecules regulating spindle orientation in other models



B Kinesins



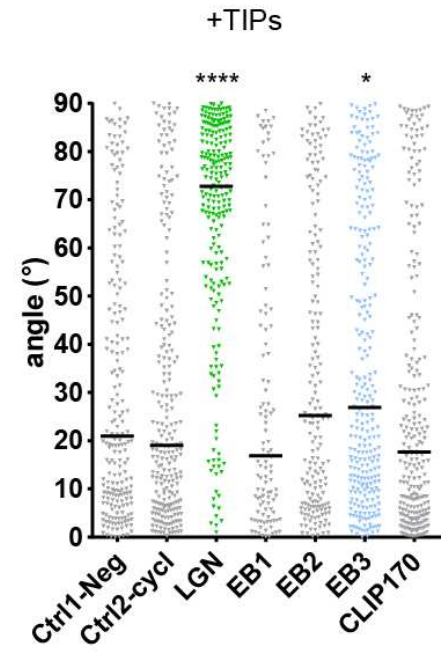
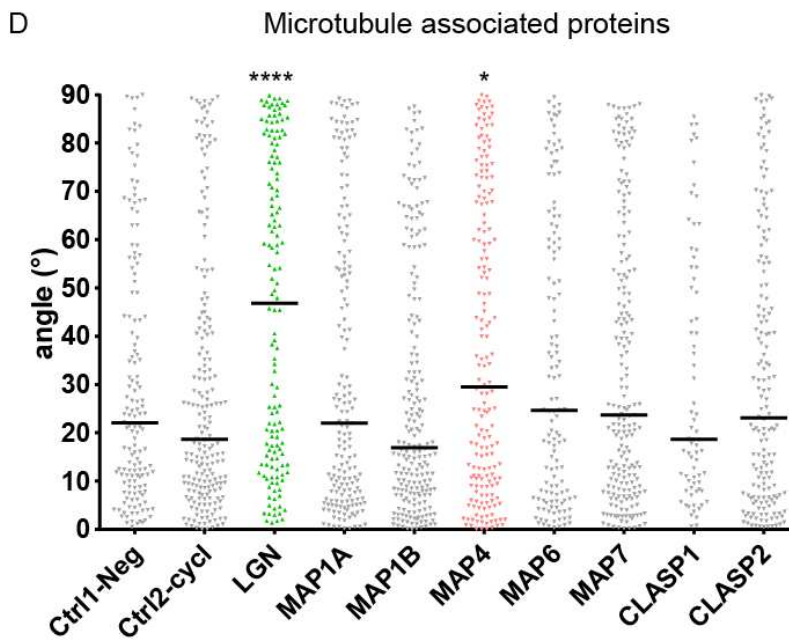
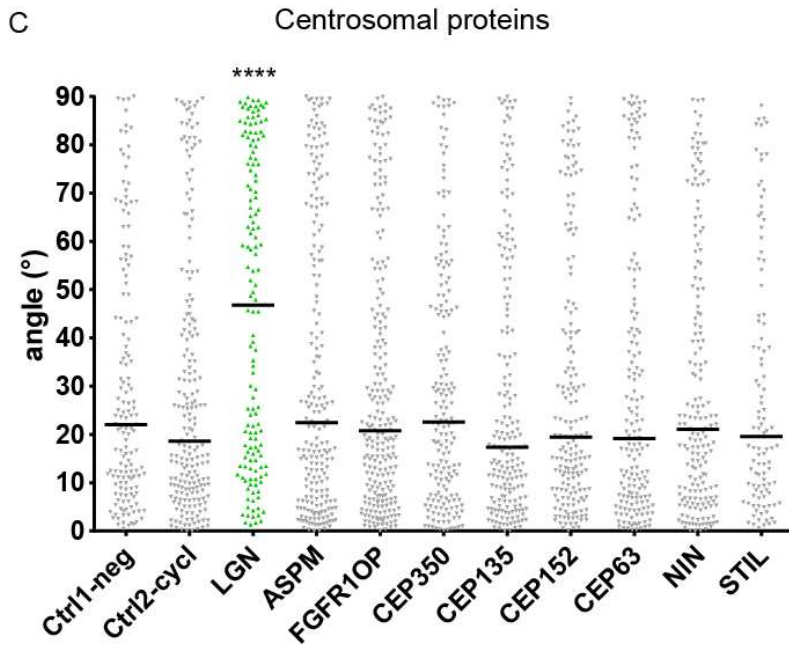
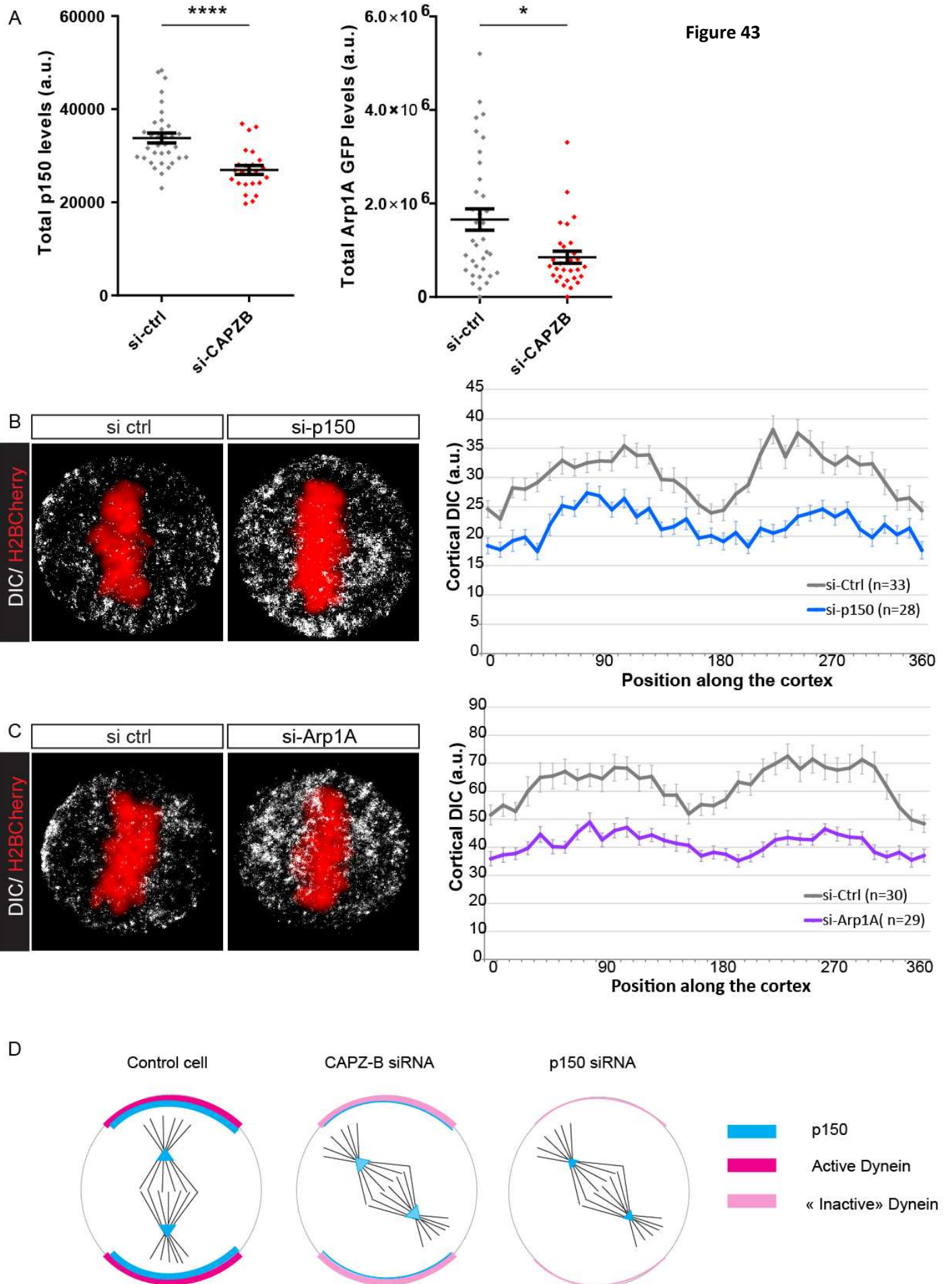


Figure 43



APPENDIX 2: METHODS

CELL CULTURE

HeLa cells were cultured in DMEM Glutamax™ (Life technologies) 10% Fetal Bovine Serum (FBS), 1% Penicillin/Streptomycin at 37°C and 5% CO₂. Specific cell lines were maintained in selection antibiotics. FACS sorting was regularly used to enrich for cells with high expression levels of each exogenous protein. To induce EdGFP-Gai expression, cells were treated with 1 µg/ml Doxycycline for 24hr before FACS. For live imaging of EB3-GFP, DHC-GFP and CAPZ-B-GFP, HeLa cells were cultured in Fluorobrite™ DMEM Medium (Life Technologies) complemented with 10% FBS, L-Glutamine and antibiotics.

For small scale experiments using micropatterns, cells were seeded on coverslips with fibronectin coated-micropatterns of different geometry acquired from Cytoo® or prepared as described in (Fink et al., 2011), and culture chambers (Cytoo®) were used for time-lapse acquisitions.

For the RNAi screen, cells were transfected with siRNAs in 96 well plates. On the third day after transfection, cells were dissociated using Accutase (StemPro® Accutase® Thermo Fisher Scientific) and seeded on 96 well plates printed with 30 µm circular micropatterns (Cytooplates®) for imaging.

For experiments on non-micropatterned substrates, cells were cultured on glass slides or glass bottom Matek® plates coated with Fibronectin (25 µg/ml).

TRANSFECTION

For siRNA experiments, cells were transfected with 25 nM siRNA concentration using HiPerFect (Qiagen) following the manufacturer's instructions, and imaged 72 hr after transfection. For plasmid transfection, Lipofectamine 2000 (Invitrogen) or Attractene (Qiagen) reagents were used following manufacturer's protocols.

RNAI LIBRARY

For the RNAi screen, we used an On target Plus® siRNA customized (Cherry-picking) library of 107 candidates +controls (Dharmacon). In this library, each gene is targeted by a pool of 4 different siRNAs. Depletion efficiency of all dynein subunits and regulators in HeLa cells using this library was previously shown by RT-PCR by Raaijmakers and colleagues (Raaijmakers et al., 2013).

In each experiment, two independent replicates for each siRNA condition were imaged. Additional confirmation experiments were performed for all dynein subunits and regulators, as well as for some other proteins with subtle but significant phenotype.

PLASMIDS AND CELL LINES

For generating the Ed stable cell lines, I used a strategy based on the use of transposable sequences, to increase the probability of genomic integration, as well as an inducible system for the expression of Ed-fusion proteins (see Fig. 40).

The following cell lines were generated for this study using the indicated plasmids:

Cell line	Plasmids used to generate it	Type of expression
EdGFP- H2BCherry	pTol2-TRE EdGFP NeoR pTol2-TetON iresH2Cherry pCAGGS-Tol2Transposase (transient)	Dox inducible Ed-X-expression
EdGFPLGN- H2BCherry	pTol2-TRE EdGFPLGN NeoR pTol2-TetON iresH2Cherry pCAGGS-Tol2Transposase (transient)	
EdGFPGai- H2BCherry	pTol2-TRE EdGFPGα NeoR pTol2-TetON iresH2Cherry pCAGGS-Tol2Transposase (transient)	Constitutive H2B-Cherry expression
EdCherryGai-H2BCherry-LGNGFP	Base cell line: HeLa LGN GFP from Iain Cheeseman (Kiyomitsu and Cheeseman, 2012)	+LGN-GFP constitutive expression

	<p>pTol2-TREdCherryGai NeoR</p> <p>pTol2-TetON iresH2Cherry</p> <p>pCAGGS-Tol2Transposase (transient)</p>	
--	---	--

For transient transfection in cells and electroporation in chicken, the following plasmids were used: p-EGFP-CAPZ-B (0.6 ng/μl in cells, 1 μg/μl in embryos-Addgene), pCX-H2B-EGFP (300 ng/ul, gift from K. Hadjantonakis) and pCX-H2B-mRFP (100 ng/ul, gift from S. Tajbakhsh).

DRUG TREATMENT

Latrunculin A (0.5 μM for experiments shown in Figs. 26 and 40, and 0.4 μM in Fig. 32) and Nocodazole (10 nM) were added to cells before starting time lapse acquisition. For evaluating drug effects on actin and microtubules, cells were treated for at least 3 hr before fixation. For stainings performed in cell pairs on micropatterns, cells were incubated for 6 hr in ProTAME (12 μM, R&D systems) before fixation.

IMMUNOFLUORESCENCE

The following primary antibodies were used in this study: anti-NuMA (Novus Biologicals, 1: 200), anti-p150 (BD Transduction laboratories, 1:100), anti-Dynein Intermediate Chain (DIC-clone 74.1, Millipore, 1:50), anti-CAPZ-B (Millipore, 1:100), anti-α-tubulin (clone DM1A, Sigma- 1:500), anti γ-tubulin (Clone GTU88, Sigma, 1:500), anti-N-cadherin (Clone GC4, 1:100) and anti-aPKC (Santa Cruz, 1:500).

HELA CELLS

For NuMA and CAPZ-B stainings, HeLa cells were fixed for 10' in TCA 10% followed by 10' in cold MetOH, at 4°C. For p150 staining, cells were fixed at RT for 10' in Formaldehyde 4% followed by 5' in PBS-Triton 0.1%. For staining with DIC antibody, cells were fixed in PFA 2% in MetOH for 15' at -20°C. α-tubulin and Phalloidin (1:50) stainings were performed on cells fixed using PFA and Glutaraldehyde in BRB80 buffer, following the protocol described in (Fink et al., 2011). Cells were blocked in 3% BSA,

0.1% PBS Triton (for most antibodies) or 3% BSA, 0.2 % NP40 in BRB80 (for α -tubulin and Phalloidin stainings) during 1 hr at RT before incubation with phalloidin or primary antibodies

CHICKEN EMBRYOS

Whole embryos were fixed during 1 hr in Formadehyde 4% in PBS at 4°C. For en-face views, fixed embryos were cut along their midline. For γ -tubulin staining, dissected embryos were treated with acetone for 15' at -20°C and washed 3x5min in PBS-Triton 0.3%. 1 hour incubation in blocking solution (PBS-Triton 0.3% /10%FBS) was performed before immunostaining.

For cryosections, embryos were equilibrated at 4°C in PB/15% Sucrose, embedded in PB/15% Sucrose/7,5% gelatin, and flash frozen in isopentane brought to -50°C on dry ice, before sectioning at -20°C. Before immuno-staining, cryosections were equilibrated at room temperature, degelatinized in PBS at 37°C 3 times 5 minutes, before a 30 minutes blocking step in PBS-Triton 0.1%/10% FBS.

Both cells and embryos were mounted using Vectashield (Vector labs).

IN OVO ELECTROPORATION

CRISPR/Cas9 gene knock-out in chick embryos was achieved by direct electroporation of a Cas9 protein/guide RNA complex and reporter plasmid in the neural tube. In ovo electroporation was performed in E2 embryos as described (Morin et al., 2007), with the following modifications. 20 nt CRISPR/Cas9 target sequences were selected in CAPZ-B cDNA sequence, and in CAPZ-B intron 3 genomic sequence using the CRISPOR website (<http://crispor.tefor.net/>) and used to design 36 base long single stranded trRNA sequence. trRNA oligonucleotides were purchased from Integrated DNA Technologies (IDT). trRNA (100 μ M) were mixed at equimolar concentration with a tracrRNA (purchased from IDT: ALT-R™) to obtain a 50 μ M mix in 10 μ l aliquots, and annealed by heating 5 minutes to 95°C and cooling down to RT, and 1 μ l of 10x buffer (100mM Hepes pH7.5, 1.5M KCl) was added to obtain a 45 μ M gRNA mix. Purified Cas9 protein (30 μ M in 10mM Hepes, 150mM KCl, a gift from A De Cian and JP Concordet (Menoret et al., 2015) was mixed 1:1 (vol:vol) with the gRNA mix

and incubated for 20 minutes at 37°C to promote complex formation. 1µl of this mix was then complemented with Fast Green and a DNA reporter plasmid (pCAGGS-H2B-EGFP) in a total volume of 5µl. Final concentrations in the mix are Cas9 protein 3µM, gRNA duplex 4.5µM, reporter plasmid 300ng/µl (corresponding to 60nM for a 7.5kb plasmid). Typical injection volumes are 50-100nl/embryo. The most efficient sequence in chick CAPZ-B (ATTGAAGATTGCACGAGATAAGG) targets exon 3 at base 158 of the coding sequence. A trRNA sequence (CAATTGGATCTCCAGAACCGTGG) targeting the 3rd intron of CAPZ-B 535bp downstream of the exon3/intron3 boundary was used as a negative control, and gave results similar to the electroporation of the CAGGS-H2B-GFP reporter plasmid alone.

IMAGE ACQUISITION

Imaging was performed with the following microscopes: a laser scanning confocal microscope (model SP5 and SP8; Leica) with a 40x (Plan Neofluar NA 1.3 oil immersion) objective and Leica LAS software; a structured illumination microscope (Zeiss Observer Z1, inverted stand, Apotome) using a 40x objective and Zeiss software; Spinning disk confocal microscopy was performed either with an inverted microscope (Nikon Ti Eclipse) equipped with a Yokogawa CSU-X1 confocal head using a 40x water immersion objective (APO LWD, NA 1.15, Nikon) and Metamorph software (Molecular Devices) and an emCCD Camera (Evolve, Roper Scientific), or on an inverted microscope (Nikon Ti Eclipse) equipped with a Yokogawa CSU-W1 confocal head, an sCMOS Camera (Orca Flash4LT, Hamamatsu) and a 100x oil immersion objective (APO VC, NA 1.4, Nikon) using Micromanager software (Edelstein et al., 2010). Widefield imaging was performed on an inverted microscope (Nikon Ti Eclipse) with an sCMOS Camera (Orca Flash4LT, Hamamatsu) and a 10x objective (CFI Plan APO LBDA, NA 0.45, Nikon) using Micromanager software.

For time lapse microscopy experiments, cells were incubated in a microscope chamber (LIS or DigitalPixel) at 37°C, under 5% CO₂ in a humidified atmosphere.

IMAGE ANALYSIS

Fiji software (Schindelin et al., 2012) was used for image processing and data analysis (except for spindle orientation measurements in Echinoid-micropattern experiments and microtubules dynamics). When necessary, images were subjected to brightness and contrast adjustment to equilibrate channel intensities and background using Fiji software.

ANGLE MEASUREMENT IN RNAI SCREEN AND ED-GAI MODEL DEVELOPMENT EXPERIMENTS

Raw movies were screened manually and the time and x-y position of all events of interest (that is, an anaphase within a pair of isolated cells) were recorded in a Fiji Results Table. A custom macro was then used for the batch extraction of all selected division events as individual movies of 15 frames (10 before anaphase and 4 after anaphase). These manually extracted movies were then run into a custom Matlab code to determine the angle of division in anaphase. Our orientation assay uses the Ed enrichment at cell-cell contacts to position force generators. Ideally, the orientation of division in anaphase (visualized by the H2B-Cherry labelled chromosomes) should be measured relative to the EdGFP enrichment, requiring the use of two color channels in the analysis. To simplify the analysis, we reasoned that the point at mid distance between the two nuclei immediately before division could be used as a proxy for the localization of the Ed enrichment, allowing the use of only one color channel (H2B-Cherry) for the analysis. This approach was validated in a representative set of division events: we compared the angle distribution obtained by automatic measurement of anaphase angle with respect to the neighboring nucleus with manual measurements of angles with respect to the Echinoid enrichment, and observed that both types of measurements result in similar angle distributions.

Doxycycline-induced expression results in variable expression of the EdGFP transgenes; besides, we observed a progressive decay in transgene expression levels over time, possibly due to transgene silencing, so that we regularly FACS-sorted cells to enrich for high GFP expression upon Dox

induction. We also found that the ability of the EdGFP-Gai transgene to drive orientation perpendicular to the cell contact was strongly correlated to EdGFP-Gai expression levels. We therefore introduced a “GFP level filter” as a second module in the Matlab code to exclude cells with weak GFP enrichment. For each set of experiments in the screen, the GFP filter value was determined using the control siRNA experiments and the same filter value was applied to all tested conditions.

DESCRIPTION OF MATLAB SOFTWARE: NUCLEI SEGMENTATION, DIVISION ANGLE TRACKING AND GFP CLUSTER QUANTIFICATION

Microscopy images of GFP and mCherry (Fig.41a) were analysed with a Matlab procedure to determine the angle of division and the amount of clustered GFP. The following steps are implemented in the procedure:

NUCLEI SEGMENTATION

- 1) The initial nucleus image (Fig.41 b) is correlated with a Gaussian of 10 pixels spatial size (Fig. 41 c).
- 2) This image is filtered with a 10 pixel Gaussian filter (Fig. 41 d).
- 3) It is then converted into a binary image based on the level of fluorescence of the background (Fig.41 e).
- 4) Areas smaller than 400 pixels are removed as artefacts due to border effect from step (1), holes in binary regions are filled, and only area larger than 30 pixels are kept (Fig. 41 f).
- 5) Nuclei properties (numbers, areas, centroids positions) are determined using this final image.

MEASUREMENT OF THE ANGLE OF DIVISION

- 6) The division time (t_d) is determined using time sequences containing 2 nuclei, then 2 nuclei, then 3 nuclei (Fig. 41 g, h).
- 7) The cell which is not dividing is obtained by determining the largest of the 3 nuclei at time t_d
- 8) The angle of division is calculated at time t_d from the position of the centre of mass of the 3 nuclei (Fig.41 i)

DETERMINATION OF THE AMOUNT OF GFP CLUSTER

- 9) The last three time points before division (td-3, td-2 and td-1) are selected for the quantification of GFP cluster at the cell-cell contact (Fig. 41 j).
- 10) Position of the 2 nuclei obtained previously are used to automatically define a line going through the two cell (red line, Fig. 41 j)
- 11) GFP profile along this line is plotted (red dots, Fig. 41 k), averaged over the three time points and three Gaussian curves are fitted to it (black curve, Fig. 41 k). Initial values for the X position of those Gaussians are determined by the position of nuclei centre of mass.
- 12) The means and standard derivations of the Gaussian functions are determined from Gaussian fitting. Consequently, after normalization to the background, "GFP" level is calculated as the intensity of the common area (central peak) in comparison to the mean value of GFP intensity of the cells periphery (two external peaks).

QUANTIFICATION OF CORTICAL SIGNALS IN MITOTIC CELLS

The profiles of CAPZ-B GFP, Arp1A-GFP, p150 and Dynein Intermediate Chain signal at the cell cortex of metaphase HeLa cells (shown in Figs.30 and 33) were measured in Fiji software as follows: a 5 pixel wide line (circular tool) was positioned on cell contour in a confocal optical section corresponding to the middle plane of the cell. Pixel values along the line were calculated using the "Plot Profile" tool (each value corresponds to the average value of the 5 pixels on the line width). The start (and finish) point for the intensity measurement was chosen facing the chromosome plate on one side of the cell. As the absolute length of the circular line varies from cell to cell as a function of cell diameter, we designed a macro that interpolates plot values to calculate a normalized set of 360 values along the line, where positions 0 and 180 face the equatorial plate and positions 90 and 270 face the spindle poles, as illustrated in Figure 30a. For DIC profiles, averaging of 5 points was performed in order to smooth the curves (as the DIC signal is quite discontinuous). When comparing signals

between control and CAPZ-B siRNA-treated cells, these values were corrected by background measurements. Finally, average profiles were then calculated from n individual profiles.

ANALYSIS OF MT DYNAMICS USING U-TRACK

Metaphase EB3-GFP cells were imaged during 2 minutes at a 500 ms interval using a 100x objective (APO VC, NA 1.4, Nikon). Imaging was performed at a single plane containing both spindle poles. Cells with rotated spindles with respect to the growth surface such that both poles were not visible in a single plane were not considered for analysis.

Movies were subjected to analysis by the microtubule plus end tracking function contained in the u-track package (Applegate et al., 2011; Matov et al., 2010). Microtubule tracking was performed on the whole cell as the spindle density phenotype was observed both in the spindle and astral MT area. Our imaging conditions allowed to visualize astral MT without saturating the EB3-GFP signal in the spindle area. Visual inspection of the tracking movies showed correct tracking both in spindle and astral MTs. The parameters used for detection (by the watershed method), tracking and classification were the default parameters of the package. The analysis output for each cell consists in average or median values of several parameters calculated from thousands of tracks. Four independent experiments confirmed the same tendency for growth speed, shrinkage speed and growth lifetime upon CAPZ-B depletion. P150 siRNA and Arp1A siRNA were evaluated in parallel to CAPZ-B siRNA in two independent experiments.

1) Dlg1 controls planar spindle orientation in the neuroepithelium through direct interaction with LGN. Saadaoui M, Machicoane M, di Pietro F, Etoc F, Echard A, Morin X. *J Cell Biol.* 2014. 206(6):707-717.

In this project, Mehdi Saadaoui, a former postdoc in the lab, studied the function of Dlg1 during planar spindle orientation in the chick neuroepithelium. In mitotic neuroepithelial cells, LGN complex and NuMA localize in a ring at the lateral domain, and this restricted localization is essential for planar spindle orientation. However, how the lateral localization of LGN was controlled in this context was elusive: while aPKC controls LGN lateral localization in MDCK cysts (Hao et al., 2010) the group had shown that it does not in the chick neuroepithelium (Peyre et al., 2011). One potential candidate to regulate LGN localization was Dlg1, which localizes in the lateral domain in different epithelia. Moreover, Dlg family members were known to interact with LGN both in fly and vertebrates, and to regulate spindle orientation in the context of the asymmetric cell division of *Drosophila* Neuroblasts and Sensory Organ Precursors (Bellaïche et al., 2001; Siegrist and Doe, 2005). Interestingly, M. Saadaoui found that Dlg1 localizes to the basolateral domain of apical progenitors in the chick neuroepithelium. Remarkably, he showed that knock-down of Dlg1 generated a dramatic phenotype in spindle orientation in neural progenitors. Concomitantly, depletion of Dlg-1 resulted in the loss of LGN from the cortex. Importantly, using rescue experiments of both LGN and Dlg1 knock-down with mutant constructs of Dlg and LGN that were unable to mediate the interaction with each other, M. Saadaoui showed that the direct interaction between these two proteins is critical for planar spindle orientation. In parallel, Mickael Machicoane, a PhD student in Arnaud Echard's lab at the Pasteur Institute, had shown that siRNA depletion of Dlg1 generated spindle orientation defects in cells cultured on L-micropatterns. Complementing his work, I found that Dlg1 depletion in cultured cells results in a strong decrease in LGN and NuMA cortical levels, thus illustrating a parallel with the chick embryo and extending the findings to a different system. In addition, we showed that Dlg1

depletion generates a subtle spindle orientation defect with respect to the growth surface in metaphase cells.

In conclusion, we showed that Dlg-1 regulates vertebrate spindle orientation both in polarized cells *in vivo* and in non-polarized cells in culture. Interestingly, Bergstrahl and colleagues have recently found that Dlg also regulates planar spindle orientation in the *Drosophila* follicular epithelium (Bergstrahl et al., 2013). Importantly, our work demonstrated that Dlg1 regulates vertebrate spindle orientation by a different mechanism than the one observed in *Drosophila*. In particular, in the vertebrate cells, Dlg1 regulates the recruitment/stability of LGN at the cortex, in contrast to *Drosophila* epithelia where Dlg works by restricting the lateral localization of Pins (Bergstrahl et al., 2013).

Dlg1 controls planar spindle orientation in the neuroepithelium through direct interaction with LGN

Mehdi Saadaoui,^{1,2,3} Mickaël Machicoane,^{4,5,6} Florencia di Pietro,^{1,2,3,7} Fred Etoc,^{1,2,3} Arnaud Echard,^{4,5} and Xavier Morin^{1,2,3}

¹Institut de Biologie de l'École Normale Supérieure, École Normale Supérieure, F-75005 Paris, France

²Institut National de la Santé et de la Recherche Médicale, U1024, F-75005 Paris, France

³Centre National de la Recherche Scientifique, Unité Mixte de Recherche 8197, F-75005 Paris, France

⁴Membrane Traffic and Cell Division Laboratory, Institut Pasteur, F-75015 Paris, France

⁵Centre National de la Recherche Scientifique, Unité de Recherche Associée 2582, F-75015 Paris, France

⁶Cellule Pasteur–Université Pierre et Marie Curie, Université Pierre et Marie Curie, F-75015 Paris, France

⁷Institute of Doctoral Studies (IFD), Sorbonne Universités, Université Pierre et Marie Curie–Université Paris 6, F-75252 Paris, France

Oriented cell divisions are necessary for the development of epithelial structures. Mitotic spindle orientation requires the precise localization of force generators at the cell cortex via the evolutionarily conserved LGN complex. However, polarity cues acting upstream of this complex *in vivo* in the vertebrate epithelia remain unknown. In this paper, we show that Dlg1 is localized at the basolateral cell cortex during mitosis and is necessary for planar spindle orientation in the chick neuroepithelium. Live imaging revealed that Dlg1

is required for directed spindle movements during metaphase. Mechanistically, we show that direct interaction between Dlg1 and LGN promotes cortical localization of the LGN complex. Furthermore, in human cells dividing on adhesive micropatterns, homogeneously localized Dlg1 recruited LGN to the mitotic cortex and was also necessary for proper spindle orientation. We propose that Dlg1 acts primarily to recruit LGN to the cortex and that Dlg1 localization may additionally provide instructive cues for spindle orientation.

Introduction

Oriented cell divisions play a crucial role in the development, growth, and homeostasis of many tissues (Morin and Bellaïche, 2011). Divisions within the plane of epithelial structures (thereafter referred to as planar divisions) both contribute to the expansion of the tissue surface and are essential for tissue integrity through maintenance of the epithelial monolayer organization (Fleming et al., 2007). Conversely, divisions perpendicular to the epithelial plane (vertical divisions) have been shown to contribute to tissue stratification, binary fate decisions, and regulation of stem cell pools (Quyn et al., 2010; Williams et al., 2011). Defective control of spindle orientation leads to developmental and homeostasis defects and may be a step in the transformation process leading to cancer (Pease and Tirnauer, 2011; Noatynska et al., 2012).

Correspondence to Xavier Morin: xavier.morin@ens.fr

F. Etoc's present address is Center for Studies in Physics and Biology and Laboratory of Molecular Vertebrate Embryology, The Rockefeller University, New York, NY 10065.

Abbreviations used in this paper: aPKC, atypical PKC; Dlg, discs large; GPR, G protein regulatory; GUK, guanylate kinase; Insc, Inscuteable; LR, linker region; NB, neuroblast; NuMA, nuclear mitotic apparatus; PACT, Pericentrin/AKAP-450 centrosomal targeting.

In many models of oriented cell divisions, spindle orientation relies on the specific cortical subcellular localization of a core molecular complex composed of the Gα_i subunits of heterotrimeric inhibitory G proteins, of LGN (also referred to as G protein–signaling molecule 2 and as Pins in *Drosophila melanogaster*), and of nuclear mitotic apparatus (NuMA). This LGN complex recruits motor proteins (cytoplasmic dynein and its regulators) to concentrate force generators that pull on astral microtubules to position and orient the mitotic spindle along a specific axis (Morin and Bellaïche, 2011). Apical distribution of the LGN complex is required for vertical spindle orientation in the asymmetric division of both *Drosophila* neuroblasts (NBs; Yu et al., 2000) and mouse embryonic skin progenitors (Lechler and Fuchs, 2005; Williams et al., 2011), whereas its lateral enrichment controls planar spindle orientation in vertebrate neuroepithelial and MDCK cells (Zheng et al., 2010; Peyre et al., 2011).

© 2014 Saadaoui et al. This article is distributed under the terms of an Attribution–Noncommercial–Share Alike–No Mirror Sites license for the first six months after the publication date (see <http://www.rupress.org/terms>). After six months it is available under a Creative Commons License [Attribution–Noncommercial–Share Alike 3.0 Unported license, as described at <http://creativecommons.org/licenses/by-nc-sa/3.0/>].

The LGN complex appears as a generic cog in spindle orientation, taking orders from intra- and extracellular upstream polarity cues. In *Drosophila* NBs, positional information is given by the apically located Par complex, which recruits the LGN complex via the Inscutable (Insc) adapter protein (Morin and Bellaïche, 2011). Likewise, in mouse embryonic skin progenitors, integrin signaling from the basal lamina acts as a positional cue for intracellular Par-Insc-LGN localization at the apical cell cortex to promote vertical spindle orientation and skin stratification (Lechler and Fuchs, 2005; Williams et al., 2011). Insc also controls vertical and oblique spindle orientation at the expense of planar divisions in the vertebrate neuroepithelium (Žigman et al., 2005; Postiglione et al., 2011).

Polarity cues driving planar spindle orientation in vertebrate epithelia are poorly understood, and the mechanism responsible for the lateral restriction of LGN in dividing cells (Zheng et al., 2010; Peyre et al., 2011) is unclear. Experiments in 3D culture of MDCK cells indicated that apical atypical PKC (aPKC) phosphorylates LGN, locally increasing LGN affinity with a 14–3–3 protein that competes with $G\alpha_i$ for LGN interaction, thereby excluding LGN from the apical cortex (Hao et al., 2010). Although a similar role of aPKC was observed in *Drosophila* larval wing disk epithelia (Guilgur et al., 2012), it does not seem to be the case in the chick neuroepithelium (Peyre et al., 2011). Studies in *Drosophila* suggested a role of the discs large (Dlg) gene family: *dlg* mutant sensory organ precursors show defective spindle orientation and reduced accumulation of Pins at the anterior cell cortex in *Drosophila* larvae (Bellaïche et al., 2001). Dlg is also part of a nonessential microtubule-based pathway driving cortical localization of LGN– $G\alpha_i$ in fly NBs (Siegrist and Doe, 2005; Johnston et al., 2009). Finally, defects in spindle orientation were recently described in *Drosophila* *dlg* mutant larval wing disks and adult female follicular cells (Bergstrahl et al., 2013; Nakajima et al., 2013). In vitro studies have revealed biochemical interactions between LGN and several members of the Dlg family, but the functional relevance of this interaction has not been investigated in vivo (Sans et al., 2005; Johnston et al., 2009; Zhu et al., 2011).

Here, we show that vertebrate Dlg1/SAP97 (Synapse-associated protein 97) is polarized at the mitotic cell cortex and is essential for directional movements, resulting in planar spindle orientation in the chick neuroepithelium. Using point mutations in both Dlg1 and LGN, we demonstrate that the direct interaction between Dlg1 and LGN plays a key role in LGN cortical recruitment and spindle orientation in vivo. We further show that Dlg1 also controls LGN cortical accumulation and substrate-induced spindle orientation in cells cultured on adhesive micropatterns. Our data reveal a major function for Dlg1 in recruiting LGN to the mitotic cortex and in proper spindle orientation in multiple cellular contexts in vertebrates.

Results and discussion

Dlg1 is required for planar spindle orientation in chick neural progenitors

We focused on chick Dlg1/SAP97/Dlh: among the four DLG family members found in chick databases, Dlg1 is structurally

the most closely related to canonical *Caenorhabditis elegans* *dlg-1* and *Drosophila* Dlg (Assémat et al., 2008) and was found expressed in the chick neural tube at E3 (Fig. S1 A). Interestingly, a GFP-Dlg1 fusion protein was enriched at the basolateral cell cortex during mitosis upon in ovo electroporation in the chick neuroepithelium (Fig. 1, A and B; and Fig. S2 for a list of vectors used in this study).

We addressed a possible role of Dlg1 in spindle orientation using miRNA-based RNAi vectors (Das et al., 2006). Silencing efficiency was assessed by the loss of GFP-Dlg1 fusion expression (Fig. S1 B). We measured spindle orientation in en face views of flat mounted neural tubes (Figs. 1 A and S1 C; Materials and methods). Although the majority of control cells exhibited a planar orientation both in metaphase ($\alpha_{\text{mean Ctrl}} = 11.9^\circ$, $n = 85$) and anaphase ($\alpha_{\text{mean Ctrl}} = 8.3^\circ$, $n = 51$; Fig. 1, C and D), cells expressing Dlg1 miRNA showed a misoriented spindle in metaphase ($\alpha_{\text{mean Dlg}^-} = 29.3^\circ$, $n = 106$, $P < 0.0001$) and, to a minor extent, in anaphase ($\alpha_{\text{mean Dlg}^-} = 12.8^\circ$, $n = 59$, $P = 0.0048$; Fig. 1, C and D).

Drosophila Dlg is important for adherens junction structure and cell polarity in interphase cells (Woods and Bryant, 1991), and a similar role has been proposed for Dlg1 based on siRNA experiments in cultured human epithelial cells (Laprise et al., 2004). However, analysis of Dlg1 mouse mutant phenotypes in the embryonic lens and urogenital tracts did not reveal a general requirement for Dlg1 in epithelial polarity (Naim et al., 2005; Mahoney et al., 2006; Iizuka-Kogo et al., 2007; Rivera et al., 2009), although specific cell types in the lens show cell-autonomous polarity defects (Rivera et al., 2009). We investigated whether Dlg1 knockdown may disrupt cell polarity in the neuroepithelium at different time points after electroporation. Remarkably, overall tissue organization was not perturbed (Fig. 1 E, top). Subapical localization of the tight junction marker ZO-1 (Figs. 1 E and S1 D) and apical distribution of aPKC (Fig. S1 E) were not affected, even after a long period of RNAi treatment. In addition, subapical enrichment of the adherens junction markers N-cadherin and β -catenin was undistinguishable from control cells (Figs. 1 E and S1 D). Hence, Dlg1 is not required for the maintenance of cell polarity and has an essential role in planar spindle orientation of neuroepithelial cells in vivo.

Mitotic spindle movements are randomized in Dlg1 knockdown cells

To understand why Dlg1 is essential for spindle orientation, we analyzed spindle dynamics in Dlg1-depleted cells. Chick embryos were electroporated with fluorescent reporters to label centrosomes and chromosomes in control or Dlg1 RNAi-expressing cells. We imaged the neuroepithelium using an en face culture protocol (Peyre et al., 2011) and designed a semi-automated 3D centrosome-tracking routine (Materials and methods; Fig. 2 A) to analyze the behavior of dividing cells. In both control and Dlg1-depleted cells, mean spindle orientations relative to the apical surface were similar to those observed in fixed conditions in metaphase and anaphase cells (Fig. 2 B). We concentrated on spindle movements relative to the apico-basal axis (z axis in the en face view). During prophase, the two

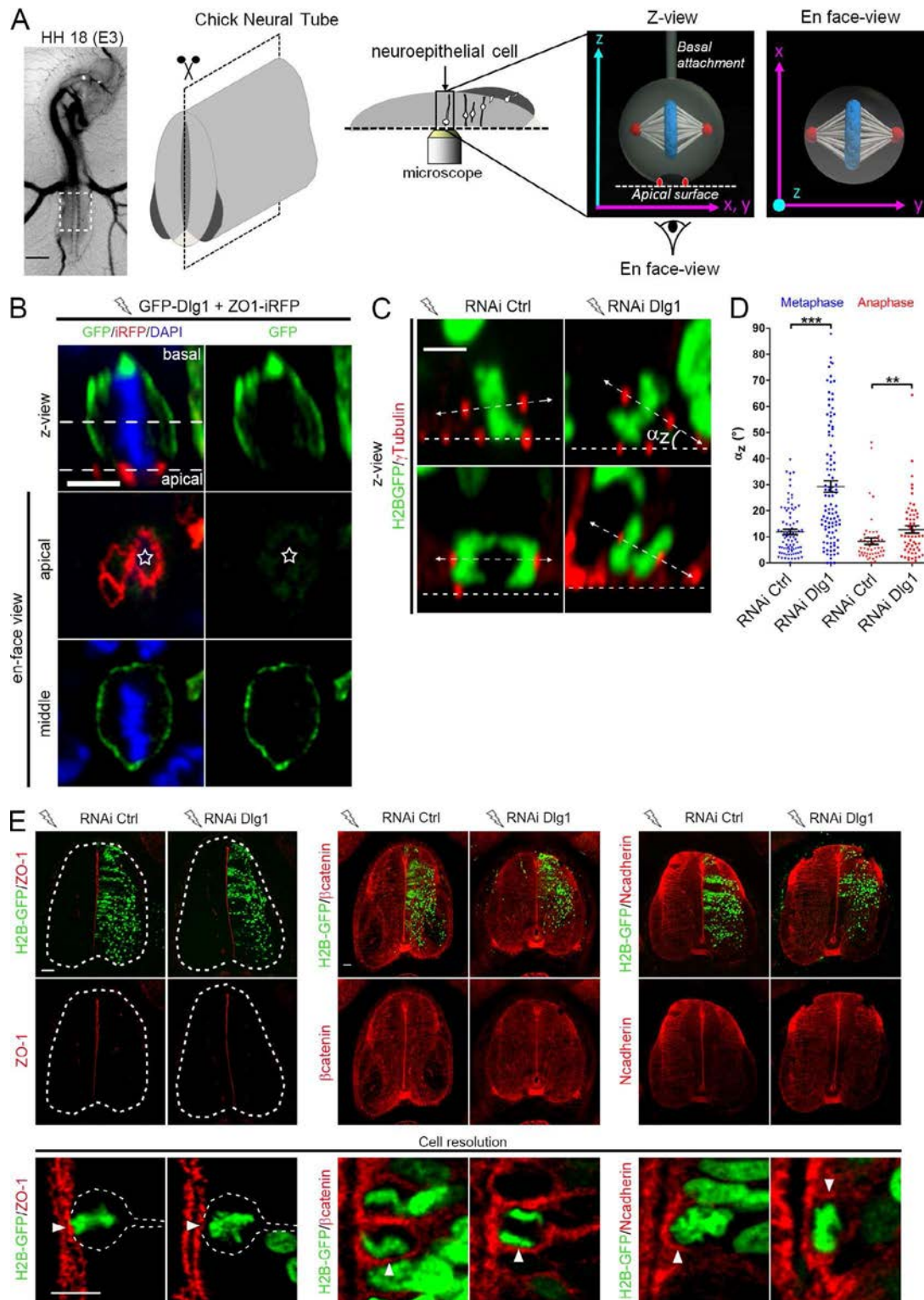


Figure 1. Dlg1 is required for planar spindle orientation in chick neural progenitors. (A) Scheme of flat mounting of the E3 (Hamburger Hamilton [HH] stage 18) chick neural tube for en face imaging of neuroepithelial cells. (B) GFP-Dlg1 is restricted to the basolateral cortex during metaphase. The z view is a reslice along the z axis of the confocal stack acquired in en face view. The four bottom images show single optical sections from the en face view (apical and middle levels). ZO-1 (red) labels tight junctions. White dashed lines on the z view show focal planes chosen for the apical and middle en face views. White stars show apical domain of the GFP-Dlg1-expressing cell. (C) Z view along the axis of the mitotic spindle of metaphase and anaphase cells expressing control (Ctrl) or Dlg1-targeting miRNAs (H2B-GFP marker). H2B-GFP and γ -tubulin label chromosomes and spindle poles, respectively. (D) Quantification of mitotic spindle α_z orientation at E3, 24 h after electroporation (means \pm SEM, $n > 50$ cells from at least three embryos). **, $P \leq 0.01$; ***, $P \leq 0.001$. (E) Tissue architecture (top) and apicobasal polarity (cell resolution images) are not affected in neural tubes electroporated with Dlg1 miRNA as illustrated by ZO-1, β -catenin, or N-cadherin staining. White arrowheads point to H2B-GFP-positive electroporated cells. Dotted lines highlight the contour of the neural tube (top) or of individual dividing cells (bottom). Bars: (A) 1.5 mm; (B and C) 5 μ m; (E, top) 50 μ m; (E, bottom) 10 μ m.

centrosomes disengage from the apical surface and move to two opposite sides of the nucleus and form the bipolar spindle upon nuclear envelope breakdown during prometaphase. The distance between spindle poles remains stable during prometaphase and metaphase and until anaphase onset. We used this distance as a means to stage progression through mitotic phases. In control cells, the mitotic spindle formed with a random orientation relative to the z axis (Fig. 2 C; Peyre et al., 2011). Within 5 min, it underwent a phase of directed z rotation away from this axis to align parallel to the apical surface. During a second phase, it remained in the planar orientation, while displaying oscillatory z rotations (Fig. 2, C and E; and Video 1). Dlg1 RNAi cells failed to undergo the directed z rotation that occurs immediately after spindle formation. Instead, spindles experienced random movements relative to the z axis throughout prometaphase and metaphase. This led to a nonplanar orientation at anaphase onset (Fig. 2, D and E; and Video 2). The ability of the spindle to move was not impaired because the absolute z rotation in 1-min intervals (our time frame in these experiments) was not different from control cells (Fig. 2 F). However, whereas control cells showed a specific directional bias of spindle movements away from the apicobasal axis during early metaphase (relative rotation $\delta_{z(t_{1-5})} = -6 \pm 1.4^\circ/\text{min}$; Fig. 2 G), this bias was lost in Dlg1-depleted cells ($\delta_{z(t_{1-5})} = -1 \pm 1.3^\circ/\text{min}$, $P = 0.0025$; Fig. 2 G). Hence, defective spindle orientation upon Dlg1 knockdown results from a failure to orient their rotation movement toward the planar orientation in early metaphase, rather than from an inability to rotate.

Dlg1 is required to orient the spindle in dissociated cells cultured on adhesive micropatterns

We then explored whether Dlg1 is also involved in spindle orientation in a nonepithelial context. In vitro, adherent cells typically divide parallel to the plane of the culture dish. We found that Dlg1-depleted HeLa cells displayed a slightly tilted angle in metaphase compared with controls ($\alpha_{z \text{ Dlg-}} = 10.6^\circ$ and $\alpha_{z \text{ Ctrl}} = 5.9^\circ$, $P = 0.0037$; Fig. 3 A). This defect was absent in anaphase, suggesting that planar orientation is delayed upon Dlg1 silencing ($\alpha_{z \text{ Dlg-}} = 5.4^\circ$ and $\alpha_{z \text{ Ctrl}} = 5.4^\circ$; Fig. 3 A). To investigate whether Dlg1 might be involved in spindle orientation in the xy plane, which depends on the geometry of cell adhesion to the substrate (Théry et al., 2005, 2007), we used cells cultured on L shape adhesive micropatterns. In this system, the mitotic spindle predominantly aligns with the hypotenuse of the triangle defined by the L shape (Fig. 3 B; Théry et al., 2005). Remarkably, Dlg1 distribution in the xy plane was homogeneous at the cell cortex of prometaphase and metaphase cells and did not display any enrichment relative to the spindle poles or the pattern geometry (Fig. 3 B). Control cells displayed a spindle angle distribution tightly centered on 45° at anaphase onset, as expected (Fig. 3 C). In contrast, Dlg1-depleted cells showed a significantly broader angle distribution, with a twofold reduction in the number of spindles correctly oriented at 45° ($23 \pm 3\%$ of Dlg1 RNAi vs. $42 \pm 6\%$ of control cells in the 15° bin centered on 45° [$P < 0.0001$ and $D = 0.124$]; Fig. 3 C).

In control cells, the spindle is only loosely oriented at the beginning of mitosis and undergoes directed rotation movements

toward the 45° orientation mainly during late prometaphase and early metaphase (Machicoane et al., 2014). The final orientation is typically reached within 15 min after metaphase onset and maintained until anaphase (Fig. 3 D). In contrast, we observed that directed rotation toward the 45° position was reduced in Dlg1-depleted cells, with movements of the spindle essentially consisting in oscillations around its initial position (Fig. 3 D).

Hence, directed spindle rotation in the xy plane during metaphase is also compromised by Dlg1 knockdown in HeLa cells cultured on adhesive micropatterns. However, in this system, Dlg1 is homogeneous at the cortex, suggesting that its localization is not instructive. Rather, its role may be permissive, allowing cells to translate cues from the adhesive pattern into a specific spindle orientation.

LGN cortical localization depends on Dlg1

Direct biochemical interactions have been described between the C-terminal guanylate kinase (GUK) domain of several Dlg family members and the central linker region (LR) domain of LGN (Figs. 3 E and 4 A; Sans et al., 2005; Johnston et al., 2009; Zhu et al., 2011). Because LGN is essential for spindle orientation, the defects observed upon Dlg1 depletion in both chick and HeLa cells might be a result of a direct effect on LGN. We thus investigated the distribution of LGN after Dlg1 knockdown.

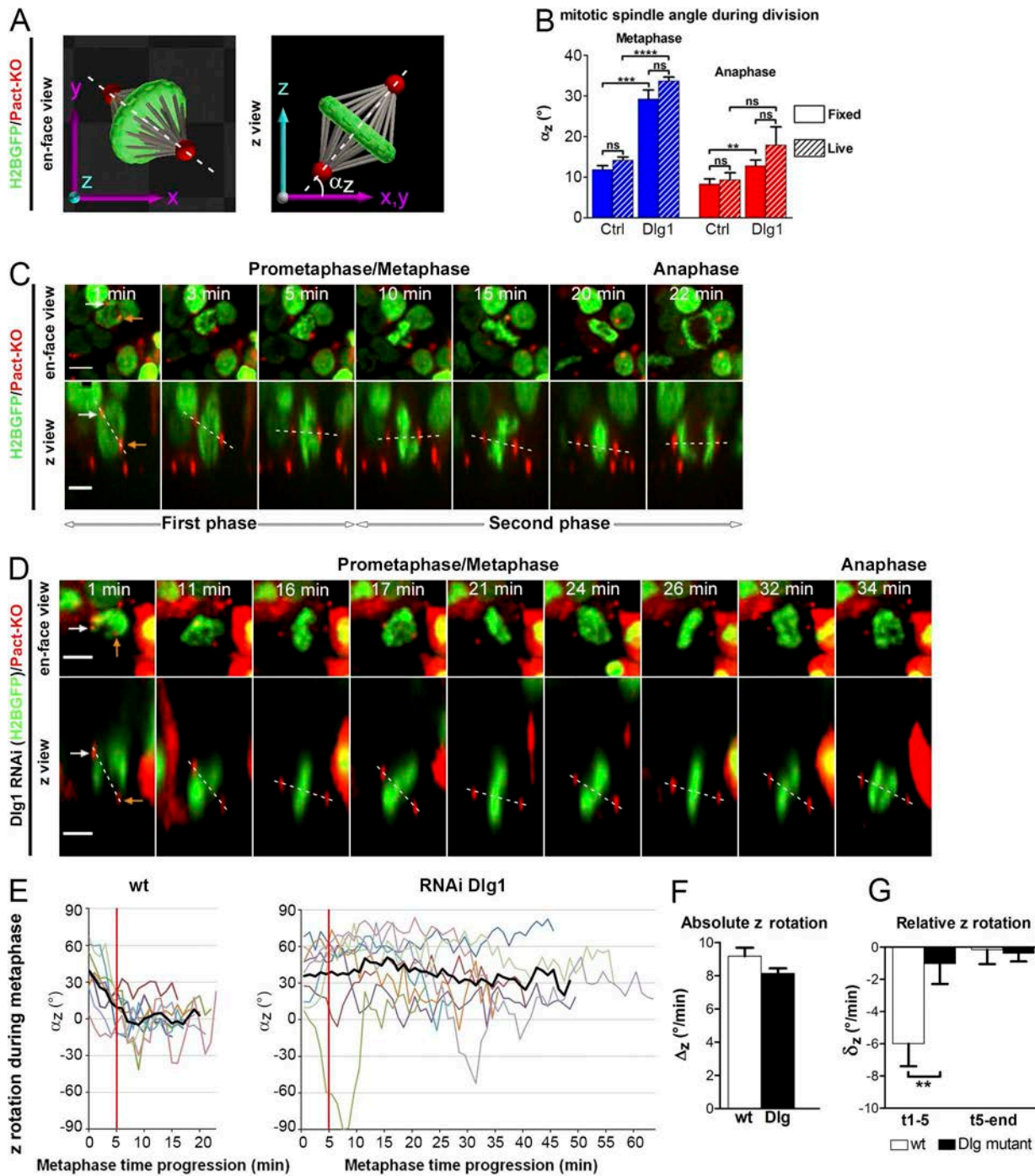
In HeLa cells in metaphase, LGN appeared as two cortical crescents with a symmetric distribution facing the spindle poles, as expected (Kiyomitsu and Cheeseman, 2012). In contrast, after Dlg1 depletion, cortical levels of LGN were decreased, and the remaining cortical LGN was distributed evenly (Fig. 3 E). Cortical localization of NuMA in metaphase relies on LGN (Peyre et al., 2011; Kiyomitsu and Cheeseman, 2013). Accordingly, NuMA was lost from the cortex in Dlg1-depleted cells, whereas it was still visible on the spindle (Fig. 3 E).

Similarly, in Dlg1-depleted cells in vivo, a GFP-LGN fusion no longer accumulated at the lateral cell cortex, with a twofold decrease of the cortical over cytoplasmic signals in metaphase compared with control cells (Fig. 4 B). Conversely, LGN knockdown did not prevent the cortical distribution of a GFP-Dlg1 fusion protein (Fig. S3 A).

Altogether, we conclude that Dlg1 acts upstream of LGN/NuMA and is essential for the cortical recruitment of LGN. In cultured cells, Dlg1 is homogenous at the cortex and therefore likely permissive for the cell to respond to external orientation cues provided by adhesive micropatterns. In epithelia, the apicobasal polarization of Dlg1 distribution may additionally provide an instructive cue for planar orientation.

Direct LGN-Dlg1 interaction is necessary for mitotic spindle orientation

Dlg1 involvement in LGN localization led us to dissect the functional domains of LGN necessary for its cortical distribution. Because LGN is also known to interact with cortically anchored GDP-bound $G\alpha_i$ subunits via the four G protein regulatory (GPR) domains located at its C terminus (Fig. 4 A; Willard et al., 2004; Morin et al., 2007; Peyre et al., 2011), we addressed the specific requirement of LGN binding domains



to $\text{G}\alpha_i$ and Dlg1 in its cortical localization through analysis of the localization of GFP-tagged truncated forms of LGN. Individually, LGN linker (LR) and GPR domains were detectable

at the cell cortex over a strong cytoplasmic signal. In contrast, combining both domains (LR-GPR) led to a much stronger and almost exclusive cortical localization (Fig. 4 C).

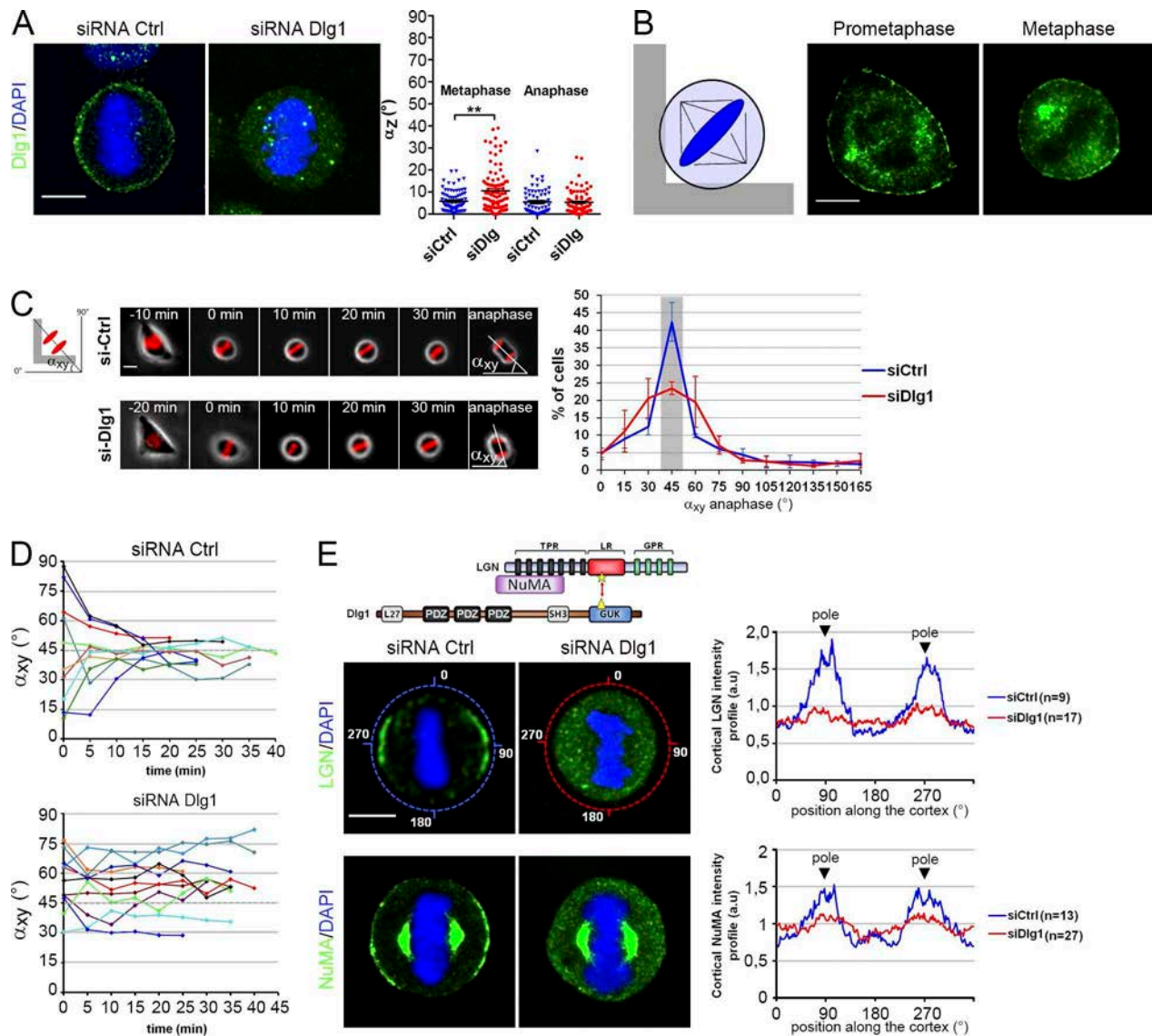


Figure 3. Dlg1 is required to orient the spindle in dissociated cells cultured on adhesive micropatterns. (A, left) Cortical localization of Dlg1 in HeLa cells cultured on nonpatterned coverslips. Dlg1 staining was lost upon siRNA treatment. (right) Distribution of the mitotic spindle angles relative to the coverslip in control and Dlg1 RNAi cells (α_z , means \pm SEM, $n > 70$ cells). **, $P \leq 0.01$. (B) Cortical localization of Dlg1 during prometaphase and metaphase in cells cultured on L shape fibronectin micropatterns, as schematized on the left. (C) Control and Dlg1 siRNA-treated H2B-Cherry-expressing HeLa cells were cultured on L shape patterns and recorded by time-lapse microscopy. (left) Representative examples of time-lapse sequences of control or siDlg1 cells. A scheme of L shape micropattern and orientation of the mitotic spindle at anaphase onset is provided. (right) Distribution of mitotic spindle angles relative to pattern orientation (α_{xy}) at anaphase onset (means \pm SD, $n > 750$ cells from three independent experiments). The gray box highlights the 15° bin centered around 45° . (D) Evolution of the mitotic spindle α_{xy} orientation during mitosis plotted for a dozen cells from C. (E, top left) Dlg1–LGN–NuMA interacting domains. Yellow star and triangle represent amino acids necessary for Dlg1–LGN interaction: P769 in Dlg1 and S401 in LGN, respectively. (bottom left) Confocal slices of nonpatterned control and Dlg1 siRNA-transfected metaphase cells stained for LGN and NuMA. (right) Graph showing mean LGN and NuMA cortical intensity profiles for control and Dlg1 siRNA-treated cells. Cortical coordinates along the plot correspond to the blue and red circles depicted in the LGN images. a.u., arbitrary unit; Ctrl, control; TPR, tetratricopeptide repeat; PDZ, PSD95/Dlg/ZO-1 domain. Bars: (A, B, and E) 10 μ m; (C) 5 μ m.

In vitro, phosphorylation of a serine residue corresponding to S401 of LGN increases by 500-fold the affinity of a peptide located in the LGN LR toward purified Dlg1 (Zhu et al., 2011). Interestingly, substitution of an alanine at this position reduced the cortical enrichment of the LR-GPR GFP fusion in vivo (S401A; Fig. 4 D). Together, these results show that Dlg1–LGN and G α_i –LGN interactions are both required for proper cortical localization of LGN during division.

To confirm the role of Dlg1–LGN interaction in LGN localization by another approach, we overexpressed the LGN

interacting domain of Dlg1 (GUK domain; Fig. 4 A) together with GFP-LGN in neuroepithelial cells. As anticipated, the GUK domain behaved as a dominant negative that displaced GFP-LGN from the cell cortex and caused spindle orientation defects (Fig. S3, B and C). In *Drosophila*, the interaction between Dlg and the Pins linker depends on a conserved proline residue in the GUK domain (Johnston et al., 2011). Accordingly, substitution of this proline for a serine residue in the chick Dlg1 GUK domain abolished its dominant-negative effect on LGN cortical localization and spindle orientation (Fig. S3, B and C).

To demonstrate that the mutual interaction between Dlg1 and LGN is necessary for spindle orientation, we performed RNAi rescue experiments *in vivo* using RNAi-resistant forms of LGN and Dlg1. Whereas wild-type mouse LGN displayed a clear cortical localization and efficiently rescued spindle orientation defects caused by chick LGN knockdown, mouse LGN-S401A was poorly recruited to the cortex (Fig. S3 D) and, accordingly, did not rescue spindle orientation (Fig. 4 E). Similarly, a full-length RNAi-resistant Dlg1 rescued both LGN-GFP cortical localization and spindle orientation defects caused by Dlg1 knockdown, whereas these defects were not rescued by the mutant version of full-length Dlg1 with a proline to serine substitution in the GUK domain (Figs. S3 E and 4 F). Hence, point mutations that suppress the direct interaction between Dlg1 and LGN are sufficient to recapitulate the loss-of-function phenotypes in the neuroepithelium. We conclude that this direct interaction is necessary for their function in spindle orientation *in vivo*.

Our results show a requirement for Dlg in spindle orientation in a variety of cellular contexts. This may reveal an ancestral and possibly universal role for the Dlg/LGN pair, which may even predate the involvement of Dlg in apico-basal polarity that has so far attracted most of the interest. In the light of the present study, it will be interesting to determine whether and how Dlg1 controls spindle orientation in cell types that undergo developmentally regulated switches between planar and vertical modes of division, such as skin progenitors and intestinal or mammary stem cells (Lechler and Fuchs, 2005; Quyn et al., 2010; Williams et al., 2011; Elias et al., 2014).

Materials and methods

Electroporation and plasmids

Electroporation in the chick neural tube was performed at embryonic day 2 (E2) as described previously (Morin et al., 2007). For gain- or loss-of-function experiments, plasmids were used at 1 $\mu\text{g}/\mu\text{l}$. For rescue experiments, 6-Myc-tagged LGN and Dlg1 expression constructs under the CAGGS promoter were added at 0.2 $\mu\text{g}/\mu\text{l}$. Mouse and chick LGNs are very closely related, and GFP-tagged versions of the two proteins display identical subcellular distribution (this study; Peyre et al., 2011); besides, mouse LGN was previously shown to be able to substitute for both chick LGN and *Drosophila* Pins (Yu et al., 2003; Morin et al., 2007). We therefore used mouse LGN to investigate cortical recruitment and to rescue chick LGN RNAi phenotypes. For Dlg1 RNAi rescue experiments, an RNAi-resistant 6-Myc-tagged chick Dlg1 construct was generated by targeted mutagenesis, introducing five silent base substitutions in the region targeted by the Dlg1 1135 miRNA construct. GFP-tagged LGN and Dlg1 expression constructs under the cytomegalovirus promoter were used at 1 $\mu\text{g}/\mu\text{l}$. Full-length cDNA of chick Dlg1-SAP97 and short cDNA of Dlg1, 2, and 3 and GAPDH used in RT-PCR experiments were amplified from chick neural tube cDNA samples prepared with the first-strand synthesis system (SuperScript III; Invitrogen). Several targets were chosen to down-regulate chick Dlg1 according to described recommendations (Das et al., 2006). The most effective construct was Dlg1 1135, which targets bases 1,135–1,155 in the Dlg1 cDNA: 5'-TTAGAAGAAGTTACTCATGAA-3'. Expression vectors used in this study are listed in Fig. S2. Pericentrin/AKAP-450 centrosomal targeting (PACT)-mKO1 was a gift from F. Matsuzaki (RIKEN Center for Developmental Biology, Kobe, Japan).

Immunohistochemistry

For antibody staining, chick embryos were fixed for 1 h in ice-cold 4% formaldehyde/PBS. For cryosections, embryos were washed three times in 0.12 M phosphate buffer (PB), pH 7.2, and equilibrated overnight at 4°C

in PB/15% sucrose. Embryos were then embedded in PB/15% sucrose/7.5% gelatin for cryoprotection before sectioning. Before immunostaining, cryosections were equilibrated at RT, degelatinized in PBS at 37°C for 5 min, and permeabilized 10 min in PBS/0.1% Triton X-100 (PBT 0.1%) before a 30-min blocking step in PBT 0.1%/10% FCS. For en face views, embryos were cut along their midline and permeabilized for 15 min in PBS/0.3% Triton X-100 (PBT 0.3%) before a 1-h blocking step in PBT 0.3%/10% FCS. For cell culture, HeLa cells were fixed for 20 min at RT in 4% formaldehyde/PBS, rinsed with PBS, and permeabilized in PBT 0.1% for 5 min.

Primary antibodies used in this study are mouse anti-GFP (Torrey Pines Biolabs), mouse anti- γ -tubulin (clone GTU-88), mouse anti-cMyc (clone 9E10), rabbit anti-cMyc, mouse anti-N-cadherin (clone GC-4) obtained from Sigma-Aldrich, mouse anti-ZO-1 (Invitrogen), mouse anti- β -catenin (BD), rabbit anti-aPKC- ζ (sc-206), rabbit anti-Dlg1 (sc-25661) from Santa Cruz Biotechnology, Inc., and rabbit anti-LGN (a gift from F. Matsuzaki). For the γ -tubulin antibody, embryos were incubated for 5 min in 100% acetone pre-equilibrated at -20°C and rinsed twice in PBS at RT before the blocking step. Secondary antibodies coupled to Alexa Fluor 488, Cy3, or Cy5 were obtained from Jackson ImmunoResearch Laboratories, Inc. and typically used at 1:400 dilutions. Vectashield with DAPI (Vector Laboratories) was used as a mounting medium.

Image acquisition

Optical sections of fixed samples (en face views from half-embryos or transverse sections from cryosections) were obtained on a confocal microscope (SP5; Leica) using 20 and 40 \times (Plan Neofluar NA 1.3 oil immersion) objectives and LAS software (Leica). Fiji software (Schindelin et al., 2012) was used for images processing (Gaussian blur) and data analysis (spindle orientation measurement). When necessary, images were subjected to brightness and contrast adjustment to equilibrate channel intensities and background using Photoshop CS4 software (Adobe).

3D measurement of spindle orientation in fixed samples

Spindle orientation was measured on en face mounted neural tubes from E3 embryos labeled with an anti- γ -tubulin antibody to reveal spindle poles and with DAPI dye to label chromosomes. Electroporated cells were identified by their expression of a Histone2B-GFP reporter protein (carried by the miRNA plasmid), also revealing the chromosomal plate of dividing cells. In addition, for rescue and dominant-negative experiments (Figs. 4, E and F; and S4 C), expression of Myc-tagged expression constructs was revealed by an anti-Myc antibody. En face image stacks (0.5- μm z interval) were acquired at 40 \times magnification. Z views and spindle orientation quantification were performed in Fiji software (Schindelin et al., 2012) using custom-designed macros. Scrolling through the z levels, the x and y position of both centrosomes of all metaphase and anaphase cells in a field were recorded using the Point tool in ImageJ/Fiji (National Institutes of Health) with Add to ROI Manager selected. A custom-written ImageJ/Fiji macro was used to treat all cells as a batch as follows (zip file 1): for each cell, xy coordinates were used to define a 100-pixel-long line joining both centrosomes and centered on the midpoint between them. A resliced stack of five parallel images centered on this line (0.25- μm interval) was generated and projected (Z Projection tool with Max Intensity setting) to generate a single image of 1- μm -thick volume along the spindle axis. Images of all these cells were then assembled in a montage (one example is given in Fig. S2 C). Note that in each of the images, the apical surface is delineated by the position of subapical centrosomes located at the basis of the cilium of neighboring interphase cells. For each cell in the montage, four points were then defined and recorded as follows: first, two points defining the apical surface (typically corresponding to two apical centrosomes in interphase cells) and two points defining the spindle axis (one point for each centrosome of the dividing cell). Using a custom-written macro, all cells in the montage were treated as a batch, and their spindle orientation was calculated as the angle between the line that joins the two first and the line that joins the two last points (in the 0–90° range).

Time-lapse microscopy and analysis of cultured chick neural tube

En face live imaging. En face culture of the embryonic neuroepithelium was performed at E3 (24 h after electroporation). After removal of extraembryonic membranes, embryos were transferred to 37°C F12 medium and slit along their midline from the hindbrain to the caudal end. The electroporated side of the neural tube was peeled off with dissection forceps and transferred in F12 medium to a glass-bottom culture dish. 200 μl of 1% agarose F12 medium (penicillin/streptomycin and 1 mM sodium pyruvate) preheated at 42°C was gently pipetted up and down several times

to soak the neural tubes. Excess medium was then removed so that the neural tubes would flatten with their apical surface adhering to the bottom of the dish, and an additional thin layer of agarose medium was then added on top. After agarose polymerization, the whole dish was covered with 3 ml liquid F12/penicillin/streptomycin/sodium pyruvate medium and transferred to 37°C for 1 h for recovery before imaging. Imaging was performed with a 40x water immersion objective (Apochromat LWD NA 1.15; Nikon) on an inverted microscope (Ti Eclipse; Nikon) equipped with a heating enclosure and a spinning-disk confocal head (CSU-X1; Yokogawa Electric Corporation). We recorded 30- μm -thick z stacks (1 μm between individual sections) at 1-min intervals for 4–6 h using MetaMorph software (Molecular Devices) and an electron-multiplying charge-coupled device camera (Evolve; Roper Scientific).

3D tracking of the centrosomes. Based on 4D imaging of mitotic cells expressing a centrosome reporter (PACT domain of pericentrin fused to mKO1; Konno et al., 2008), we implemented a homemade MATLAB routine (MathWorks, Inc.; zip file 2) to measure the three spatial coordinates x , y , and z of each centrosome during the time course of the division. The routine runs on regions of interest centered on single dividing cells that are manually selected and cropped (x , y , and temporal) beforehand from the full-length acquisition. In brief, our software uncouples tracking in the xy plane and tracking in the z direction, and both operations are performed successively. First, the user creates a maximum intensity projection in the xy plane for each z stack of the video and defines manually an intensity threshold to segment the signal arising from the centrosomes. This operation results in the segmentation of multiple clusters of bright pixels, two of them being the centrosomes from the cell of interest. Cluster positions are defined as the barycenter of the fluorescence signal in the pixels inside each cluster. Clusters smaller than 2 pixels typically correspond to noise or mislocalized reporter and are therefore filtered out and removed from the analysis. Tracking of each centrosome in the xy plane is performed successively by selecting in the first frame the cluster associated to the centriole of interest. Then, the software tracks its position in the following frame by choosing the closest cluster, repeats this operation frame by frame in the whole video, and finally returns the associated trajectory in the xy plane. To get a robust tracking method, we implemented a semimanual procedure to correct for tracking mistakes arising, for example, from the localization of a centrosome close to a bright fluorescent spot in the background of the cell, which can lead to an incorrect localization in the following frame. In this case, the user can come back to the frame where the error occurred and select the correct cluster associated to the centrosome being tracked. Once the tracking in the xy plane is performed for the pair of centrosomes, the x and y coordinates are used to slice the imaging volume in the vertical direction, in the plane linking both centrosomes. A video with the two centrosomes in the vertical direction is thus generated, and the same tracking procedure as presented before is used to get the z coordinate of each centrosome. At the end of the procedure, the spatial coordinates $x(t)$, $y(t)$, and $z(t)$ are returned for each centrosome and used to compute for each time point the distance between centrosomes, α_{xy} (the angle of the projection of the spindle axis in the xy plane), α_z (the angle of the spindle axis relative to the xy plane), and the distance covered by each centrosome in the xy plane and along the z axis since the previous time point.

The relative and absolute z rotations calculated in early (t_1 – t_5) and late (t_5 –end) metaphase presented in Fig. 2 (F and G) were calculated as follows for each cell, between two time points i and j :

$$\text{absolute } z \text{ rotation per minute, } \Delta_{z(t_{ij})} = \frac{\sum_{t=i}^{j-1} |\alpha_{z(t+1)} - \alpha_{z(t)}|}{\Delta t_{ij}};$$

$$\text{relative } z \text{ rotation per minute, } \delta_{z(t_{ij})} = \frac{\sum_{t=i}^{j-1} (\alpha_{z(t+1)} - \alpha_{z(t)})}{\Delta t_{ij}}.$$

Cell culture and transfection

HeLa cells expressing mCherry-H2B were cultured as previously described (Fink et al., 2011). For siRNA transfections, cells were treated following the manufacturer's instructions using HiPerFect (QIAGEN) for 72 h. Coverslips with L shape micropatterns were prepared and used as described in Fink et al. (2011). In brief, coverslips were first covered with poly-L-lysine-g-polyethylene glycol to passivate the surface. After UV illumination through a mask destroying the poly-L-lysine-g-polyethylene glycol in the unprotected

areas, fibronectin (Sigma-Aldrich) was added at 50 $\mu\text{g}/\text{ml}$ for 1 h. Fibrinogen coupled to Cy5 (Molecular Probes) was added to fibronectin for pattern visualization.

Time-lapse microscopy and measurement of spindle orientation of HeLa cells on micropatterns

HeLa cells expressing mCherry-H2B plated on L shape micropatterns were placed in a 37°C chamber (Chamlide; Live Cell Instrument) equilibrated with 5% CO_2 . Single cells were imaged every 5 min using an inverted microscope (Ti Eclipse) equipped with a 10x air objective. Mitotic plates were followed throughout mitosis using the mCherry channel. Spindle orientation was calculated in early anaphase based on the angle measured between separated chromosomes and the micropattern using the angle tool of ImageJ (Fig. 3 B).

Statistical analysis

Statistical analyses were performed using a Mann–Whitney test performed with Prism (GraphPad Software), except for HeLa cell α_{xy} measurements, in which a Kolmogorov–Smirnov test was performed.

Quantification of cortical signals in mitotic cells

The profiles of LGN or NuMA signal at the cell cortex of metaphase HeLa cells shown in Fig. 3 D were measured in Fiji software as follows: a 5-pixel-wide line (Freehand Line tool) was manually traced following the cell contour in a confocal optical section corresponding to the middle plane of the cell. The start (and finish) point of this circular line was chosen facing the chromosome plate on one side of the cell. Pixel values along the line were calculated using the Plot Profile tool (each value corresponds to the mean value of the 5 pixels on the line width). As the absolute length of the circular line varies from cell to cell as a function of cell diameter, we designed a macro that interpolates plot values to calculate a normalized set of 360 values along the line, where positions 0 and 180 face the equatorial plate and positions 90 and 270 face the spindle poles, as illustrated in Fig. 3 D. For control and Dlg1 siRNA-treated cells, mean profiles were then calculated from n individual profiles. For both LGN and NuMA data, mean profiles were normalized through division by the mean value of the mean control profile.

To quantify the amount of LGN fusion proteins localized at the cell cortex of dividing chick neuroepithelial cells, we generated en face images of cells of interest and selected the plane of the cell largest width, corresponding to the “equator.” We aimed at precisely disentangling the fluorescence signals arising from the cortex and the cytoplasm. We hypothesized that each image was a linear combination of a cortical component and a cytoplasmic component. We thus have $P = P_{\text{cortical}} + P_{\text{cytoplasm}}$, in which P is the image of the protein of interest. The cytoplasmic component was probed by the expression of an independent cytoplasmic reporter m (mRFP). Assuming that the cytoplasmic fraction of the protein of interest should adopt a similar spatial distribution as the cytoplasmic reporter, we adjusted, by a least squared optimization, the signal from the cytoplasmic reporter, measured in a small reference region (refR) of the cytoplasm distant from the cortex and the chromosomes (typically a square of 10-pixel sides), to the signal in the same region but measured for the protein of interest: $P_{\text{refR}} = \alpha \times M_{\text{refR}}$, in which M_{refR} is the image of the cytoplasmic reporter m in the reference region. The calculated proportionality coefficient α between the two signals was then used to recover the cortical component of protein p using the following operation: $P_{\text{cortical}} = P - \alpha M$, and allowing us to deduce $P_{\text{cytoplasm}}$ as well. Finally, the image P_{cortical} was used to analyze 15 intensity profiles spanning the cell length, starting from the cell center and equally distributed along 360°. At this stage, most of the profiles consisted of a bell-shaped signal around the membrane location. To quantify the extent of this cortical signal, we thus fitted a Gaussian profile centered on the maximum value of the profile. The fit was performed on the four adjacent pixel values around the membrane location on each profile. The integrated intensity of the fitted Gaussian was finally calculated and interpreted as the amount of protein p cortical recruitment at the membrane location on the profile. The cytoplasmic signal on a same profile was measured on $P_{\text{cytoplasm}}$ as the integrated intensity along the same line, from the cell center to the membrane location. In the end, the ratio of cortical signal over cytoplasmic signal for each of the 15 profiles was averaged to get a final relative level of protein p recruitment at the membrane in the cell of interest.

Online supplemental material

Fig. S1 presents a characterization of chick Dlg family members' expression in the chick neural tube and the experimental validation of Dlg1

miRNA efficiency. Fig. S2 summarizes all the gain-of-function, loss-of-function, and reporter constructs used in this study. Fig. S3 shows that the direct interaction between the GUK domain of Dlg1 and the linker domain of LGN is necessary for LGN cortical localization and for planar spindle orientation in the neuroepithelium, in complement to data presented in Fig. 4. Videos show the 3D spindle movements of dividing control (Video 1) or Dlg1 knockdown (Video 2) chick neuroepithelial cells expressing H2B-GFP and PACT-mKO1 reporters of chromosomes and centrosomes. Zip file 1 contains a PDF document that explains the procedure for the successive use of two Fiji macros to perform batch measurements of mitotic spindle orientation relative to the apical surface of the tissue and the two Fiji macro files. Zip file 2 contains a PDF file describing the two MATLAB procedures and two folders containing the MATLAB code. Online supplemental material is available at <http://www.jcb.org/cgi/content/full/jcb.201405060/DC1>.

We thank Fumio Matsuzaki for PACT-mKO1 and the LGN antibody and Sonia Garel and Samuel Tozer for discussions and critical comments on the manuscript. We acknowledge Benjamin Mathieu and the Institut de Biologie de l'École Normale Supérieure imaging platform for excellent assistance. Imaging equipment was acquired through the generous help of the Neuropole de Recherche Francilien (NeRF).

Work in X. Morin's laboratory is supported by an Institut National de la Santé et de la Recherche Médicale Avenir grant (R08221JS), the Fondation pour la Recherche Médicale (FRM; implantation nouvelle équipe), the Fondation Association pour la Recherche contre le Cancer (ARC; ARC Livespin 2012), and the Agence Nationale pour la Recherche (ANR; ANR Blanche 2012). M. Saadaoui was the recipient of postdoctoral fellowships from the Institut National de la Santé et de la Recherche Médicale (Avenir) and NeRF. Work in A. Echard's laboratory is supported by the Institut Pasteur, the Centre National de la Recherche Scientifique, the FRM (Equipe FRM DEQ20120323707), and the Fondation ARC (to M. Machicoane). This work has received support under the program Investissements d'Avenir launched by the French government and implemented by the ANR (references: ANR-10-LABX-54 MEMO LIFE and ANR-11-IDEX-0001-02 PSL* Research University).

The authors declare no competing financial interests.

Submitted: 26 May 2014

Accepted: 7 August 2014

References

- Assémat, E., E. Bazellières, E. Pallesi-Pocachard, A. Le Bivic, and D. Massey-Harroche. 2008. Polarity complex proteins. *Biochim. Biophys. Acta*. 1778:614–630. <http://dx.doi.org/10.1016/j.bbame.2007.08.029>
- Bellaïche, Y., A. Radovic, D.F. Woods, C.D. Hough, M.L. Parmentier, C.J. O'Kane, P.J. Bryant, and F. Schweisguth. 2001. The Partner of Inscuteable/Discs-large complex is required to establish planar polarity during asymmetric cell division in *Drosophila*. *Cell*. 106:355–366. [http://dx.doi.org/10.1016/S0092-8674\(01\)00444-5](http://dx.doi.org/10.1016/S0092-8674(01)00444-5)
- Bergstrahl, D.T., H.E. Lovegrove, and D. St Johnston. 2013. Discs large links spindle orientation to apical-basal polarity in *Drosophila* epithelia. *Curr. Biol.* 23:1707–1712. <http://dx.doi.org/10.1016/j.cub.2013.07.017>
- Das, R.M., N.J. Van Hateren, G.R. Howell, E.R. Farrell, F.K. Bangs, V.C. Porteous, E.M. Manning, M.J. McGrew, K. Ohyama, M.A. Sacco, et al. 2006. A robust system for RNA interference in the chicken using a modified microRNA operon. *Dev. Biol.* 294:554–563. <http://dx.doi.org/10.1016/j.ydbio.2006.02.020>
- Elias, S., M.S. Thion, H. Yu, C.M. Sousa, C. Lasgi, X. Morin, and S. Humbert. 2014. Huntingtin regulates mammary stem cell division and differentiation. *Stem Cell Rev.* 2:491–506. <http://dx.doi.org/10.1016/j.stemcr.2014.02.011>
- Fink, J., N. Carpi, T. Betz, A. Bétard, M. Chebah, A. Azioune, M. Bornens, C. Sykes, L. Fetler, D. Cuvelier, and M. Piel. 2011. External forces control mitotic spindle positioning. *Nat. Cell Biol.* 13:771–778.
- Fleming, E.S., M. Zajac, D.M. Moschenross, D.C. Montrose, D.W. Rosenberg, A.E. Cowan, and J.S. Tirnauer. 2007. Planar spindle orientation and asymmetric cytokinesis in the mouse small intestine. *J. Histochem. Cytochem.* 55:1173–1180. <http://dx.doi.org/10.1369/jhc.7A7234.2007>
- Guilgur, L.G., P. Prudêncio, T. Ferreira, A.R. Pimenta-Marques, and R.G. Martinho. 2012. *Drosophila* aPKC is required for mitotic spindle orientation during symmetric division of epithelial cells. *Development*. 139:503–513. <http://dx.doi.org/10.1242/dev.071027>
- Hao, Y., Q. Du, X. Chen, Z. Zheng, J.L. Balsbaugh, S. Maitra, J. Shabanowitz, D.F. Hunt, and I.G. Macara. 2010. Par3 controls epithelial spindle orientation by aPKC-mediated phosphorylation of apical Pins. *Curr. Biol.* 20:1809–1818. <http://dx.doi.org/10.1016/j.cub.2010.09.032>
- Iizuka-Kogo, A., T. Ishida, T. Akiyama, and T. Senda. 2007. Abnormal development of urogenital organs in Dlg1-deficient mice. *Development*. 134:1799–1807. <http://dx.doi.org/10.1242/dev.02830>
- Johnston, C.A., K. Hiron, K.E. Prehoda, and C.Q. Doe. 2009. Identification of an Aurora-A/Pins/LINKER/Dlg spindle orientation pathway using induced cell polarity in S2 cells. *Cell*. 138:1150–1163. <http://dx.doi.org/10.1016/j.cell.2009.07.041>
- Johnston, C.A., D.S. Whitney, B.F. Volkman, C.Q. Doe, and K.E. Prehoda. 2011. Conversion of the enzyme guanylate kinase into a mitotic-spindle orienting protein by a single mutation that inhibits GMP-induced closing. *Proc. Natl. Acad. Sci. USA*. 108:E973–E978. <http://dx.doi.org/10.1073/pnas.1104365108>
- Kiyomitsu, T., and I.M. Cheeseman. 2012. Chromosome- and spindle-pole-derived signals generate an intrinsic code for spindle position and orientation. *Nat. Cell Biol.* 14:311–317.
- Kiyomitsu, T., and I.M. Cheeseman. 2013. Cortical dynein and asymmetric membrane elongation coordinately position the spindle in anaphase. *Cell*. 154:391–402. <http://dx.doi.org/10.1016/j.cell.2013.06.010>
- Konno, D., G. Shioi, A. Shitamukai, A. Mori, H. Kiyonari, T. Miyata, and F. Matsuzaki. 2008. Neuroepithelial progenitors undergo LGN-dependent planar divisions to maintain self-renewability during mammalian neurogenesis. *Nat. Cell Biol.* 10:93–101.
- Laprise, P., A. Viel, and N. Rivard. 2004. Human homolog of disc-large is required for adherens junction assembly and differentiation of human intestinal epithelial cells. *J. Biol. Chem.* 279:10157–10166. <http://dx.doi.org/10.1074/jbc.M309843200>
- Lechler, T., and E. Fuchs. 2005. Asymmetric cell divisions promote stratification and differentiation of mammalian skin. *Nature*. 437:275–280. <http://dx.doi.org/10.1038/nature03922>
- Machicoane, M., C.A. de Frutos, J. Fink, M. Rocancourt, Y. Lombardi, S. Garel, M. Piel, and A. Echard. 2014. SLK-dependent activation of ERMs controls LGN–NuMA localization and spindle orientation. *J. Cell Biol.* 205:791–799. <http://dx.doi.org/10.1083/jcb.201401049>
- Mahoney, Z.X., B. Sammut, R.J. Xavier, J. Cunningham, G. Go, K.L. Brim, T.S. Stappenbeck, J.H. Miner, and W. Swat. 2006. Discs-large homolog 1 regulates smooth muscle orientation in the mouse ureter. *Proc. Natl. Acad. Sci. USA*. 103:19872–19877. <http://dx.doi.org/10.1073/pnas.0609326103>
- Morin, X., and Y. Bellaïche. 2011. Mitotic spindle orientation in asymmetric and symmetric cell divisions during animal development. *Dev. Cell*. 21:102–119. <http://dx.doi.org/10.1016/j.devcel.2011.06.012>
- Morin, X., F. Jaouen, and P. Durbec. 2007. Control of planar divisions by the G-protein regulator LGN maintains progenitors in the chick neuroepithelium. *Nat. Neurosci.* 10:1440–1448. <http://dx.doi.org/10.1038/nn1984>
- Naim, E., A. Bernstein, J.F. Bertram, and G. Caruana. 2005. Mutagenesis of the epithelial polarity gene, discs large 1, perturbs nephrogenesis in the developing mouse kidney. *Kidney Int.* 68:955–965. <http://dx.doi.org/10.1111/j.1523-1755.2005.00489.x>
- Nakajima, Y., E.J. Meyer, A. Kroesen, S.A. McKinney, and M.C. Gibson. 2013. Epithelial junctions maintain tissue architecture by directing planar spindle orientation. *Nature*. 500:359–362. <http://dx.doi.org/10.1038/nature12335>
- Noatynska, A., M. Gotta, and P. Meraldi. 2012. Mitotic spindle (DIS) orientation and DISease: cause or consequence? *J. Cell Biol.* 199:1025–1035. <http://dx.doi.org/10.1083/jcb.201209015>
- Pease, J.C., and J.S. Tirnauer. 2011. Mitotic spindle misorientation in cancer—out of alignment and into the fire. *J. Cell Sci.* 124:1007–1016. <http://dx.doi.org/10.1242/jcs.081406>
- Peyre, E., F. Jaouen, M. Saadaoui, L. Haren, A. Merdes, P. Durbec, and X. Morin. 2011. A lateral belt of cortical LGN and NuMA guides mitotic spindle movements and planar division in neuroepithelial cells. *J. Cell Biol.* 193:141–154. <http://dx.doi.org/10.1083/jcb.201101039>
- Postiglione, M.P., C. Jüschke, Y. Xie, G.A. Haas, C. Charalambous, and J.A. Knoblich. 2011. Mouse inscuteable induces apical-basal spindle orientation to facilitate intermediate progenitor generation in the developing neocortex. *Neuron*. 72:269–284. <http://dx.doi.org/10.1016/j.neuron.2011.09.022>
- Quyn, A.J., P.L. Appleton, F.A. Carey, R.J. Steele, N. Barker, H. Clevers, R.A. Ridgway, O.J. Sansom, and I.S. Näthke. 2010. Spindle orientation bias in gut epithelial stem cell compartments is lost in precancerous tissue. *Cell Stem Cell*. 6:175–181. <http://dx.doi.org/10.1016/j.stem.2009.12.007>
- Rivera, C., I.F. Yamben, S. Shatadal, M. Waldof, M.L. Robinson, and A.E. Griep. 2009. Cell-autonomous requirements for Dlg-1 for lens epithelial cell structure and fiber cell morphogenesis. *Dev. Dyn.* 238:2292–2308. <http://dx.doi.org/10.1002/dvdy.22036>

- Sans, N., P.Y. Wang, Q. Du, R.S. Petralia, Y.X. Wang, S. Nakka, J.B. Blumer, I.G. Macara, and R.J. Wenthold. 2005. mPins modulates PSD-95 and SAP102 trafficking and influences NMDA receptor surface expression. *Nat. Cell Biol.* 7:1179–1190.
- Schindelin, J., I. Arganda-Carreras, E. Frise, V. Kaynig, M. Longair, T. Pietzsch, S. Preibisch, C. Rueden, S. Saalfeld, B. Schmid, et al. 2012. Fiji: an open-source platform for biological-image analysis. *Nat. Methods.* 9:676–682. <http://dx.doi.org/10.1038/nmeth.2019>
- Siegrist, S.E., and C.Q. Doe. 2005. Microtubule-induced Pins/Goi cortical polarity in *Drosophila* neuroblasts. *Cell.* 123:1323–1335. <http://dx.doi.org/10.1016/j.cell.2005.09.043>
- Théry, M., V. Racine, A. Pépin, M. Piel, Y. Chen, J.B. Sibarita, and M. Bornens. 2005. The extracellular matrix guides the orientation of the cell division axis. *Nat. Cell Biol.* 7:947–953.
- Théry, M., A. Jiménez-Dalmaroni, V. Racine, M. Bornens, and F. Jülicher. 2007. Experimental and theoretical study of mitotic spindle orientation. *Nature.* 447:493–496. <http://dx.doi.org/10.1038/nature05786>
- Willard, F.S., R.J. Kimple, and D.P. Siderovski. 2004. Return of the GDI: the GoLoco motif in cell division. *Annu. Rev. Biochem.* 73:925–951. <http://dx.doi.org/10.1146/annurev.biochem.73.011303.073756>
- Williams, S.E., S. Beronja, H.A. Pasolli, and E. Fuchs. 2011. Asymmetric cell divisions promote Notch-dependent epidermal differentiation. *Nature.* 470:353–358. <http://dx.doi.org/10.1038/nature09793>
- Woods, D.F., and P.J. Bryant. 1991. The discs-large tumor suppressor gene of *Drosophila* encodes a guanylate kinase homolog localized at septate junctions. *Cell.* 66:451–464. [http://dx.doi.org/10.1016/0092-8674\(81\)90009-X](http://dx.doi.org/10.1016/0092-8674(81)90009-X)
- Yu, F., X. Morin, Y. Cai, X. Yang, and W. Chia. 2000. Analysis of partner of inscuteable, a novel player of *Drosophila* asymmetric divisions, reveals two distinct steps in inscuteable apical localization. *Cell.* 100:399–409. [http://dx.doi.org/10.1016/S0092-8674\(00\)80676-5](http://dx.doi.org/10.1016/S0092-8674(00)80676-5)
- Yu, F., X. Morin, R. Kaushik, S. Bahri, X. Yang, and W. Chia. 2003. A mouse homologue of *Drosophila* pins can asymmetrically localize and substitute for pins function in *Drosophila* neuroblasts. *J. Cell Sci.* 116:887–896. <http://dx.doi.org/10.1242/jcs.00297>
- Zheng, Z., H. Zhu, Q. Wan, J. Liu, Z. Xiao, D.P. Siderovski, and Q. Du. 2010. LGN regulates mitotic spindle orientation during epithelial morphogenesis. *J. Cell Biol.* 189:275–288. <http://dx.doi.org/10.1083/jcb.200910021>
- Zhu, J., Y. Shang, C. Xia, W. Wang, W. Wen, and M. Zhang. 2011. Guanylate kinase domains of the MAGUK family scaffold proteins as specific phospho-protein-binding modules. *EMBO J.* 30:4986–4997. <http://dx.doi.org/10.1038/emboj.2011.428>
- Žigman, M., M. Cayouette, C. Charalambous, A. Schleiffer, O. Hoeller, D. Dunican, C.R. McCudden, N. Firnberg, B.A. Barres, D.P. Siderovski, and J.A. Knoblich. 2005. Mammalian inscuteable regulates spindle orientation and cell fate in the developing retina. *Neuron.* 48:539–545. <http://dx.doi.org/10.1016/j.neuron.2005.09.030>

2) Predictive Spatiotemporal Manipulation of Signaling Perturbations using optogenetics. Valon L, Etoc F, Remorino A, di Pietro F, Faqir F, Morin X, Dahan M, Coppey M. *Biophys J.* 2015. 109(9):1785-97.

At the beginning of my thesis, we established a collaboration with the team of Maxime Dahan (initially at IBENS, then at the Biophysics Unit at the Curie Institute) to work on the optimization and characterization of optogenetic tools to induce the activation of proteins with a fine spatio-temporal control in the cell. We focused on the Cry2-CIBN optogenetic pair derived from the plant *Arabidopsis thaliana* (Kennedy et al., 2010). In this system, the interaction between Cry2 and CIBN is inducible by blue light illumination. Thus, in a cell in which CIBN is anchored to the membrane and Cry2 is cytoplasmic, blue light activation of the Cry2-CIBN interaction results in Cry2 recruitment to the cell cortex.

The general aim was to apply these tools to control signaling pathways in a localized manner and use this to approach to study the dynamics of different cellular processes both in interphase and mitotic cells. In particular, our group's interest in this system was to recruit members of the LGN complex to the cell cortex in a regulated manner, both in space and in time, in order to probe the biophysical parameters of spindle orientation/reorientation in a highly controlled fashion. Unfortunately we found that the Cry2-CIBN system performed very poorly in mitotic cells compared to interphase, which we tentatively attribute to an unidentified inhibitory nuclear protein released in mitosis. On the other side, a second and more general objective was to characterize the stimulation parameters required to obtain a defined level of Cry2 recruitment with a high level of spatiotemporal resolution. Because the group of M. Dahan is a biophysics team, we collaborated to bring our expertise in molecular and cellular biology mainly at the beginning of this project. I worked mainly in collaboration with Léo Valon, a former PhD student. In particular, we introduced fluorescently-tagged Cry2 and CIBN constructs in HeLa cells and we demonstrated robust and reproducible global recruitment of Cry2 to the cellular cortex, as previously shown by Kennedy and colleagues (Kennedy et al., 2010). In addition, we performed local activation of CIBN using a FRAP illumination system and

observed localized Cry2 recruitment by TIRF microscopy. Moreover, we applied this local activation approach to cells cultured on circular micropatterns, which allowed us to obtain reproducible gradients of Cry2 recruitment at the basal membrane, which were reversible in accordance to the half-life of Cry2-CIBN interaction. Léo Valon went on with this project by characterizing the optogenetic system in detail. In particular, he studied how Cry2 recruitment is modified in response to changes in the illuminations parameters such as the intensity, frequency of pulse and exposure time. He also proposed theoretical models for Cry2 recruitment considering the illumination parameters, the dissociation kinetics and the diffusion components, and showed that these models are useful to predict the levels and spatial distribution of Cry2 recruitment in response to a defined light stimulus. These results represent an important contribution as optogenetic tools are increasingly being used to study diverse cellular processes in several systems. Finally, he applied this optogenetic approach to locally activate the Rho GTPase Cdc42 observing the formation of actin based protrusions specifically in the area of activation, and in consequence, cell migration.

Article

Predictive Spatiotemporal Manipulation of Signaling Perturbations Using Optogenetics

Leo Valon,¹ Fred Etoc,² Amanda Remorino,¹ Florencia di Pietro,³ Xavier Morin,³ Maxime Dahan,¹ and Mathieu Coppey^{1,*}

¹Laboratoire Physico-Chimie, Institut Curie, Centre National de la Recherche Scientifique UMR168, Paris-Science Lettres, Université Pierre et Marie Curie-Paris 6, Paris, France; ²Center for Studies in Physics and Biology, The Rockefeller University, New York, New York; and ³Institut de Biologie de l'École Normale Supérieure, École Normale Supérieure, Paris, France

ABSTRACT Recently developed optogenetic methods promise to revolutionize cell biology by allowing signaling perturbations to be controlled in space and time with light. However, a quantitative analysis of the relationship between a custom-defined illumination pattern and the resulting signaling perturbation is lacking. Here, we characterize the biophysical processes governing the localized recruitment of the Cryptochrome CRY2 to its membrane-anchored CIBN partner. We develop a quantitative framework and present simple procedures that enable predictive manipulation of protein distributions on the plasma membrane with a spatial resolution of 5 μm . We show that protein gradients of desired levels can be established in a few tens of seconds and then steadily maintained. These protein gradients can be entirely relocalized in a few minutes. We apply our approach to the control of the Cdc42 Rho GTPase activity. By inducing strong localized signaling perturbation, we are able to monitor the initiation of cell polarity and migration with a remarkable reproducibility despite cell-to-cell variability.

INTRODUCTION

Over the last couple of years, the development of optogenetics actuators for cell biology has dramatically increased. The toolbox of light-gated molecular systems is continuously expanding, with photosensitive proteins covering almost all the spectrum from UV to far red (reviewed in Pathak et al. (1)). It is now possible to control many intracellular processes (reviewed in Tischer and Weiner (2)), such as receptor transduction (3), protein degradation (4), protein localization (5), or protein sequestration (6) with an optogenetic approach. This success can be attributed to the fact that optogenetic tools are genetically encoded, triggered by light such that they can be easily modulated in time and space, have fast kinetics and excellent reactivity, and that most of them are reversible.

One of the most striking benefits of optogenetics is the ability to perform transient and spatially confined signaling perturbations (7). Indeed, most of the usual genetic and pharmacologic approaches induce only permanent and global perturbations on protein signaling. But, in their natural context, almost all signaling proteins in the cell display rich spatiotemporal patterns of activity as observed with fluorescent reporters and biosensors (8,9). One important question is to know whether the spatiotemporal features of optogenetically controlled activity patterns can match those of endogenous signaling activities. In fact, a proper characterization of the spatial and temporal resolutions that can be

achieved with contemporary optogenetic tools is still lacking. Here we address this problem by developing a quantitative biophysical approach enabling a predictive manipulation of protein distribution at the subcellular scale.

Among the optogenetic molecular systems proposed recently to control cell polarity and migration (10–13) or intracellular signaling through protein localization (14–16), the CRY2/CIBN dimerizer system (17) appears especially promising (18) and versatile (6). Importantly, it presents a low dark activity but a strong and robust binding upon light activation without the need for a cofactor (19). In a 2012 study on lipid signaling, Idevall-Hagren et al. (15) demonstrated that local CRY2 protein recruitment to the plasma membrane was achievable. Yet, a comprehensive framework for the quantitative control in space and time of protein recruitment to the membrane is still lacking.

Here we present a predictive subcellular control of protein distribution on the plasma membrane. By studying the biophysical parameters governing the molecular processes of the CRY2/CIBN optogenetic system for plasma membrane targeting, we report a simple, easy to set up, reproducible, and versatile method to control signaling activities at a subcellular scale and with a temporal control of a few tens of seconds. Importantly we provide a set of rules allowing an inexperienced user to apply spatially restricted signaling perturbations within the cell. Eventually, we demonstrate the efficiency of the CRY2/CIBN system to activate endogenous signaling pathways by inducing cell migration through local and sustained subcellular activations of cdc42.

Submitted February 23, 2015, and accepted for publication August 3, 2015.

*Correspondence: mathieu.coppey@curie.fr

Editor: Klaus Hahn.

© 2015 by the Biophysical Society
0006-3495/15/11/1785/13



MATERIALS AND METHODS

Cloning

The Intersectin DH PH domain linker (ITSN(DHPH)-Linker) gene was amplified from ITSN(DHPH)-Linker-YFP-PIF (gift from O. Weiner, University of California, San Francisco) and cloned into CRY2PHR-mCherry (gift from C. Tucker (University of Colorado, Denver), hereafter called “CRY2”) using *Nhe1* and *Xho1* enzyme sites that resulted in ITSN(DHPH)-Linker-CRY2PHR-mCherry. All plasmids contain the generic CMV promoter (backbone pmCherryN1 from Clontech Laboratories, Mountain View, CA).

Cell culture and transfection

NIH 3T3 fibroblasts and HeLa cells were cultured at 37°C in 5% CO₂ in DMEM (Dulbecco’s modified Eagle’s medium) supplemented with 10% fetal calf serum. Transfections were performed using X-tremeGENE 9 (Roche Applied Science, Penzburg, Bavaria, Germany) according to the manufacturer’s instructions using an equal amount of cDNA for the two dimerizer CIBN and CRY2 (1 μg/mL).

Live cell imaging

Twenty-five-mm glass coverslips were prepared both with and without round patterns of fibronectin bovine protein (Life Technologies, Carlsbad, CA) as described in Azioune et al. (20). For imaging, cells were dissociated using Accutase (Life Technologies) and incubated on those coverslips for at least 45 min. Experiments were performed at 37°C in 5% CO₂ in a heating chamber (Pecon, Meyer Instruments, Houston, TX) placed on an inverted microscope model No. IX71 equipped with a 60× objective with NA 1.45 (Olympus, Melville, NY). The microscope was controlled with the software Metamorph (Molecular Devices, Eugene, OR). Differential interference contrast (DIC) imaging was performed with a far red filter in the illumination path to avoid CRY2 activation. Total internal reflection fluorescence (TIRF) images were acquired using an azimuthal TIRF module (ilas²; Roper Scientific, Tucson, AZ) and laser power and exposure time were chosen to prevent photobleaching.

Fluorescence quantification and cell segmentation

We analyzed movies with custom-built routines in MATLAB (The MathWorks, Natick, MA). We removed background from raw images, and extracted kymographs and mean fluorescence in a region of interest (ROI) over time. The segmentation of cell borders (for example) was performed on fluorescence images using a threshold based on the average level of the noise (MATLAB function “Graythresh”). The membrane ruffling activity (see Fig. 6 d) was determined using DIC images on which we applied a detection of pixel intensity changes (using MATLAB function edges).

Normalization

All recruitment curves obtained from TIRF images were normalized to the fold increase of fluorescence (relative changes): after background subtraction, the value of fluorescence for each time point was divided by the initial fluorescence (averaged over the first frames without activation). The curves in Fig. 6 d were normalized between 0 and 1 to compare the kinetics. The curves in Figs. 2, e and f, and 3, a–c, were normalized between 0 and 1, where 1 stands for the maximal recruitment. The exponential gradients of Fig. 4 e were normalized using the same procedure as in Gregor et al. (21) to align the distributions of CRY2 coming from different cells without introducing a spatial bias in the averaging procedure.

Fluorescence recovery after photobleaching experiments and photoactivation

For fluorescence recovery after photobleaching (FRAP) experiments on CIBN-GFP-CAAX, we used a 50-mW 405-nm laser at full power controlled by a FRAP head (Roper Scientific) to photobleach a round area with a diameter of 3 μm during 1 s. To photoactivate CRY2, we used the same FRAP head, but we used a 488-nm laser at low laser power (5–10%). The FRAP data were analyzed considering a purely diffusive process in two dimensions, which leads to the recovery (22)

$$C_{\text{tot}}(t) = \int C dx dy = \exp\left(-\frac{2\tau_D}{t}\right) \left[I_0\left(\frac{2\tau_D}{t}\right) + I_1\left(\frac{2\tau_D}{t}\right) \right],$$

where C is the amount of plasma membrane CIBN at positions x, y and time t , $\tau_D = a^2/4D$ is the diffusion time (a being the radius of the bleached area), and I_0 and I_1 are the modified Bessel functions of the first kind. Experimentally, $C_{\text{tot}}(t)$ was obtained by integrating the fluorescence intensity over the whole ROI used for photobleaching. We determined the value of the diffusion coefficient D by fitting the experimental recovery curve to the theoretical expectation (Fig. S1, a–c, in the Supporting Material).

To measure the dissociation kinetics of the CRY2/CIBN dimer, we assumed a first-order dissociation process such that

$$M_{\text{tot}}(t) \propto \exp(-k_{\text{off}}t),$$

where $M_{\text{tot}}(t)$ is the total amount of plasma membrane CRY2, and k_{off} is the dissociation rate. By fitting the experimental data with an exponentially decaying function (Fig. S1, d–f) we obtained the dissociation time as $\tau_{\text{off}} = 1/k_{\text{off}}$.

RESULTS

Local recruitment of CRY2-mCherry at the basal plasma membrane

The plasma membrane CRY2/CIBN optogenetic system is composed of two proteins that are expressed by the cell: CIBN-GFP-CAAX (CIBN) localized at the cell membrane with a CAAX anchor and CRY2PHR-mCherry (CRY2), which is initially cytoplasmic (17). Under blue illumination (<525 nm), CRY2 changes conformation and gains the ability to bind to CIBN. In cells expressing these two proteins, the formation of the dimer leads to a relocalization of CRY2 from the cytoplasm to the cell membrane. In our experiments, we used a 488-nm focalized scanning laser beam at low power (4–20 μW) to shine light in a selected ROI. We quantified the amount of CRY2 at the basal plasma membrane (pmCRY2) by imaging the cell in TIRF mode, thereby imaging CRY2 proteins only when they become recruited.

By periodically shining blue light in a restricted area of a cell (6 pulses of 100 ms spaced out by 80 s in the indicated *red box* followed by six pulses in the indicated *green box*, Fig. 1, a and b, and Movie S1 in the Supporting Material), we recruited CRY2 locally at the plasma membrane, in the region of activation. After a pulse, the cytoplasmic volume partly depleted of CRY2 is refilled in a few seconds

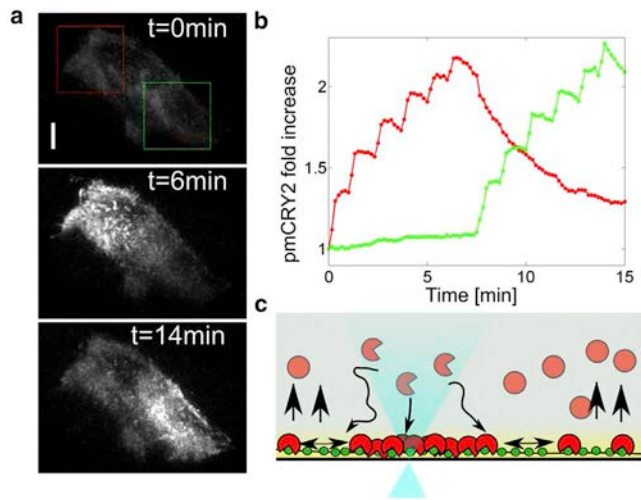


FIGURE 1 Physical processes responsible for local recruitment of pmCRY2. (a) CRY2-mCherry TIRF images before illumination (*top*) and after six local activations in the indicated red box (*middle*) and after six activations in the indicated green box (*bottom*). (b) Quantification of the relative increase of signal in the red and green region over time. (c) Scheme of the biophysical processes involved in CRY2-mCherry localization at the plasma membrane. Inactive cytoplasmic CRY2 (*solid red circles*) changes conformation upon illumination into an active state (*open red circle*) that diffuses to the membrane and binds CIBN (*solid green circles*). (*Yellow region*) Evanescent TIRF field. (*Black arrows*) Diffusion-limited membrane recruitment, lateral diffusion, and dimer dissociation altogether representing the cycle of CRY2 in a steady and localized stimulation (*blue cone of light*). To see this figure in color, go online.

with fresh nonactivated CRY2. This replenishment allows the recruitment of more CRY2 as observed by the increasing amount of pmCRY2 each time a pulse of light is applied (*Fig. 1 b*). The evolution of pmCRY2 between each light pulse and after the total illumination sequence is controlled by the lateral diffusion and natural dissociation of the light

activated CRY2/CIBN dimer. On the one hand, the lateral diffusion of the dimer at the plasma membrane tends to homogenize the pmCRY2 concentration over the whole cell membrane. This is revealed by the slight but continuous increase of fluorescence in the green region while recruitment is done in the red region (*Fig. 1 b*, from 0 to 7 min). In addition, the complex dissociation decreases the amount of pmCRY2, as observed in the red region when no light is shone (*Fig. 1 b*, from 7 to 15 min). Therefore, the binding, diffusion, and dissociation processes (summarized in *Fig. 1 c*) are the key parameters controlling the level and the spatial distribution of pmCRY2. In the following sections, we quantify the biophysical characteristics of these processes to set up a predictive framework of pmCRY2 dynamics.

CRY2 membrane distribution following a single pulse of light

To map the relationship between the illumination properties and pmCRY2 initial distribution, we first characterized the elementary response to a single localized pulse of light. Right after a pulse, the maximal pmCRY2 recruitment is observed after a characteristic time of $\tau_{\text{on}} = 2.2 \text{ s} \pm 0.4 \text{ s}$ ($N = 10$) (*Fig. S1, g–i*). This time is very fast in comparison to all other characteristic times of this system and is similar to the characteristic time for the replenishment of the activated volume by a cytoplasmic protein diffusing with a diffusion coefficient of $\sim 10 \mu\text{m}^2/\text{s}$. For a $3\text{-}\mu\text{m}$ diameter pulse of blue light of 100-ms duration, the pmCRY2 initial distribution is well fitted by a Gaussian function (*Fig. 2 a*) with a standard deviation of $6 \pm 1 \mu\text{m}$. The use of a focused laser together with the large numerical aperture of the objective leads to the activation of CRY2 in a relatively wide

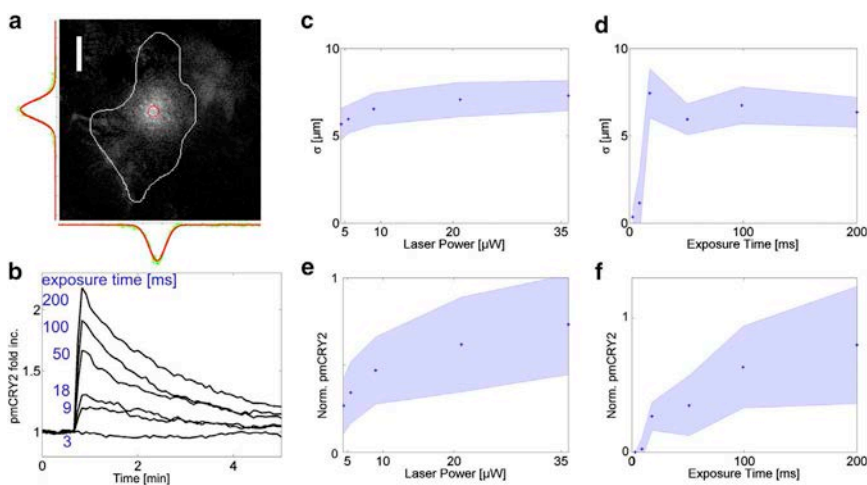


FIGURE 2 CRY2 recruitment as a function of illumination characteristics. (a) Differential TIRF image of pmCRY2 3s after the illumination with a local pulse of blue light. (*White line*) Contour of the cell. (*Side curves*) pmCRY2 intensity (*green*) and Gaussian fit (*red*) along a line across the activation area (*red circle*). Scale bar = $10 \mu\text{m}$. (b) Quantification of the mean intensity in the activation area (*red circle, a*) divided by its mean value before activation as a function of time for activating pulses of different duration in a single cell. The exposure times were chosen equal to 3, 9, 18, 50, 100, and 200 ms. Images are taken every 5 s. The temporal decay ($\sim 80 \text{ s}$) is governed by lateral diffusion because the diffusion time is smaller than the complex dissociation (185 s) for such point activations. (c–f) Mean values (*blue dots*) and standard deviation (*blue-shaded regions*) of pmCRY2 initial Gaussian

distribution after a single pulse of activation. The average width σ (c and d), and total integrated amount (e and f) calculated from the integral of the Gaussian $2\pi\sigma_x\sigma_y A$ are plotted as a function of laser power (c and e) and exposure time (d and f). In (d) and (f) the laser power is fixed at $5.5 \mu\text{W}$ and the pulse durations are 3, 9, 18, 50, 100, and 200 ms ($N = 15$ cells). In (c) and (e) the exposure is fixed at 50 ms and the laser power is set to 4.5, 5.5, 9, 21, and $36 \mu\text{W}$ ($N = 25$ cells). To see this figure in color, go online.

conical volume. Assuming an angle of divergence of $\sim 45^\circ$, the maximal lateral extension of the cone of light will be of the order of the height L of the cell, estimated to be $L \sim 3\text{--}5 \mu\text{m}$. Once activated, CRY2 proteins diffuse through the cytoplasm before reaching the plasma membrane and binding to CIBN. The distribution of the distance traveled laterally, before the binding event, is known (23), and it follows an exponential function of characteristic length $\sim L/\sqrt{3}$. The overall Gaussian shape of pmCRY2 then results from the convolution of the cone of activation with the spatial profile set by the three-dimensional diffusion of light-activated CRY2 and capture at the plasma membrane.

We defined the total amount of pmCRY2 being recruited in a single pulse as the integral of the initial Gaussian distribution, namely $M_{sp} = 2\pi\sigma_x\sigma_yA$, where σ_x , σ_y are the widths along the two major axes and A is the amplitude of the Gaussian distribution. By increasing the exposure time (T_{exp}) of the blue pulse from 3 to 200 ms (the laser power P being fixed to $5.5 \mu\text{W}$; see [Movie S2](#)), we could increase A in a progressive manner ([Fig. 2 b](#)). We also varied independently P from 4.5 to $36 \mu\text{W}$ with $T_{exp} = 50$ ms and systematically assessed the dependence of M_{sp} on these two parameters. M_{sp} increases as a function of P and T_{exp} up to a plateau, which is reached when all CRY2 proteins in the illuminated volume are activated ([Fig. 2, e and f](#)). By further increasing T_{exp} on a timescale comparable to τ_{on} , the quantity M_{sp} would start to increase slowly over the plateau because a diffusive flux of inactivated CRY2 would appear in the illuminated volume. This diffusive regime is not easily quantifiable and we restricted our analysis to short pulses.

Importantly, we did not observe any dependency of σ as increasing amounts of pmCRY2 were recruited ([Fig. 2, c and d](#)). This means that the membrane anchor CIBN is not limiting and that large local concentrations of pmCRY2 can be achieved. This is coherent with our observation that, in our configuration of transient transfections, the small CIBN-GFP protein (~ 50 kDa) was always expressed by the cell in a larger amount than the CRY2-mCherry protein (~ 100 kDa).

Altogether, the amount of pmCRY2 recruited in a single pulse, M_{sp} , behaves as expected for a first-order Michaelis-Menten law,

$$M_{sp} \propto C \frac{PT_{exp}}{[PT_{exp}]_{1/2} + PT_{exp}}, \quad (1)$$

where $[PT_{exp}]_{1/2}$ is the value of the product PT_{exp} needed to achieve half of the maximal recruitment (for instance $[PT_{exp}]_{1/2}$ is reached for $P = 9 \mu\text{W}$ and $T_{exp} = 50$ ms), and C is the cytoplasmic concentration of CRY2 (we checked that M_{sp} was proportional to C for given values of P and T_{exp} ; data not shown).

CRY2/CIBN lateral diffusion and dissociation

The initial pmCRY2 distribution obtained after a pulse of light is subsequently smoothed out by the lateral diffusion of CIBN-GFP. Using FRAP experiments, we characterized the diffusion of either the CIBN-GFP protein alone or in complex with CRY2-mCherry ([Fig. S1, a–c](#)). We measured a similar diffusion coefficient of $0.1 \mu\text{m}^2/\text{s} \pm 0.03 \mu\text{m}^2/\text{s}$ in both cases ([Fig. S1 c](#)), which is in good agreement with the diffusion coefficient expected for a phospholipid or a protein anchored in the membrane (24). This value sets the characteristic time for diffusion, which is 100 min to diffuse over the whole length ($\sim 50 \mu\text{m}$) of the basal plasma membrane and 20 s for a small activation region of $\sim 3 \mu\text{m}$ size.

The total amount of pmCRY2 decreases over time due to the dissociation of the CRY2/CIBN dimer. We experimentally characterized this process by quantifying the pmCRY2 decay over time after inducing a recruitment on the whole cell ([Fig. S1, d and e](#)). We observed a single exponential decay of pmCRY2 signal, indicative of a one-step dissociation process. The characteristic dissociation time $\tau = 1/k_{off}$ is 185 ± 40 s, which means that 63% of the pmCRY2 disappears in 3 min and 95% in 9 min, in agreement with prior reports (17).

Quantitative control of pmCRY2 level with frequency modulation

Because the CRY2/CIBN complex dissociates, we can expect that steady levels of pmCRY2 can be maintained over time through continuous illumination with blue light. The actual steady-state value would be determined by the intensity of activating light as it was done previously for the PhyB/PIF6 system (14). In this study, a determined level of recruitment was targeted by finely tuning the intensity of light using a computer-assisted feedback loop (25). Here, we explored a different, and possibly simpler, strategy to perform a direct control of pmCRY2 steady-state levels. Rather than continuously illuminating the cell with blue light, we recruited CRY2 in successive batches using periodic pulses. Indeed, the amount of pmCRY2 recruited with a single pulse can be characterized, allowing us to then predictively target a selected steady-state value by only modulating the frequency of light pulses. From a practical standpoint, this periodic approach fits naturally with standard routines commonly used to acquire time-lapse movies with multiple wavelengths. In the following section, we develop the modeling framework describing pmCRY2 dynamics under periodic stimulations.

We call M_n and M_n^* the number of CRY2 proteins bound to plasma membrane before and after the n th activation pulse. C_n represents the number of CRY2 proteins in the cytoplasm. We assume the following hypotheses: 1) the total number of CRY2 proteins, $C_0 = M_n + C_n$, is conserved over time; 2) the quantity of protein recruited after a pulse

is proportional to the number of cytoplasmic CRY2 through a factor f (smaller than 1): $M_n^* = M_n + f \times C_n$; and 3) pmCRY2 is released with a rate $k_{\text{off}} = 1/\tau$ such that $M_{n+1} = M_n^* \exp(-\Delta t/\tau)$, where Δt is the time interval between two light pulses. Hence, the number of pmCRY2 proteins at time $n+1$ is

$$M_{n+1} = [M_n(1-f) + f C_0] e^{-\frac{\Delta t}{\tau}}, \quad (2)$$

which yields the solution

$$M_n = \frac{1 - (1-f)^n e^{-n\frac{\Delta t}{\tau}}}{1 - (1-f)e^{-\frac{\Delta t}{\tau}}} f C_0 e^{-\frac{\Delta t}{\tau}}. \quad (3)$$

For many applications, we are just interested in the final steady amount of recruited protein, which corresponds to the limit $M_{n+1} = M_n = M_\infty$. In this limit, Eq. 3 reduces to

$$M_\infty = \frac{f C_0}{e^{\frac{\Delta t}{\tau}} - (1-f)}. \quad (4)$$

We first checked our ability to modify the pmCRY2 steady-state level by tuning Δt on a single cell. By activating the same cell with three different periods (2, 20, and 60 s) while

letting it rest to its basal level between each round of activation, we induced three pmCRY2 steady-state levels (Fig. 3 a). To validate our theoretical expressions for M_∞ and M_n , we extracted the values of f and C_0 from the curve corresponding to $\Delta t = 2$ s. The value of C_0 was obtained from the steady-state level of pmCRY2 reached for $\Delta t = 2$ s, which was then normalized to 1. We assumed that for this stimulation condition all the cytoplasmic CRY2 was bound to the plasma membrane since $\Delta t \ll \tau$. The value of f was then determined from the step increase of pmCRY2 after the first pulse, which is equal to $f C_0$ ($f = 0.2$). As seen in Fig. 3 a, for the two other conditions ($\Delta t = 20$ s and $\Delta t = 60$ s), the agreement between the expected theoretical values of M_n and experiment is excellent. The full dependency of the steady-state level as a function of Δt is plotted in red in Fig. 3 b. This curve can be used to predict the interval duration between light pulses that should be used to achieve a desired steady-state value of pmCRY2, expressed as a fraction of the maximal value (constant illumination). Note that the steady-state level of pmCRY2 can be modified in real time by changing the periodicity of the pulses (Fig. 3 c).

Although the predictive approach described above does work, the determination of the two central parameters C_0

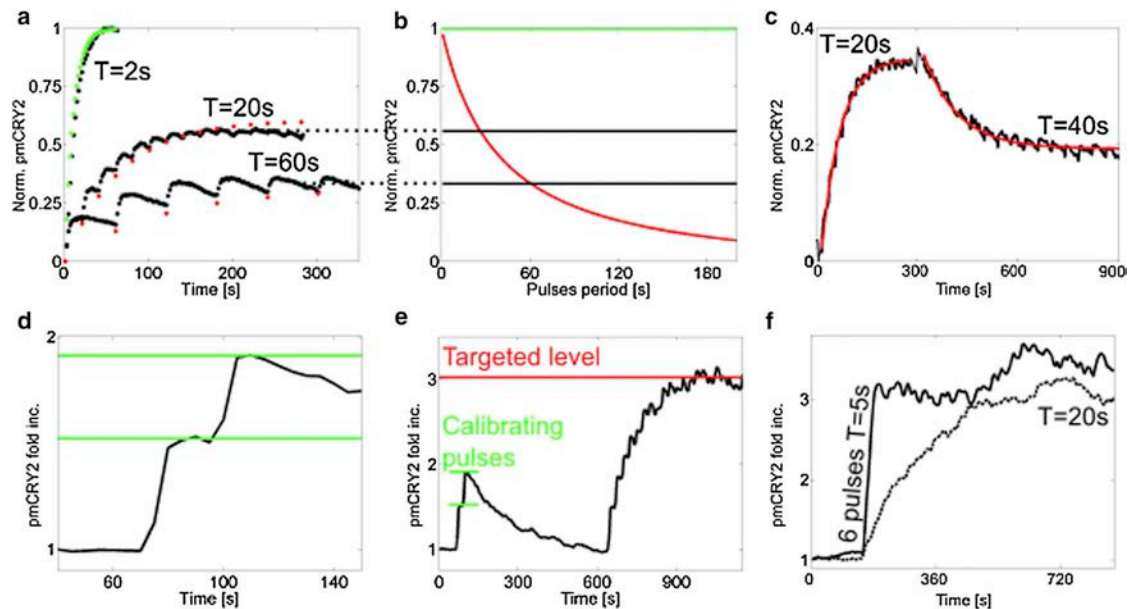


FIGURE 3 Level control of pmCRY2 using pulse frequency. (a) Experimental TIRF intensity of pmCRY2 (black) as a function of time in the same cell for different activation frequencies (one pulse of 50 ms and 21 μW every 2, 20, and 60 s). The intensity is normalized by the final level of the curve with the period of 2 s. The parameters f and C_0 were obtained from the fitted theoretical values of M_n (green dots) to the experimental curve of period 2 s. These parameters were used to predict the theoretical values of M_n for periods of 20 and 60 s (red dots). (b) Theoretical dependency of the pmCRY2 steady-state value (red) on the period of the activating pulses for f and C_0 extracted in (a). (Black lines) Final level of pmCRY2 for the experimental curves (shown in black) in (a), which correspond theoretically to periods of 26 and 61 s. (c) Experimental values of pmCRY2 over time for a single cell (black). After 5 min, the initial stimulations done every 20 s have been modified to one pulse every 40 s. The experimental curve was fitted with exponentially relaxing functions (red). The normalization is done with regards to the maximal steady value as in (a) and (b). (d and e) pmCRY2 over time after 2 pulses of blue light spaced out by 25 s and then regular periodic pulses (a period of 25 s after 10 min). (d) Initial 150 s of this experiment (one image every 5 s) with the two calibrating response levels used to extract the parameters f and C_0 (green lines). (e) pmCRY2 over time (black) for the total duration of the experiment with the targeted level (computed using f and C_0 from (d), red line). (f) pmCRY2 over time for a local activation with a constant frequency either with (black) or without (dashed black) a first round of activation at high frequency (six pulses with periodicity of 5 s). In both cases, the steady state is maintained with one pulse every 20 s (50 ms at 9 μW power). To see this figure in color, go online.

and f requires us first to induce a full recruitment of pmCRY2. Those two parameters can be alternatively obtained by simply shining two calibrating pulses of blue light. These two pulses need to be spaced by a time larger than the characteristic time needed to equilibrate concentration in the cytosol by diffusion ($\tau_{\text{on}} \sim 3$ s) but shorter than the characteristic time of the lateral diffusion at the cell membrane and of the complex disassociation (~ 180 s). Once the two successive levels of pmCRY2 M_1^* and M_2^* are known, we can express the values of f and C_0 as

$$f = 1 - (M_2^*/M_1^* - 1)e^{-\frac{\Delta t}{\tau}},$$

$$C_0 = M_1^*/f.$$

We measured the two levels M_1^* and M_2^* for a representative cell activated with two pulses spaced by 25 s (Fig. 3 d). From those two values, we determined the parameters f and C_0 and used them to predict the steady state that would be achieved with a period $\Delta t = 25$ s (Fig. 3 e). Using this predictive approach, the targeted level is reached with a relative error of 30% ($N = 5$), which is mainly due to the uncertainties in the determination of M_1^* and M_2^* . Compared to the first method based on a first full recruitment of pmCRY2, the two-pulses method is less accurate, but only requires a relatively small recruitment—which could be beneficial when dealing with signaling perturbations.

Shortening the time to reach the steady state

As predicted by our model (Eq. 3) and observed by fitting the data (Fig. 3 c), the steady-state levels are reached exponentially with time with a characteristic time τ . However, one can shorten this time by first doing a high-frequency activation to directly target this steady value. We have to determine from Eqs. 3 and 4 the number of activating pulses needed to reach a fraction x of the steady state $M_n = xM_\infty$ (under the condition that $\Delta t > \tau_{\text{on}}$):

$$n = \frac{\ln(1-x)}{\ln(1-f) - \Delta t/\tau}.$$

Taking a numerical example, we can see that seven pulses are needed to reach 90% ($x = 0.9$) of the steady value corresponding to an interval between pulses of $\Delta t = 20$ s and a fraction of the total CRY2 recruited in one pulse of $f = 0.2$. In addition, we calculated the number of fast pulses of period $\Delta t_f \ll \Delta t$ needed to reach the fraction x of the steady state corresponding to the period Δt as

$$n_f = \frac{\ln(1-x_f)}{\ln(1-f) - \Delta t_f/\tau},$$

where $x_f = (e^{\Delta t_f/\tau} - (1-f))/(e^{\Delta t/\tau} - (1-f))$ is the fraction of the fast frequency steady state equaling the slow fre-

quency steady state. Coming back to our numerical example, only four pulses of period $\Delta t_f = 5$ s are needed to reach the steady value corresponding to the period $\Delta t = 20$ s. In this case, the steady state is reached in ~ 20 s instead of the ~ 140 s we would need with a constant frequency of pulses. Using this approach, we can induce and maintain the steady-state level predicted for $\Delta t = 20$ s with a fast off/on control (Fig. 3 f).

Spatial distribution of pmCRY2

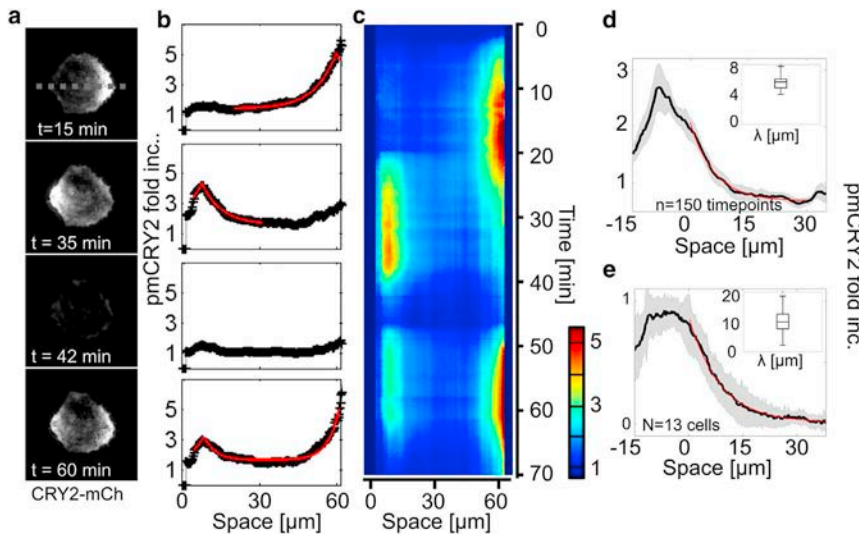
We now consider the subcellular distribution of pmCRY2 following a spatially localized activation. The processes of binding to the plasma membrane, lateral diffusion, and dissociation can be combined in the following diffusion-reaction equation satisfied by the number of recruited pmCRY2 as a function of time and position on the membrane,

$$\frac{\partial M(x,y,t)}{\partial t} = D\Delta_{2d}M(x,y,t) - k_{\text{off}}M(x,y,t) + S(x,y,t), \quad (5)$$

where Δ_{2d} is the Laplacian operator in two dimensions and $S(x,y,t)$ is the source term, which is directly related to the characteristics of the activating blue light: laser power, exposure time, frequency of pulses, and spatial extension of the illuminated area.

Equation 5 is found in many other biological contexts. Indeed, a localized source with diffusion and degradation is a general physical process known to generate molecular gradients as illustrated by the morphogen gradients that pattern tissues during embryogenesis (26). This equation introduces a typical length scale $\lambda = \sqrt{D/k_{\text{off}}}$, which is the key parameter dictating the spatial distribution of pmCRY2. This characteristic length scale sets the lower limit of the size over which CRY2 can be recruited. In our case, considering the value of D and k_{off} previously determined, we obtain $\lambda = 4.5 \mu\text{m}$. This value explains why we can achieve local recruitment in a HeLa cell (Fig. 1 a), which is ~ 10 times larger.

To underline the role of λ , cells were initially plated on 50- μm -diameter round pattern of fibronectin to obtain calibrated cellular shapes. We performed experiments with periodic stimulations in a circular region with diameter 3 μm and chose a period of pulses (25 s) smaller than the dissociation time. We could establish and maintain a subcellular gradient of pmCRY2 (Fig. 4, a–e, and Movies S3 and S4) quantified by the fluorescence profile at steady state along a line going through two extremities of the cell. As expected from the solution of Eq. 5 for a one-dimensional infinite space with a point source, the distribution of pmCRY2 at steady state (M_{ss}^*) is well fitted with an exponentially decaying function,



each time point ($n = 150$), $\lambda_{\text{exp}} = 6.3 \pm 1 \mu\text{m}$. (e) Quantification of the variability of the exponential gradient for different cells. For each of the 13 cells, we used the time-averaged distribution of pmCRY2 to compute the average and SD of the pmCRY2 exponential gradient (see Materials and Methods for the normalization procedure). (Inset) Boxplot of the decay lengths measured for each cell, $\lambda_{\text{exp}} = 10.5 \pm 5 \mu\text{m}$. To see this figure in color, go online.

$$M_{ss}^*(x|x_0) \propto e^{-\frac{|x-x_0|}{\lambda_{\text{exp}}}},$$

where x_0 is the position of the point source and λ_{exp} the experimental decay length of the exponential function. We measured a characteristic length $\lambda_{\text{exp}} = 10.5 \pm 5 \mu\text{m}$ (Fig. 4 e). This value is approximately twice larger than the theoretical expectation $\lambda = 4.5 \mu\text{m}$ because the source term in our experiments is not perfectly punctual. Indeed, the activations are performed in a disk and CRY2 proteins diffuse laterally in the cytoplasm before binding to CIBN.

Thanks to the dynamic property of the steady state, the exponential gradient of pmCRY2 could be entirely reversed by moving the activating spot of light within a timescale $3\tau \sim 9$ min, which is limited by the dissociation kinetics (Fig. 4, a–c). Note that the amplitudes of the left and right exponential gradients differ because the local geometry of the cell contributes to the amount of pmCRY2 recruited in one batch (the parameter f). Thus, to perform a local recruitment with a precisely targeted level, the calibration pulses need to be done in the same region. Overall, the temporal variability of the exponential gradient (15% variations in λ_{exp} , Fig. 4 d and Movie S4) is much lower than the intercellular variability (45% variations in λ_{exp} , Fig. 4 e).

The knowledge of pmCRY2 profiles at steady state for a punctual illumination can be used to compute the relation between any light pattern and pmCRY2 spatial distribution. The distribution of pmCRY2 at steady state (M_{ss}) is the convolution of the illumination distribution $S(x_0)$ and the propagator M_{ss}^* :

$$M_{ss}(x) = \int dx_0 M_{ss}^*(x|x_0)S(x_0). \quad (6)$$

FIGURE 4 pmCRY2 spatial distribution for a punctual activation. (a–c) CRY2-mCherry TIRF signals of a cell being successively activated in different points (a) and its corresponding kymograph (c) showing the quantified pmCRY2 profile along a horizontal line as exemplified for $t = 15$, 35, 42, and 60 min (b). First activations between time $t = 2$ min and $t = 20$ min in the right of the cell (one pulse every 25s). Second activation routine between $t = 20$ min and $t = 35$ min on the left of the cell. Third set of activations between $t = 46$ and 60 min on both sides. The decaying spatial distributions at steady state (black) were fitted with exponentially decreasing functions (red). The cell is initially plated on a 50- μm -diameter round pattern of fibronectin. (d) Quantification of the variability of the exponential gradient over time. An exponential gradient was established on one side of a round cell and maintained for >30 min (Movie S4). (Black line) Average gradient over 30 min; (gray shadow) 1 standard deviation. (Inset) Boxplot of the decay lengths measured for

In Fig. S2, a and b, we illustrated theoretically this convolution by replacing the integral by a sum of exponentially decaying curves with a weight depending on the illumination characteristics. For example, if the activation is done uniformly in a rectangular region, the source term in one dimension will be a rectangle function and the corresponding steady-state concentration will be a plateau with exponentially decaying tails on the sides of the activated region (Fig. S2 a). A linear pattern of light will lead to a linear pmCRY2 profile in the central region surrounded by exponentially decaying tails on its border (Fig. S2 b).

Experimentally, the source term is not pointlike because of CRY2 cytoplasmic diffusion. As shown in Fig. 2 a, a single pulse leads to a Gaussian distribution of pmCRY2, which depends on cell height. The steady-state solution of the diffusion-reaction equation can also be solved with a Gaussian source term (27), but the solution is more complex. However, the effect of this extended source is minor for large regions of activation. By shining light in a square region, we observe a plateau of pmCRY2 in the illuminated region surrounded by decaying tails of characteristic length λ_{exp} (Fig. S2, c and d).

Altogether, using Eq. 6 we can achieve any desired spatial profile of pmCRY2 provided that its local sharpness is not greater than the 10- μm exponential decaying function. Importantly, if we are not entirely depleting the cytoplasm from CRY2, changing the frequency of pulses affects only the overall amount of recruitment. One can thus control the level of pmCRY2 independently of its spatial profile, and the predictive control of pmCRY2 levels with the frequency of pulses presented above still applies for spatially heterogeneous illuminations.

Subcellular control of Cdc42 activity

The presented optogenetic approach allows the manipulation of protein distribution with a spatial resolution of a few microns and a temporal resolution of a few minutes. This makes it a good candidate to perturb Rho GTPase signaling, which presents spatiotemporal patterns of activities with similar characteristics (8,9). As a matter of fact, the endogenous mechanisms giving rise to patterns of Rho GTPase activation most probably rely on diffusion-reaction processes similar to the ones described above (28,29).

We demonstrate here our approach to the Rho GTPase Cdc42 with a similar strategy to that developed initially with the PhyB/PIF6 optogenetic system (14). The strategy is based on the local recruitment to the plasma membrane of the Intersectin (ITSN) guanine exchange factor (GEF) catalytic domain (DHPH domain). The catalytic domain of ITSN is specific to Cdc42 and triggers the transition from its inactive GDP-loaded state to its active GTP-loaded state. By itself, the catalytic domain does not localize to the plasma membrane and is expected to remain inactive in the cytosol. We fused this domain to CRY2-mCherry so that light could be used to rescue its membrane localization and induce Cdc42 signaling. When the fusion was expressed in cells and in the absence of activating light, we did not notice any phenotypical change due to a constitutive activation of Cdc42 in the dark. However, under blue light illumination, ITSN-DHPH-CRY2-mCherry (optoGEF-Cdc42) was recruited at the plasma membrane and led to the activation of the endogenous pool of Cdc42.

Following a sustained activation in a subcellular region, the recruitment of optoGEF-Cdc42 (Fig. 5 *a*) showed characteristics similar to the pmCRY2 distributions presented above with a constant value inside the region of activation and an exponential tail of decay length $\lambda_{\text{exp}} = 9 \pm 1.5 \mu\text{m}$ (Fig. S3). This subcellular recruitment induced Cdc42 activity, as observed by the localization of the effector Pak1 Binding Domain fused to the infraRed Fluorescent Protein (PBD-iRFP). Remarkably, the optoGEF-Cdc42 and PBD-iRFP signals are enriched at the same place (Fig. 5, *a* and *b*), and we did not observe a significant spatial extension of the signaling activity despite the catalytic nature of our optogenetic actuator OptoGEF Cdc42. As noted

previously for Rac1 (30), this suggests that either Cdc42 proteins have a reduced mobility when activated or that activated Cdc42 proteins are rapidly deactivated before they move away from the region of activation. In terms of kinetics, optoGEF-Cdc42 and PBD-iRFP recruitments are similar with almost no delay (Fig. 5 *c*). Thus, the relationship between optoGEF-Cdc42 distribution and Cdc42 activation can be assumed immediate and linear.

At the morphological level, by applying and maintaining a subcellular gradient of optoGEF-Cdc42 (Fig. 6, *a-d* and Movie S5) we provoked a direct and major effect on the cell phenotype. A couple of minutes after recruitment (Fig. 6 *b*), we observed a large increase in membrane activity, the formation of filopodia, membrane extrusions, and macropinocytotic vesicles (Fig. 6, *c* and *d*). These events came along with alternating phases of membrane protrusion and retraction, with a timing of few minutes. In addition to these local morphological effects, our optogenetic perturbation also affected the global phenotype of the cell. After a period of 10 min, the cell barycenter started to move (Fig. 6 *d*). The optoGEF-Cdc42 pattern is extending as the cell gets into the activation region and the cell retracts at its opposite side. From an initially unpolarized state, the cell adopted a clear front-to-rear polarized migrating phenotype. Such optogenetic initiation of migration was extremely robust; even blebbing cells or cells engaged in cell-to-cell contact could be triggered into a migratory state (Movies S6 and S7).

We then performed sharp off-on local Cdc42 optogenetic activation on a large number of HeLa cells (Fig. 7, *a* and *b* and Movies S8 and S9) to quantify the time course of polarity formation and migration initiation. By segmenting the cell contour over time (Fig. 7 *c*), we extracted the time course of the cell barycenter displacement (Fig. 7 *d*) and cell front/rear displacements and areas along the migration axis (summarize in Fig. 7 *e*). Following the optogenetic activation, the front of the cell started to move in <2 min while the rear of the cell started to retract after a delay of ~10 min (Fig. 7 *f*). These dynamics are consistent with what has been observed recently using a light-activated Rac1-GPCR system to induce immune cell migration (13). In all cases, the displacement of the nucleus was following the rear of the cell (data not shown), suggesting that a net movement

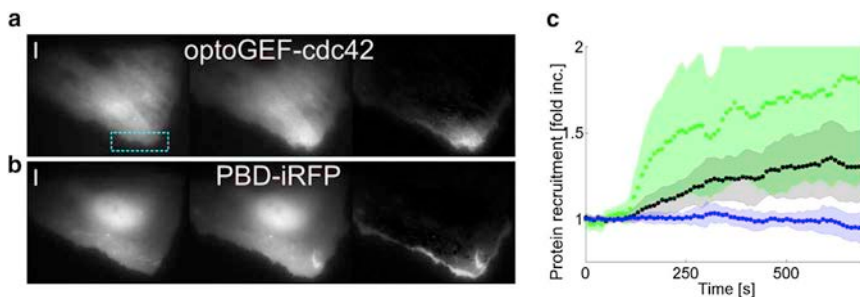
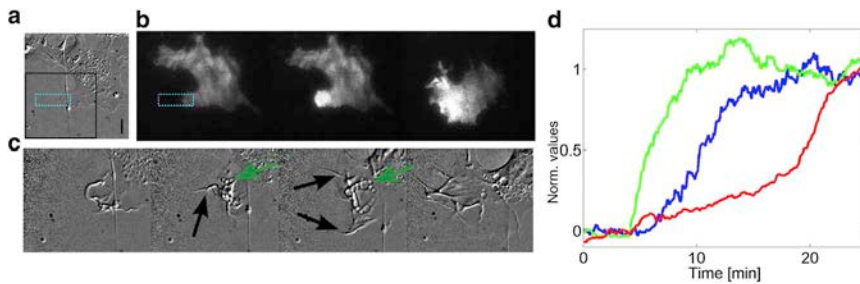


FIGURE 5 Local recruitment of optoGEF-Cdc42 activates Cdc42. (*a* and *b*) TIRF images of OptoGEF-Cdc42 (*a*) and PBD-iRFP (*b*) before activation (*left*), 6 min after activation (*middle*), and differential images (*right*). (*Blue rectangle*) Activations. (*c*) Average time courses (*dots*) and standard deviation (*shaded regions*) over $N = 10$ cells of OptoGEF-Cdc42 (*green*) and PBD-iRFP (*black*) in the activated region (one image every 10 s, one activation every frame starting at time 100 s). PBD quantification in another region of the cell is represented as a control (*blue*). To see this figure in color, go online.



(green arrows) localization of vesicles. (d) Quantification of pmCRY2 recruitment in the activation area (green), of membrane activity (blue) and of cell barycenter displacement (red) over time normalized between 0 and 1. To see this figure in color, go online.

FIGURE 6 Local activation of Cdc42 in fibroblast cell generates membrane activity and cell barycenter displacement. (a–c) DIC images (a and c) and TIRF images (b) of a fibroblast illuminated locally by a rectangular ROI (1 pulse every 20 s, blue region). (a) The cell is represented before the activation routine. Scale bar = 10 μm . (b) TIRF images before, at 1 min, and 50 min after activation. (c) Zoom-in of the black area of (a) for 8, 17, 30, and 50 min after the beginning of the activation routine. (Black arrows) Presence of filopodia;

of the cell was achieved only when the back of the cell started to retract. The time course of the front and rear areas (Fig. 7 g) showed that both increased initially. This unexpected small extension of the rear area could be either due to an unmeasurable leakage of the optogenetic activation or to a global cellular response to the local strong increase of Cdc42 activity.

DISCUSSION

The use of optogenetic molecular systems to perform intracellular signaling perturbations is rapidly increasing. The main advantage of using light compared to other approaches such as chemically induced dimerization methods (31) is the ability to apply spatially restricted perturbations. Yet, the conditions required to achieve a given subcellular spatial resolution depend on precise knowledge of the biophysical processes involved during the optogenetic activation. Using the CRY2/CIBN light-inducible dimerization system for manipulating protein distribution on the plasma membrane, we provided an in-depth characterization of these processes. We showed that the two intrinsic parameters controlling the dynamics of membrane-bound dimers are the lateral diffusion coefficient D of the dimer and its lifetime τ .

The recruitment of CRY2 to the plasma membrane occurs in a few seconds, enabling fast perturbations. For most of the intracellular signaling pathways, this timing is one order-of-magnitude faster than the cellular response, and the perturbation can be assumed instantaneous. However, the lifetime of the complex limits the shutdown of induced perturbations and 10 min are needed to go back to the resting state. Thus, one inconvenience of the CRY2/CIBN system is that it precludes the temporal dissection of intracellular signal processing at frequencies $>1/600 = 0.0025$ Hz, as recently done for the Ras/ERK pathway using the PhyB/PIF6 system (32). Yet, in many cases, one is interested in dissecting the temporal order of events after a signal is imposed. In this situation, the only requirement is to be able to impose a fast off/on perturbation and to maintain it over time. We showed an example of such an approach for dissecting the initiation of cell migration with a localized cdc42 perturbation, as discussed further below.

We achieved a control in the level of membrane-recruited CRY2 through the modulation of the frequency of activating light pulses. The advantage of this method compared to continuous illumination is that it allows a predictive control of the steady-state level and it limits the exposure of cell to light. Ideally, activating pulses should be short and strong enough to activate all CRY2 present in the illuminated volume of the cytoplasm without entering into the three-dimensional diffusive replenishment regime. Thus each batch of activated CRY2 will be maximal and more reproducible. Typically, the pulses are 100-ms long with a light intensity comparable to the one used for imaging.

The steady-state level of CRY2 recruitment reached for a maintained pulsatile activation depends only on two parameters: the initial cytoplasmic concentration of CRY2 and the fraction of this concentration, which is depleted in one pulse. We showed that these two parameters could be measured before the establishment of a targeted level by applying two successive light pulses. Yet, this calibration needs to be done before each specific activation in a cell, which can be problematic for high-throughput approaches. To overcome this limitation, further quantitative analyses should be performed on stable cell lines expressing a titrated amount of each optogenetic partner (using lentiviral infection and FACS sorting as done in Toettcher et al. (32), for example) and making use of adhesive micropatterns to normalize cell shapes (20).

However, not all experiments require a specified steady value. The relatively slow dissociation of the CRY2/CIBN dimer allows sparse stimulations. As a general guideline, one pulse every 5 s will give a high steady-state value and one pulse every 100 s is close to the lowest limit. In between, the steady state depends exponentially on the frequency of pulses (Fig. 3 b). This general rule applies independently of the actual experimental details such as cell height, volume of illumination, etc. Yet, to perform a fast off/on recruitment and to maintain it steadily, it is necessary to quantify the recruitment parameters beforehand. For more complex time courses of CRY2 recruitment, we refer to the recent publication (33) on the optogenetic control of gene transcription, which relies on the same principle of frequency modulation.

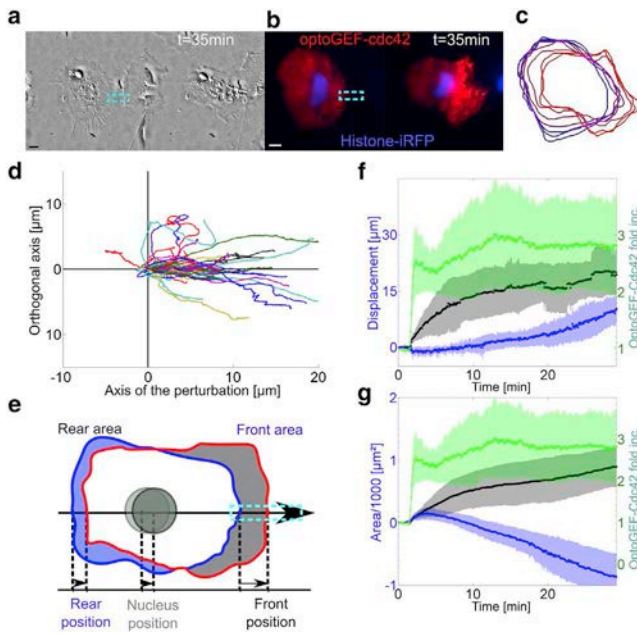


FIGURE 7 Quantitative measurement of HeLa cell movement in response to optoGEF-Cdc42 gradient. (a and b) Local activation of Cdc42 in a HeLa cell expressing OptoGEF-Cdc42 and H2B-iRFP. DIC images (a) and fluorescent images (b) showing mCherry (red) and iRFP (blue) at two time points, before (left) and 28 min after activation (right). (Dashed-blue rectangles) Area of blue illumination. (c) Outline of the cell for increasing time points (from blue to red) over 30 min. The outer border of the cell was segmented from TIRF mCherry images every 4 min. (d) Quantification of the displacement of the cell barycenter for 30 min moves along and perpendicularly to the main axis of the cell for $N = 36$ cells. The main axis is defined by a line passing through the cell barycenter at $t = 0$ min and the position of the recruitment. (e–g) Quantification of cell movement induced by local Cdc42 activation for $N = 5$ cells. (e) Scheme of the different elements being quantified: cell front, rear, and nucleus displacement along the migration axis and the evolution of the areas of the front and the rear. (f and g) Quantification of OptoGEF-Cdc42 in the photoactivated region (green) and of the barycenter displacement (f) and area (g) of the front (black) and the rear (blue) of the cell. The photoactivation was done with six pulses of 50 ms every 5 s, followed by pulses of 50 ms every 25 s. (Shaded areas) Mean \pm SD (dots). To see this figure in color, go online.

One should note that all quantifications were based on relative fold increases from an initial background value and not on absolute concentrations. The quantification was done on TIRF images and we found that the background value was mainly due to the leaking signal from the initial cytoplasmic CRY2. Thus, both the background value and the absolute amount of recruitment scale with the level of CRY2 expression. Even though for signaling only the absolute concentration of activated proteins matters, the relative fold increase still provides an easy way to characterize perturbation intensities and to compare different optogenetic systems. In this regard, we remarked that we could achieve much higher levels of recruitment using the CRY2/CIBN system than with the PhyB/PIF6 (14) or TULIPS (16) systems. This observation can be explained

by the cytosolic photosensitive protein being always in deficit with respect to the number of binding sites on the membrane. Through the successive recruitment of cytoplasmic batches, the local concentration of membrane dimers can be increased to high levels.

For local recruitment, we showed that the distribution of CRY2 on the plasma membrane was restricted by the length scale $\lambda = \sqrt{D\tau} \sim 5 \mu\text{m}$. The elementary steady-state response for a pointlike illumination is an exponential distribution with a decay length of λ . When the illumination is done in extended regions, the steady-state distribution is the convolution of the exponential distribution with the illumination pattern. This means that sharp spatial borders cannot be achieved and that the distribution of CRY2 on the membrane will always present exponential tails at the edge of the illuminated region. This inherent limitation of the CRY2/CIBN dimerizer could be optimized in the future by decreasing the lifetime of the complex or by immobilizing the membrane anchor. Note that this limitation is not specific to this case, but can be extended to all other optogenetic systems that are passively reversible. More generally, the reaction-diffusion processes we described in this work are common to all optogenetic systems. For example, the PA-Rac diffuses with a coefficient $D = 0.55 \mu\text{m}^2/\text{s}$ and reverses to a dark state in 43 s (10). This means that the length scale associated with this system is $\lambda = \sqrt{D\tau} \sim 5 \mu\text{m}$, similar to the CRY2/CIBN system. Recently, there has been an increased interest in the control of clustering and oligomerization processes with optogenetics (6,34). In these cases, the clusters induced by light are probably larger than the typical size of the intracellular meshwork of actin (35,36) (~ 100 nm) and will remain almost immobile ($D \sim 0$), thus enabling sharp local activations ($\lambda \sim 0$). The actively reversible systems, such as the PhyB/PIF6 (14) and Dronpa (37) systems, are not subjected to an inherent spatial limitation as the reversion is inducible with light and thus sharp local activation can be achieved (38).

In our experimental conditions, the membrane-anchored CIBN was systematically expressed in large excess compared to the cytosolic CRY2. On the contrary, in our hands the PhyB/PIF6 and TULIPS systems tend to be in the opposite situation with a large excess of the cytoplasmic component. The imbalance of concentrations toward the membrane anchor has practical implications, as follows. First, because the membrane anchor is not limiting, the spatial distribution of membrane-bound CRY2 does not depend on the amount of recruited CRY2. Indeed, we have never observed any spatial spreading of the pmCRY2 signal exceeding our predicted value. If CIBN proteins were limiting, we would expect to see an extension of the pmCRY2 signal because the local saturation of CIBN sites would require activated CRY2 to bind further away. Thus, the level can be controlled independently of the spatial distribution and vice versa. Second, when CRY2 proteins are

recruited locally, the distribution of the whole cellular amount of CRY2 is redistributed. Indeed, at steady state most of the CRY2 proteins will be depleted from the cytoplasm and will be bound on the plasma membrane. For local stimulations, CRY2 is depleted away from the region of activation and gets concentrated there. This overall manipulation of protein distribution enables the imaging of CRY2 relocalization in epifluorescence. Moreover, it allows the imaging of GFP signals if the acquisition is done once in a while to interfere minimally with the local stimulation.

Altogether, thanks to its low background and excellent reactivity (19), the CRY2/CIBN optogenetic system allows the manipulation of protein distribution on the plasma membrane over a wide dynamic range, using a simple procedure for its spatiotemporal control. This makes it a tool of choice for signaling perturbations. We assessed its potential by designing a fusion of CRY2 with the catalytic domain of Intersectin, a specific GEF for the Rho GTPase Cdc42. A similar strategy was previously developed with the PhyB-PIF6 dimerization system (14). In this study, Levskaya et al. (14) reported Cdc42 activation through the recruitment of the Cdc42 GTP binding domain of WASP (WASP-GBD). In another study, using the Dronpa system to gate the activity of ITSN on the plasma membrane, Zhou et al. (37) demonstrated local and global formation of filopodia. Using a light-gated, constitutively active form of Cdc42, Wu et al. (10) reported filopodia and membrane ruffle formation. Our optoGEF-Cdc42 construct had a strong potency in locally activating the endogenous pool of Cdc42 as well as forming filopodia, membrane ruffles, and macropinocytotic vesicles. Compared to the previous optogenetic activation of Cdc42, our perturbative approach was strong enough to induce cell migration. In this regard, an increasing number of optogenetic strategies have been proposed to control cell migration, including photoactivable Rac, optogenetic trapping (6), GPCR control (13), or light activation of growth factor receptors (3). In comparison to these methods, our optogenetic tool has the advantage of activating only the endogenous pool of the Rho GTPase (no overexpression) in a direct fashion (no intermediates). Importantly, we showed that the pattern of activated Cdc42 was matching the pattern of recruited optoGEF-Cdc42. Thus, the imaging of CRY2 recruitment provides a faithful measure of the imposed signaling perturbation. This information is of prime interest when performing quantitative analyses of input-output relationships along the Cdc42 signaling pathway.

Cell polarity and migration are highly complex processes that involve the spatiotemporal regulation of many signaling pathways, effectors, and the cell cytoskeleton. Migrating cells are characterized by a front and a back that are tightly coordinated to ensure net movement. There are many modalities of cell migration, depending on environmental cues or cellular specificities (39). Thus, there is

no consensus on a universal mechanism by which cells polarize and migrate; many functional modules (9) and mechanical processes can cooperate or act individually in specific contexts to polarize cells (40). Rho GTPases are frequently involved in cell polarity and migration but the numerous feedbacks arising from signaling cross talks and cytoskeleton dynamics render difficult the identification of their role in the initiation and maintenance of a polarized state. The use of optogenetics to induce signaling perturbation offers a unique tool to overcome this complexity. We showed here that, by applying and maintaining a spatially restricted Cdc42 activity, we were able to sequence in time the events leading to cell polarization and migration in a reproducible fashion. The induction of a fast and strong perturbation shifts the functioning point of the intracellular signaling system on a timescale shorter than the ones on which feedbacks operate. Hence, such perturbations reveal the causality in signal transduction by temporarily holding down the feedbacks that are responsible for the high degree of correlation among all elements of the intracellular circuitry.

CONCLUSIONS

In this work, we presented a quantitative framework allowing the predictive manipulation of protein gradients with the CRY2/CIBN optogenetic dimerizer system. We provided a comprehensive description of the CRY2 plasma membrane recruitment and we measured the relevant biophysical parameters. Cell shape and geometry have a large impact on CRY2 membrane distribution and the implementation of a spatiotemporal feedback system would provide a significantly higher degree of control. A closed loop system requires the segmentation of the cell contour, the quantification of pmCRY2 distribution, and the application of a computed correction with the illumination. With regard to this last task, our quantitative framework will be of use to build the feedback model required to converge toward a targeted distribution of the optogenetic actuator.

We applied the CRY2/CIBN optogenetic system to dissect the initiation of cell migration following Cdc42 activation on a coarse scale by only monitoring the cellular morphology. Future works should include a more exhaustive analysis of the dynamics of selected intracellular components. In particular, we observed that even if we induced very large local concentrations of optoGEF-Cdc42, we did not saturate the endogenous pool of Cdc42. The dynamics of our reporter of Cdc42 activity, PBD-iRFP, appeared linear in space and time. It would be interesting to assess systematically if this relation holds for all perturbations and for downstream components. The front and back antagonistic functions require a nonlinear integration at some level of the transduction machinery, and optogenetics could help to pinpoint the mechanisms underlying this task.

SUPPORTING MATERIAL

Three figures and nine movies are available at [http://www.biophysj.org/biophysj/supplemental/S0006-3495\(15\)00924-8](http://www.biophysj.org/biophysj/supplemental/S0006-3495(15)00924-8).

AUTHOR CONTRIBUTIONS

L.V. performed the experiments; L.V. and M.C. analyzed the data; F.E. and F.d.P. performed preliminary experiments; A.R. performed experiments for the revision of the work; X.M. participated in the discussion of the results; L.V., F.E., M.D., and M.C. designed the research; and L.V., M.D., and M.C. wrote the article.

ACKNOWLEDGMENTS

M.C. acknowledges financial support from the French National Research Agency (ANR) (LICOP grant No. ANR-12-JSV5-0002-01). M.C. and M.D. acknowledge funding from the French National Research Agency Paris-Science-Lettres Program (grant No. ANR-10-IDEX-0001-02 PSL), Labex CelTisPhyBio (grant No. ANR-10-LBX-0038), and the France-BioImaging Infrastructure supported by French National Research Agency grant No. ANR-10-INSE-04 (Investments for the Future). X.M. acknowledges financial support from the French National Research Agency (ANR Blanche 2012 LIVESPIN).

REFERENCES

- Pathak, G. P., J. D. Vrana, and C. L. Tucker. 2013. Optogenetic control of cell function using engineered photoreceptors. *Biol. Cell.* 105:59–72.
- Tischer, D., and O. D. Weiner. 2014. Illuminating cell signalling with optogenetic tools. *Nat. Rev. Mol. Cell Biol.* 15:551–558.
- Kim, N., J. M. Kim, ..., W. D. Heo. 2014. Spatiotemporal control of fibroblast growth factor receptor signals by blue light. *Chem. Biol.* 21:903–912.
- Renicke, C., D. Schuster, ..., C. Taxis. 2013. A LOV2 domain-based optogenetic tool to control protein degradation and cellular function. *Chem. Biol.* 20:619–626.
- Yang, X., A. P. Jost, ..., C. Tang. 2013. A light-inducible organelle-targeting system for dynamically activating and inactivating signaling in budding yeast. *Mol. Biol. Cell.* 24:2419–2430.
- Lee, S., H. Park, ..., W. D. Heo. 2014. Reversible protein inactivation by optogenetic trapping in cells. *Nat. Methods.* 11:633–636.
- Karunaratne, W. K., P. R. O'Neill, and N. Gautam. 2015. Subcellular optogenetics—controlling signaling and single-cell behavior. *J. Cell Sci.* 128:15–25.
- Machacek, M., L. Hodgson, ..., G. Danuser. 2009. Coordination of Rho GTPase activities during cell protrusion. *Nature.* 461:99–103.
- Pertz, O. 2010. Spatio-temporal Rho GTPase signaling—where are we now? *J. Cell Sci.* 123:1841–1850.
- Wu, Y. I., D. Frey, ..., K. M. Hahn. 2009. A genetically encoded photoactivatable Rac controls the motility of living cells. *Nature.* 461:104–108.
- Wang, X., L. He, ..., D. J. Montell. 2010. Light-mediated activation reveals a key role for Rac in collective guidance of cell movement in vivo. *Nat. Cell Biol.* 12:591–597.
- Yoo, S. K., Q. Deng, ..., A. Huttenlocher. 2010. Differential regulation of protrusion and polarity by PI3K during neutrophil motility in live zebrafish. *Dev. Cell.* 18:226–236.
- Karunaratne, W. K., L. Giri, ..., N. Gautam. 2013. Optical control demonstrates switch-like PIP3 dynamics underlying the initiation of immune cell migration. *Proc. Natl. Acad. Sci. USA.* 110:E1575–E1583.
- Levskaia, A., O. D. Weiner, ..., C. A. Voigt. 2009. Spatiotemporal control of cell signalling using a light-switchable protein interaction. *Nature.* 461:997–1001.
- Idevall-Hagren, O., E. J. Dickson, ..., P. De Camilli. 2012. Optogenetic control of phosphoinositide metabolism. *Proc. Natl. Acad. Sci. USA.* 109:E2316–E2323.
- Strickland, D., Y. Lin, ..., M. Glotzer. 2012. TULIPS: tunable, light-controlled interacting protein tags for cell biology. *Nat. Methods.* 9:379–384.
- Kennedy, M. J., R. M. Hughes, ..., C. L. Tucker. 2010. Rapid blue-light-mediated induction of protein interactions in living cells. *Nat. Methods.* 7:973–975.
- Kim, B., and M. Z. Lin. 2013. Optobiology: optical control of biological processes via protein engineering. *Biochem. Soc. Trans.* 41:1183–1188.
- Pathak, G. P., D. Strickland, ..., C. L. Tucker. 2014. Benchmarking of optical dimerizer systems. *ACS Synth. Biol.* 3:832–838.
- Azioune, A., M. Storch, ..., M. Piel. 2009. Simple and rapid process for single cell micro-patterning. *Lab Chip.* 9:1640–1642.
- Gregor, T., E. F. Wieschaus, ..., D. W. Tank. 2007. Stability and nuclear dynamics of the bicoid morphogen gradient. *Cell.* 130:141–152.
- Soumpasis, D. M. 1983. Theoretical analysis of fluorescence photobleaching recovery experiments. *Biophys. J.* 41:95–97.
- Berezhkovskii, A. M., L. Batsilas, and S. Y. Shvartsman. 2004. Ligand trapping in epithelial layers and cell cultures. *Biophys. Chem.* 107:221–227.
- Jacobson, K., D. O'Dell, and J. T. August. 1984. Lateral diffusion of an 80,000-Dalton glycoprotein in the plasma membrane of murine fibroblasts: relationships to cell structure and function. *J. Cell Biol.* 99:1624–1633.
- Toettcher, J. E., D. Gong, ..., O. D. Weiner. 2011. Light-based feedback for controlling intracellular signaling dynamics. *Nat. Methods.* 8:837–839.
- Grimm, O., M. Coppey, and E. Wieschaus. 2010. Modelling the Bicoid gradient. *Development.* 137:2253–2264.
- Berezhkovskii, A. M., M. Coppey, and S. Y. Shvartsman. 2009. Signaling gradients in cascades of two-state reaction-diffusion systems. *Proc. Natl. Acad. Sci. USA.* 106:1087–1092.
- Jilkine, A., and L. Edelstein-Keshet. 2011. A comparison of mathematical models for polarization of single eukaryotic cells in response to guided cues. *PLOS Comput. Biol.* 7:e1001121.
- Muñoz-García, J., and B. N. Kholodenko. 2010. Signalling over a distance: gradient patterns and phosphorylation waves within single cells. *Biochem. Soc. Trans.* 38:1235–1241.
- Etoc, F., D. Lisse, ..., M. Dahan. 2013. Subcellular control of Rac-GTPase signalling by magnetogenetic manipulation inside living cells. *Nat. Nanotechnol.* 8:193–198.
- Inoue, T., W. D. Heo, ..., T. Meyer. 2005. An inducible translocation strategy to rapidly activate and inhibit small GTPase signaling pathways. *Nat. Methods.* 2:415–418.
- Toettcher, J. E., O. D. Weiner, and W. A. Lim. 2013. Using optogenetics to interrogate the dynamic control of signal transmission by the Ras/Erk module. *Cell.* 155:1422–1434.
- Olson, E. J., L. A. Hartsough, ..., J. J. Tabor. 2014. Characterizing bacterial gene circuit dynamics with optically programmed gene expression signals. *Nat. Methods.* 11:449–455.
- Taslimi, A., J. D. Vrana, ..., C. L. Tucker. 2014. An optimized optogenetic clustering tool for probing protein interaction and function. *Nat. Commun.* 5:4925.
- Luby-Phelps, K., P. E. Castle, ..., F. Lanni. 1987. Hindered diffusion of inert tracer particles in the cytoplasm of mouse 3T3 cells. *Proc. Natl. Acad. Sci. USA.* 84:4910–4913.
- Kalwarczyk, T., N. Ziebaczyk, ..., R. Hołyst. 2011. Comparative analysis of viscosity of complex liquids and cytoplasm of mammalian cells at the nanoscale. *Nano Lett.* 11:2157–2163.

37. Zhou, X. X., H. K. Chung, ..., M. Z. Lin. 2012. Optical control of protein activity by fluorescent protein domains. *Science*. 338: 810–814.
38. Toettcher, J. E., C. A. Voigt, ..., W. A. Lim. 2011. The promise of optogenetics in cell biology: interrogating molecular circuits in space and time. *Nat. Methods*. 8:35–38.
39. Bear, J. E., and J. M. Haugh. 2014. Directed migration of mesenchymal cells: where signaling and the cytoskeleton meet. *Curr. Opin. Cell Biol.* 30:74–82.
40. Parent, C. A., and O. D. Weiner. 2013. The symphony of cell movement: how cells orchestrate diverse signals and forces to control migration. *Curr. Opin. Cell Biol.* 25:523–525.

3) Detection and tracking of overlapping cell nuclei for large scale mitosis analyses. Li Y., Rose F., di Pietro F., Morin X, Genovesio A. *BMC Bioinformatics*, 2016. DOI 10.1186.

We aimed at developing software to fully automate the analysis of cell division angles in our Ed-Gai and micropattern-based model of spindle orientation, as this was particularly needed to facilitate data analysis in the frame of the screen. We thus worked in collaboration with Yingbo Li, a postdoc in our lab, and France Rose and Auguste Genovesio from the Bioinformatics team of IBENS. The most complex part of the analysis was to extract the movies of interest from raw data (i.e. all the movies containing a division within a pair of isolated cells) by using the H2B-Cherry images. Raw movies consisted in imaging fields containing more than 250 micropatterns arranged in a honeycomb fashion, filmed over 56 hr. During the duration of the movie, each micropattern contains a variable and varying number of cells (between 0 and 8 in general) depending on the number of cells initially seeded on the pattern, the number of division events and cell death. Developing of automatic extraction of individual micropattern movies was straight-forward thanks to the acquisition of a fluorescent image of the micropatterns which were marked with fibrinogen-650. The next step was to detect the passage of 2 to 3 cells -if any- in these movies. Standard segmentation methods proved not useful for this step as cells on round micropatterns tend to be too packed. This is particularly evident when more than two cells are accommodated in a pattern; in these cases overlapping of nuclei can induce errors in segmentation routines. Similarly, even when only 2 cells are present on a pattern, temporary overlapping of nuclei as cells move on the pattern complicates the segmentation process. To solve these problems, our collaborators proposed a new approach to identify the transition from two to three nuclei based on the application of Gaussian mixture models. In particular, they observed that the difference between the errors of fitting a 2 component vs a 3 component Gaussian model to the whole image sequence peaks in coincidence with the transition from two to three cells. This is because the 3 component Gaussian model fits much better than the 2 component model when there are three cells on the patterns. This method was successful to

recognize a subset of events of interests. However, the method needed further optimization as many false positives and false negatives were included in the first tests of this approach. Considering further features of the Gaussian mixture model, such as the distance between the closest Gaussian components in the 3 components model, helped to improve the accuracy of the detection. Importantly, angle measurement on automatically extracted movies for three different conditions resulted in similar angle distributions compared to the “ground truth” I had obtained by manually extracting events from the same data set, thus providing validation of the proposed method. The analysis method developed in this work could be useful for further screening using our spindle orientation model or for cell nuclei detection in packed cluster of cells in other experimental contexts.

METHODOLOGY ARTICLE

Open Access



Detection and tracking of overlapping cell nuclei for large scale mitosis analyses

Yingbo Li^{1,2†}, France Rose^{1†}, Florencia di Pietro², Xavier Morin² and Auguste Genovesio^{1*}

Abstract

Background: Cell culture on printed micropatterns slides combined with automated fluorescent microscopy allows for extraction of tens of thousands of videos of small isolated growing cell clusters. The analysis of such large dataset in space and time is of great interest to the community in order to identify factors involved in cell growth, cell division or tissue formation by testing multiples conditions. However, cells growing on a micropattern tend to be tightly packed and to overlap with each other. Consequently, image analysis of those large dynamic datasets with no possible human intervention has proven impossible using state of the art automated cell detection methods.

Results: Here, we propose a fully automated image analysis approach to estimate the number, the location and the shape of each cell nucleus, in clusters at high throughput. The method is based on a robust fit of Gaussian mixture models with two and three components on each frame followed by an analysis over time of the fitting residual and two other relevant features. We use it to identify with high precision the very first frame containing three cells. This allows in our case to measure a cell division angle on each video and to construct division angle distributions for each tested condition. We demonstrate the accuracy of our method by validating it against manual annotation on about 4000 videos of cell clusters.

Conclusions: The proposed approach enables the high throughput analysis of video sequences of isolated cell clusters obtained using micropatterns. It relies only on two parameters that can be set robustly as they reduce to the average cell size and intensity.

Keywords: Image analysis, Gaussian mixture, High throughput, Mitosis, Time-lapse microscopy, Cell detection

Background

Mitosis, the eukaryotes division, is a complex cellular process involving multiple proteins. In multicellular organisms, the precise orientation of cell divisions relative to their environment plays a crucial role in the development, growth, and homeostasis of many tissues [1]. For example, divisions within the plane of epithelial structures contribute to the expansion of the tissue surface and to the maintenance of the epithelial monolayer organization [2], while divisions perpendicular to the epithelial plane contribute to tissue stratification, binary fate decisions and regulation of stem cell pools [3, 4]. Defective control of spindle orientation may be a step in the transformation

process leading to cancer [5, 6]. In vertebrate cells, multiple molecular pathways contribute to spindle orientation in response to a variety of stimuli that include intrinsic cell polarity, adhesion to the extracellular matrix, and contacts with their neighbors [1]. Remarkably, these mechanisms are shared by cells grown in a culture dish, and in vitro studies in adherent cells have contributed a lot to our current understanding of spindle orientation.

The aim of the biological study, for which the following development was set, is to identify new regulators involved in the orientation of cell division through a mid-throughput RNAi screen in vitro. To this end, we have developed a specific model of oriented cell division between pairs of cells grown on adhesive micropatterned disks. The precise molecular design of this spindle orientation assay is beyond the scope of the current study and will be described elsewhere, in combination with the results of the RNAi screen (di Pietro et al. in preparation).

*Correspondence: auguste.genovesio@ens.fr

†Equal Contributors

¹Scientific Center for Computational Biology, Institut de Biologie de l'Ecole Normale Supérieure, CNRS-INSERM-ENS, PSL Research University, 46, rue d'Ulm, 75005 Paris, France

Full list of author information is available at the end of the article

Here, we present the image analysis approach that we designed with the aim to automatically 1) identify events of cell divisions and 2) measure their orientation relative to their neighbors. Cell culture on micro-patterned surfaces is increasingly used in cell and developmental biology studies using single [7–9], pairs [10], or larger groups of cells [11, 12], owing to the possibility that micropatterning offers to control numerous parameters of the cells environment and therefore reduce intercellular variability. Hence the proposed method for the first step can be generally useful to the parallel study of any event of interest arising in a growing cluster of cells.

Human cells (HeLa cells) genetically modified to express the H2B-mCherry chromosomal fluorescent reporter were seeded onto thousands of 30 μm diameter micropatterned disks coated with fibronectin [13] and imaged over 60 h every 7 min using fluorescence time-lapse microscopy. The honeycomb regular spacing of the adhesive fibronectin patterns, microprinted on a cytorepellent surface, enabled to obtain hundreds of isolated growing clusters of cells per condition (see Fig. 1).

The development of scripts to detect all pattern positions and extract all single cluster video sequences is fairly straightforward. The purpose of this paper is not to describe this process but rather how we resolved unexpected difficulties inherent to the large variety of cell cluster sequences we had to deal with in the next step of the process. We seek to detect, for each of those sequences, the precise time point when a cluster switches from two to three cells in order to measure the division

angle of the occurring division versus the axis formed by the previously existing two cells (see Fig. 2). Hence, only patterns with one cell or two cells at the beginning of the experiment are of interest; however the cell seeding process results in patterns without any cell (which can easily be discarded from the analysis), and patterns with more (3 or more) cells than required, which are therefore densely packed on the pattern. Despite the fact that this description sounds rather simple, in practice, we faced a variety of challenges (see Fig. 3) that made this operation intractable with the most advanced and popular cell detection methods currently available.

For low throughput microscopy image analysis, a variety of semi-automated methods were proposed and are currently largely used to detect cells [14]. By semi-automated we mean an imaging throughput that is low enough (a few images or videos) for manual intervention to help or correct the detection. An exhaustive description of those available semi-automatic methods is out of the scope of this paper. However, as soon as full automation is required because of the throughput, the number of concretely working methods shrink to a few and require the data to meet with some strong hypotheses. One of those hypotheses is that cells must contain a single nucleus [15]. Another important hypothesis that is often made is that nuclei can touch each other but should not overlap [16]. Eventually, the accurate monitoring of topological changes, that is tracking splitting objects over time, highly relies on the accuracy of the cell identification process at each time frame.

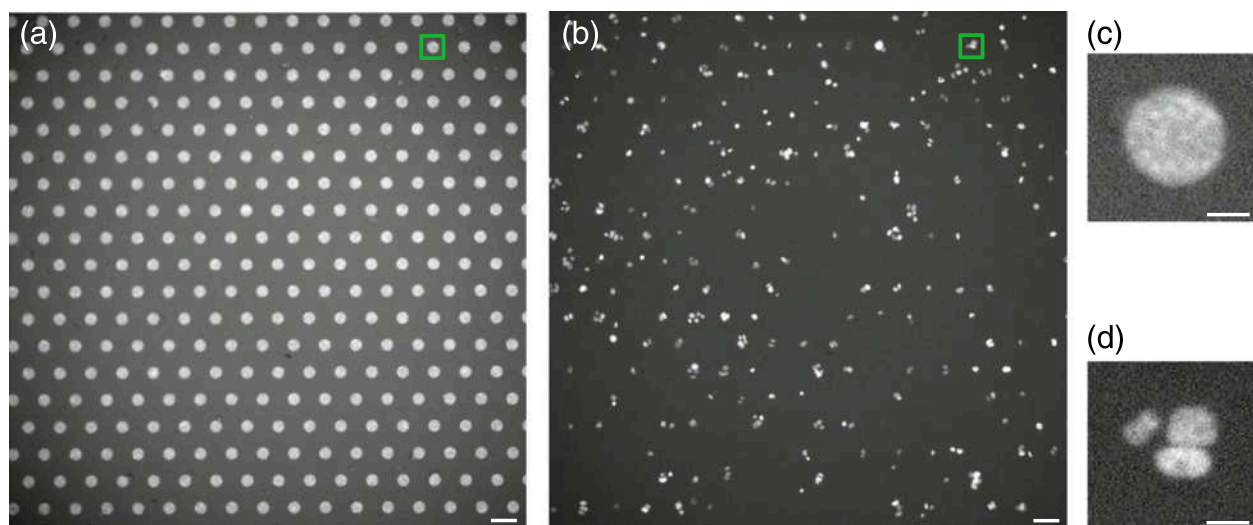


Fig. 1 Large series of cell cluster acquisitions using Fibronectin micro-patterns. **a** shows an image displaying all micro pattern positions of a given field of view. This image is captured once at the beginning of the sequence to locate cell patterns. **b** shows an acquisition of one time frame of the H2B-mCherry signal for the same field of view. This image contains the cell clusters. **c** shows one of the pattern position (corresponding to the green square on the top right of the field of view in image **a**) and **d** shows the corresponding cell cluster located on it. A movie is automatically extracted from each pattern positions containing cells. The thousands of movies extracted this way from multiple fields of view are then analyzed using the proposed method. Scalebars are 80 μm for **(a)** and **(b)** and 20 μm for **(c)** and **(d)**

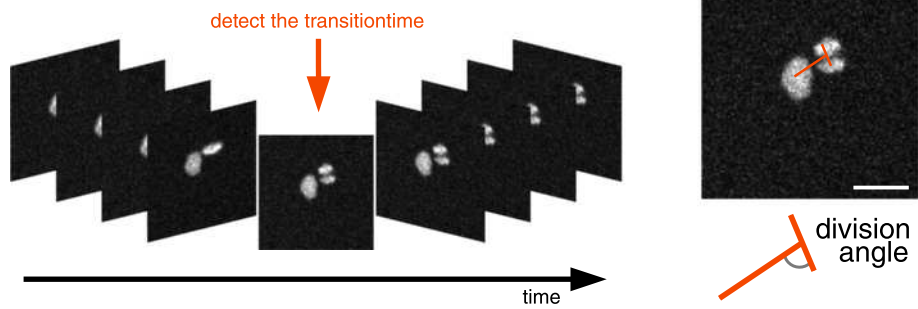


Fig. 2 Goal. Automated identification of the first frame containing three cells in the video and computation of the division angle on this frame. Scalebar is 20 μm

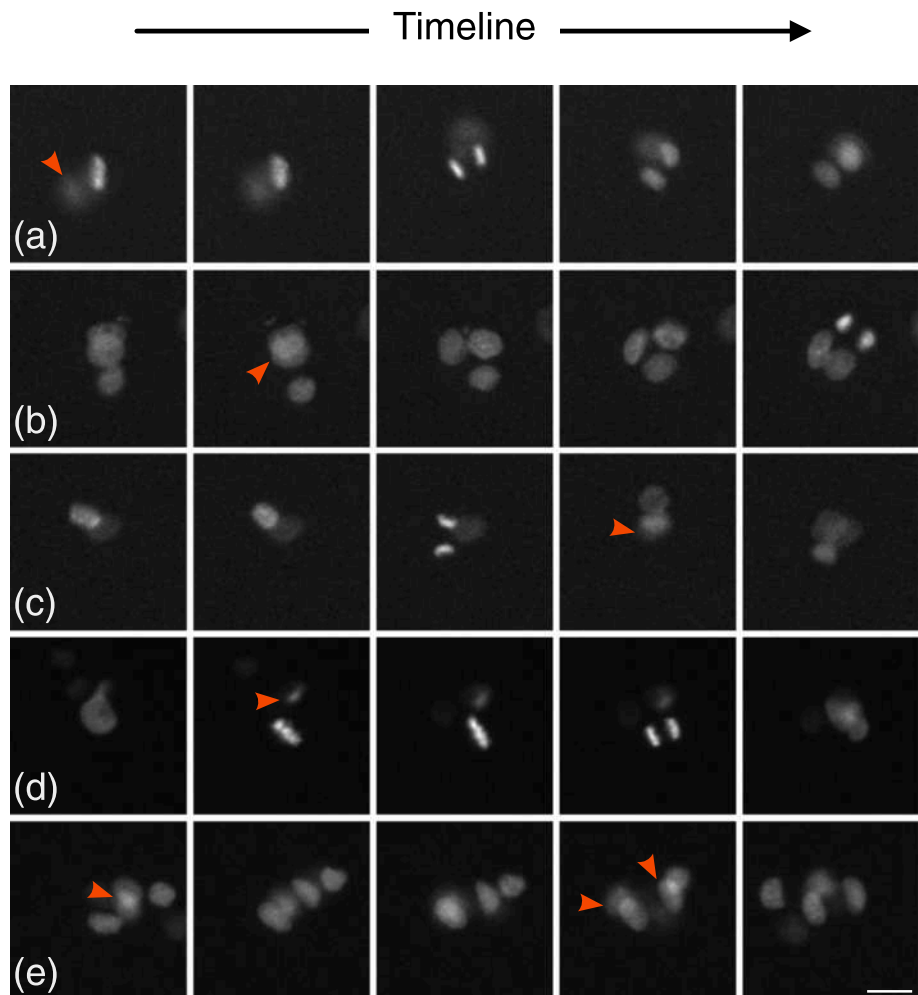


Fig. 3 Difficulties. Cell number and location in a packed cluster cannot be robustly assessed with known methods and even sometimes by human vision. Each row shows 5 consecutive frames of a video example that illustrates the variety of difficulties this assay presented. **a** a frequent case where one of the cell is out of focus, **(b)** another frequent case where cells are overlapping, **(c)** a case showing both overlapping and out of focus cells, **(d)** a case where a cell enters the field of view just before mitosis, **(e)** another case showing overlapping cells. Scalebar is 20 μm

Despite fruitful debates about the capabilities of levelset methods to uncover the topological changes in a group of objects to detect at low throughput [17], methods currently used at high throughput for cells detection are rarely based on those approaches because of their lack of robustness in a fully automated process. Instead, the cell detection relies most often on two steps: seed identification followed by segmentation [18–20]. The identification step consists in defining a seed for each object and the segmentation step consists in applying a region growing algorithm initialized by those seeds to uncover objects boundaries. An example of naive approach to seed detection is the local maxima detection after smoothing, which is heavily used at high throughput because of its simplicity, its speed and its robustness for many cell based applications. Regarding the detection step, seeded watershed and coupled explicit or implicit active contours can be used [21–24]. The former methods are currently common practice and proved to be very efficient in detecting millions of regular cells in monolayer where nuclei do not overlap [25] while the later are more rarely seen in practice because of their inherent instability. However the whole process depends primarily on the identification step. That is, the results tend to significantly degrade when nuclei overlap with one another and that seed cannot be correctly identified (see Fig. 3). This is precisely the problem we ran into while using micropatterns.

In the literature, those small fibronectin patterns have mostly been used for experiments with a single cell per pattern (a few exceptions with two cells or more do exist but the pattern makes the position of cells obvious and non overlapping [7, 10]). Moreover, most of the studies were not dynamic and focused on getting reproducible cell shape in order to quantify cytoskeleton organization [26]. Therefore, with a few exceptions, tracking cells on single micropatterns has not yet been an issue using this technology.

In our experiment, the chosen pattern is a disk and the number of cells growing onto them is variable and unknown. Furthermore, the pattern introduces physical constraints that tend to pack cells together as they are dividing, making their individual detection or even a simple counting often difficult (see Fig. 3). Indeed when more than two cells are present on a pattern, their shape differ from cells duplicating freely on an unbounded fibronectin slide. Consequently, nuclei shape and distances between nuclei are impacted. Furthermore, when clusters contain three or more cells, they often overlap with each other, making the detection intractable with previously cited methods. We therefore had to propose a new way to extract information from those packed clusters of cells.

In order to detect in each sequence the first frame showing three cells, our approach consisted in modeling the cell cluster by Gaussian Mixture Models. Hence, a selection

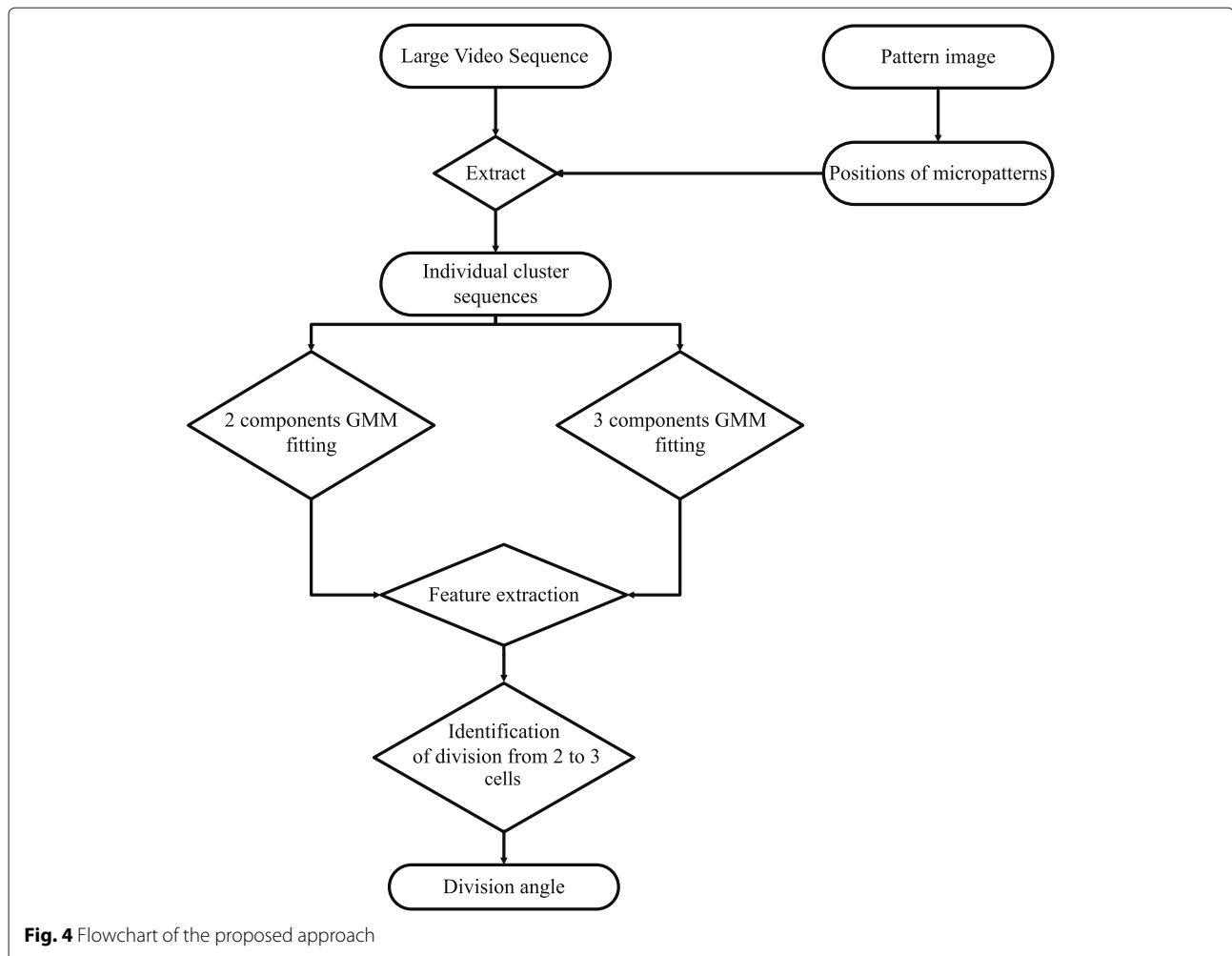
process based on the sequence would allow us to determine the number of cells and their positions at each frame. Since the event we were looking for in our study was the second mitosis (that is when one of the two cells divides in a cluster of two cells only), we proposed to fit two hypothesis models to the cell cluster at each time frame: a 2-component and a 3-component 2D Gaussian mixture models (GMM). Fitting a GMM to count and detect biological objects in microscopy images was proposed in the past mostly to model small fluorescent spots or on static images. Thomann et al. [27] used a 3D Gaussian model to approach the point spread function and detect the number of spots reaching super-resolution. A χ^2 test was then used to choose the right number of Gaussians in the Gaussian mixture. However, the number of degrees of freedom of the χ^2 test was defined as the number of pixels lying on the object (a few in the case of spots) which would be unrealistic in our case. Other methods are based on mutual information [28] or are dedicated to mitosis detection in histopathology images [29] but they gave poor results on our data because the cells are more densely packed on micropatterns. However, a close approach was proposed in [30] where numerous cells are tracked in 3D using GMM. The difference with our approach lies in the fact that because the throughput is much higher in our case, images could not be acquired in 3D. Therefore, unlike in 3D imaging, the view is incomplete and cells can overlap with each other and appear out of focus which are the major issues we had to deal with (see Fig. 3).

Method

The proposed approach is composed of four steps described in this section. The first step consists in localizing the fibronectin patterns and cropping the whole video at those locations to obtain individual cluster sequences, the second step consists in fitting 2- and 3-components Gaussian Mixture Model (GMM) onto each frame of each video sequence and the third step consists in the identification of the first frame containing three cells (the transition from 2 cells to 3 cells) using the fitting error difference and other features computed from the GMM parameters. The final step consists in the computation of the angle of division in the identified frame. The whole proposed approach is illustrated in Fig. 4 (and the code is freely available at <https://github.com/biocompibens/livespin>).

Extraction of individual sequences from a video

Figure 1 shows the pattern image obtained at the beginning of the sequence acquisition. Each bright area in the pattern image is a micropattern possibly containing an individual and isolated cell cluster. We name a cell cluster a set of cells close to each other that mostly originate from a single cell. Figure 1 also shows a random frame of the video sequence of the H2B-mCherry signal corresponding



to the same field of view. Each condition of a screen will be made of two such acquisitions. Since each cell cluster is independent from the other, we set up a system to automatically crop a window around each micropattern over time, thus producing one video sequence per micropattern with a possible cluster on it (see Fig. 1).

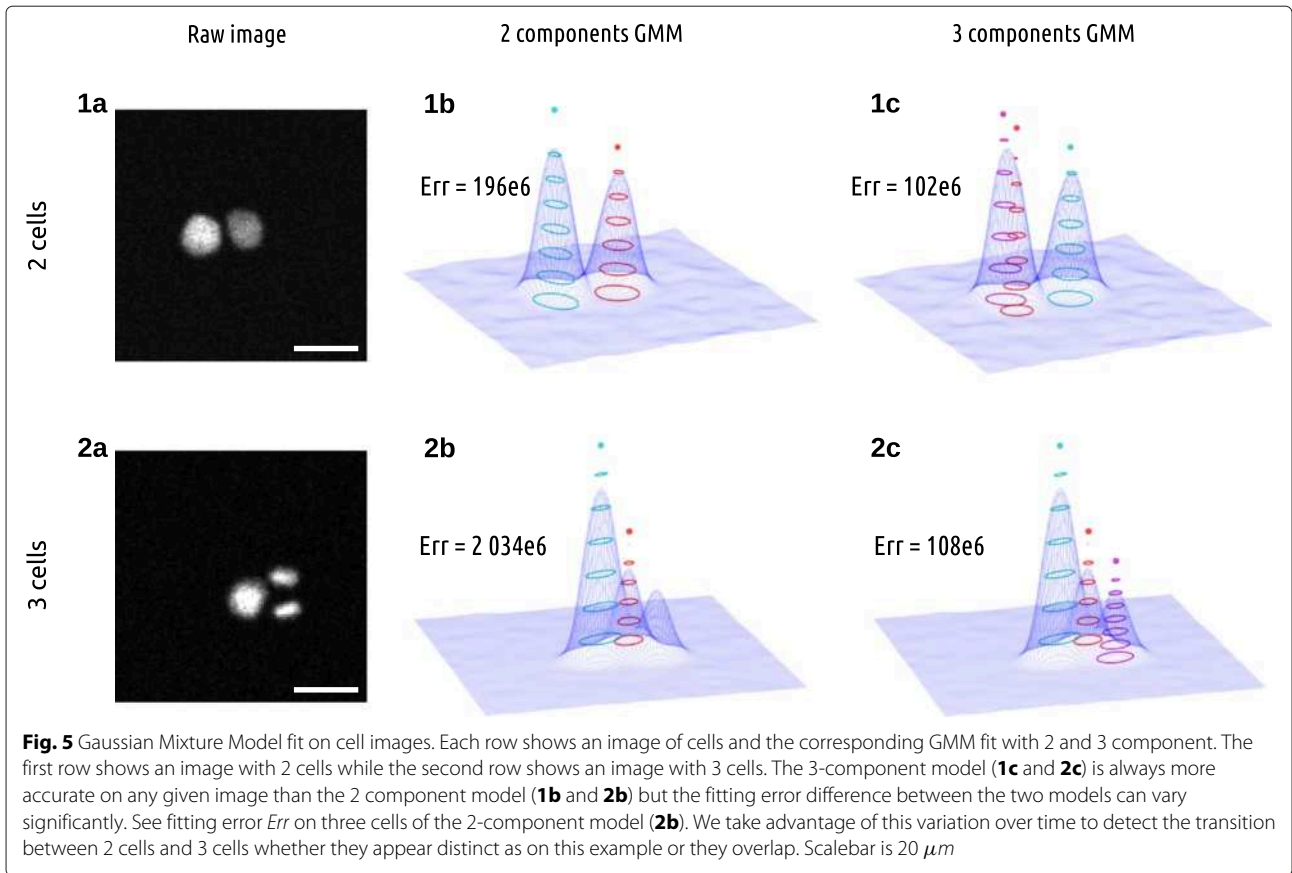
In order to take into account the illumination bias (on Fig. 1, intensity at the center of the image is brighter than around the borders) we applied an adaptive equalization of the histogram [31]. Once corrected, the pattern image is fairly easy to segment and a smoothing followed by a cropping around local maxima was sufficient to obtain hundreds of cropped movies, each containing one micropattern location as shown by Fig. 1. From this point, those movies could be analysed independently with the following proposed method.

Characterization of cell nuclei by Gaussian mixture model *GMM as a cell cluster model*

Nuclei of cells expressing H2B-mCherry and imaged via fluorescence microscope exhibit an ovoid structure which

can be approximated by a 2D Gaussian distribution of grey level intensity around its center, as shown in Fig. 5. Therefore, an image containing N cells could in principle be modelled reasonably well by a Gaussian mixture model (GMM) with at least N components. The final goal of the study is to measure the variation of the orientation of the cell division when a cluster goes from two to three cells. Thus our approach consists in comparing the relative quality of reconstruction of the observed cluster by two GMM models with two and three components. This would allow for resolution of both the number of cells and also their positions provided by the model.

In theory, whatever the signal, more components in a GMM leads to a better reconstruction. It is therefore not possible to directly compare the fitting residuals obtained by the two models as the 3-component model would always show a lower error. This model selection issue was discussed in general in the literature and universal criteria for model selection were proposed in the past as the Akaike Information Criterion (AIC) [32] or the Bayesian Information Criterion (BIC) [33]. Our experience using



those criteria independently at each time frame of the sequence led to a totally erroneous identification of the correct cell division frame. We therefore took a different approach as we describe further. However, prior to discussion on model selection, we describe how an accurate fit of the two GMM with two and three components could be achieved at high throughput: that is, on each of the 400 frames of each of the thousand individual movies of cluster we extracted.

Fitting the model to the data

The formulation of a 2D Gaussian mixture we used for fitting is the following:

$$f(\mathbf{x}, \Theta_K) = \sum_{k=1}^K w_k e^{-\frac{1}{2}(\mathbf{x}-\mu_k)'S_k^{-1}(\mathbf{x}-\mu_k)} \quad (1)$$

where K is the number of components of the mixture, w_k is a scalar value indicating the weight (or the intensity at the peak) of the component k , $\mu_k = (\mu(x), \mu(y))'$ is the 2D location of the component k in the plane and S_k is its covariance matrix that reads:

$$S_k = \begin{bmatrix} \sigma_1^2 & \sigma_{12} \\ \sigma_{12} & \sigma_2^2 \end{bmatrix} \quad (2)$$

So each component is fully characterized by a set of 6 parameters $P_k = \{w, \mu(x), \mu(y), \sigma_1, \sigma_2, \sigma_{12}\}$ and the concatenated set of parameters $\Theta_K = \{P_1, \dots, P_K\}$ fully characterizes a K components mixture. Following the two hypotheses model with two and three components we are interested in testing, we build GMMs with 12 or 18 parameters respectively. We use the Powell algorithm [34] to minimize the least-square residual between a frame image I and the K component GMM image model M_K that reads: $f_{err} = \sum_{x,y} [I(x,y) - M_K(x,y)]^2$.

Parameters initialization

One of the main difficulties in minimizing such a residual is that given the large number of parameters (12 or 18), the convergence toward the global minimum is not systematic. In order to ease this convergence, it is therefore crucial to set the initial parameters with values close to the optimal solution.

For the first image of the sequence, we take advantage of the fact that an average nucleus diameter \bar{d}_{nuc} and intensity \bar{w}_{nuc} can be easily estimated from the data. As \bar{d}_{nuc} can be modeled as the Full Width at Half Maximum [35], we first define a 2D Gaussian kernel with $\bar{\sigma}_{nuc} = \bar{d}_{nuc}/(2\sqrt{2\ln(2)})$. Local maximas are then detected on an image smoothed by this kernel and limited by a

foreground defined with the Otsu method [36]. Those local maximas are then used as initial values for Gaussian component locations. If the number of detected maximas is lower than the number of components of the model (e.g. when cells overlap), then additional random locations on the foreground are added. The intensity \bar{w}_{nuc} is directly used to initialize w . The remaining parameters σ_1 , σ_2 and σ_{12} are initialized with median values of a set of previously fitted GMM components with random initialization.

For the rest of the frames in the sequence, parameters are initialized with values obtained from the fitting at previous frames and from observations obtained from the current frame. In two consecutive frames with no mitotic event (that is in the large majority of the cases), the position, the intensity and the shape of the cells are not supposed to change much given the time interval between video frames (in video duration of 7 min). Therefore, the parameters μ and w could be initialized on the next frame by the values obtained for the same parameter at the last frame. This would read $\hat{\mu}_t = \mu_{t-1}$ and $\hat{w}_t = w_{t-1}$. However, in the case where mitosis happens, the location and the intensity of some of the cells suddenly change. To take into account this event, local maximas of the image are also precomputed on each image and the locations (resp. the intensity) of each component are initialized by a value half way between the location (resp. the intensity) obtained at the previous frame and the location (resp. the intensity) of the closest local maxima possibly detected on the current frame. This reads $\hat{\mu}_t = (\mu_{t-1} + \mu_t^D)/2$ and $\hat{w}_t = (w_{t-1} + I(\mu_t^D))/2$ where μ_t^D is the location of the closest detected maxima on frame t . This simple method ensures that the fitting process will be initialized a priori as close as possible from the optimal solution while it is not known if a mitotic event occurs or not.

Furthermore, we observed that while the shape of a nucleus is not changing much between two consecutive frames (except at a mitotic event time), on the contrary its orientation is quite dynamic (cells are often rotating). Therefore, we decided to uncouple the shape and the orientation of each component at each time frame in order to properly initialize the fitting process on the next frame for each of those parameters. In the formulation we use, shape and rotation are mixed into the covariance matrix. By diagonalizing the covariance matrix $S_{k,t-1}$ of each component k resulting from the previous frame we obtain λ_1 and λ_2 the eigenvalues corresponding respectively to the length of the major and the minor axes of the ellipse and the corresponding eigenvectors v_1 and v_2 from which the angle of the ellipse's major axis can be computed: $\theta_{k,t-1} = \arctan(v_1(y)/v_1(x))$.

When the nucleus rotates, solely the angle θ varies, not the shape represented by λ_1 and λ_2 . Therefore, we proposed an initialization of the angle to be a linear extrapolation of the two previous frames (constant speed rotation)

with $\delta_{k,t-1} = \theta_{k,t-1} - \theta_{k,t-2}$ leading to the following rotation matrix:

$$\hat{R}_{k,t} = \begin{bmatrix} \cos(\delta_{k,t-1}) & -\sin(\delta_{k,t-1}) \\ \sin(\delta_{k,t-1}) & \cos(\delta_{k,t-1}) \end{bmatrix} \quad (3)$$

Eventually, the covariance matrix containing the parameters $\hat{\sigma}_1$, $\hat{\sigma}_2$ and $\hat{\sigma}_{12}$ is initialized by rotating the covariance matrix obtained at previous frame the following way:

$$\hat{S}_{k,t} = \hat{R}_{k,t} S_{k,t-1} \hat{R}_{k,t}^{-1} \quad (4)$$

Constraints to ensure convergence

As our model includes 12 parameters in the case of 2 components and 18 parameters in the case of 3 components, even with a precise initialization the fitting process may diverge (e.g. one component may easily collapse or move outside the frame). We enforced the convergence by adding penalty terms to our error function.

The first penalty term concerns the locations μ_k of the Gaussian components. A reasonable hypothesis made on those locations is that they should lie onto the intensity foreground. Therefore, we computed a distance matrix D which is the size of the image. Each position of D maps to 0 inside the foreground and to the distance to the closest foreground pixel outside the foreground. In order to prevent the Gaussian components to move away from the foreground we use this matrix in the following penalty term that rapidly increases the error when a component location moves away from the foreground:

$$f_{\text{loc}} = \sum_{k=1}^K D(\mu_k)^2 \quad (5)$$

The second penalty term concerns the area of the nuclei that we know is about a given value $\bar{A}_{\text{nuc}} = \pi \bar{d}_{\text{nuc}}^2/4$ entirely defined by our prior estimation of \bar{d}_{nuc} . It ensures that the final area of the component represented by the determinant of the covariance matrix is not exaggeratedly different from this given area and it reads:

$$f_{\text{vol}} = \sum_{k=1}^K (|S_k| - \bar{A}_{\text{nuc}})^2 \quad (6)$$

The last penalty term concerns the intensity of the nucleus that should not collapse and that we know is about a previously defined \bar{w}_{nuc} . Indeed, we observe that without this term, one of the components could easily end up modeling the background. It reads:

$$f_{\text{int}} = \sum_{k=1}^K (w_k - \bar{w}_{\text{nuc}})^2 \quad (7)$$

The global error, now penalized by those terms, reads:

$$f_{\text{global}} = f_{\text{err}} \cdot (1 + f_{\text{loc}} + f_{\text{vol}} + f_{\text{int}}) \quad (8)$$

Note that each of those additional constraints prevents the optimization process to move toward absurd values by artificially increasing the total error outside an acceptable range. Therefore, they drastically modify the objective function outside an acceptable range of parameter values while they preserve the function within this range. The consequence is that they do not modify significantly the minimum of the function.

Time features computed from the GMMs

At this stage, large sets of data can be fully automatically processed by extracting all single pattern videos and automatically fitting a 2-component GMM and a 3-component GMM on each of their time frames. Two parameters only need to be set: the approximated nuclear diameter \bar{d}_{nuc} and intensity \bar{w}_{nuc} . Those values can be easily recovered.

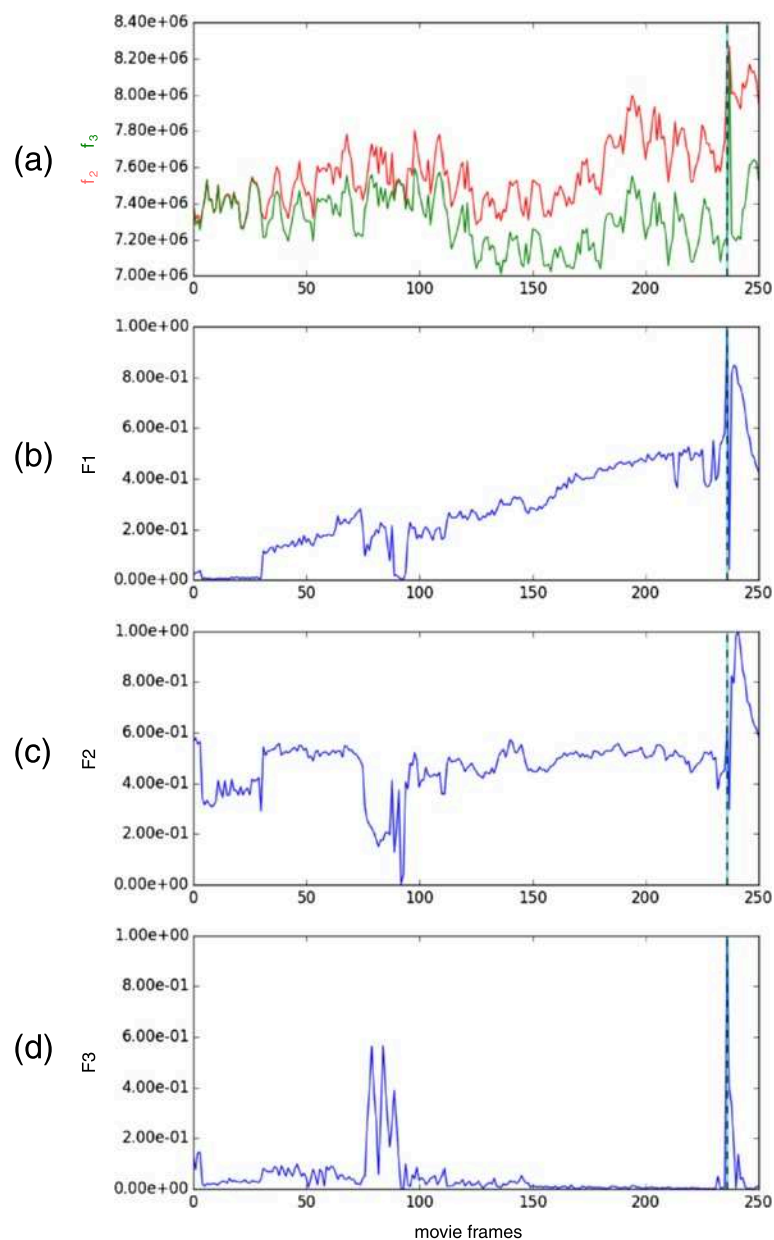


Fig. 6 Time features F_1 , F_2 and F_3 on an example video. The dashed vertical line indicates the event of interest we are seeking to identify when a third cell appears. **a** residual f_2 of the 2-component model in red, f_3 of the 3-component model in green and **(b)** F_1 , their ratio. **c** F_2 , the distance between the two closest centers of the 3-components model. **d** F_3 , the variance of the intensity values between the two closest centers of the 3-component model

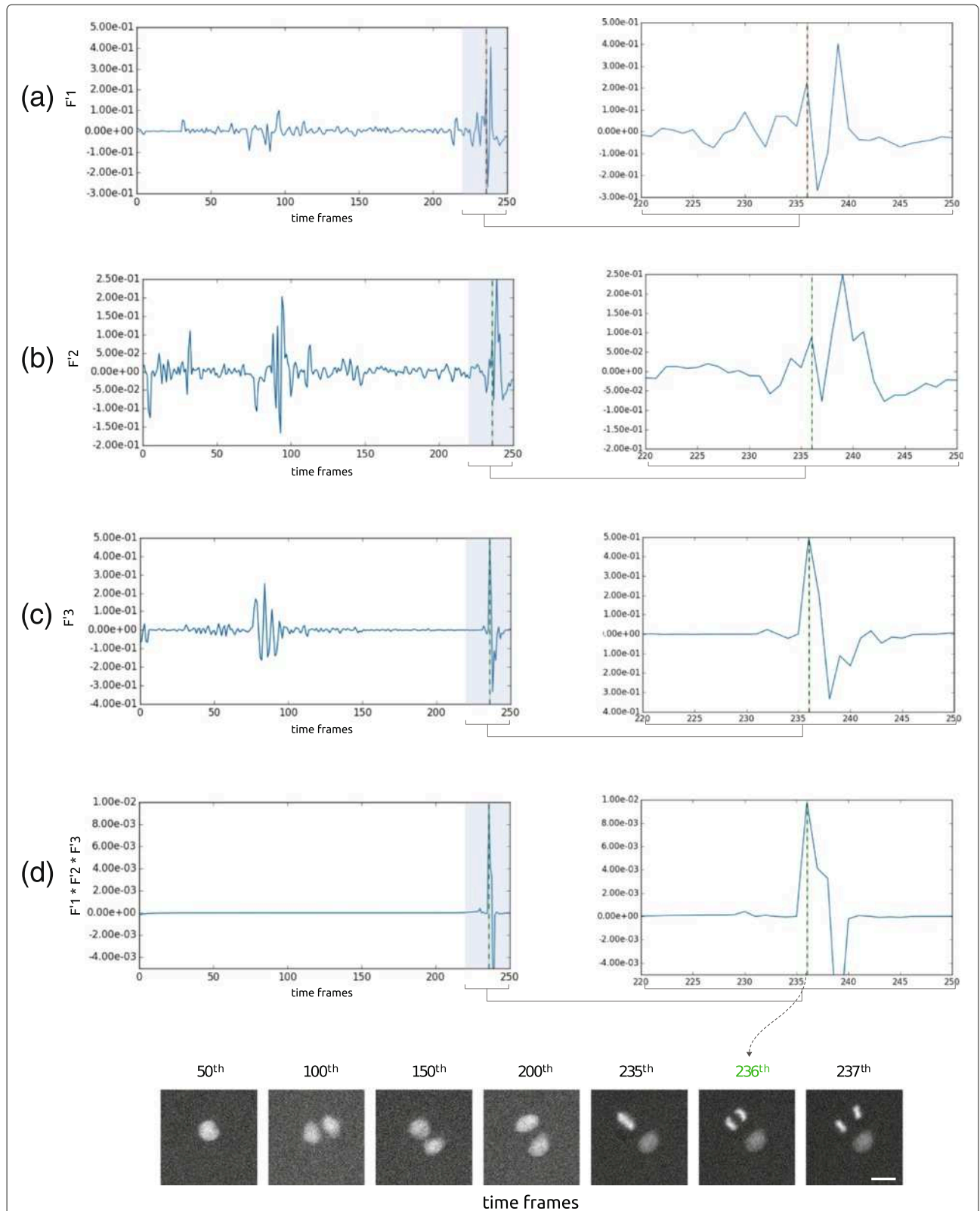


Fig. 7 Derivatives of the time features (corresponding to the example given in Fig. 6) (a) F_1 , (b) F_2 , (c) F_3 and (d) their product over time. The right panels are zooms in the peak region. A first clear peak of the feature derivatives product can be observed at the frame of interest. Scalebar is 20 μm

In order to identify the first frame onto which three cells can be observed (that is right at the second division) on each of those videos, we propose to compute the derivative over time of three features. Those features are the fitting error ratio between both models, the minimum distance between the three component centers and the variance of intensity between the closest component centers. None of those require any parameter and they are described below.

F₁: fitting error ratio

We are interested in finding a specific anaphase event: the first frame onto which three objects can clearly be identified (see Fig. 2). In theory, a GMM with three components (residual f_3) should always fit better to the signal than a GMM with two components (residual f_2). This is illustrated on a single image by Fig. 5 and on a whole sequence by Fig. 6a where f_3 is constantly lower than f_2 . However, our rationale is that the transition time from two to three nuclei will be the moment when the residual ratio between both GMM fitting suddenly becomes significantly higher. Such a pattern can be observed from the derivative over time of the residual ratio $F_1(t) = f_3(t)/f_2(t)$ across the entire sequence right when this event is happening (see Fig. 7a and b).

F₂: distance between the closest components

As shown in Fig. 6c, the distance between the two closest centers in the 3-component model $F_2(t) = \min\{\|\mu_i(t) - \mu_j(t)\|_2, \forall (i, j) \in \{1, 2, 3\}^2, i \neq j\}$ becomes much larger when the mitotic event of interest happens. This is because when a 3-component GMM is used to model two cells, one of the cells ends up being modeled by two components and therefore shows two very close centers. However, when one of the cells splits into two, the 3-component GMM correctly models the cluster, and each component matches a single cell. Consequently, the minimum distance between any two centers suddenly increases.

F₃: variance of intensity between the closest components

Along with the distance between the closest centers, the intensity variation of the pixels between those two closest centers also provides information. Indeed, if the variance is high, it denotes that both foreground and background pixels were considered in the calculation, while if the variance is low, it means that only foreground pixels were used. Therefore, this feature tends to measure whether or not the two closest components of a 3-component model are separated by some background or not and therefore if they model or not the same cell. The feature F_3 over time for an example cluster can be seen in Fig. 6d.

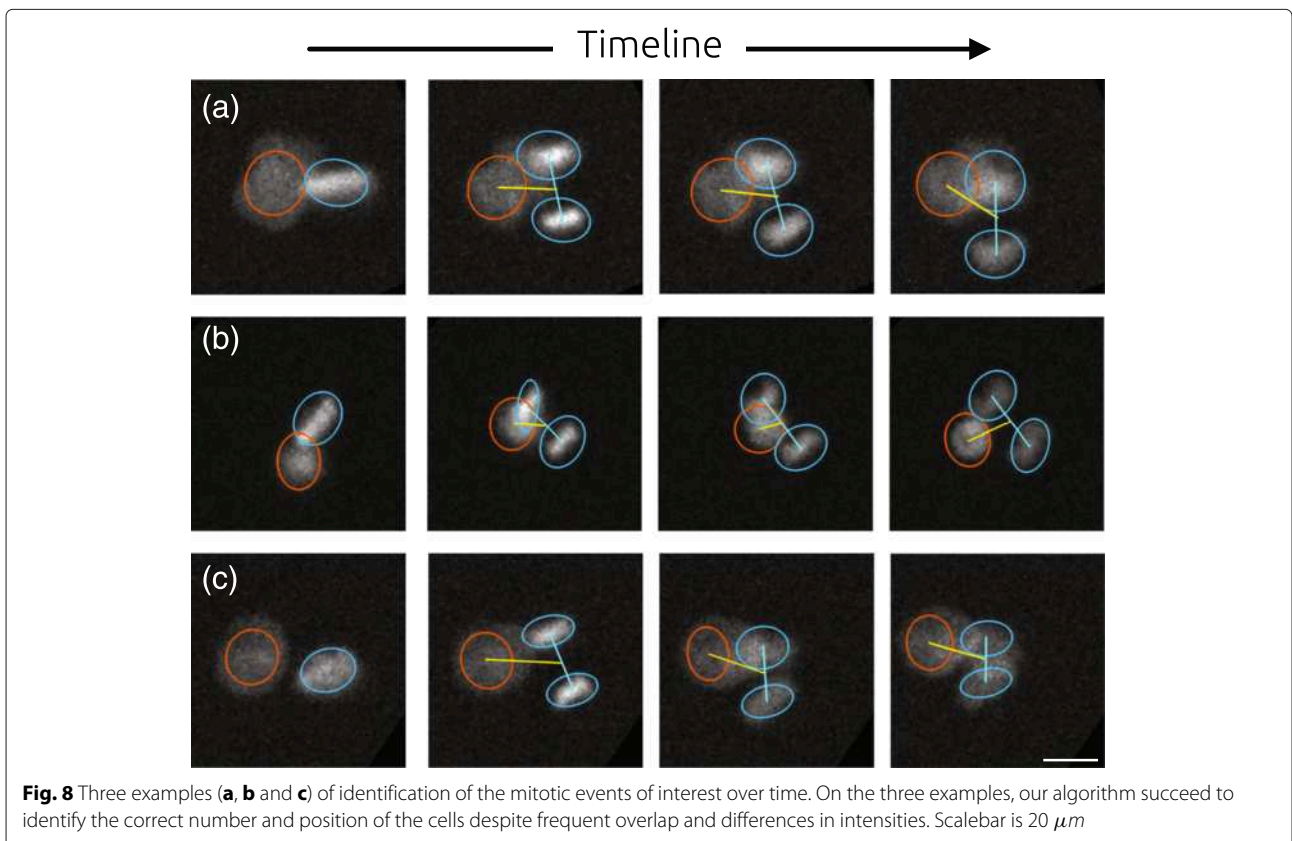


Fig. 8 Three examples (a, b and c) of identification of the mitotic events of interest over time. On the three examples, our algorithm succeed to identify the correct number and position of the cells despite frequent overlap and differences in intensities. Scalebar is 20 μm

Table 1 Pattern count on raw data (A and B), after a rough preprocessing step (C, D and E) to discard empty patterns or patterns containing obviously more than 2 cells on the first frame of the sequence. Eventually, the number of pattern where a transition from two to three cell was detected automatically (F) or manually (G). While a lower number of event is selected automatically, more than 80 % of the events selected automatically were also part of the manual selection whatever the experimental condition

	Cyclophilin siRNA	LGN siRNA	p62 siRNA
A) Total number of fields of view (=large videos)	4	5	6
B) Total number of micropatterns (=single cluster videos)	1116	1393	1668
C) Micropatterns with no cells (excluded)	400	607	719
D) Micropatterns with too many cells at time 0 (excluded)	51	64	120
E) Micropatterns with a low number of cells at time 0	665	722	829
F) Events selected automatically from (E)	122	135	97
G) Events selected manually	184	197	227
H) Proportion of (F) also in (G)	85.9 %	82.5 %	81.8 %

Identification of the division time of interest

In order to detect sudden changes over time using the features described above, we compute their derivatives. Hence we search for a sudden peak in those features' derivatives (see Fig. 7). In practice, there is a large variability of events we have to deal with when processing hundreds of videos of that kind. Using those three features simultaneously increases the ability of the approach to detect the division time of interest. We show on an example (see Fig. 7) and on a larger study (data not shown) that using the product of those features' derivatives over time allows to extract this event with a better accuracy than using only one or two of them.

Computation of the division angle

The method described above enables detection of the time of the first anaphase image on a movie with two cells. Detecting the right time is essential in order to measure the correct angle, because cells move and rotate from one time point to the next, especially when there are more than two cells on a pattern. Moreover cells can die or image acquisition can have started when three or more cells were already on the pattern. In those last cases, the error model would not fit. This allows us to exclude sequences where a division angle cannot be measured.

Once the right image is selected, the parameters of the fitting give the positions μ_k and sizes $|\mathcal{S}_k|$ of the corresponding underlying nuclei (see Fig. 5). From those

Table 2 The angle samples obtained from a manual selection or an automated analysis are similar: the null hypothesis of a KS test ("both samples come from the same angle distribution") cannot be rejected at a 10 % significance level

	Manual (M)		Automated (A)		(M) vs (A) KS-test <i>p</i> -value
	median	stdev	median	stdev	
Cyclophilin siRNA	23	30	31	31	0.229
LGN siRNA	71	26	72	25	0.620
p62 siRNA	62	28	54	30	0.246

measures, nuclei issued from the last division are chosen to be the two smallest Gaussian objects. Using those, the extraction of the angle described by the Fig. 2 is straightforward.

Results

To our knowledge, no available software could provide a full solution dedicated to the type of assay we propose (i.e. an automated tracking of overlapping cells on thousands of individual movies). Therefore, it was not possible to strictly compare our approach to another possibly existing method. However, a freely available software program that could have matched our need was Cellprofiler [25] because in principle, it enables the tracking of cells over time in a large set of image sequences, using the Hungarian algorithm. However, cell detection in Cellprofiler is based on a maxima detection followed by a seeded Watershed segmentation so we expected it not to perform well in detecting overlapping and dividing cells. In accordance, the results we obtained were dramatically poor. A quantitative comparison here would be meaningless, as almost no mitotic event could be identified this way. However, it was possible to compare our automated approach to a large set of data (4000 sequences) that has been exhaustively analyzed by a human tester, and considered thereafter as the "ground truth" for our method.

Experimental data

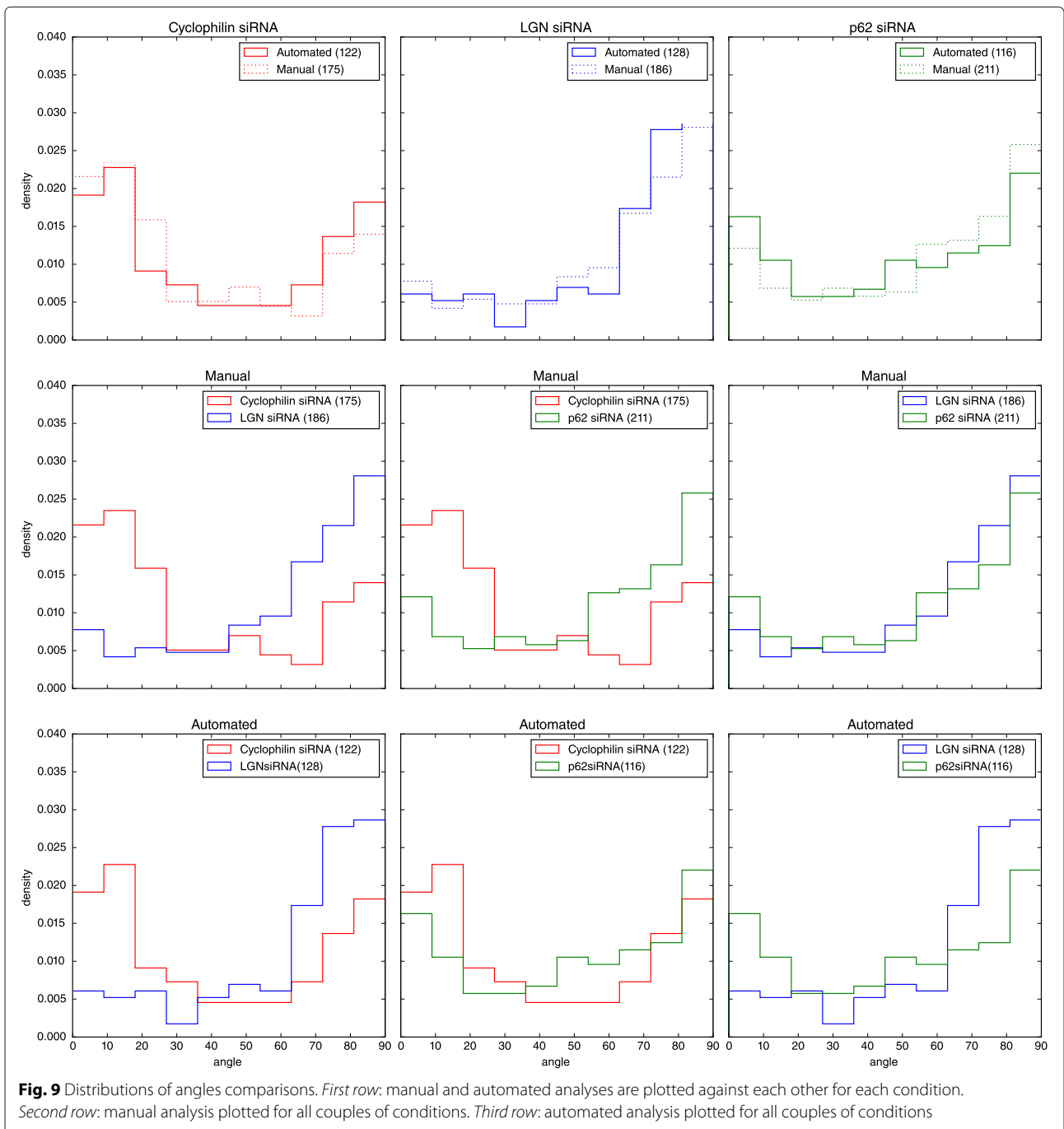
The dataset we created to validate the method is made of several videos of hundreds of cell divisions under

Table 3 The angle distributions obtained from a manual selection and an automated analysis reach similar conclusions: the null hypothesis of a KS test ("both samples come from the same angle distribution") is rejected for any two couple of conditions at a 10 % significance level

KS-test <i>p</i> -value	Cyclophilin siRNA vs LGN siRNA	Cyclophilin siRNA vs p62 siRNA	LGN siRNA vs p62 siRNA
	Manual	3.22e-15	9.47e-11
Automated	2.09e-07	1.65e-02	2.72e-04

three biological conditions. Those conditions are as follows: as a negative control, we used an siRNA targeting Cyclophilin, which is proposed as one of several standard negative controls by GE-Dharmacon in their ON-target+ human siRNA libraries. LGN (Leucine-Glycine-Asparagine repeat protein) was used as a positive control: LGN is an adaptor molecule involved in the localized recruitment of dynein motor complexes at the cell membrane, which direct forces exerted on astral microtubules.

LGN is a central regulator of spindle orientation in many animal cell types (reviewed in [1]). Our paired-cell assay (di Pietro et al, in preparation) is designed to specifically depend on the “LGN-complex” molecular cascade. siRNA against LGN therefore significantly alters spindle orientation in this assay. The third siRNA targets p62, which is part of the dynactin molecular complex and as such a candidate for the regulation of dynein activity and spindle orientation. It is therefore expected to differ significantly



from the negative control, and to yield results similar (but not necessarily identical) to the positive control. As we aim at using this method on a large set of conditions for which we will have a variation in the number of patterns we will obtain per condition, each condition for our test was respectively made of 4, 5 and 6 videos covering each field of view. Each field of view was made of about 250 frames of size 2048×2048 pixels. Figure 1 shows a frame of such a video captured by a wide field fluorescence microscope and containing about 280 patterns (excluding those touching the borders).

The fitting process is the most time-consuming step of the analysis. It takes 2 seconds for each image on a PC with Intel Core i7-4800MQ 2.7 GHz with 16 GB RAM. As analyzing one sequence requires to test two models on 250 frames, the overall process for one cluster containing cells takes 25 min. However, we used a computing cluster to process hundreds of cell clusters simultaneously.

Precision of the event detection

The dataset proposed was subject to a fully manual analysis on one hand and a fully automated analysis on the other hand. In both cases, the goal was to retrieve the sequences containing a transition from two to three cells and the exact time frame of this transition in order to measure the division angle. Figure 8 shows a few examples of those transition events automatically detected. Table 1 describes in detail the pattern and event count along the process. In summary, about 40 % of the pattern contained no cells, 10 % contained obviously too many cells at the beginning of the sequence to be processed further and 50 % were processed further using the proposed analysis to search for a possible transition from two to three cells. Eventually, the manual analysis identified that 15 % of the sequence contained a transition from two to three cells, while the automated analysis only found 10 %. Interestingly,

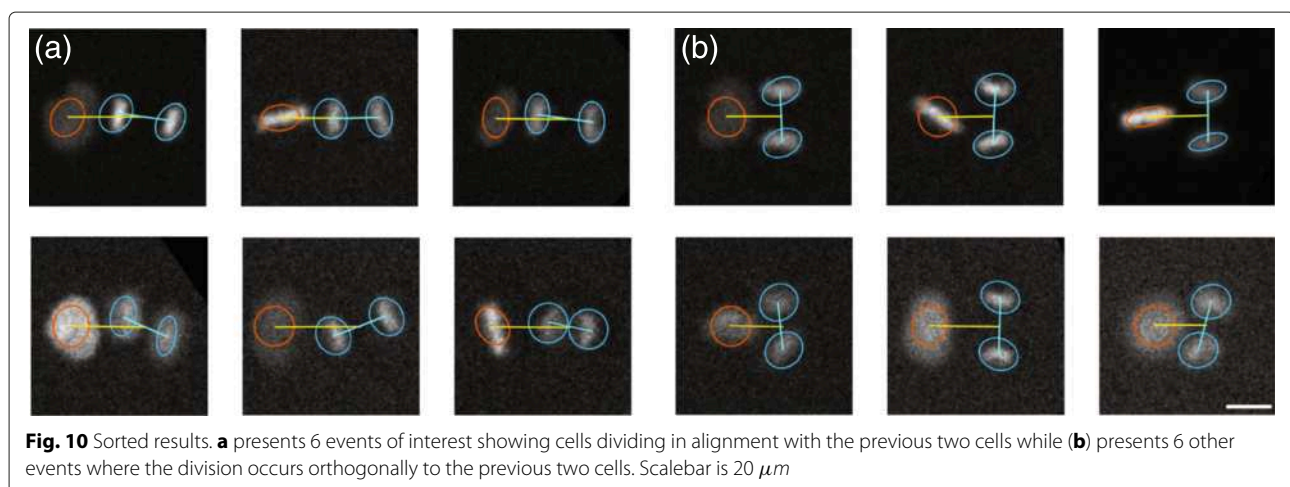
for any condition, at least 80 % of the events found automatically were also part of the event found manually (this could be called the precision as we are confident in our case that our manual analysis is very close to the ground truth). A tedious investigation of the differences between the manual and the automated analysis led to the conclusion that the automated method could sometimes fail in the case where some debris crossed the field of view, in case of dead cells or when two cells divided at the same time to produce four cells. Eventually, the event could also be missed when no clear significant peak arises in the derivative of the feature over time, due to extreme cases of simultaneous out of focus and overlapping.

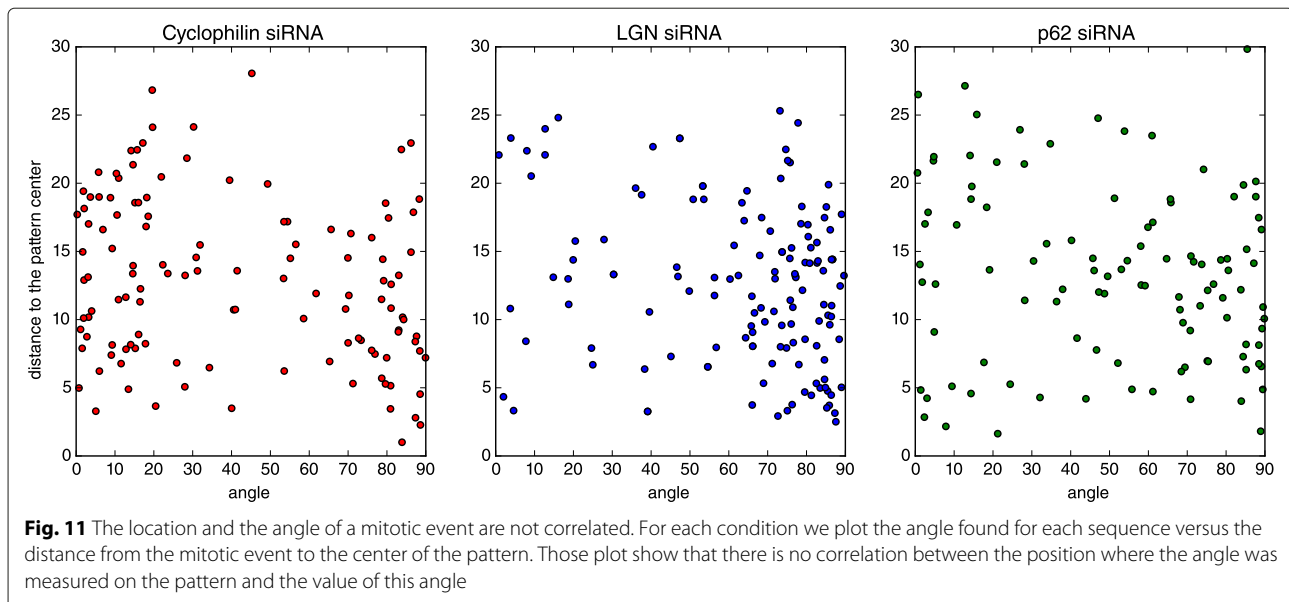
Accuracy of the angle distributions

Most importantly, whatever the error rate the algorithm or a human could make, we could assess here that both reach the same conclusion regarding the impact of a perturbation at a 10 % significance level. This can be observed on two statistical analyses. On one hand, in Table 2 a Kolmogorov-Smirnov test cannot reject the hypothesis of similarity between the angle distributions obtained manually and automatically for each condition. On the other hand, Table 3 shows that the comparison between any two pairs of conditions reaches also a similar conclusion: the similarity between distributions is systematically rejected. It should also be noted that while the difference between controls (Cyclophilin vs LGN) is still confirmed by the two approaches at a 5 % significance level, the automated analysis seems to remain less accurate than the manual one at detecting a more subtle change in the distribution produced by the siRNA against p62.

Discussion

In order to factor out some possible issues that may have occurred we performed additional tests.





Possible bias induced by the statistical test

Interestingly, Fig. 9 shows that the distributions of angles we obtained were not mono-modal or Gaussian-like as we may have expected, but rather bimodal (extreme case examples of those two phenotypes could be retrieved from the automated analysis, see Fig. 10). In order to take into account this, statistical tests known to be more sensitive to the sides of a distribution, such as the Anderson-Darling test, were also tried but they reached very similar conclusions (data not shown).

Possible bias produced by the pattern

As the pattern's edge forms a barrier and the pattern's size is in the order of the cell size, division is constrained. However, we investigated if there was any relation between the angle and the position of the cells on the pattern (e.g. are cells dividing closer to the edge more likely to divide orthogonally?). The Fig. 11 shows that the position on the pattern has no effect on the angle.

Conclusion

In this paper we proposed a high throughput method to automatically detect the transition of a cell cluster from two to three cells in thousands of videos. The proposed algorithm performs a robust implicit tracking of cells even when they are packed, overlap or are not clearly distinguishable. The approach is based on a robust fitting of two-dimensional Gaussian mixture models with two and three components on each frame of the video. We showed that the derivatives of the residual ratio between the two models, the distance between the two closest centers and the variation of intensity between them was sufficient to detect the exact time of an event of interest. We showed,

using three independent conditions, that the distributions of angles obtained automatically were very similar to those obtained through a very tedious manual annotation that took several days and would be impossible to concretely extend to hundreds of conditions. While the focus of our study was to monitor the division orientation, the same principle can easily be extended to many other questions through the calculation of other features obtained using the proposed approach.

Availability of data and materials

All code and data necessary to reproduce the results of this paper is freely available on GitHub

- **Project name:** livespin
- **Project home page:** <https://github.com/biocompibens/livespin>
- **Archived version:** <https://github.com/biocompibens/livespin.git>
- **Operating system(s):** Platform independent
- **Programming language:** Python
- **Other requirements:** Python 2.7
- **License:** GNU GPL 3.0

Competing interests

The authors declare that they have no competing interests.

Declarations

Publication charges for this article have been funded by Institut de Biologie de l'École Normale Supérieure.

Authors' contributions

XM conceived the high throughput experiment on mitotic division orientation. FDP made the experiments, acquired all the videos and annotated the data. FR and AG proposed the GMM approach, YL proposed additional features, FR and YL implemented the method. AG, FR and YL wrote the manuscript. All authors edited the manuscript. All authors read and approved the final manuscript.

Acknowledgements

We thank ANR-10-LABX-54 MEMO LIFE, ANR-11-IDEX-0001-02 PSL* Research University, ANR-12-LIVESPIN and ARC for funding, Felipe Delestro Matos for helping with the figure forming and Mary Ann Letellier for helpful comments on the manuscript. We acknowledge Léo Valon, for helpful discussions and his initial work at testing various methods to perform an automated analysis.

Author details

¹Scientific Center for Computational Biology, Institut de Biologie de l'Ecole Normale Supérieure, CNRS-INSERM-ENS, PSL Research University, 46, rue d'Ulm, 75005 Paris, France. ²Division cellulaire et neurogenèse, Institut de Biologie de l'Ecole Normale Supérieure, PSL Research University, 46, rue d'Ulm, 75005 Paris, France.

Received: 10 March 2016 Accepted: 9 April 2016

Published online: 26 April 2016

References

- Morin X, Bellaïche Y. Mitotic spindle orientation in asymmetric and symmetric cell divisions during animal development. *Dev Cell*. 2011;21(1):102–19. doi:10.1016/j.devcel.2011.06.012.
- Fleming ES, Zajac M, Moschenross DM, Montrose DC, Rosenberg DW, Cowan AE, Tirnauer JS. Planar spindle orientation and asymmetric cytokinesis in the mouse small intestine. *J Histochem Cytochem*. 2007;55(11):1173–1180.
- Williams SE, Beronja S, Pasolli HA, Fuchs E. Asymmetric cell divisions promote Notch-dependent epidermal differentiation. *Nature*. 2011;470(7334):353–8.
- Quyn AJ, Appleton PL, Carey FA, Steele RJ, Barker N, Clevers H, Ridgway RA, Sansom OJ, Nathke IS. Spindle orientation bias in gut epithelial stem cell compartments is lost in precancerous tissue. *Cell Stem Cell*. 2010;6(2):175–81.
- Noatynska A, Gotta M, Meraldi P. Mitotic spindle (dis) orientation and disease: cause or consequence? *J Cell Biol*. 2012;199(7):1025–1035.
- Pease JC, Tirnauer JS. Mitotic spindle misorientation in cancer—out of alignment and into the fire. *J Cell Sci*. 2011;124(Pt 7):1007–1016.
- They M, Racine V, Pepin A, Piel M, Chen Y, Sibarita JB, Bornens M. The extracellular matrix guides the orientation of the cell division axis. *Nat Cell Biol*. 2005;7(10):947–53.
- Saadaoui M, Machicoane M, di Pietro F, Etoc F, Echard A, Morin X. Dlg1 controls planar spindle orientation in the neuroepithelium through direct interaction with LGN. *J Cell Biol*. 2014;206(6):707–17.
- They M, Jimenez-Dalmaroni A, Racine V, Bornens M, Julicher F. Experimental and theoretical study of mitotic spindle orientation. *Nature*. 2007;447(7143):493–6.
- Tsong Q, Duchemin-Pelletier E, Deshiere A, Balland M, Guillou H, Filhol O, Théry M. Spatial organization of the extracellular matrix regulates cell–cell junction positioning. *Proc Natl Acad Sci*. 2012;109(5):1506–1511.
- Dupin I, Sakamoto Y, Etienne-Manneville S. Cytoplasmic intermediate filaments mediate actin-driven positioning of the nucleus. *J Cell Sci*. 2011;124(Pt 6):865–72.
- Warmflash A, Sorre B, Etoc F, Siggia ED, Brivanlou AH. A method to recapitulate early embryonic spatial patterning in human embryonic stem cells. *Nat Methods*. 2014;11(8):847–54.
- Degot S, Auzan M, Chapuis V, Béghin A, Chadeyras A, Nelep C, Calvo-Muñoz ML, Young J, Chatelain F, Fuchs A. Improved visualization and quantitative analysis of drug effects using micropatterned cells. *J Vis Exp*. 2010;46. doi:10.3791/2514.
- Meijering E. Cell segmentation: 50 years down the road [life sciences]. *IEEE Signal Proc Mag*. 2012;29(5):140–5.
- Wählby C, Lindblad J, Vondrus M, Bengtsson E, Björkstén L. Algorithms for cytoplasm segmentation of fluorescence labelled cells. *Anal Cell Pathol*. 2002;24(2–3):101–11.
- Mathew B, Schmitz A, Muñoz-Descalzo S, Ansari N, Pampaloni F, Stelzer EH, Fischer SC. Robust and automated three-dimensional segmentation of densely packed cell nuclei in different biological specimens with lines-of-sight decomposition. *BMC Bioinforma*. 2015;16(1):187.
- McInemey T, Terzopoulos D. Topology adaptive deformable surfaces for medical image volume segmentation. *IEEE Trans Med Imaging*. 1999;18(10):840–50.
- Gauch JM. Image segmentation and analysis via multiscale gradient watershed hierarchies. *IEEE Trans Image Process*. 1999;8(1):69–79.
- Meyer F, Beucher S. Morphological segmentation. *J Vis Commun Image Represent*. 1990;1(1):21–46.
- Yang F, Mackey MA, Ianzini F, Gallardo G, Sonka M. Cell segmentation, tracking, and mitosis detection using temporal context. *Med Image Comput Comput Assist Interv*. 2005;8(Pt 1):302–9.
- Lindblad J, Wählby C, Bengtsson E, Zaltsman A. Image analysis for automatic segmentation of cytoplasm and classification of rac1 activation. *Cytometry Part A*. 2004;57(1):22–33.
- Jones TR, Carpenter A, Golland P. Voronoi-based segmentation of cells on image manifolds. In: *Proceeding CVBIA'05 Proceedings of the First international conference on Computer Vision for Biomedical Image Applications*; 2005. p. 535–43.
- Zimmer C, Olivo-Marín JC. Coupled parametric active contours. *IEEE Trans Pattern Anal Mach Intell*. 2005;27(11):1838–1842. doi:10.1109/TPAMI.2005.214.
- Zhang B, Zimmer C, Olivo-Marín JC. Tracking fluorescent cells with coupled geometric active contours. In: *Biomedical Imaging: Nano to Macro, 2004. IEEE International Symposium on*; 2004. Vol. 1. p. 476–9. doi:10.1109/ISBI.2004.1398578.
- Kamentsky L, Jones TR, Fraser A, Bray MA, Logan DJ, Madden KL, Ljosa V, Rueden C, Eliceiri KW, Carpenter AE. Improved structure, function and compatibility for cellprofiler: modular high-throughput image analysis software. *Bioinformatics*. 2011;27(8):1179–1180.
- Duong T, Goud B, Schauer K. Closed-form density-based framework for automatic detection of cellular morphology changes. *Proc Natl Acad Sci*. 2012;109(22):8382–387.
- Thomann D, Rines DR, Sorger PK, Danuser G. Automatic fluorescent tag detection in 3D with super-resolution: application to the analysis of chromosome movement. *J Microsc*. 2002;208(Pt 1):49–64.
- Yang ZR, Zwolinski MSM. Mutual Information Theory for Adaptive Mixture Models. *IEEE Trans Pattern Anal Mach Intell*. 2001;23(4):396–403.
- Khan AM, ElDaly H, Rajpoot N. A gamma-gaussian mixture model for detection of mitotic cells in breast cancer histopathology images. *J Pathol Inform*. 2013;4:11. doi:10.4103/2153-3539.112696.
- Amat F, Lemon W, Mossing DP, McDole K, Wan Y, Branson K, Myers EW, Keller PJ. Fast, accurate reconstruction of cell lineages from large-scale fluorescence microscopy data. *Nat Methods*. 2014;11(9):951–8.
- Stark JA. Adaptive image contrast enhancement using generalizations of histogram equalization. *IEEE Trans Image Process*. 2000;9(5):889–96.
- Akaike H. A new look at the statistical model identification. *IEEE Trans Autom Control*. 1974;19(6):716–23. doi:10.1109/TAC.1974.1100705.
- Schwarz G. Estimating the dimension of a model. *Ann Statist*. 1978;6(2):461–4. doi:10.1214/aos/1176344136.
- Powell MJ. An efficient method for finding the minimum of a function of several variables without calculating derivatives. *Comput J*. 1964;7(2):155–162.
- Weisstein EW. Full width at half maximum. *MathWorld—A Wolfram Web Resource*. <http://mathworld.wolfram.com/FullWidthatHalfMaximum.html>.
- Otsu N. A threshold selection method from Gray-level histograms. *IEEE Trans Syst Man Cybern*. 1979;9(1):62–6. doi:10.1109/tsmc.1979.4310076.

REFERENCES

- Afshar, K., Willard, F.S., Colombo, K., Johnston, C.A., McCudden, C.R., Siderovski, D.P., and Gonczy, P. (2004). RIC-8 is required for GPR-1/2-dependent Galpha function during asymmetric division of *C. elegans* embryos. *Cell* *119*, 219-230.
- Almonacid, M., Terret, M.E., and Verlhac, M.H. (2014). Actin-based spindle positioning: new insights from female gametes. *J Cell Sci* *127*, 477-483.
- Applegate, K.T., Besson, S., Matov, A., Bagonis, M.H., Jaqaman, K., and Danuser, G. (2011). plusTipTracker: Quantitative image analysis software for the measurement of microtubule dynamics. *Journal of structural biology* *176*, 168-184.
- Arbeille, E., Reynaud, F., Sanyas, I., Bozon, M., Kindbeiter, K., Causeret, F., Pierani, A., Falk, J., Moret, F., and Castellani, V. (2015). Cerebrospinal fluid-derived Semaphorin3B orients neuroepithelial cell divisions in the apicobasal axis. *Nat Commun* *6*, 6366.
- Arquint, C., and Nigg, E.A. (2014). STIL microcephaly mutations interfere with APC/C-mediated degradation and cause centriole amplification. *Curr Biol* *24*, 351-360.
- Ayloo, S., Lazarus, J.E., Dodda, A., Tokito, M., Ostap, E.M., and Holzbaur, E.L. (2014). Dynactin functions as both a dynamic tether and brake during dynein-driven motility. *Nat Commun* *5*, 4807.
- Azoury, J., Lee, K.W., Georget, V., Hikal, P., and Verlhac, M.H. (2011). Symmetry breaking in mouse oocytes requires transient F-actin meshwork destabilization. *Development* *138*, 2903-2908.
- Azoury, J., Lee, K.W., Georget, V., Rassinier, P., Leader, B., and Verlhac, M.H. (2008). Spindle positioning in mouse oocytes relies on a dynamic meshwork of actin filaments. *Curr Biol* *18*, 1514-1519.
- Baena-Lopez, L.A., Baonza, A., and Garcia-Bellido, A. (2005). The orientation of cell divisions determines the shape of *Drosophila* organs. *Curr Biol* *15*, 1640-1644.
- Bartolini, F., Ramalingam, N., and Gundersen, G.G. (2012). Actin-capping protein promotes microtubule stability by antagonizing the actin activity of mDia1. *Molecular biology of the cell* *23*, 4032-4040.
- Bearer, E.L. (1991). Direct observation of actin filament severing by gelsolin and binding by gCap39 and CapZ. *J Cell Biol* *115*, 1629-1638.
- Bellaiche, Y., Radovic, A., Woods, D.F., Hough, C.D., Parmentier, M.L., O'Kane, C.J., Bryant, P.J., and Schweisguth, F. (2001). The Partner of Inscuteable/Discs-large complex is required to establish planar polarity during asymmetric cell division in *Drosophila*. *Cell* *106*, 355-366.
- Bergstralh, D.T., Lovegrove, H.E., Kujawiak, I., Dawney, N.S., Zhu, J., Cooper, S., Zhang, R., and St Johnston, D. (2016). Pins is not required for spindle orientation in the *Drosophila* wing disc. *Development* *143*, 2573-2581.
- Bergstralh, D.T., Lovegrove, H.E., and St Johnston, D. (2013). Discs large links spindle orientation to apical-basal polarity in *Drosophila* epithelia. *Curr Biol* *23*, 1707-1712.
- Bergstralh, D.T., Lovegrove, H.E., and St Johnston, D. (2015). Lateral adhesion drives reintegration of misplaced cells into epithelial monolayers. *Nat Cell Biol* *17*, 1497-1503.
- Betschinger, J., Mechtler, K., and Knoblich, J.A. (2006). Asymmetric segregation of the tumor suppressor brat regulates self-renewal in *Drosophila* neural stem cells. *Cell* *124*, 1241-1253.
- Bhabha, G., Johnson, G.T., Schroeder, C.M., and Vale, R.D. (2016). How Dynein Moves Along Microtubules. *Trends Biochem Sci* *41*, 94-105.

- Borisy, G.G., and Svitkina, T.M. (2000). Actin machinery: pushing the envelope. *Curr Opin Cell Biol* 12, 104-112.
- Bosveld, F., Markova, O., Guirao, B., Martin, C., Wang, Z., Pierre, A., Balakireva, M., Gaugue, I., Ainslie, A., Christophorou, N., *et al.* (2016). Epithelial tricellular junctions act as interphase cell shape sensors to orient mitosis. *Nature* 530, 495-498.
- Bouissou, A., Verollet, C., de Forges, H., Haren, L., Bellaiche, Y., Perez, F., Merdes, A., and Raynaud-Messina, B. (2014). gamma-Tubulin Ring Complexes and EB1 play antagonistic roles in microtubule dynamics and spindle positioning. *Embo J* 33, 114-128.
- Bowman, S.K., Neumuller, R.A., Novatchkova, M., Du, Q., and Knoblich, J.A. (2006). The Drosophila NuMA Homolog Mud regulates spindle orientation in asymmetric cell division. *Dev Cell* 10, 731-742.
- Bradshaw, N.J., Hennah, W., and Soares, D.C. (2013). NDE1 and NDEL1: twin neurodevelopmental proteins with similar 'nature' but different 'nurture'. *Biomolecular concepts* 4, 447-464.
- Bremner, K.H., Scherer, J., Yi, J., Vershinin, M., Gross, S.P., and Vallee, R.B. (2009). Adenovirus transport via direct interaction of cytoplasmic dynein with the viral capsid hexon subunit. *Cell host & microbe* 6, 523-535.
- Burgess, S.A., Walker, M.L., Sakakibara, H., Knight, P.J., and Oiwa, K. (2003). Dynein structure and power stroke. *Nature* 421, 715-718.
- Busson, S., Dujardin, D., Moreau, A., Dompierre, J., and De Mey, J.R. (1998). Dynein and dynactin are localized to astral microtubules and at cortical sites in mitotic epithelial cells. *Curr Biol* 8, 541-544.
- Cabernard, C., and Doe, C.Q. (2009). Apical/basal spindle orientation is required for neuroblast homeostasis and neuronal differentiation in Drosophila. *Dev Cell* 17, 134-141.
- Cadart, C., Zlotek-Zlotkiewicz, E., Le Berre, M., Piel, M., and Matthews, H.K. (2014). Exploring the function of cell shape and size during mitosis. *Dev Cell* 29, 159-169.
- Campinho, P., Behrndt, M., Ranft, J., Risler, T., Minc, N., and Heisenberg, C.P. (2013). Tension-oriented cell divisions limit anisotropic tissue tension in epithelial spreading during zebrafish epiboly. *Nat Cell Biol* 15, 1405-1414.
- Capalbo, L., D'Avino, P.P., Archambault, V., and Glover, D.M. (2011). Rab5 GTPase controls chromosome alignment through Lamin disassembly and relocation of the NuMA-like protein Mud to the poles during mitosis. *Proc Natl Acad Sci U S A* 108, 17343-17348.
- Carlier, M.F., and Pantaloni, D. (1997). Control of actin dynamics in cell motility. *J Mol Biol* 269, 459-467.
- Carminati, M., Gallini, S., Pirovano, L., Alfieri, A., Bisi, S., and Mapelli, M. (2016). Concomitant binding of Afadin to LGN and F-actin directs planar spindle orientation. *Nature structural & molecular biology* 23, 155-163.
- Carreno, S., Kouranti, I., Glusman, E.S., Fuller, M.T., Echard, A., and Payre, F. (2008). Moesin and its activating kinase Slik are required for cortical stability and microtubule organization in mitotic cells. *J Cell Biol* 180, 739-746.
- Carter, A.P., Cho, C., Jin, L., and Vale, R.D. (2011). Crystal structure of the dynein motor domain. *Science* 331, 1159-1165.
- Carter, A.P., Garbarino, J.E., Wilson-Kubalek, E.M., Shipley, W.E., Cho, C., Milligan, R.A., Vale, R.D., and Gibbons, I.R. (2008). Structure and functional role of dynein's microtubule-binding domain. *Science* 322, 1691-1695.
- Casella, J.F., Craig, S.W., Maack, D.J., and Brown, A.E. (1987). Cap Z(36/32), a barbed end actin-capping protein, is a component of the Z-line of skeletal muscle. *J Cell Biol* 105, 371-379.
- Castanon, I., Abrami, L., Holtzer, L., Heisenberg, C.P., van der Goot, F.G., and Gonzalez-Gaitan, M. (2013). Anthrax toxin receptor 2a controls mitotic spindle positioning. *Nat Cell Biol* 15, 28-39.

- Caussinus, E., and Gonzalez, C. (2005). Induction of tumor growth by altered stem-cell asymmetric division in *Drosophila melanogaster*. *Nat Genet* *37*, 1125-1129.
- Chaigne, A., Campillo, C., Gov, N.S., Voituriez, R., Azoury, J., Umana-Diaz, C., Almonacid, M., Queguiner, I., Nassoy, P., Sykes, C., *et al.* (2013). A soft cortex is essential for asymmetric spindle positioning in mouse oocytes. *Nat Cell Biol* *15*, 958-966.
- Chan, Y.W., Fava, L.L., Uldschmid, A., Schmitz, M.H., Gerlich, D.W., Nigg, E.A., and Santamaria, A. (2009). Mitotic control of kinetochore-associated dynein and spindle orientation by human Spindly. *J Cell Biol* *185*, 859-874.
- Chang, W., Dynek, J.N., and Smith, S. (2005). NuMA is a major acceptor of poly(ADP-ribosyl)ation by tankyrase 1 in mitosis. *Biochem J* *391*, 177-184.
- Chen, C.T., Hehnlly, H., Yu, Q., Farkas, D., Zheng, G., Redick, S.D., Hung, H.F., Samtani, R., Jurczyk, A., Akbarian, S., *et al.* (2014). A unique set of centrosome proteins requires pericentrin for spindle-pole localization and spindle orientation. *Curr Biol* *24*, 2327-2334.
- Chenn, A., and McConnell, S.K. (1995). Cleavage orientation and the asymmetric inheritance of Notch1 immunoreactivity in mammalian neurogenesis. *Cell* *82*, 631-641.
- Cheong, F.K., Feng, L., Sarkeshik, A., Yates, J.R., 3rd, and Schroer, T.A. (2014). Dynactin integrity depends upon direct binding of dynamitin to Arp1. *Molecular biology of the cell* *25*, 2171-2180.
- Cho, C., Reck-Peterson, S.L., and Vale, R.D. (2008). Regulatory ATPase sites of cytoplasmic dynein affect processivity and force generation. *J Biol Chem* *283*, 25839-25845.
- Choksi, S.P., Southall, T.D., Bossing, T., Edoff, K., de Wit, E., Fischer, B.E., van Steensel, B., Micklem, G., and Brand, A.H. (2006). Prospero acts as a binary switch between self-renewal and differentiation in *Drosophila* neural stem cells. *Dev Cell* *11*, 775-789.
- Chowdhury, S., Ketcham, S.A., Schroer, T.A., and Lander, G.C. (2015). Structural organization of the dynein-dynactin complex bound to microtubules. *Nature structural & molecular biology* *22*, 345-347.
- Clark, A.G., Dierkes, K., and Paluch, E.K. (2013). Monitoring actin cortex thickness in live cells. *Biophys J* *105*, 570-580.
- Clark, S.W., Staub, O., Clark, I.B., Holzbaur, E.L., Paschal, B.M., Vallee, R.B., and Meyer, D.I. (1994). Beta-centractin: characterization and distribution of a new member of the contractin family of actin-related proteins. *Molecular biology of the cell* *5*, 1301-1310.
- Cockell, M.M., Baumer, K., and Gonczy, P. (2004). *lis-1* is required for dynein-dependent cell division processes in *C. elegans* embryos. *J Cell Sci* *117*, 4571-4582.
- Cong, L., Ran, F.A., Cox, D., Lin, S., Barretto, R., Habib, N., Hsu, P.D., Wu, X., Jiang, W., Marraffini, L.A., *et al.* (2013). Multiplex genome engineering using CRISPR/Cas systems. *Science* *339*, 819-823.
- Cooper, J.A., Caldwell, J.E., Gattermeir, D.J., Torres, M.A., Amatruda, J.F., and Casella, J.F. (1991). Variant cDNAs encoding proteins similar to the alpha subunit of chicken CapZ. *Cell Motil Cytoskeleton* *18*, 204-214.
- Cooper, J.A., and Sept, D. (2008). New insights into mechanism and regulation of actin capping protein. *International review of cell and molecular biology* *267*, 183-206.
- Courtois, A., Schuh, M., Ellenberg, J., and Hiiragi, T. (2012). The transition from meiotic to mitotic spindle assembly is gradual during early mammalian development. *J Cell Biol* *198*, 357-370.
- Couwenbergs, C., Labbe, J.C., Goulding, M., Marty, T., Bowerman, B., and Gotta, M. (2007). Heterotrimeric G protein signaling functions with dynein to promote spindle positioning in *C. elegans*. *J Cell Biol* *179*, 15-22.

- Couwenbergs, C., Spilker, A.C., and Gotta, M. (2004). Control of embryonic spindle positioning and Galpha activity by *C. elegans* RIC-8. *Curr Biol* 14, 1871-1876.
- Culver-Hanlon, T.L., Lex, S.A., Stephens, A.D., Quintyne, N.J., and King, S.J. (2006). A microtubule-binding domain in dynactin increases dynein processivity by skating along microtubules. *Nat Cell Biol* 8, 264-270.
- da Silva, S.M., and Vincent, J.P. (2007). Oriented cell divisions in the extending germband of *Drosophila*. *Development* 134, 3049-3054.
- Das, R.M., and Storey, K.G. (2012). Mitotic spindle orientation can direct cell fate and bias Notch activity in chick neural tube. *EMBO Rep* 13, 448-454.
- David, N.B., Martin, C.A., Segalen, M., Rosenfeld, F., Schweisguth, F., and Bellaiche, Y. (2005). *Drosophila* Ric-8 regulates Galphai cortical localization to promote Galphai-dependent planar orientation of the mitotic spindle during asymmetric cell division. *Nat Cell Biol* 7, 1083-1090.
- Davis, D.A., Wilson, M.H., Giraud, J., Xie, Z., Tseng, H.C., England, C., Herscovitz, H., Tsai, L.H., and Delalle, I. (2009). Capzb2 interacts with beta-tubulin to regulate growth cone morphology and neurite outgrowth. *PLoS Biol* 7, e1000208.
- Delalle, I., Pflieger, C.M., Buff, E., Lueras, P., and Hariharan, I.K. (2005). Mutations in the *Drosophila* orthologs of the F-actin capping protein alpha- and beta-subunits cause actin accumulation and subsequent retinal degeneration. *Genetics* 171, 1757-1765.
- Dewey, E.B., Sanchez, D., and Johnston, C.A. (2015). Warts phosphorylates mud to promote pins-mediated mitotic spindle orientation in *Drosophila*, independent of Yorkie. *Curr Biol* 25, 2751-2762.
- DeWitt, M.A., Chang, A.Y., Combs, P.A., and Yildiz, A. (2012). Cytoplasmic dynein moves through uncoordinated stepping of the AAA+ ring domains. *Science* 335, 221-225.
- di Pietro, F., Echard, A., and Morin, X. (2016). Regulation of mitotic spindle orientation: an integrated view. *EMBO Rep*.
- Du, Q., and Macara, I.G. (2004). Mammalian Pins is a conformational switch that links NuMA to heterotrimeric G proteins. *Cell* 119, 503-516.
- Du, Q., Stukenberg, P.T., and Macara, I.G. (2001). A mammalian Partner of inscuteable binds NuMA and regulates mitotic spindle organization. *Nat Cell Biol* 3, 1069-1075.
- Dumont, J., Million, K., Sunderland, K., Rassinier, P., Lim, H., Leader, B., and Verlhac, M.H. (2007). Formin-2 is required for spindle migration and for the late steps of cytokinesis in mouse oocytes. *Dev Biol* 301, 254-265.
- Dunsch, A.K., Hammond, D., Lloyd, J., Schermelleh, L., Gruneberg, U., and Barr, F.A. (2012). Dynein light chain 1 and a spindle-associated adaptor promote dynein asymmetry and spindle orientation. *J Cell Biol* 198, 1039-1054.
- Echeverri, C.J., Paschal, B.M., Vaughan, K.T., and Vallee, R.B. (1996). Molecular characterization of the 50-kD subunit of dynactin reveals function for the complex in chromosome alignment and spindle organization during mitosis. *J Cell Biol* 132, 617-633.
- Edelstein, A., Amodaj, N., Hoover, K., Vale, R., and Stuurman, N. (2010). Computer control of microscopes using microManager. *Current protocols in molecular biology* / edited by Frederick M Ausubel [et al] *Chapter 14*, Unit14 20.
- Elias, S., Thion, M., Yu, H., Moreira Sousa, C., Lasgi, C., Morin, X., and Humbert, S. (2014). Huntingtin Regulates Mammary Stem Cell Division and Differentiation. *Stem Cells Reports* 2, 491-506.
- Faulkner, N.E., Dujardin, D.L., Tai, C.Y., Vaughan, K.T., O'Connell, C.B., Wang, Y., and Vallee, R.B. (2000). A role for the lissencephaly gene LIS1 in mitosis and cytoplasmic dynein function. *Nat Cell Biol* 2, 784-791.

Fehon, R.G., McClatchey, A.I., and Bretscher, A. (2010). Organizing the cell cortex: the role of ERM proteins. *Nat Rev Mol Cell Biol* *11*, 276-287.

Feng, Y., Olson, E.C., Stukenberg, P.T., Flanagan, L.A., Kirschner, M.W., and Walsh, C.A. (2000). LIS1 regulates CNS lamination by interacting with mNudE, a central component of the centrosome. *Neuron* *28*, 665-679.

Feng, Y., and Walsh, C.A. (2004). Mitotic spindle regulation by Nde1 controls cerebral cortical size. *Neuron* *44*, 279-293.

Fink, J., Carpi, N., Betz, T., Betard, A., Chebah, M., Azioune, A., Bornens, M., Sykes, C., Fetler, L., Cuvelier, D., *et al.* (2011). External forces control mitotic spindle positioning. *Nat Cell Biol* *13*, 771-778.

Fischer, E., Legue, E., Doyen, A., Nato, F., Nicolas, J.F., Torres, V., Yaniv, M., and Pontoglio, M. (2006). Defective planar cell polarity in polycystic kidney disease. *Nat Genet* *38*, 21-23.

Fish, J.L., Kosodo, Y., Enard, W., Paabo, S., and Huttner, W.B. (2006). Aspm specifically maintains symmetric proliferative divisions of neuroepithelial cells. *Proc Natl Acad Sci U S A* *103*, 10438-10443.

Fleming, E.S., Temchin, M., Wu, Q., Maggio-Price, L., and Tirnauer, J.S. (2009). Spindle misorientation in tumors from APC(min/+) mice. *Mol Carcinog* *48*, 592-598.

Frank, D.J., Hopmann, R., Lenartowska, M., and Miller, K.G. (2006). Capping protein and the Arp2/3 complex regulate nonbundle actin filament assembly to indirectly control actin bundle positioning during *Drosophila melanogaster* bristle development. *Molecular biology of the cell* *17*, 3930-3939.

Fumoto, K., Hoogenraad, C.C., and Kikuchi, A. (2006). GSK-3beta-regulated interaction of BICD with dynein is involved in microtubule anchorage at centrosome. *Embo J* *25*, 5670-5682.

Gaetz, J., and Kapoor, T.M. (2004). Dynein/dynactin regulate metaphase spindle length by targeting depolymerizing activities to spindle poles. *J Cell Biol* *166*, 465-471.

Gallini, S., Carminati, M., De Mattia, F., Pirovano, L., Martini, E., Oldani, A., Asteriti, I.A., Guarguaglini, G., and Mapelli, M. (2016). NuMA Phosphorylation by Aurora-A Orchestrates Spindle Orientation. *Curr Biol* *26*, 458-469.

Gassmann, R., Essex, A., Hu, J.S., Maddox, P.S., Motegi, F., Sugimoto, A., O'Rourke, S.M., Bowerman, B., McLeod, I., Yates, J.R., 3rd, *et al.* (2008). A new mechanism controlling kinetochore-microtubule interactions revealed by comparison of two dynein-targeting components: SPDL-1 and the Rod/Zwilch/Zw10 complex. *Genes Dev* *22*, 2385-2399.

Gee, M.A., Heuser, J.E., and Vallee, R.B. (1997). An extended microtubule-binding structure within the dynein motor domain. *Nature* *390*, 636-639.

Geiser, J.R., Schott, E.J., Kingsbury, T.J., Cole, N.B., Totis, L.J., Bhattacharyya, G., He, L., and Hoyt, M.A. (1997). *Saccharomyces cerevisiae* genes required in the absence of the CIN8-encoded spindle motor act in functionally diverse mitotic pathways. *Molecular biology of the cell* *8*, 1035-1050.

Geldmacher-Voss, B., Reugels, A.M., Pauls, S., and Campos-Ortega, J.A. (2003). A 90-degree rotation of the mitotic spindle changes the orientation of mitoses of zebrafish neuroepithelial cells. *Development* *130*, 3767-3780.

Gillies, T.E., and Cabernard, C. (2011). Cell division orientation in animals. *Curr Biol* *21*, R599-609.

Godin, J.D., Colombo, K., Molina-Calavita, M., Keryer, G., Zala, D., Charrin, B.C., Dietrich, P., Volvert, M.L., Guillemot, F., Dragatsis, I., *et al.* (2010). Huntingtin is required for mitotic spindle orientation and mammalian neurogenesis. *Neuron* *67*, 392-406.

Gonczy, P., Pichler, S., Kirkham, M., and Hyman, A.A. (1999). Cytoplasmic dynein is required for distinct aspects of MTOC positioning, including centrosome separation, in the one cell stage *Caenorhabditis elegans* embryo. *J Cell Biol* *147*, 135-150.

- Gong, Y., Mo, C., and Fraser, S.E. (2004). Planar cell polarity signalling controls cell division orientation during zebrafish gastrulation. *Nature* *430*, 689-693.
- Good, M.C., Vahey, M.D., Skandarajah, A., Fletcher, D.A., and Heald, R. (2013). Cytoplasmic volume modulates spindle size during embryogenesis. *Science* *342*, 856-860.
- Gotta, M., and Ahringer, J. (2001). Distinct roles for Galpha and Gbetagamma in regulating spindle position and orientation in *Caenorhabditis elegans* embryos. *Nat Cell Biol* *3*, 297-300.
- Gotta, M., Dong, Y., Peterson, Y.K., Lanier, S.M., and Ahringer, J. (2003). Asymmetrically distributed *C. elegans* homologs of AGS3/PINS control spindle position in the early embryo. *Curr Biol* *13*, 1029-1037.
- Grill, S.W., Gonczy, P., Stelzer, E.H., and Hyman, A.A. (2001). Polarity controls forces governing asymmetric spindle positioning in the *Caenorhabditis elegans* embryo. *Nature* *409*, 630-633.
- Grill, S.W., Howard, J., Schaffer, E., Stelzer, E.H., and Hyman, A.A. (2003). The distribution of active force generators controls mitotic spindle position. *Science* *301*, 518-521.
- Gruber, R., Zhou, Z., Sukchev, M., Joerss, T., Frappart, P.O., and Wang, Z.Q. (2011). MCPH1 regulates the neuroprogenitor division mode by coupling the centrosomal cycle with mitotic entry through the Chk1-Cdc25 pathway. *Nat Cell Biol* *13*, 1325-1334.
- Habib, S.J., Chen, B.C., Tsai, F.C., Anastassiadis, K., Meyer, T., Betzig, E., and Nusse, R. (2013). A localized Wnt signal orients asymmetric stem cell division in vitro. *Science* *339*, 1445-1448.
- Hammesfahr, B., and Kollmar, M. (2012). Evolution of the eukaryotic dynactin complex, the activator of cytoplasmic dynein. *BMC evolutionary biology* *12*, 95.
- Hampoelz, B., Hoeller, O., Bowman, S.K., Dunican, D., and Knoblich, J.A. (2005). *Drosophila* Ric-8 is essential for plasma-membrane localization of heterotrimeric G proteins. *Nat Cell Biol* *7*, 1099-1105.
- Hao, Y., Du, Q., Chen, X., Zheng, Z., Balsbaugh, J.L., Maitra, S., Shabanowitz, J., Hunt, D.F., and Macara, I.G. (2010). Par3 Controls Epithelial Spindle Orientation by aPKC-Mediated Phosphorylation of Apical Pins. *Curr Biol* *20*, 1809-1818.
- Haren, L., and Merdes, A. (2002). Direct binding of NuMA to tubulin is mediated by a novel sequence motif in the tail domain that bundles and stabilizes microtubules. *J Cell Sci* *115*, 1815-1824.
- Hart, M.C., and Cooper, J.A. (1999). Vertebrate isoforms of actin capping protein beta have distinct functions In vivo. *J Cell Biol* *147*, 1287-1298.
- Hart, M.C., Korshunova, Y.O., and Cooper, J.A. (1997). Vertebrates have conserved capping protein alpha isoforms with specific expression patterns. *Cell Motil Cytoskeleton* *38*, 120-132.
- Hehnly, H., and Doxsey, S. (2014). Rab11 endosomes contribute to mitotic spindle organization and orientation. *Dev Cell* *28*, 497-507.
- Hertwig, O. (1884). Das Problem der Befruchtung und der Isotropie des Eies, eine Theory der Vererbung. *Jenaische Zeitschrift fuer Naturwissenschaft* *18*, 21-23.
- Hess, H.A., Roper, J.C., Grill, S.W., and Koelle, M.R. (2004). RGS-7 completes a receptor-independent heterotrimeric G protein cycle to asymmetrically regulate mitotic spindle positioning in *C. elegans*. *Cell* *119*, 209-218.
- Higgins, J., Midgley, C., Bergh, A.M., Bell, S.M., Askham, J.M., Roberts, E., Binns, R.K., Sharif, S.M., Bennett, C., Glover, D.M., *et al.* (2010). Human ASPM participates in spindle organisation, spindle orientation and cytokinesis. *BMC cell biology* *11*, 85.
- Hirokawa, N., and Noda, Y. (2008). Intracellular transport and kinesin superfamily proteins, KIFs: structure, function, and dynamics. *Physiological reviews* *88*, 1089-1118.

- Hirose, H., Arasaki, K., Dohmae, N., Takio, K., Hatsuzawa, K., Nagahama, M., Tani, K., Yamamoto, A., Tohyama, M., and Tagaya, M. (2004). Implication of ZW10 in membrane trafficking between the endoplasmic reticulum and Golgi. *Embo J* *23*, 1267-1278.
- Holleran, E.A., Ligon, L.A., Tokito, M., Stankewich, M.C., Morrow, J.S., and Holzbaur, E.L. (2001). beta III spectrin binds to the Arp1 subunit of dynactin. *J Biol Chem* *276*, 36598-36605.
- Holubcova, Z., Howard, G., and Schuh, M. (2013). Vesicles modulate an actin network for asymmetric spindle positioning. *Nat Cell Biol* *15*, 937-947.
- Homem, C.C., and Knoblich, J.A. (2012). *Drosophila* neuroblasts: a model for stem cell biology. *Development* *139*, 4297-4310.
- Hoogenraad, C.C., and Akhmanova, A. (2016). Bicaudal D Family of Motor Adaptors: Linking Dynein Motility to Cargo Binding. *Trends Cell Biol* *26*, 327-340.
- Hook, P., and Vallee, R.B. (2006). The dynein family at a glance. *J Cell Sci* *119*, 4369-4371.
- Hook, P., Yagi, T., Ghosh-Roy, A., Williams, J.C., and Vallee, R.B. (2009). The dynein stalk contains an antiparallel coiled coil with region-specific stability. *Biochemistry* *48*, 2710-2713.
- Hopmann, R., Cooper, J.A., and Miller, K.G. (1996). Actin organization, bristle morphology, and viability are affected by actin capping protein mutations in *Drosophila*. *J Cell Biol* *133*, 1293-1305.
- Hopmann, R., and Miller, K.G. (2003). A balance of capping protein and profilin functions is required to regulate actin polymerization in *Drosophila* bristle. *Molecular biology of the cell* *14*, 118-128.
- Hug, C., Jay, P.Y., Reddy, I., McNally, J.G., Bridgman, P.C., Elson, E.L., and Cooper, J.A. (1995). Capping protein levels influence actin assembly and cell motility in dictyostelium. *Cell* *81*, 591-600.
- Hurst, S., Howes, E.A., Coadwell, J., and Jones, R. (1998). Expression of a testis-specific putative actin-capping protein associated with the developing acrosome during rat spermiogenesis. *Molecular reproduction and development* *49*, 81-91.
- Hutchins, J.R., Toyoda, Y., Hegemann, B., Poser, I., Heriche, J.K., Sykora, M.M., Augsburg, M., Hudecz, O., Buschhorn, B.A., Bulkescher, J., *et al.* (2010). Systematic analysis of human protein complexes identifies chromosome segregation proteins. *Science* *328*, 593-599.
- Huttner, W.B., and Brand, M. (1997). Asymmetric division and polarity of neuroepithelial cells. *Curr Opin Neurobiol* *7*, 29-39.
- Isenberg, G., Aebi, U., and Pollard, T.D. (1980). An actin-binding protein from *Acanthamoeba* regulates actin filament polymerization and interactions. *Nature* *288*, 455-459.
- Izumi, Y., Ohta, N., Hisata, K., Raabe, T., and Matsuzaki, F. (2006). *Drosophila* Pins-binding protein Mud regulates spindle-polarity coupling and centrosome organization. *Nat Cell Biol* *8*, 586-593.
- Izumi, Y., Ohta, N., Itoh-Furuya, A., Fuse, N., and Matsuzaki, F. (2004). Differential functions of G protein and Baz-aPKC signaling pathways in *Drosophila* neuroblast asymmetric division. *J Cell Biol* *164*, 729-738.
- Jaffe, A.B., Kaji, N., Durgan, J., and Hall, A. (2008). Cdc42 controls spindle orientation to position the apical surface during epithelial morphogenesis. *J Cell Biol* *183*, 625-633.
- Janody, F., and Treisman, J.E. (2006). Actin capping protein alpha maintains vestigial-expressing cells within the *Drosophila* wing disc epithelium. *Development* *133*, 3349-3357.
- Jo, Y.J., Jang, W.I., Namgoong, S., and Kim, N.H. (2015). Actin-capping proteins play essential roles in the asymmetric division of maturing mouse oocytes. *J Cell Sci* *128*, 160-170.

- Johansson, M., Rocha, N., Zwart, W., Jordens, I., Janssen, L., Kuijl, C., Olkkonen, V.M., and Neefjes, J. (2007). Activation of endosomal dynein motors by stepwise assembly of Rab7-RILP-p150Glued, ORP1L, and the receptor betaIII spectrin. *J Cell Biol* 176, 459-471.
- Johnston, C.A., Doe, C.Q., and Prehoda, K.E. (2012). Structure of an enzyme-derived phosphoprotein recognition domain. *PLoS ONE* 7, e36014.
- Johnston, C.A., Hirono, K., Prehoda, K.E., and Doe, C.Q. (2009). Identification of an Aurora-A/PinsLINKER/Dlg spindle orientation pathway using induced cell polarity in S2 cells. *Cell* 138, 1150-1163.
- Johnston, C.A., Manning, L., Lu, M.S., Golub, O., Doe, C.Q., and Prehoda, K.E. (2013). Formin-mediated actin polymerization cooperates with Mushroom body defect (Mud)-Dynein during Frizzled-Dishevelled spindle orientation. *J Cell Sci* 126, 4436-4444.
- Kahana, J.A., Schlenstedt, G., Evanchuk, D.M., Geiser, J.R., Hoyt, M.A., and Silver, P.A. (1998). The yeast dynactin complex is involved in partitioning the mitotic spindle between mother and daughter cells during anaphase B. *Molecular biology of the cell* 9, 1741-1756.
- Kalebic, N., Taverna, E., Tavano, S., Wong, F.K., Suchold, D., Winkler, S., Huttner, W.B., and Sarov, M. (2016). CRISPR/Cas9-induced disruption of gene expression in mouse embryonic brain and single neural stem cells in vivo. *EMBO Rep* 17, 338-348.
- Kardon, J.R., Reck-Peterson, S.L., and Vale, R.D. (2009). Regulation of the processivity and intracellular localization of *Saccharomyces cerevisiae* dynein by dynactin. *Proc Natl Acad Sci U S A* 106, 5669-5674.
- Kardon, J.R., and Vale, R.D. (2009). Regulators of the cytoplasmic dynein motor. *Nat Rev Mol Cell Biol* 10, 854-865.
- Karki, S., and Holzbaur, E.L. (1995). Affinity chromatography demonstrates a direct binding between cytoplasmic dynein and the dynactin complex. *J Biol Chem* 270, 28806-28811.
- Kennedy, M., Hughes, R., Peteya, L., Schwartz, J., Ehlers, M., and Tucker, C. (2010). Rapid blue-light-mediated induction of protein interactions in living cells. *Nature Methods* 7, 973.
- Kim, H., Ling, S.C., Rogers, G.C., Kural, C., Selvin, P.R., Rogers, S.L., and Gelfand, V.I. (2007a). Microtubule binding by dynactin is required for microtubule organization but not cargo transport. *J Cell Biol* 176, 641-651.
- Kim, K., McCully, M.E., Bhattacharya, N., Butler, B., Sept, D., and Cooper, J.A. (2007b). Structure/function analysis of the interaction of phosphatidylinositol 4,5-bisphosphate with actin-capping protein: implications for how capping protein binds the actin filament. *J Biol Chem* 282, 5871-5879.
- Kim, T., Cooper, J.A., and Sept, D. (2010). The interaction of capping protein with the barbed end of the actin filament. *J Mol Biol* 404, 794-802.
- King, S.J., Brown, C.L., Maier, K.C., Quintyne, N.J., and Schroer, T.A. (2003). Analysis of the dynein-dynactin interaction in vitro and in vivo. *Molecular biology of the cell* 14, 5089-5097.
- King, S.J., and Schroer, T.A. (2000). Dynactin increases the processivity of the cytoplasmic dynein motor. *Nat Cell Biol* 2, 20-24.
- Kitagawa, D., Kohlmaier, G., Keller, D., Strnad, P., Balestra, F.R., Fluckiger, I., and Gonczy, P. (2011). Spindle positioning in human cells relies on proper centriole formation and on the microcephaly proteins CPAP and STIL. *J Cell Sci* 124, 3884-3893.
- Kiyomitsu, T., and Cheeseman, I.M. (2012). Chromosome- and spindle-pole-derived signals generate an intrinsic code for spindle position and orientation. *Nat Cell Biol* 14, 311-317.
- Kiyomitsu, T., and Cheeseman, I.M. (2013). Cortical dynein and asymmetric membrane elongation coordinately position the spindle in anaphase. *Cell* 154, 391-402.

- Knoblich, J.A. (2008). Mechanisms of asymmetric stem cell division. *Cell* **132**, 583-597.
- Knoblich, J.A. (2010). Asymmetric cell division: recent developments and their implications for tumour biology. *Nat Rev Mol Cell Biol* **11**, 849-860.
- Kon, T., Nishiura, M., Ohkura, R., Toyoshima, Y.Y., and Sutoh, K. (2004). Distinct functions of nucleotide-binding/hydrolysis sites in the four AAA modules of cytoplasmic dynein. *Biochemistry* **43**, 11266-11274.
- Kon, T., Oyama, T., Shimo-Kon, R., Imamula, K., Shima, T., Sutoh, K., and Kurisu, G. (2012). The 2.8 Å crystal structure of the dynein motor domain. *Nature* **484**, 345-350.
- Kon, T., Sutoh, K., and Kurisu, G. (2011). X-ray structure of a functional full-length dynein motor domain. *Nature structural & molecular biology* **18**, 638-642.
- Konno, D., Shioi, G., Shitamukai, A., Mori, A., Kiyonari, H., Miyata, T., and Matsuzaki, F. (2008). Neuroepithelial progenitors undergo LGN-dependent planar divisions to maintain self-renewability during mammalian neurogenesis. *Nat Cell Biol* **10**, 93-101.
- Kosodo, Y., Roper, K., Haubensak, W., Marzesco, A.M., Corbeil, D., and Huttner, W.B. (2004). Asymmetric distribution of the apical plasma membrane during neurogenic divisions of mammalian neuroepithelial cells. *Embo J* **23**, 2314-2324.
- Kotak, S., Afshar, K., Busso, C., and Gonczy, P. (2016). Aurora A kinase regulates proper spindle positioning in *C. elegans* and in human cells. *J Cell Sci*.
- Kotak, S., Busso, C., and Gonczy, P. (2012). Cortical dynein is critical for proper spindle positioning in human cells. *J Cell Biol* **199**, 97-110.
- Kotak, S., Busso, C., and Gonczy, P. (2013). NuMA phosphorylation by CDK1 couples mitotic progression with cortical dynein function. *Embo J* **32**, 2517-2529.
- Kotak, S., Busso, C., and Gonczy, P. (2014). NuMA interacts with phosphoinositides and links the mitotic spindle with the plasma membrane. *Embo J* **33**, 1815-1830.
- Kotak, S., and Gonczy, P. (2014). NuMA phosphorylation dictates dynein-dependent spindle positioning. *Cell Cycle* **13**, 177-178.
- Kraut, R., Chia, W., Jan, L.Y., Jan, Y.N., and Knoblich, J.A. (1996). Role of inscuteable in orienting asymmetric cell divisions in *Drosophila*. *Nature* **383**, 50-55.
- Krendel, M., and Mooseker, M.S. (2005). Myosins: tails (and heads) of functional diversity. *Physiology (Bethesda)* **20**, 239-251.
- Kunda, P., Pelling, A.E., Liu, T., and Baum, B. (2008). Moesin controls cortical rigidity, cell rounding, and spindle morphogenesis during mitosis. *Curr Biol* **18**, 91-101.
- Kwon, M., Bagonis, M., Danuser, G., and Pellman, D. (2015). Direct Microtubule-Binding by Myosin-10 Orients Centrosomes toward Retraction Fibers and Subcortical Actin Clouds. *Dev Cell* **34**, 323-337.
- Lam, C., Vergnolle, M.A., Thorpe, L., Woodman, P.G., and Allan, V.J. (2010). Functional interplay between LIS1, NDE1 and NDEL1 in dynein-dependent organelle positioning. *J Cell Sci* **123**, 202-212.
- Lancaster, O.M., and Baum, B. (2014). Shaping up to divide: coordinating actin and microtubule cytoskeletal remodelling during mitosis. *Semin Cell Dev Biol* **34**, 109-115.
- Lancaster, O.M., Le Berre, M., Dimitracopoulos, A., Bonazzi, D., Zlotek-Zlotkiewicz, E., Picone, R., Duke, T., Piel, M., and Baum, B. (2013). Mitotic rounding alters cell geometry to ensure efficient bipolar spindle formation. *Dev Cell* **25**, 270-283.

Lansbergen, G., Komarova, Y., Modesti, M., Wyman, C., Hoogenraad, C.C., Goodson, H.V., Lemaitre, R.P., Drechsel, D.N., van Munster, E., Gadella, T.W., Jr., *et al.* (2004). Conformational changes in CLIP-170 regulate its binding to microtubules and dynactin localization. *J Cell Biol* *166*, 1003-1014.

Lazaro-Diequez, F., Ispolatov, I., and Musch, A. (2015). Cell shape impacts on the positioning of the mitotic spindle with respect to the substratum. *Molecular biology of the cell* *26*, 1286-1295.

Lazarus, J.E., Moughamian, A.J., Tokito, M.K., and Holzbaur, E.L. (2013). Dynactin subunit p150(Glued) is a neuron-specific anti-catastrophe factor. *PLoS Biol* *11*, e1001611.

Lechler, T., and Fuchs, E. (2005). Asymmetric cell divisions promote stratification and differentiation of mammalian skin. *Nature* *437*, 275-280.

Lee, C.Y., Wilkinson, B.D., Siegrist, S.E., Wharton, R.P., and Doe, C.Q. (2006). Brat is a Miranda cargo protein that promotes neuronal differentiation and inhibits neuroblast self-renewal. *Dev Cell* *10*, 441-449.

Lee, W.L., Kaiser, M.A., and Cooper, J.A. (2005). The offloading model for dynein function: differential function of motor subunits. *J Cell Biol* *168*, 201-207.

Lee, W.L., Oberle, J.R., and Cooper, J.A. (2003). The role of the lissencephaly protein Pac1 during nuclear migration in budding yeast. *J Cell Biol* *160*, 355-364.

Legoff, L., Rouault, H., and Lecuit, T. (2013). A global pattern of mechanical stress polarizes cell divisions and cell shape in the growing *Drosophila* wing disc. *Development* *140*, 4051-4059.

Li, J., Lee, W.L., and Cooper, J.A. (2005). NudEL targets dynein to microtubule ends through LIS1. *Nat Cell Biol* *7*, 686-690.

Li, Y., Rose, F., di Pietro, F., Morin, X., and Genovesio, A. (2016). Detection and tracking of overlapping cell nuclei for large scale mitosis analyses. *BMC bioinformatics* *17*, 183.

Li, Y.Y., Yeh, E., Hays, T., and Bloom, K. (1993). Disruption of mitotic spindle orientation in a yeast dynein mutant. *Proc Natl Acad Sci U S A* *90*, 10096-10100.

Lizarraga, S.B., Margossian, S.P., Harris, M.H., Campagna, D.R., Han, A.P., Blevins, S., Mudbhary, R., Barker, J.E., Walsh, C.A., and Fleming, M.D. (2010). Cdk5rap2 regulates centrosome function and chromosome segregation in neuronal progenitors. *Development* *137*, 1907-1917.

Loisel, T.P., Boujemaa, R., Pantaloni, D., and Carlier, M.F. (1999). Reconstitution of actin-based motility of *Listeria* and *Shigella* using pure proteins. *Nature* *401*, 613-616.

Lu, M.S., and Prehoda, K.E. (2013). A NudE/14-3-3 pathway coordinates dynein and the kinesin Khc73 to position the mitotic spindle. *Dev Cell* *26*, 369-380.

Luxenburg, C., Pasolli, H.A., Williams, S.E., and Fuchs, E. (2011). Developmental roles for Srf, cortical cytoskeleton and cell shape in epidermal spindle orientation. *Nat Cell Biol* *13*, 203-214.

Macara, I.G., Guyer, R., Richardson, G., Huo, Y., and Ahmed, S.M. (2014). Epithelial homeostasis. *Curr Biol* *24*, R815-825.

Machicoane, M., de Frutos, C.A., Fink, J., Rocancourt, M., Lombardi, Y., Garel, S., Piel, M., and Echard, A. (2014). SLK-dependent activation of ERMs controls LGN-NuMA localization and spindle orientation. *J Cell Biol* *205*, 791-799.

Makokha, M., Hare, M., Li, M., Hays, T., and Barbar, E. (2002). Interactions of cytoplasmic dynein light chains Tctex-1 and LC8 with the intermediate chain IC74. *Biochemistry* *41*, 4302-4311.

Mallik, R., Carter, B.C., Lex, S.A., King, S.J., and Gross, S.P. (2004). Cytoplasmic dynein functions as a gear in response to load. *Nature* *427*, 649-652.

- Mao, Y., Tournier, A.L., Bates, P.A., Gale, J.E., Tapon, N., and Thompson, B.J. (2011). Planar polarization of the atypical myosin Dachs orients cell divisions in *Drosophila*. *Genes Dev* 25, 131-136.
- Mao, Y., Tournier, A.L., Hoppe, A., Kester, L., Thompson, B.J., and Tapon, N. (2013). Differential proliferation rates generate patterns of mechanical tension that orient tissue growth. *Embo J* 32, 2790-2803.
- Markus, S.M., Kalutkiewicz, K.A., and Lee, W.L. (2012). Astral microtubule asymmetry provides directional cues for spindle positioning in budding yeast. *Exp Cell Res* 318, 1400-1406.
- Markus, S.M., and Lee, W.L. (2011a). Microtubule-dependent path to the cell cortex for cytoplasmic dynein in mitotic spindle orientation. *Bioarchitecture* 1, 209-215.
- Markus, S.M., and Lee, W.L. (2011b). Regulated offloading of cytoplasmic dynein from microtubule plus ends to the cortex. *Dev Cell* 20, 639-651.
- Marthiens, V., and French-Constant, C. (2009). Adherens junction domains are split by asymmetric division of embryonic neural stem cells. *EMBO Rep* 10, 515-520.
- Marthiens, V., Rujano, M.A., Pennetier, C., Tessier, S., Paul-Gilloteaux, P., and Basto, R. (2013). Centrosome amplification causes microcephaly. *Nat Cell Biol* 15, 731-740.
- Maruyama, K. (2002). beta-Actinin, Cap Z, connectin and titin: what's in a name? *Trends Biochem Sci* 27, 264-266.
- Matanis, T., Akhmanova, A., Wulf, P., Del Nery, E., Weide, T., Stepanova, T., Galjart, N., Grosveld, F., Goud, B., De Zeeuw, C.I., *et al.* (2002). Bicaudal-D regulates COPI-independent Golgi-ER transport by recruiting the dynein-dynactin motor complex. *Nat Cell Biol* 4, 986-992.
- Matov, A., Applegate, K., Kumar, P., Thoma, C., Krek, W., Danuser, G., and Wittmann, T. (2010). Analysis of microtubule dynamic instability using a plus-end growth marker. *Nat Methods* 7, 761-768.
- Matsumura, S., Hamasaki, M., Yamamoto, T., Ebisuya, M., Sato, M., Nishida, E., and Toyoshima, F. (2012). ABL1 regulates spindle orientation in adherent cells and mammalian skin. *Nat Commun* 3, 626.
- McGrail, M., and Hays, T.S. (1997). The microtubule motor cytoplasmic dynein is required for spindle orientation during germline cell divisions and oocyte differentiation in *Drosophila*. *Development* 124, 2409-2419.
- McKenney, R.J., Huynh, W., Tanenbaum, M.E., Bhabha, G., and Vale, R.D. (2014). Activation of cytoplasmic dynein motility by dynactin-cargo adapter complexes. *Science* 345, 337-341.
- McKenney, R.J., Vershinin, M., Kunwar, A., Vallee, R.B., and Gross, S.P. (2010). LIS1 and NudE induce a persistent dynein force-producing state. *Cell* 141, 304-314.
- McNally, F.J. (2013). Mechanisms of spindle positioning. *J Cell Biol* 200, 131-140.
- Mejillano, M.R., Kojima, S., Applewhite, D.A., Gertler, F.B., Svitkina, T.M., and Borisy, G.G. (2004). Lamellipodial versus filopodial mode of the actin nanomachinery: pivotal role of the filament barbed end. *Cell* 118, 363-373.
- Menoret, S., De Cian, A., Tesson, L., Remy, S., Usal, C., Boule, J.B., Boix, C., Fontaniere, S., Creneguy, A., Nguyen, T.H., *et al.* (2015). Homology-directed repair in rodent zygotes using Cas9 and TALEN engineered proteins. *Scientific reports* 5, 14410.
- Merdes, A., Ramyar, K., Vechio, J.D., and Cleveland, D.W. (1996). A complex of NuMA and cytoplasmic dynein is essential for mitotic spindle assembly. *Cell* 87, 447-458.
- Mesngon, M.T., Tarricone, C., Hebbar, S., Guillotte, A.M., Schmitt, E.W., Lanier, L., Musacchio, A., King, S.J., and Smith, D.S. (2006). Regulation of cytoplasmic dynein ATPase by Lis1. *J Neurosci* 26, 2132-2139.

Mi, N., Chen, Y., Wang, S., Chen, M., Zhao, M., Yang, G., Ma, M., Su, Q., Luo, S., Shi, J., *et al.* (2015). CapZ regulates autophagosomal membrane shaping by promoting actin assembly inside the isolation membrane. *Nat Cell Biol* *17*, 1112-1123.

Mikami, A., Tynan, S.H., Hama, T., Luby-Phelps, K., Saito, T., Crandall, J.E., Besharse, J.C., and Vallee, R.B. (2002). Molecular structure of cytoplasmic dynein 2 and its distribution in neuronal and ciliated cells. *J Cell Sci* *115*, 4801-4808.

Minc, N., Burgess, D., and Chang, F. (2011). Influence of cell geometry on division-plane positioning. *Cell* *144*, 414-426.

Minc, N., and Piel, M. (2012). Predicting division plane position and orientation. *Trends Cell Biol* *22*, 193-200.

Mitsushima, M., Aoki, K., Ebisuya, M., Matsumura, S., Yamamoto, T., Matsuda, M., Toyoshima, F., and Nishida, E. (2010). Revolving movement of a dynamic cluster of actin filaments during mitosis. *J Cell Biol* *191*, 453-462.

Mochizuki, N., Cho, G., Wen, B., and Insel, P.A. (1996). Identification and cDNA cloning of a novel human mosaic protein, LGN, based on interaction with G alpha i2. *Gene* *181*, 39-43.

Moon, H.M., Youn, Y.H., Pemble, H., Yingling, J., Wittmann, T., and Wynshaw-Boris, A. (2014). LIS1 controls mitosis and mitotic spindle organization via the LIS1-NDEL1-dynein complex. *Hum Mol Genet* *23*, 449-466.

Moore, J.K., Li, J., and Cooper, J.A. (2008). Dynactin function in mitotic spindle positioning. *Traffic* *9*, 510-527.

Moore, J.K., Stuchell-Brereton, M.D., and Cooper, J.A. (2009). Function of dynein in budding yeast: mitotic spindle positioning in a polarized cell. *Cell Motil Cytoskeleton* *66*, 546-555.

Mora-Bermudez, F., Matsuzaki, F., and Huttner, W.B. (2014). Specific polar subpopulations of astral microtubules control spindle orientation and symmetric neural stem cell division. *eLife* *3*.

Morin, X., and Bellaïche, Y. (2011). Mitotic spindle orientation in asymmetric and symmetric cell divisions during animal development. *Dev Cell* *21*, 102-119.

Morin, X., Jaouen, F., and Durbec, P. (2007). Control of planar divisions by the G-protein regulator LGN maintains progenitors in the chick neuroepithelium. *Nat Neurosci* *10*, 1440-1448.

Morris, E.J., Assi, K., Salh, B., and Dedhar, S. (2015). Integrin-linked kinase links dynactin-1/dynactin-2 with cortical integrin receptors to orient the mitotic spindle relative to the substratum. *Scientific reports* *5*, 8389.

Muhua, L., Karpova, T.S., and Cooper, J.A. (1994). A yeast actin-related protein homologous to that in vertebrate dynactin complex is important for spindle orientation and nuclear migration. *Cell* *78*, 669-679.

Mukherjee, K., Ishii, K., Pillalamarri, V., Kammin, T., Atkin, J.F., Hickey, S.E., Xi, Q.J., Zepeda, C.J., Gusella, J.F., Talkowski, M.E., *et al.* (2016). Actin capping protein CAPZB regulates cell morphology, differentiation, and neural crest migration in craniofacial morphogenesis. *Hum Mol Genet* *25*, 1255-1270.

Muresan, V., Stankewich, M.C., Steffen, W., Morrow, J.S., Holzbaur, E.L., and Schnapp, B.J. (2001). Dynactin-dependent, dynein-driven vesicle transport in the absence of membrane proteins: a role for spectrin and acidic phospholipids. *Mol Cell* *7*, 173-183.

Nakajima, Y., Meyer, E.J., Kroesen, A., McKinney, S.A., and Gibson, M.C. (2013). Epithelial junctions maintain tissue architecture by directing planar spindle orientation. *Nature* *500*, 359-362.

Narita, A., Takeda, S., Yamashita, A., and Maeda, Y. (2006). Structural basis of actin filament capping at the barbed-end: a cryo-electron microscopy study. *Embo J* *25*, 5626-5633.

Navarro, C., Puthalakath, H., Adams, J.M., Strasser, A., and Lehmann, R. (2004). Egalitarian binds dynein light chain to establish oocyte polarity and maintain oocyte fate. *Nat Cell Biol* *6*, 427-435.

Nguyen-Ngoc, T., Afshar, K., and Gonczy, P. (2007). Coupling of cortical dynein and G alpha proteins mediates spindle positioning in *Caenorhabditis elegans*. *Nat Cell Biol* 9, 1294-1302.

Niethammer, M., Smith, D.S., Ayala, R., Peng, J., Ko, J., Lee, M.S., Morabito, M., and Tsai, L.H. (2000). NUDEL is a novel Cdk5 substrate that associates with LIS1 and cytoplasmic dynein. *Neuron* 28, 697-711.

Noatynska, A., Gotta, M., and Meraldi, P. (2012). Mitotic spindle (DIS)orientation and DISease: cause or consequence? *J Cell Biol* 199, 1025-1035.

Noctor, S.C., Martinez-Cerdeno, V., and Kriegstein, A.R. (2008). Distinct behaviors of neural stem and progenitor cells underlie cortical neurogenesis. *J Comp Neurol* 508, 28-44.

O'Connell, C.B., and Wang, Y.L. (2000). Mammalian spindle orientation and position respond to changes in cell shape in a dynein-dependent fashion. *Molecular biology of the cell* 11, 1765-1774.

Ogienko, A.A., Karagodin, D.A., Lashina, V.V., Baiborodin, S.I., Omelina, E.S., and Baricheva, E.M. (2013). Capping protein beta is required for actin cytoskeleton organisation and cell migration during *Drosophila* oogenesis. *Cell biology international* 37, 149-159.

Paridaen, J.T., Wilsch-Brauninger, M., and Huttner, W.B. (2013). Asymmetric inheritance of centrosome-associated primary cilium membrane directs ciliogenesis after cell division. *Cell* 155, 333-344.

Pavlov, D., Muhrlad, A., Cooper, J., Wear, M., and Reisler, E. (2007). Actin filament severing by cofilin. *J Mol Biol* 365, 1350-1358.

Pawlisz, A.S., Mutch, C., Wynshaw-Boris, A., Chenn, A., Walsh, C.A., and Feng, Y. (2008). Lis1-Nde1-dependent neuronal fate control determines cerebral cortical size and lamination. *Hum Mol Genet* 17, 2441-2455.

Pazour, G.J., Dickert, B.L., and Witman, G.B. (1999). The DHC1b (DHC2) isoform of cytoplasmic dynein is required for flagellar assembly. *J Cell Biol* 144, 473-481.

Pease, J.C., and Tirnauer, J.S. (2011). Mitotic spindle misorientation in cancer--out of alignment and into the fire. *J Cell Sci* 124, 1007-1016.

Peyre, E., Jaouen, F., Saadaoui, M., Haren, L., Merdes, A., Durbec, P., and Morin, X. (2011). A lateral belt of cortical LGN and NuMA guides mitotic spindle movements and planar division in neuroepithelial cells. *J Cell Biol* 193, 141-154.

Peyre, E., and Morin, X. (2012). An oblique view on the role of spindle orientation in vertebrate neurogenesis. *Development, growth & differentiation* 54, 287-305.

Pfender, S., Kuznetsov, V., Pleiser, S., Kerkhoff, E., and Schuh, M. (2011). Spire-type actin nucleators cooperate with Formin-2 to drive asymmetric oocyte division. *Curr Biol* 21, 955-960.

Pfister, K.K., Shah, P.R., Hummerich, H., Russ, A., Cotton, J., Annuar, A.A., King, S.M., and Fisher, E.M. (2006). Genetic analysis of the cytoplasmic dynein subunit families. *PLoS Genet* 2, e1.

Postiglione, M.P., Juschke, C., Xie, Y., Haas, G.A., Charalambous, C., and Knoblich, J.A. (2011). Mouse *inscuteable* induces apical-basal spindle orientation to facilitate intermediate progenitor generation in the developing neocortex. *Neuron* 72, 269-284.

Qiu, W., Derr, N.D., Goodman, B.S., Villa, E., Wu, D., Shih, W., and Reck-Peterson, S.L. (2012). Dynein achieves processive motion using both stochastic and coordinated stepping. *Nature structural & molecular biology* 19, 193-200.

Quesada-Hernandez, E., Caneparo, L., Schneider, S., Winkler, S., Liebling, M., Fraser, S.E., and Heisenberg, C.P. (2010). Stereotypical cell division orientation controls neural rod midline formation in zebrafish. *Curr Biol* 20, 1966-1972.

- Quyn, A.J., Appleton, P.L., Carey, F.A., Steele, R.J., Barker, N., Clevers, H., Ridgway, R.A., Sansom, O.J., and Nathke, I.S. (2010). Spindle orientation bias in gut epithelial stem cell compartments is lost in precancerous tissue. *Cell stem cell* **6**, 175-181.
- Raaijmakers, J.A., Tanenbaum, M.E., and Medema, R.H. (2013). Systematic dissection of dynein regulators in mitosis. *J Cell Biol* **201**, 201-215.
- Rebollo, E., Roldan, M., and Gonzalez, C. (2009). Spindle alignment is achieved without rotation after the first cell cycle in *Drosophila* embryonic neuroblasts. *Development* **136**, 3393-3397.
- Reck-Peterson, S.L., Yildiz, A., Carter, A.P., Gennerich, A., Zhang, N., and Vale, R.D. (2006). Single-molecule analysis of dynein processivity and stepping behavior. *Cell* **126**, 335-348.
- Redemann, S., Pecreaux, J., Goehring, N.W., Khairy, K., Stelzer, E.H., Hyman, A.A., and Howard, J. (2010). Membrane invaginations reveal cortical sites that pull on mitotic spindles in one-cell *C. elegans* embryos. *PLoS ONE* **5**, e12301.
- Roberts, A.J., Kon, T., Knight, P.J., Sutoh, K., and Burgess, S.A. (2013). Functions and mechanics of dynein motor proteins. *Nat Rev Mol Cell Biol* **14**, 713-726.
- Roberts, A.J., Numata, N., Walker, M.L., Kato, Y.S., Malkova, B., Kon, T., Ohkura, R., Arisaka, F., Knight, P.J., Sutoh, K., *et al.* (2009). AAA+ Ring and linker swing mechanism in the dynein motor. *Cell* **136**, 485-495.
- Rocheteau, P., Gayraud-Morel, B., Siegl-Cachedenier, I., Blasco, M.A., and Tajbakhsh, S. (2012). A subpopulation of adult skeletal muscle stem cells retains all template DNA strands after cell division. *Cell* **148**, 112-125.
- Roghi, C., and Allan, V.J. (1999). Dynamic association of cytoplasmic dynein heavy chain 1a with the Golgi apparatus and intermediate compartment. *J Cell Sci* **112** (Pt 24), 4673-4685.
- Saadaoui, M., Machicoane, M., di Pietro, F., Etoc, F., Echard, A., and Morin, X. (2014). Dlg1 controls planar spindle orientation in the neuroepithelium through direct interaction with LGN. *J Cell Biol* **206**, 707-717.
- Saburi, S., Hester, I., Fischer, E., Pontoglio, M., Eremina, V., Gessler, M., Quaggin, S.E., Harrison, R., Mount, R., and McNeill, H. (2008). Loss of Fat4 disrupts PCP signaling and oriented cell division and leads to cystic kidney disease. *Nat Genet* **40**, 1010-1015.
- Samora, C.P., Mogessie, B., Conway, L., Ross, J.L., Straube, A., and McAinsh, A.D. (2011). MAP4 and CLASP1 operate as a safety mechanism to maintain a stable spindle position in mitosis. *Nat Cell Biol* **13**, 1040-1050.
- Sans, N., Wang, P.Y., Du, Q., Petralia, R.S., Wang, Y.X., Nakka, S., Blumer, J.B., Macara, I.G., and Wenthold, R.J. (2005). mPins modulates PSD-95 and SAP102 trafficking and influences NMDA receptor surface expression. *Nat Cell Biol* **7**, 1179-1190.
- Sasaki, S., Shionoya, A., Ishida, M., Gambello, M.J., Yingling, J., Wynshaw-Boris, A., and Hirotsune, S. (2000). A LIS1/NUDEL/cytoplasmic dynein heavy chain complex in the developing and adult nervous system. *Neuron* **28**, 681-696.
- Schaefer, M., Petronczki, M., Dorner, D., Forte, M., and Knoblich, J.A. (2001). Heterotrimeric G proteins direct two modes of asymmetric cell division in the *Drosophila* nervous system. *Cell* **107**, 183-194.
- Schaefer, M., Shevchenko, A., and Knoblich, J.A. (2000). A protein complex containing Inscuteable and the G α -binding protein Pins orients asymmetric cell divisions in *Drosophila*. *Curr Biol* **10**, 353-362.
- Schafer, D.A., Gill, S.R., Cooper, J.A., Heuser, J.E., and Schroer, T.A. (1994a). Ultrastructural analysis of the dynactin complex: an actin-related protein is a component of a filament that resembles F-actin. *J Cell Biol* **126**, 403-412.
- Schafer, D.A., Hug, C., and Cooper, J.A. (1995). Inhibition of CapZ during myofibrillogenesis alters assembly of actin filaments. *J Cell Biol* **128**, 61-70.

- Schafer, D.A., Korshunova, Y.O., Schroer, T.A., and Cooper, J.A. (1994b). Differential localization and sequence analysis of capping protein beta-subunit isoforms of vertebrates. *J Cell Biol* *127*, 453-465.
- Schafer, D.A., Mooseker, M.S., and Cooper, J.A. (1992). Localization of capping protein in chicken epithelial cells by immunofluorescence and biochemical fractionation. *J Cell Biol* *118*, 335-346.
- Schindelin, J., Arganda-Carreras, I., Frise, E., Kaynig, V., Longair, M., Pietzsch, T., Preibisch, S., Rueden, C., Saalfeld, S., Schmid, B., *et al.* (2012). Fiji: an open-source platform for biological-image analysis. *Nat Methods* *9*, 676-682.
- Schlager, M.A., Serra-Marques, A., Grigoriev, I., Gumy, L.F., Esteves da Silva, M., Wulf, P.S., Akhmanova, A., and Hoogenraad, C.C. (2014). Bicaudal d family adaptor proteins control the velocity of Dynein-based movements. *Cell reports* *8*, 1248-1256.
- Schroer, T.A. (2004). Dynactin. *Annu Rev Cell Dev Biol* *20*, 759-779.
- Schuh, M., and Ellenberg, J. (2008). A new model for asymmetric spindle positioning in mouse oocytes. *Curr Biol* *18*, 1986-1992.
- Segalen, M., and Bellaiche, Y. (2009). Cell division orientation and planar cell polarity pathways. *Semin Cell Dev Biol* *20*, 972-977.
- Segalen, M., Johnston, C.A., Martin, C.A., Dumortier, J.G., Prehoda, K.E., David, N.B., Doe, C.Q., and Bellaiche, Y. (2010). The Fz-Dsh planar cell polarity pathway induces oriented cell division via Mud/NuMA in *Drosophila* and zebrafish. *Dev Cell* *19*, 740-752.
- Seldin, L., Muroyama, A., and Lechler, T. (2016). NuMA-microtubule interactions are critical for spindle orientation and the morphogenesis of diverse epidermal structures. *eLife* *5*, e12504.
- Seo, J.S., Kim, H.N., Kim, S.J., Bang, J., Kim, E.A., Sung, K.S., Yoon, H.J., Yoo, H.Y., and Choi, C.Y. (2014). Cell cycle-dependent SUMO-1 conjugation to nuclear mitotic apparatus protein (NuMA). *Biochem Biophys Res Commun* *443*, 259-265.
- Sheeman, B., Carvalho, P., Sagot, I., Geiser, J., Kho, D., Hoyt, M.A., and Pellman, D. (2003). Determinants of *S. cerevisiae* dynein localization and activation: implications for the mechanism of spindle positioning. *Curr Biol* *13*, 364-372.
- Shu, T., Ayala, R., Nguyen, M.D., Xie, Z., Gleeson, J.G., and Tsai, L.H. (2004). Ndel1 operates in a common pathway with LIS1 and cytoplasmic dynein to regulate cortical neuronal positioning. *Neuron* *44*, 263-277.
- Siegrist, S.E., and Doe, C.Q. (2005). Microtubule-induced Pins/Galphai cortical polarity in *Drosophila* neuroblasts. *Cell* *123*, 1323-1335.
- Siller, K.H., Cabernard, C., and Doe, C.Q. (2006). The NuMA-related Mud protein binds Pins and regulates spindle orientation in *Drosophila* neuroblasts. *Nat Cell Biol* *8*, 594-600.
- Siller, K.H., and Doe, C.Q. (2008). Lis1/dynactin regulates metaphase spindle orientation in *Drosophila* neuroblasts. *Dev Biol* *319*, 1-9.
- Siller, K.H., Serr, M., Steward, R., Hays, T.S., and Doe, C.Q. (2005). Live imaging of *Drosophila* brain neuroblasts reveals a role for Lis1/dynactin in spindle assembly and mitotic checkpoint control. *Molecular biology of the cell* *16*, 5127-5140.
- Sinnar, S.A., Antoku, S., Saffin, J.M., Cooper, J.A., and Halpain, S. (2014). Capping protein is essential for cell migration in vivo and for filopodial morphology and dynamics. *Molecular biology of the cell* *25*, 2152-2160.
- Skop, A.R., and White, J.G. (1998). The dynactin complex is required for cleavage plane specification in early *Caenorhabditis elegans* embryos. *Curr Biol* *8*, 1110-1116.

Small, J.V., Stradal, T., Vignal, E., and Rottner, K. (2002). The lamellipodium: where motility begins. *Trends Cell Biol* *12*, 112-120.

Solinet, S., Mahmud, K., Stewman, S.F., Ben El Kadhi, K., Decelle, B., Talje, L., Ma, A., Kwok, B.H., and Carreno, S. (2013). The actin-binding ERM protein Moesin binds to and stabilizes microtubules at the cell cortex. *J Cell Biol* *202*, 251-260.

Speicher, S., Fischer, A., Knoblich, J., and Carmena, A. (2008). The PDZ protein Canoe regulates the asymmetric division of *Drosophila* neuroblasts and muscle progenitors. *Curr Biol* *18*, 831-837.

Spradling, A., Fuller, M.T., Braun, R.E., and Yoshida, S. (2011). Germline stem cells. *Cold Spring Harbor perspectives in biology* *3*, a002642.

Srinivasan, D.G., Fisk, R.M., Xu, H., and van den Heuvel, S. (2003). A complex of LIN-5 and GPR proteins regulates G protein signaling and spindle function in *C elegans*. *Genes Dev* *17*, 1225-1239.

Stehman, S.A., Chen, Y., McKenney, R.J., and Vallee, R.B. (2007). NudE and NudEL are required for mitotic progression and are involved in dynein recruitment to kinetochores. *J Cell Biol* *178*, 583-594.

Stewart, M.P., Helenius, J., Toyoda, Y., Ramanathan, S.P., Muller, D.J., and Hyman, A.A. (2011). Hydrostatic pressure and the actomyosin cortex drive mitotic cell rounding. *Nature* *469*, 226-230.

Suzuki, A., and Ohno, S. (2006). The PAR-aPKC system: lessons in polarity. *J Cell Sci* *119*, 979-987.

Svitkina, T.M., Bulanova, E.A., Chaga, O.Y., Vignjevic, D.M., Kojima, S., Vasiliev, J.M., and Borisy, G.G. (2003). Mechanism of filopodia initiation by reorganization of a dendritic network. *J Cell Biol* *160*, 409-421.

Swan, A., Nguyen, T., and Suter, B. (1999). *Drosophila* Lissencephaly-1 functions with Bic-D and dynein in oocyte determination and nuclear positioning. *Nat Cell Biol* *1*, 444-449.

Tai, C.Y., Dujardin, D.L., Faulkner, N.E., and Vallee, R.B. (2002). Role of dynein, dynactin, and CLIP-170 interactions in LIS1 kinetochore function. *J Cell Biol* *156*, 959-968.

Tame, M.A., Raaijmakers, J.A., Afanasyev, P., and Medema, R.H. (2016). Chromosome misalignments induce spindle-positioning defects. *EMBO Rep* *17*, 317-325.

Tame, M.A., Raaijmakers, J.A., van den Broek, B., Lindqvist, A., Jalink, K., and Medema, R.H. (2014). Astral microtubules control redistribution of dynein at the cell cortex to facilitate spindle positioning. *Cell Cycle* *13*, 1162-1170.

Tanaka, T., Serneo, F.F., Higgins, C., Gambello, M.J., Wynshaw-Boris, A., and Gleeson, J.G. (2004). Lis1 and doublecortin function with dynein to mediate coupling of the nucleus to the centrosome in neuronal migration. *J Cell Biol* *165*, 709-721.

Tawk, M., Araya, C., Lyons, D.A., Reugels, A.M., Girdler, G.C., Bayley, P.R., Hyde, D.R., Tada, M., and Clarke, J.D. (2007). A mirror-symmetric cell division that orchestrates neuroepithelial morphogenesis. *Nature* *446*, 797-800.

They, M., Jimenez-Dalmaroni, A., Racine, V., Bornens, M., and Julicher, F. (2007). Experimental and theoretical study of mitotic spindle orientation. *Nature* *447*, 493-496.

They, M., Racine, V., Pepin, A., Piel, M., Chen, Y., Sibarita, J.B., and Bornens, M. (2005). The extracellular matrix guides the orientation of the cell division axis. *Nat Cell Biol* *7*, 947-953.

Thornton, G.K., and Woods, C.G. (2009). Primary microcephaly: do all roads lead to Rome? *Trends Genet* *25*, 501-510.

Toyoshima, F., Matsumura, S., Morimoto, H., Mitsushima, M., and Nishida, E. (2007). PtdIns(3,4,5)P3 regulates spindle orientation in adherent cells. *Dev Cell* *13*, 796-811.

- Toyoshima, F., and Nishida, E. (2007). Integrin-mediated adhesion orients the spindle parallel to the substratum in an EB1- and myosin X-dependent manner. *Embo J* 26, 1487-1498.
- Tsai, J.W., Chen, Y., Kriegstein, A.R., and Vallee, R.B. (2005). LIS1 RNA interference blocks neural stem cell division, morphogenesis, and motility at multiple stages. *J Cell Biol* 170, 935-945.
- Tseng, Q., Duchemin-Pelletier, E., Deshiere, A., Balland, M., Guillou, H., Filhol, O., and Thery, M. (2012). Spatial organization of the extracellular matrix regulates cell-cell junction positioning. *Proc Natl Acad Sci U S A* 109, 1506-1511.
- Tuncay, H., and Ebnet, K. (2016). Cell adhesion molecule control of planar spindle orientation. *Cell Mol Life Sci* 73, 1195-1207.
- Tynan, S.H., Gee, M.A., and Vallee, R.B. (2000). Distinct but overlapping sites within the cytoplasmic dynein heavy chain for dimerization and for intermediate chain and light intermediate chain binding. *J Biol Chem* 275, 32769-32774.
- Uchida, C., Hattori, T., Takahashi, H., Yamamoto, N., Kitagawa, M., and Taya, Y. (2014). Interaction between RB protein and NuMA is required for proper alignment of spindle microtubules. *Genes to cells : devoted to molecular & cellular mechanisms* 19, 89-96.
- Urnavicius, L., Zhang, K., Diamant, A.G., Motz, C., Schlager, M.A., Yu, M., Patel, N.A., Robinson, C.V., and Carter, A.P. (2015). The structure of the dynactin complex and its interaction with dynein. *Science* 347, 1441-1446.
- Vallee, R.B., McKenney, R.J., and Ori-McKenney, K.M. (2012). Multiple modes of cytoplasmic dynein regulation. *Nat Cell Biol* 14, 224-230.
- Vassilev, L.T., Tovar, C., Chen, S., Knezevic, D., Zhao, X., Sun, H., Heimbrosk, D.C., and Chen, L. (2006). Selective small-molecule inhibitor reveals critical mitotic functions of human CDK1. *Proc Natl Acad Sci U S A* 103, 10660-10665.
- Vaughan, K.T., and Vallee, R.B. (1995). Cytoplasmic dynein binds dynactin through a direct interaction between the intermediate chains and p150Glued. *J Cell Biol* 131, 1507-1516.
- Vitriol, E.A., Uetrecht, A.C., Shen, F., Jacobson, K., and Bear, J.E. (2007). Enhanced EGFP-chromophore-assisted laser inactivation using deficient cells rescued with functional EGFP-fusion proteins. *Proc Natl Acad Sci U S A* 104, 6702-6707.
- von Bulow, M., Rackwitz, H.R., Zimbelmann, R., and Franke, W.W. (1997). CP beta3, a novel isoform of an actin-binding protein, is a component of the cytoskeletal calyx of the mammalian sperm head. *Exp Cell Res* 233, 216-224.
- Walczak, C.E., Gayek, S., and Ohi, R. (2013). Microtubule-depolymerizing kinesins. *Annu Rev Cell Dev Biol* 29, 417-441.
- Wang, H., Ng, K.H., Qian, H., Siderovski, D.P., Chia, W., and Yu, F. (2005). Ric-8 controls Drosophila neural progenitor asymmetric division by regulating heterotrimeric G proteins. *Nat Cell Biol* 7, 1091-1098.
- Wang, X., Tsai, J.W., Imai, J.H., Lian, W.N., Vallee, R.B., and Shi, S.H. (2009). Asymmetric centrosome inheritance maintains neural progenitors in the neocortex. *Nature* 461, 947-955.
- Watson, P., Forster, R., Palmer, K.J., Pepperkok, R., and Stephens, D.J. (2005). Coupling of ER exit to microtubules through direct interaction of COPII with dynactin. *Nat Cell Biol* 7, 48-55.
- Wear, M.A., Yamashita, A., Kim, K., Maeda, Y., and Cooper, J.A. (2003). How capping protein binds the barbed end of the actin filament. *Curr Biol* 13, 1531-1537.
- Wee, B., Johnston, C.A., Prehoda, K.E., and Doe, C.Q. (2011). Canoe binds RanGTP to promote Pins(TPR)/Mud-mediated spindle orientation. *J Cell Biol* 195, 369-376.

Wei, C., Bhattaram, V.K., Igwe, J.C., Fleming, E., and Tirnauer, J.S. (2012). The LKB1 tumor suppressor controls spindle orientation and localization of activated AMPK in mitotic epithelial cells. *PLoS ONE* 7, e41118.

Wilcock, A.C., Swedlow, J.R., and Storey, K.G. (2007). Mitotic spindle orientation distinguishes stem cell and terminal modes of neuron production in the early spinal cord. *Development* 134, 1943-1954.

Willard, F.S., Kimple, R.J., and Siderovski, D.P. (2004). Return of the GDI: the GoLoco motif in cell division. *Annu Rev Biochem* 73, 925-951.

Williams, S.E., Beronja, S., Pasolli, H.A., and Fuchs, E. (2011). Asymmetric cell divisions promote Notch-dependent epidermal differentiation. *Nature* 470, 353-358.

Williams, S.E., Ratliff, L.A., Postiglione, M.P., Knoblich, J.A., and Fuchs, E. (2014). Par3-mInsc and Galphai3 cooperate to promote oriented epidermal cell divisions through LGN. *Nat Cell Biol* 16, 758-769.

Wodarz, A., Ramrath, A., Grimm, A., and Knust, E. (2000). Drosophila atypical protein kinase C associates with Bazooka and controls polarity of epithelia and neuroblasts. *J Cell Biol* 150, 1361-1374.

Woodard, G.E., Huang, N.N., Cho, H., Miki, T., Tall, G.G., and Kehrl, J.H. (2010). Ric-8A and Gi{alpha} Recruit LGN, NuMA, and Dynein to the Cell Cortex to Help Orient the Mitotic Spindle. *Mol Cell Biol* 30, 3519-3530.

Woodruff, J.B., Drubin, D.G., and Barnes, G. (2009). Dynein-driven mitotic spindle positioning restricted to anaphase by She1p inhibition of dynactin recruitment. *Molecular biology of the cell* 20, 3003-3011.

Woolner, S., O'Brien, L.L., Wiese, C., and Bement, W.M. (2008). Myosin-10 and actin filaments are essential for mitotic spindle function. *J Cell Biol* 182, 77-88.

Wyatt, T.P., Harris, A.R., Lam, M., Cheng, Q., Bellis, J., Dimitracopoulos, A., Kabla, A.J., Charras, G.T., and Baum, B. (2015). Emergence of homeostatic epithelial packing and stress dissipation through divisions oriented along the long cell axis. *Proc Natl Acad Sci U S A* 112, 5726-5731.

Xia, J., Swiercz, J.M., Banon-Rodriguez, I., Matkovic, I., Federico, G., Sun, T., Franz, T., Brakebusch, C.H., Kumanogoh, A., Friedel, R.H., *et al.* (2015). Semaphorin-Plexin Signaling Controls Mitotic Spindle Orientation during Epithelial Morphogenesis and Repair. *Dev Cell* 33, 299-313.

Xiang, X., Beckwith, S.M., and Morris, N.R. (1994). Cytoplasmic dynein is involved in nuclear migration in *Aspergillus nidulans*. *Proc Natl Acad Sci U S A* 91, 2100-2104.

Xiang, X., Han, G., Winkelmann, D.A., Zuo, W., and Morris, N.R. (2000). Dynamics of cytoplasmic dynein in living cells and the effect of a mutation in the dynactin complex actin-related protein Arp1. *Curr Biol* 10, 603-606.

Xie, T., and Spradling, A.C. (2000). A niche maintaining germ line stem cells in the *Drosophila* ovary. *Science* 290, 328-330.

Yamashita, A., Maeda, K., and Maeda, Y. (2003a). Crystal structure of CapZ: structural basis for actin filament barbed end capping. *Embo J* 22, 1529-1538.

Yamashita, Y.M., Jones, D.L., and Fuller, M.T. (2003b). Orientation of asymmetric stem cell division by the APC tumor suppressor and centrosome. *Science* 301, 1547-1550.

Yasumi, M., Sakisaka, T., Hoshino, T., Kimura, T., Sakamoto, Y., Yamanaka, T., Ohno, S., and Takai, Y. (2005). Direct binding of Lgl2 to LGN during mitosis and its requirement for normal cell division. *J Biol Chem* 280, 6761-6765.

Yeh, T.Y., Quintyne, N.J., Scipioni, B.R., Eckley, D.M., and Schroer, T.A. (2012). Dynactin's pointed-end complex is a cargo-targeting module. *Molecular biology of the cell* 23, 3827-3837.

Yingling, J., Youn, Y.H., Darling, D., Toyo-Oka, K., Pramparo, T., Hirotsune, S., and Wynshaw-Boris, A. (2008). Neuroepithelial stem cell proliferation requires LIS1 for precise spindle orientation and symmetric division. *Cell* 132, 474-486.

- Yu, F., Morin, X., Cai, Y., Yang, X., and Chia, W. (2000). Analysis of partner of inscuteable, a novel player of *Drosophila* asymmetric divisions, reveals two distinct steps in inscuteable apical localization. *Cell* *100*, 399-409.
- Yu, F., Wang, H., Qian, H., Kaushik, R., Bownes, M., Yang, X., and Chia, W. (2005). Locomotion defects, together with Pins, regulates heterotrimeric G-protein signaling during *Drosophila* neuroblast asymmetric divisions. *Genes Dev* *19*, 1341-1353.
- Yuzawa, S., Kamakura, S., Iwakiri, Y., Hayase, J., and Sumimoto, H. (2011). Structural basis for interaction between the conserved cell polarity proteins Inscuteable and Leu-Gly-Asn repeat-enriched protein (LGN). *Proc Natl Acad Sci U S A* *108*, 19210-19215.
- Zeng, X., Sigoillot, F., Gaur, S., Choi, S., Pfaff, K.L., Oh, D.C., Hathaway, N., Dimova, N., Cuny, G.D., and King, R.W. (2010). Pharmacologic inhibition of the anaphase-promoting complex induces a spindle checkpoint-dependent mitotic arrest in the absence of spindle damage. *Cancer cell* *18*, 382-395.
- Zhang, J., Li, S., Fischer, R., and Xiang, X. (2003). Accumulation of cytoplasmic dynein and dynactin at microtubule plus ends in *Aspergillus nidulans* is kinesin dependent. *Molecular biology of the cell* *14*, 1479-1488.
- Zhang, Q., Wang, F., Cao, J., Shen, Y., Huang, Q., Bao, L., and Zhu, X. (2009). Nudel promotes axonal lysosome clearance and endo-lysosome formation via dynein-mediated transport. *Traffic* *10*, 1337-1349.
- Zheng, Z., Wan, Q., Liu, J., Zhu, H., Chu, X., and Du, Q. (2013). Evidence for dynein and astral microtubule-mediated cortical release and transport of Galphai/LGN/NuMA complex in mitotic cells. *Molecular biology of the cell* *24*, 901-913.
- Zheng, Z., Zhu, H., Wan, Q., Liu, J., Xiao, Z., Siderovski, D.P., and Du, Q. (2010). LGN regulates mitotic spindle orientation during epithelial morphogenesis. *J Cell Biol* *189*, 275-288.
- Zhu, J., Shang, Y., Xia, C., Wang, W., Wen, W., and Zhang, M. (2011). Guanylate kinase domains of the MAGUK family scaffold proteins as specific phospho-protein-binding modules. *Embo J* *30*, 4986-4997.
- Zhu, M., Settele, F., Kotak, S., Sanchez-Pulido, L., Ehret, L., Ponting, C.P., Gonczy, P., and Hoffmann, I. (2013). MISP is a novel Plk1 substrate required for proper spindle orientation and mitotic progression. *J Cell Biol* *200*, 773-787.
- Zigman, M., Trinh le, A., Fraser, S.E., and Moens, C.B. (2011). Zebrafish neural tube morphogenesis requires Scribble-dependent oriented cell divisions. *Curr Biol* *21*, 79-86.